ROMA TRE
UNIVERSITÀ DEGLI STUDI

SCUOLA DOTTORALE IN GEOLOGIA DELL'AMBIENTE E DELLE RISORSE
SDIGAR

CICLO XXVII

SYSTEMATICS AND EVOLUTIONARY DYNAMICS WITHIN TALPIDAE (MAMMALIA): PHYLOGENY AND FUNCTIONAL MORPHOLOGY

Dottorando: Gabriele Sansalone

Docente Guida: Prof. Tassos Kotsakis

Coordinatore: Prof. Claudio Faccenna

INDEX

INTRODUCTION AND OBJECTIVES

Diverse lifestyles have evolved among the Talpidae. This family is distributed throughout Eurasia and North America and includes species that are ambulatory (the shrew-like moles), semi-aquatic (desmans), semi- fossorial (shrew moles) and fully fossorial (Hutchison, 1976; Yates and Moore, 1990). Head and body length is 63-215 mm and tail length is 15-215 mm, usually 15-85 mm. *Desmana*, the Russian desman, is the largest member of the family, and the several genera of shrew-moles and the long tailed mole, *Scaptonyx*, are the smallestin head and body length. Moles and desmans have elongated, cylindrical, bodies. The long, tubular, naked, though muzzle extends beyond the margin of the lower lip. In the star-nosed mole of North America, *Condylura*, the nose is divided at the end into 22 fleshy appendages. The eyes are minute, hidden in the pelage or nearly so, and in some cases covered by skin. There is no external ear. The neck is short. The limbs are short and have five digits. The hand is permanently turned outward because the radius articulates with the humerus in a S-shaped cavity. The humerus is massive (in particular in the highly fossorial moles) and articulates with the short, thick clavicle. The scapula is long and narrow, and the sternum is large, projected anteriorly, and, in the deeply fossorial forms, highly keeled. The tibia and the fibula are joined along their distal half. Females have three or four pairs of mammae. The penis is directed toward the rear of the body, and the scrotum is represented by only a slight bulge in the skin.

In the most forms of moles, almost all the hairs are about the same length, soft, flexible, and of small diameter. The fur is as much velvet and can lie in every direction, anabling a mole to go forward and backward in small burrows. Desmans have long, oily guard hairs interspersed with the shorter hairs.

The dental formula is: (i 2-3/1-3, c 1/0-1, pm 3-4/3-4, m 3/3) x 2 = 32-44.

This family includes forms that burrows extensively, spending most of their lives underground, and some acquatic or semi-acquatic forms that occasionally burrow. Moles make tunnels of two types: shallow subsurface tunnels, usually marked by surface ridges of soil that the moles have pushed up with their backs; deeper tunnels, generally marked by cone-shaped surface mounds of earth. These are the familiar "mole-hills", composed of earth that has been pushed out through the tunnel. Surface mounds are not formed if the mole copresses the soil around the deep tunnel sufficiently to provide the required space. The more permanent deep tunnels are used for shelter and for rearing the young, while the shallow tunnels are used for feeding and resting. Urotrichini and Neurotrchini (shrew-moles) are often active on the ground and make very shallow tunnels. Desmans and *Condylura* use all of their limbs and tail when swimming. They shelter in burrows often located in stream banks.

These different life-styles are reflected in the postcranial skeleton, and, in particular, in the humerus. There is a longstanding debate on the phylogentic relationships inside the Talpidae (Whidden, 2000; Shinohara et al., 2003; Motokawa, 2004; Cabria, 2006; Sanchez-Villagra et al., 2006; Crumpton and Thompson, 2013; He et al., 2014; Shinohara et al., 2014). The fully fossorial taxa evolved a unique humeral morphology (Gambaryan et al., 2003; Sanchez-Villagra et al., 2004). Despite many authors qualitatively described the evolutionary modifications experienced by the talpids humerus (Dobson, 1882; Freeman, 1889; Edwards, 1937; Campbell, 1939;

Yalden, 1966; among others), very few studies quantitatively assessed the pattern of evolutionary transformations that occurred in this bone (Gambaryan et al., 2003). Moreover the interaction between shape, function and phylogeny has not been evaluated, by means of modern comparative methods.

In this framework, in order to investigate the phylogenetic relationships of Talpidae, a cladistic analysis, based on the morphometrics and morphology of informative skeletal elements, will be performed. Sanchez-Villagra et al. (2006) performed a similar analysis on talpids, though their work was aimed to investigate the talpids phylogeny at genus level, and with solely extant taxa included. The new analysis will include all extant and extinct species belonging to Talpidae family.

The burrowing ability is a distinctive trait of moles, in order to quantitatively assess the digging performance of moles a Finite Elements Analysis will be performed on the humerus at the generic level. Such analysis, coupled with modern comparative methods, could reveal the adaptive dynamics undergoing the evolution of the fossorial lifestyle among talpids. The Finite Elements Analysis will be extended, in a comparative fashion, also to the extinct family of Proscalopidae whose species present morphologies that do not have homologues among extant ones. The evolution of the fossorial lifestyle is likely to have influenced the whole anatomy of moles, in order to characterize the patterns of morphological evolution a Geometric Morphometrics analysis will be performed on the mandible, the first lower molar and the humerus. The comparative analyses of different skeletal elements, related to vital functions such as locomotion and feeding, could shed new lights on tempo and modes of moles adaptation to the fossorial lifestyle, at this purpose the interaction between shape, function and phylogeny will be evaluated, by means of comparative methods, in order to understand which of these features could be the most influential on morphological evolution. As reported before the humerus is the talpid bone that experienced the most remarkable modifications. In this work we will evaluate the potential phylogenetic and taxonomic signal in this highly derived skeletal element.

CHAPTER I

SYSTEMATICS AND PHYLOGENETIC RELATIONSHIPS

Introduction

The family Talpidae consists of the fossorial moles, the shrew moles and the desmans. Different lifestyles occur among various taxa, including strictly fossorial, semifossorial, ambulatory and semi-aquatic species. Although the Talpidae are distributed widely throughout the temperate areas of the Holartic, each extant genus is currently restricted to a single continent and the alternative phylogenetic hypotheses that have been published for this group have differing implications for their biogeographical history (Hutchison, 1968, 1974; Yates and Moore, 1990; Whidden, 2000). Talpids probably originated in Eurasia, considering that the oldest occurrence of the group is in the Late Eocene of Europe (McKenna and Bell, 1997). They, probably, then dispersed to North America. However, it is not clear how many invasions there were, what route(s) the animals took, and if there were any back-migrations. Relationships among talpids are controversial as demonstrated by recent molecular and morphological studies (Whidden, 2000; Shinohara et al., 2003;

Motokawa, 2004; Cabria, 2006; SanchezVillagra et al., 2006; Crumpton and Thompson, 2013; He et al., 2014; Shinohara et al., 2014). Recent investigations in extant talpid taxonomy recognized 17 genera and 44 species. When dealing with fossils the evolutionary scenario becomes even more complicated. Talpids diversity was extremely higher in the past, particulary in the early Miocene (e.g., Ziegler, 1990, Van den Hoek Ostende 2001). The oldest known talpid from Europe is *Eotalpa anglica* from the Late Eocene of England (Sigé et al., 1977). In the genus *Eotalpa* is included another species: *E. belgica* (Smith, 2007), from the Early Oligocene (MP 21). The oldest American talpid is *Oreotalpa florissantensis* (Lloyd and Eberle, 2008), also from the Latest Eocene. The oldest Asian talpid was unfortunately not determined even to genus level; it was found in the Latest Eocene of Kazakhstan (Lloyd and Eberle, 2008). In the Late Oligocene of North-America, another talpid *Quadrodens wilsoni* (Gunnell et al., 2008) is present, however, with no subfamily attribution. The Talpidae incertae sedis *Mongolopala tathue* (Ziegler et al., 2007) is known from Late Oligocene of Mongolia only. Another Late Oligocene genus from Mongolia is *Mongoloscapter zhegalloi* (Lopatin, 2002).

The only taxon attributed to a subfamily Suleimaninae, today extinct, is the monospecific genus *Suleimania ruemkae* (Van den Hoek Ostende, 2001) from the Early Miocene localities of Harami, Kilçak, and Keseköy in Anatolia.

Uropsilinae

The least fossorial talpid subfamily (Van den Hoek Ostende 2001, Van den Hoek Ostende and Fejfar 2006, Piras et al. 2012), the Uropsilinae, were represented, in Europe, by the genus *Desmanella*. The first occurrence of *Desmanella* is from latest Oligocene of Germany (Van den Hoek Ostende 1989, Ziegler 1998b). It was widespread in Asia and Europe during the Miocene and the last occurrence is from European Pliocene (García-Alix et al., 2011). The genus *Desmanella* includes 13 species and it is one of the most diverse among talpid genera: *D. gudrunae*, *D. engesseri*, *D. fejfari*, *D. sickenbergi*, *D. storchi*, *D. sthelini*, *D. cingulata*, *D. crusafonti*, *D. rietscheli*, *D. amasyaei, D. dubia*, *D. wolfersheimensis*, *D. gardiolensis* (Engesser, 1980; Qiu, 1996; Storch and Dahlmann, 2000). *Asthenoscapter*, was present in Europe from the Late Oligocene (Engesser and Storch, 2008) to the Middle Miocene (van den Hoek Ostende et al., 2005, Ziegler, 2006b). The genus *Asthenoscapter* includes two species, *A. meini* (Hutchinson, 1974) and *A. ziegleri* (Engesser and Storch 2008). The genus *Theratiskos* is present in the Early Miocene of Anatolia (van den Hoek Ostende, 2001) with two species: *Theratiskos rutgeri* and *T. metcheldae*. A third species, *T. compactus* (firstly described as *Myxomygale asiaprima*, Lopatin, 2004), was present in the Late Oligocene of Kazakhstan (Bendukidze et al., 2009). The Uropsilinae were present in North America with the Miocene genus *Mystipterus* (Hutchison, 1968), this genus includes three species: *M. vespertilio*, *M. martini* and *M. pacificus*. The monospecific North-American Middle-Late Miocene *Gallardia thomsoni* has been included in the Uropsilinae by Gunnel et al. (2008). The monospecific *Mygatalpa avernensis* is known from the Latest Oligocene to the Earliest Miocene (Remy et al., 1987; Ziegler, 1999) of Europe, generally considered as a desman, has been included in the Uropsilinae by van den Hoek Ostende (2001). The extant genus *Uropsilus* includes 4 species: *U. soricipes*, *U. gracilis*, *U. investigator* and *U. andersoni* from South-Eastern Asia, though recent molecular studies (Tu et al., 2014) suggest the presence of two more species. The genus *Uropsilus* is known from the Pleistocene only (Qiu and Storch, 2005; Liu et al., 2009).

Desmaninae

The only American member of the Desmaninae, *Lemoynea biradicularis* (Bown, 1980) was found in localities from Late Miocene or Early Pliocene times (Bown 1980). In Europe the extinct genus *Archaeodesmana* accounts for 14 species, is known from the Late Miocene to the Pliocene (Rumke, 1985; Martin-Suarez et al., 2010), it includes: *A. primigenia*, *A. vinea*, *A. turolense*, *A. adroveri*, *A. luteyni*, *A. pontica*, *A. major*, A. *dekkersi*, *A. baetica*, *A. verestchagini*, *A. bifida*, *A. brailloni*, *A. elvirae* and *A. acies* (Rumke, 1985). The genus *Galemys* has been present from the Late Miocene to recent times, it includes 3 species: the extant *G.s pyrenaicus*, *G. kormosi* and *G. sulimski* (Rumke, 1985). The genus *Desmana* has been present from the Pliocene to recent times (Van den Hoek Ostende et al. 2005, Hutterer 2005). It includes 5 species: the sole extant *D. moschata* and the extinct *D. nehringi*, *D. thermalis*, *D. kowalskae* and *D. inflata*. However, from the Pliocene and Pleistocene of Eastern Europe many species have been reported: *D. kujalnikensis*, *D. radulescui*, *D. meridionalis*, *D. nogaica*, *D. gureevi*, *D. jalpugensis*, *D. moldavica*, *D. polonica* Topachesky and Pashkov, 1990; Pashkov and Topachesky, 1990), these species have been instituted on the basis of few teeth only and without any humerus attributed. It is challenging, without direct access to the material, to investigate the systematic of these taxa. The genus *Mygalea* was present in the Miocene of Europe (Van den Hoek Ostende et al. 2005, Rzebik-Kowalska 2005a). It includes 3 species: *M. jaegeri*, *M. schreuderae* and *M. magna* (Ziegler, 1999; Ziegler, 2003; Van den Hoek Ostende, 2006). The monospecific *Mygalinia hungarica* (Gureev, 1964; Ziegler, 1999) is present in the Miocene of Central Europe. Klietmann (2013) considered *Mygalinia* to be not determinable at subfamily level, nevertheless, some features of the humerus as the hooked process of the medial epicondyle lead us to maintain the attribution of *Mygalinia* to the subfamily Desmaninae. The genus *Gerhardstorchia* includes 4 species: *G. wedrevis*, *G. meszaroshi*, *G. biradicata* and *G. quinquecuspidata*, this genus was present from the Middle-Late Miocene to the Pliocene of Europe (Dahlmann and Dogan, 2011).

Urotrichini

The tribe Urotrichini includes the Japanese endemic extant shrew moles *Urotrichus talpoides* and *Dymecodon pilirostris*, these 2 monospecific genera are know from the Pleistocene of Japan (Kawamura, 1991). Ziegler (2003) described the species *Urotrichus giganteus*; this very odd species was present in the Middle Miocene of the Middle Europe. *Urotrichus giganteus* is known from few very large humeri (Ziegler, 2003), morphologically indistinguishable from the extant species. The monospecific *Tenuibrachiatum storchi* was present in the Miocene of Central Europe (Ziegler, 2003). The genus *Myxomygale* is known from the Early Oligocene to the Middle Miocene (Ziegler, 2003; Ziegler, 2012) of Europe, this genus includes 6 species: *M. antiqua*, *M. engesseri*, *M. hutchinsoni*, *M. gracilis*, *M. minor*, *M. vauclusensis* (Ziegler, 1999, 2003, 2012). The monospecific *Nuragha schreuderae*, is known in the Early Miocene of Sardinia only (De Brujin and Rumke, 1974). The monospecific *Pseudoparatalpa lavroi* is present in the Late Oligocene of Kazakhstan (Bendukidze et al., 2009). The genus *Paratalpa* occurred in Europe from the Latest Oligocene (Hugueney, 1972, Ziegler, 1998b; Engesser and Storch, 2008) to the Early Miocene. This genus includes 3 species: *P. micheli*, *P. brachychir* and *P. meyeri*. This genus has been considerd by several authors as incertae sedis (van den Hoek Ostende, 1997; Ziegler, 2003; Klietmann, 2013;). We tentatively include *Paratalpa* in the Urotrichini, as already suggested by Hugueney (1972). Some features of the humerus as the large and flat teres tubercle, the reduced greater tuberosity, the wide bicipital notch and the unfused bicipital tunnel are very similar to the Urotrichine condition. However our inclusion is tentative and further investigations are required in order to assess the systematic status of this highly debated genus. The same follows for the genus *Desmanodon*, that replaced *Paratalpa* during the Early Miocene (van den Hoek Ostende, 1989; 1997). In this case we are even more doubtful due to the robust configuration of the humerus of *Desmanodon* spp. Again a detailed revision of this genus is required. The genus *Desmanodon* includes 9 species: *D. minor, D. major, D. antiquus, D. ziegleri, D. burkarti, D. daamsi, D. fluegeli*, *D. crocheti* and *D. larsi* (Engesser, 1980; Ziegler, 1985; Van den Hoek Ostende, 1997; Prieto, 2010; Prieto et al., 2010). According to Doukas and Van den Hoek Ostende (2006), the species *D. meuleni* must be considered a junior synonym of *D. antiquus*.

Neurotrichini

The Neurotrichini include the North-American extant taxon *Neurotrichus gibbsii*; no fossil record is documented for this species (Gunnel et al., 2008). The Polish fossil species *Neurorichus skoczeni* and *N. polonicus* have been attributed to the new genus *Rzebikia* (see Chapter 5 for extensive discussion about this topic). The genus *Quyania* was present in the Middle-Late Miocene of China and in the Pliocene of Poland (Storch and Qiu, 1983; 2005; Rzebik-Kowalska, 2014). This genus includes 2 species: *Q. chowi* and *Q. europaea*.

Condylurini

The Condylurini include the extant species *Condylura cristata,* present in North-America since the Pleistocene (Gunnell et al., 2008), and 2 extinct species from the Pliocene of Poland: *C. izabellae* and *C. kowalskii* (Skoczen, 1976; Rzebik-Kowalska, 2014). The monospecific *Achlyoscapter longirostris* was present from the Middle Miocene to the Late Pliocene of North-America (Hutchinson, 1968). We tentatively include this genus in the Condylurini following Hutchinson (1968), we observe that the upper premolar row of *Achlyoscapter* presents diastemas and a complete, brachyodont, dentition as in the modern *Condylura*.

Scalopini

The Scalopini included Asian, European and North-American forms. The monospecific *Yunoscaptor scalprum* is known from the Late Miocene of China (Qiu and Storch, 2005). The genus *Yanshuella* includes the North-American species *Y. columbiana* (Hutchinson, 1968; Storch and Qiu, 1983), present from the Late Miocene to the Early Pliocene, and the Asian species *Y. primaeva* (Storch and Qiu, 1983) that was present in the Miocene and Pliocene (Qiu and Storch, 2005) of China. The Gansu mole *Scapanulus oweni,* unknown from the fossil record, is the only extant Asian species. The genus also includes the fossil species *S. lampounensis* from the Early Miocene (Mein and Ginsburg, 1977) of southeastern Asia. The European Scalopini were a successful and diversified group. The most diversified genus was *Proscapanus*, present from the Early Miocene, that includes 6 species: *P. sansaniensis*, *P. intercedens*, *P. minor*, *P. metastylidus*, *P. austriacus* and *P. lehmani* (Gibert, 1975; Ziegler, 1985; 2003; 2006; Van den Hoek Ostende, 1989). *Proscapanus* completely disappear after the MN9 (Gibert, 1975; Ziegler, 2006). The monospecific *Hugueneya primitiva* (Van den Hoek Ostende, 1989) is known from the

Early Miocene. The genus *Leptoscaptor* is present in the late Middle Miocene only (Ziegler, 2003). This genus includes 2 species: *L. bavaricum* and *L. robustior*, which are indistinguishable in the teeth morphology but very different in the humerus overall robustness. In North-America, The genus *Wilsonius* (Kretzoi and Kretzoi, 2001 noted as *Scalopoides* was a preoccupied name as it was already used by Bode, 1953 to describe the coleopteran genus *Scalopoides*) is present from the Latest Oligocene to the Late Miocene (Gunnel et al., 2008) and includes 2 species: *W. isodens* and *W. ripafodiator* (Hutchinson, 1968). The rare monospecific *Scapanoscapter simplicidens* (Hutchinson, 1968) was present in the Early Miocene of North-America and was thought to be the possible ancestor of *Scapanus* (Hutchinson, 1987). The genus *Domninoides* (Green, 1956) is present from the Early Miocene to the Early Pliocene (Gunnell et al., 2008), this genus includes 5 species: *D. valentinensis*, *D. hessei*, *D. riparensis*, *D. knoxjonesi*, *D. mimicus* and the Spanish species *D. santafei* (Green, 1956; Gibert, 1974; Reed, 1962; Wilson, 1968; Dalquest et al., 1996). Though we have to report that *D. knoxjonesi* and *D. hessei* have been described on the basis of very fragmentary teeth material and one humerus only (Dalquest et al., 1996). Unfortunately, we were not able to directly access at the material and keep the specific attributions as valid. The extant North-American monospecific *Parascalops breweri* has been reported from the middle Pleistocene only (Gunnel et al., 2008). Skoczen (1980) described the species *Parascalops fossilis* from the Pliocene of Poland. Unfortunately the material belonging to the Polish species has been lost (Rzebik-Kowalska, 2014) and only one humerus has been "saved". *Parascalops fossilis* shows several affinities in the humeral morphology with *Proscapanus*. However the possibility that the specimens described by Skoczen in fact belonged to *Proscapanus* will remain untested. The genus *Scalopus* is present in North-America since the Late Miocene (Gunnel et al., 2008), it includes the extant species *S. acquaticus* and 5 extinct species: *S. sewardensis*, *S. blancoensis*, *S. rexroadi*, *S. mcgrewi* and *S. ruficervus* (Gunnel et al., 2008). The North-American genus *Scapanus* is present since the Middle Miocene (Gunnel et al., 2008), it includes 3 extant species: *S. latimanus*, *S. orarius* and the very large *S. townsendii*; the genus includes also 4 fossil species: *S. malatinus*, *S. hagermanensis*, *S. schultzi* and *S. proceridens* (Hutchinson, 1968, 1987).

Talpini

The Talpini include only Eurasian forms. The basal genus is thought to be *Geotrypus* (Sanchez-Villagra et al., 2004; Schwermann and Martin, 2012; Ziegler, 2012) it is known from the Late Oligocene to the Early Miocene (Schwermann and Martin, 2012; Ziegler, 2012). It includes 9 species: *G. antiquus*, *G. minor*, *G. acutidentatus*, *G. montisasini*, *G. tomerdingensis*, *G. haramiensis*, *G. kesekoyensis*, *G. ehrensteinensis* and *G. oschiriensis* (Rumke, 1974; Zielger, 1990; van den Hoek Ostende, 2001; Ziegler, 2012). The material belonging to *Geotrypus* is often scarce and fragmentary, and specimens with very different morphology have been included in this genus. In this framework we keep these attributions as valid, but the morphological analysis that will be shown in the following chapters suggest that a revision of this genus will be required. The genus *Talpa* is present from the Early Miocene (Ziegler, 1990), it is the most diversified of the family Talpidae. The genus *Talpa* includes 16 species, the 7 European extinct species: *T. tenuidentata*, *T. minuta*, *T. gilothi*, *T. vallesensis*, *T.minor*, *T. fossilis* and *T. episcopalis* (Kormos, 1930; Ziegler, 1990, 1999, 2003, 2006; Storch, 1978; Engesser, 2009). The genus includes 9 extant species *T. altaica*, *T. caucasica*, *T. levantis*, *T. stankovici*, *T. davidiana*, *T.romana*, *T.caeca*, *T. occidentalis* and *T. europaea* (Hutterer, 2005). Following Krystufek et al. (2001), the fossil species *Talpa chtonia*, from the Late Pleistocene of Israel, is a synonym of *T. davidiana*. The Eastern and South- Eastern Asian genus *Euroscaptor* is present form the Late Pleistocene only and no fossil species have been assigned to this genus. It includes 8 extant species: *E. subanura*, *E. micrura*, *E. malayana*, *E. mizura*, *E. parvidens*, *E. longirostris*, *E. grandis*, and *E. klossi* (Hutterer, 2005; Kawada et al., 2007; Kawada et al., 2012; Shinohara et al., 2014).

The East Asian genus *Mogera* was present from the Early Pleistocene (Huang and Fang, 1991; Kawamura, 1991; Qiu and Storch, 2005) and does not have any fossil species assigned. It includes 8 extant species: *M. wogura*, *M. imaizumii*, *M. tokudae*, *M. insularis*, *M. kanoana*, *M. latouchei*, *M. uchidai* and *M. etigo* (Shinohara et al., 2014). The East Asian monospicific *Parascaptor leucura* is not known from the fossil record. The monospecific Chinese *Scaptochirus moschatus* is known since the Pliocene (Flynn and Wu, 1994; Qiu and Storch, 2005). Recently have been reported two fossil species *Scaptochirus minor* (Li et al., 2013) and *S. jignanensis* (Jin and Liu, 2009). Unfortunately these species have been described in Chinese master thesis without figures.

The South-Eastern Asia genus *Scaptonyx* is the most elusive and ambigous taxon. There is a complete lack of resolution about its phylogenetic position (Sanchez-Villagra et al., 2006; Cabria, 2006; Crumpton and Thompson, 2013). We tentatively include it in the Talpini as it, though resembling a shrew-mole in its external morphology, show some very derived features of the internal anatomy, like a more robust humerus (Sanchez-Villagra et al., 2006).

In summary Talpidae include 49 extinct and extant genera and ~180 species.

The purpose of this section is to complete the first comprehensive phylogenetic analysis of extant and extinct talpids based on morphology. This study begins by extracting phylogenetic characters from previous papers (Motokawa et al., 2004; Sanchez-Villagra et al., 2006). Representatives from every genus for which there was enough material to code the morphological characters was included in the analysis.

Cladistic analysis

We performed a cladistics analysis with a parsimony approach using the TNT software (Goloboff et al., 2005), using a traditional search algorithm. We used the species hedgehog *Erinaceus europaeus* and the shrews species *Blarina brevicauda* and *Sorex araneus* as outgroups. We sampled 10 best trees and then calculated the consensus tree. We selected 69 morphological characters from the list proposed by Sanchez-Villagra et al. (2006), including the dental and humeral characters only. Teeth and humeri are the most abundant remains found in fossil assemblages. The fragmentary nature of the Talpidae fossil record imposed this choice in order to have the fewer missing data as possible. We were able to code a satisfactory number of characters for 123 extant and extinct species (see Supplementary Appendix 1 to chapter 1 to visualize the tree).

Our analysis supports the Uropsilinae as the basal calde of Talpidae. Though we found the genus *Desmanella* to be more advanced than *Uropsilus*. Moreover we found that *Asthenoscapter* and *Theratiskos* clustered with Urotrichini. Klietmann (2013) reported the humerus of *Desmanella engesseri* to have an elliptical caput of the humerus when compared with *D. gudrunae* (Van den Hoek Ostende and Fejfar, 2006), which have a round one as in the modern Uropsilinae.The elliptical caput of the humerus is an autopomorphy of the derived Talpidae clades. Klietmann proposed that *Desmanella engesseri* could be in a somewhat more advanced evolutionary step when compared with *Desmanella gudrunae*. *Asthenoscapter* and *Theratiskos* both have an elliptical caput of the humerus and an overall more derived structure of the humerus, these evidences could explain the inclusion of these genera in the Urotrichini by the cladistics analysis. The Desmaninae clusterd well togheter, in fact desmans share a highly similar humeral morphology (see also chapter 2 and 3) and a very conservative tooth morphology (Ruemke, 1985). The lack of resolution we found in the internal nodes of Desmaninae could reflect the high morphological constraints. The Urotrichini grouped well togheter, although other taxa grouped with the shrew-moles. Finding the Neurotrichine genera (*Quyania*, *Rzebikia* and *Neurotrichus*) grouping with Urotrichini was not surprising, several molecular works were not able to resolve their realtionships (Shinohara et al., 2004; Cabria, 2006; Crumpton and Thompson, 2013).

The inclusion of the genus *Paratalpa* in the Urotrichini appears to be supported by our results. *Geotrypus oschiriensis* also grouped with Urotrichini. Van den Hoek Ostende (2001) reported this species to have a very short M2 and Crochet (1995) suggested the specimens from Oschiri not to be a *Geotrypus*. Our results support the exclusion of this species from the genus *Geotrypus*, however we are cautious in ascribing the material from Oschiri to the Urotrichini tribe or to a new taxon, thus suggesting the revision of the material. *Achlyoscapter longirostris* also grouped with the Urotrichini. Hutchinson (1968) hypothesize also that this species could be tentatively placed in the evolutionary line of Urotrichini. In particular he found some morphological affinities in the lower molars. Again we want to be cautious in attributing such taxon to the Urotrichini.

The highly fossorial moles well clustered togheter, the cladistic analysis evidenced the distinction between Talpini and Scalopini. Notably, *Scaptonyx* was placed in a basal position to Talpini. The absence of resolution in the internal nodes of the topology among Talpini is striking. The close similarities in the external and internal morphology of Talpini are well known (Filippucci et al., 1987; Kawada et al., 2005). Only in recent times and with the help of modern molecular methodologies, it has been possible to solve many taxonomical issues concerning Talpini genera (Filippucci et al., 1987; Kawada et al., 2001; Colangelo et al., 2010, Kawada et al., 2013, Shinohara et al., 2014). It is interesting to note that *Desmanodon* grouped with Scalopini. This association has never been proposed before. We hypothesize that the analysis could be influenced by the presence of a robust humerus and, in particular, of a deeply divided mesostyle in the upper molars that is typical of the *Desmanodon* species. These features are also shared by many Scalopini taxa (Sanchez-Villagra, 2006). Our results, however, strongly suggest the need of a review of the genus *Desmanodon* as our analyses indicate it to be one of the most ambiguous taxa among Talpidae.

Finally, our analysis supported the presence of the Talpidae clades identified in the introduction. However, the cladistics analysis showed a poor performance in solving the internal nodes in the topology, suggesting that strong functional morphology signal in different lineages could have severely influenced the topology. Nevertheless, cladistic analysis proved to be very useful in evidencing hidden taxonomical and systematic issues, and revealing new rooms for further investigations.

Further improvements will require expanding the characters matrix and the number of species as well.

Synthetic phylogeny

The cladistic analysis did not offer a great contribution in solving the intra-generic phylogenetic relationships. In order to have a phylogenetic tree with a higher degree of resolution we built a synthetic time calibrated phylogeny. To achieve that we initially built a tree including the extant species solely using the information provided by the most recent advances in molecular phylogenetics (Colangelo et al., 2010; Crumpton and Thompson, 2013; He et al., 2014; Shinohara et al., 2014). Then we started adding fossils (a similar strategy has been used in Chapter 3). Adding fossil was challenging, our efforts were focused in reviewing the entire bulk of literature available (when possible). We investigated 1) the taxonomic validity of all known extant and extinct genera and species; 2) their stratigraphic range; 3) the phylogenetic position of the genera and species recognized as valid. Polytomies in the tree represent the absolute lack of resolution in the phylogenetic relationships or too much divergent opinion of the authors. We recognize the limitation of this approach due to uncertain affinities. However, following this strategy, it was possible to build the most complete phylogentic tree of the family Talpidae as we included all genera and 172 species (see Supplementary Material 2 to Chapter 1 to visualize the tree).

As this synthetic phylogeny provides the highest degree of resolution, it will be used in all comparative analyses that will follow.

CHAPTER II

THE MOLES THEY ARE A-CHANGIN'

The Talpidae Morphological Variation

The study of shape

The geometric properties of a configuration of points that are invariant to changes in translation, rotation, and scale. In morphometrics, we represent the shape of an object by a point in a space of shape variables, which are measurements of a geometric object that are unchanged under similarity transformations. For data that are configurations of landmarks, there is also a representation of shapes per se, without any nuisance parameters (position, rotation, scale), as single points in a space, Kendall's shape space, with a geometry given by Procrustes distance. Other sorts of shapes (e.g., those of outlines, surfaces, or functions) correspond to quite different statistical spaces.

The analysis of shape is important for understanding patterns of morphological evolution. Variation in shape across groups such as clades or species may result from several different factors such as response to selective pressures, different functionalities, changes in developmental processes and even disease or injury (e.g. Zelditch et al., 2004). Differences in shape may also signal differences in processes of growth and morphogenesis. Shape has long been used to describe and classify taxa and often provides useful characters for phylogenetic studies. Improved understanding of shape variation may help to resolve taxonomic problems and may provide a method for finding new phylogenetic characters (see MacLeod, 2002). Studies of shape variation may also reveal the effect of ecological factors or developmental processes that override phylogenetic signal and how such demands limit or direct evolutionary change (e.g. Björklund and Merilä, 1993; Schluter, 1996; Klingenberg, 2005). Sometimes, differences in shape are adequately summarized by comparing the observed shapes to more familiar objects such as circles, kidneys or letters of the alphabet (or even, in the case of the Lower Peninsula of Michigan, a mitten). Organisms, or their parts, are then characterized as being more or less circular, reniform, C-shaped or mittenlike. Such comparisons can be extremely valuable because they help us to visualize unfamiliar organisms or to focus attention on biologically meaningful components of shape. However, they can also be vague, inaccurate or even misleading, especially when the shapes are complex and do not closely resemble familiar icons. Even under the best of circumstances, we still cannot say precisely how much more circular, reniform, or C-shaped or mitten-like one shape is than another. When we need that precision, we turn to measurement.

Morphometrics is a quantitative way of addressing the shape comparisons that have always interested paleontologists and biologists. This may not seem to be the case, because the morphological approaches once typical of the quantitative literature seem very different from the qualitative descriptions of morphology; whereas the qualitative studies produce pictures or detailed descriptions (in which analogies figure prominently), morphometric studies usually produced tables with disembodied lists of numbers. Those numbers seemed so highly abstract that we could not readily visualize them as descriptors of shape differences, and the language of morphometrics also seemed highly abstract and mathematical. As a result, morphometrics seemed closer to statistics or algebra than to morphology. In one sense that perception is entirely accurate: morphometrics is a branch of mathematical shape analysis. The way that we extract information from morphometric data involves mathematical operations rather than concepts rooted in biological intuition or classical morphology. Indeed, the pioneering work in modern geometric morphometrics had nothing at all to do with organismal morphology; the goal was to answer a question about the alignment of megalithic "standing stones" like Stonehenge (Kendall and Kendall, 1980). Nevertheless, morphometrics can be as much a branch of morphology as it is a branch of statistics. It is that when the tools of shape analysis are turned to organismal shapes, illustrating and even explaining shape differences that have been mathematically analyzed. The tools of geometric shape analysis have a tremendous advantage when it comes to these purposes: not only because it offers precise and accurate description, but also because it enables rigorous statistical analyses and serves the important purposes of visualization, interpretation and communication of results. Geometric morphometrics allows us to visualize differences among complex shapes with nearly the same facility as we can visualize differences among circles, kidneys and letters of the alphabet (Zelditch et al., 2004; Zelditch et al., 2012).

Scientific protocols

Here we will describe the general protocols we used to investigate the shape and size variation and their evolution as well. The analyses described below will be the same for all the samples under study. Though, where different methodologies were used in order to answer to particular issues (i.e. Chapter 3 and 6), they will be described in detail in their specific sections.

Geometric Morphometrics protocol

Shape and size analysis

All the specimens have been photographed in their informative views at a distance of 50 cm with a Nikon D100 camera with a Micro-Nikkor 105mm lens. We digitized landmarks and semi-landmarks using the tpsDig2 software (Rohlf, 2006). Semi-landmarks are a useful tool to capture the morphology of complex outlines due to the lack of homologous anatomical points. They assume that curves or contours are homologous among specimens (Adams et al., 2004; Perez et al., 2006). Thus, semi-landmarks are useful to depict the shape of curved lines where landmarks cannot be detected. Successively, a Generalized Procrustes Analysis (GPA; Bookstein, 1991; Goodall, 1991) implemented in the procSym() function from R-package "Morpho" (Schlager, 2014) was used to rotate, translate and scale landmark configurations to the unit centroid size (CS = the square root of the sum of squared distances of a set of landmarks from their centroid; Bookstein, 1986). Rotation of the scaled and translated landmark sets starts by comparison with a reference configuration (usually the first specimen in the dataset). Once the first rotation is completed, a mean shape is calculated and the rotation process is repeated using the mean shape as the reference configuration for the sample (including the reference-specimen configuration). This meanshape/rotation procedure is iterated to minimize rotation differences between subsequent iterations through a least-square procedure (Rohlf and Slice, 1990). The residual differences correspond to real shape differences plus measurement error. In order to visualize the ordination of the aligned specimens we performed a between group PCA (bgPCA), using the function groupPCA() included in the R-package "Morpho". The bgPCA provides a projection of the data onto the principal components of the group means, leading to an ordination of the shape variables between the group means. The new axes are orthogonal and can be computed even when data are not of full rank, such as for Procrustes shape coordinates (Mitteroecker and Bookstein, 2011). This method offers a good performance when the number of observations is smaller than the number of variables (Boulesteix, 2005), which is often the case for geometric morphometrics analyses. The significance of the observed shape differences among species was evaluated by performing a permutational multivariate analysis of variance (perMANOVA) on Procrustes coordinates using adonis() function included in the "vegan" R package (Oksanen, 2013). The significance of shape differences between species was then evaluated performing a pairwise permuted MANOVA using the pwpermanovac() wrapper function, available in supplementary online materials. Size variation was visualized using a boxplot. The significance of size differences has been evaluated by performing a permutational univariate analysis of variance (perANOVA) on CS using the function adonis(). Between species size differences were evaluated performing a pairwise permuted ANOVA using the wrapper function pwperanovac(), available in supplementary online materials. All *p*-values were corrected using "Holm" correction.

Evolutionary allometry

The relationship between size (independent variable) and shape (dependent variable) was tested performing a multivariate regression of shape on size values averaged by species. All individuals analyzed in the present were adult or subadult based on the ossification status of humeral epiphysis and diaphysis. Thus the allometric trajectories of the different clades studied here represent evolutionary allometry. To test for differences in slopes among species we ran a permutational multivariate analysis of covariance (perMANCOVA), using species (clades) as groups and size as covariate, (Zelditch et al., 2004, 2012). This analysis was performed using the function adonis(). If slopes do not differ significantly (in this case the species and size interaction of the MANCOVA is not statistically significant) it is possible to control for the allometric effect and compute size-corrected shape variables (Viscosi and Cardini, 2011; Viscosi et al., 2012; Zelditch et al., 2012). Just for the sake of visualization we performed a canonical correlation analysis (CCA), which determines an Y axis that represents the amount of Y (shape variables) that is best explained by the independent variable X (CS). As we were interested in studying interspecific (inter-clade) shape differences too, we removed the intraspecific (intra-clade) variation by performing separate per-species multivariate regressions between shape and size.

The comparative methods protocol

Phylogenetic signal

The phylogenetic signal can be described as the degree to which taxa's phylogenetic relationships are correlated with their similarities in some traits of a phenotype (Blomberg et al., 2003; Klingenberg and Gidaszewski, 2010, among others). A significant phylogenetic signal is present when closely related taxa are more similar than distantly related ones. Moreover, phylogenetic signal expresses the degree of evolutionary gradualism and expresses whether niche divergence increases gradually over time or whether niches diverge punctually, that is, independently of time (Pearman et al., 2014). These two properties can be quantified with the Pagel metrics lambda and kappa (Pagel, 1997; Pagel, 1999), which provide insightful descriptions of phylogenetic patterns of species niches.

In order to test the presence of a phylogenetic signal in multivariate shape data, Procrustes (Euclidean) distance matrix of shape data were correlated with the patristic distance matrix computed on the phylogeny by means of Mantel test (using mantel.test function available in R package ape). We performed the Mantel test also on the CS. Moreover, we performed a multivariate test on the overall shape using the permutational test (Klingenberg and Gidaszewski, 2010) implemented in the physignal() function from "geomorph" R package (Adams and Otarola-Castillo, 2013) using the multivariate K-statistic (Kmult, Adams, 2014). This value evaluates the degree of phylogenetic signal in a dataset relative to what is expected under a Brownian motion model of evolution. For geometric morphometric data, the approach is a mathematical generalization of the Kappa statistic (Blomberg et al., 2003) appropriate for highly multivariate data (see Adams, 2014).

To further investigate the phylogentic signal in each principal component extracted from shape variables (PC axes explaining up to the 90% of the total variance) as well as in centroid size we used the phylosig() function implemented in the "phytools" R package (Revell, 2013) using Lambda and Kappa statistics. To visualize the evolution of the humeral size (averaged CS) and shape variable (PC scores on averaged procrustes coordinates) over a known phylogenetic tree we used the function contMap() from the "phytools" package (Revell, 2012). This function uses an ancestral character estimation to visualize historical character states for a continuous trait along the branches of a tree.

Phylogenetic non-independence

Closely related species tend to be more similar to each other than to more distantly related taxa (Garland and Ives, 2000) and therefore species means cannot be treated as independent units of information (Harvey and Pagel 1999). We performed phylogenetic ANOVA and MANOVA on the averaged per-species shape and size variables. These analyses were performed both in their standard versions and in their comparative version (using phy.anova() and phy.manova() function implemented in GEIGER package, Harmon et al., 2014). They allowed to evaluate if differences in shape or performance were statistically supported even taking into account the phenotypic channelling due to shared ancestry.

We used the Phylogenetic Generalized Least Squares linear model (Garland and Ives 2000; Rohlf, 2001; Zelditch et al., 2012), which accounts for the increases in co-variation of continuous traits between taxa that share phylogenetic history.

Evolutionary rates

We evaluated, starting from the time-claibrated phylogenetic tree, used for comparative analyses, the evolutionary rates in different clades, for both size and shape variables. We tested their potential significant differences across different clades using the function compare.evol.tates() of R package “Geomorph” (Adams, 2014). Moreover we looked for shifts of rates in the phylogeny using the trait MEDUSA approach (Thomas and Freckleton, 2012). This method allows appreciating where accelerations or slowdowns occur within the phylogeny. We achived this using the transformPhylo.ML2() of R package "MOTMOT" (Thomas and Freckleton, 2012).

Morphological and size disparity

Phenotypic disparity was studied by performing a Levene's test on the CS variable. The morphospace occupation analysis on shape variables was performed using the betadisper() function of R package "vegan" (Oksanen et al., 2008). Following Harmon et al. (2003), we also calculated mean subclade disparity through time for body size. We compared observed body size disparity across our tree with that expected under a pure Brownian process by simulating body size evolution 10 000 times across our tree usoing the dtt() function (Harmon et al., 2014). The mean clade disparity values for the observed and simulated data were plotted against node age and the morphological disparity index (MDI) calculated. MDI quantifies the overall difference in relative disparity of a clade compared with the expectation under the null Brownian motion model (Harmon et al. 2003). Negative MDI values indicate lower clade disparity than expected under Brownian motion and are a common property of adaptively radiating clades. Positive MDI values indicate higher clade disparity than expected under Brownian motion and indicate an overall tendency toward punctualism and a trait evolution that could be rapid and independent from time. To test whether Talpidae shape and size evolution has slowed or accelerated through time, we used the node-height test (Freckleton and Harvey 2006). We computed the absolute value of standardized independent contrasts (Felsenstein, 1985) for shape and size on our tree and correlated them with the height of the node at which they are generated. Because independent contrasts are Brownian rate parameters for the branches over which they are calculated (McPeek, 1995), a significant negative relationship between node age and absolute contrast value would indicate that rates of shape and size evolution have slowed through time, consistent with the "niche-filling" theory (Freckleton and Harvey 2006). While a positive correlation would indicate that the evolution have accelerated, consistent with punctualism (Slater et al., 2010a; Slater and Pennell, 2014).

Surface analysis

We used the "SURFACE" method to identify convergent evolution without the a priori designation of ecomorphs or selective regimes locations (Ingram and Mhaler, 2013). The method takes as input only a phylogenetic tree and continuous trait data, and fits a series of Ornstein Uhlenbeck (OU, evolution with a single attractor; Felsenstein, 1988; Hansen, 1997; Butler and King, 2004) models to identify cases where multiple lineages have discovered the same selective regimes. "SURFACE" consists of a 'forward' stepwise phase in which selective regimes are added to the tree, followed by a 'backward' phase that identifies cases where the same regime is reached by multiple lineages This results in an estimate of the macroevolutionary adaptive landscape that includes measures of the extent of phenotypic convergence.

THE MOLES DENTARY

Introduction

The mammalian mandible is a complex morphological structure that consists of two symmetrical dentary bones. Several studies of mandibular morphological variation have been performed (e.g. Atchley et al., 1992; Atchley, 1993; Cheverud, 1996; Humphrey et al., 1999; Duarte et al., 2000; Badyaev and Foresman, 2004; Hylander, 2005; Monteiro et al., 2005; Rees, 2005). Examination of rodents has revealed parts of the dentary that are more or less variable than others, but these findings are based on relative landmark positions for the whole dentary (Klingenberg et al., 2003; Monteiro and dos Reis, 2005).

The dentary can be divided into different regions (Fig. 2.1).

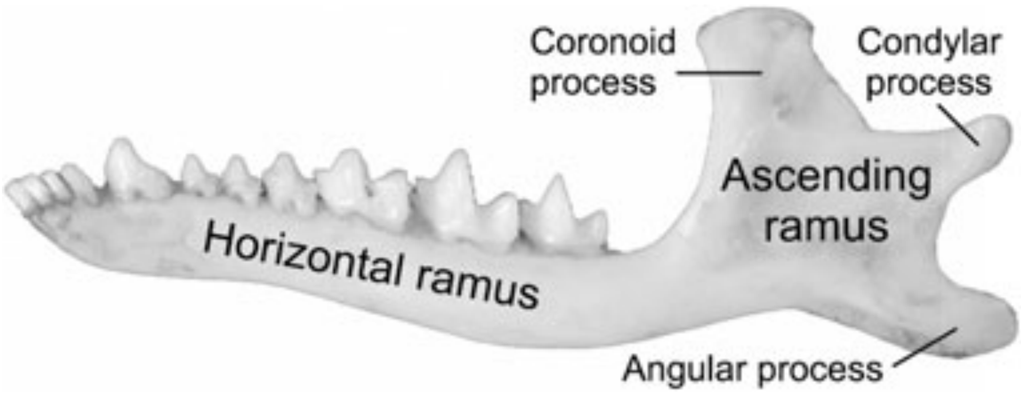

Figure 2.1. Region of the mammalian (Talpidae) dentary.

The horizontal ramus supports the teeth and the ascending ramus provides attachment sites for several masticatory muscles (Hildebrand, 1982). The ascending ramus consists of three processes. The temporalis muscle inserts onto the coronoid process and the masseter and medial pterygoid muscles onto the angular process. The condylar process provides an attachment site for the lateral pterygoid muscle as well as articulation with the cranium. These regions also correspond to the morphogenetic components described by Atchley and Hall (1991). Variation in dentary form arises from changes in the development of its components, and variability in the patterns of integration between those components into a functioning complex structure (Atchley, 1993). Development of the ascending ramus is governed by the density of mesenchymal condensations (from the neural crest cells in embryonic stages of development, see Atchley et al., 1992) followed by development of the associated muscles, whereas the horizontal ramus is mostly dependent on tooth development (Cheverud, 1996). The adult form of the mandible results from interactions between these functional and developmental processes. However, the extent to which these factors interact may vary. For example, the effect of a particular muscle on the ascending ramus only determines the form of the individual process to which the muscle attaches (Hall, 2003). Nevertheless, the structure as a whole must be able to perform effectively and at some level these processes must be integrated (Barrow and Macleod, 2008). Allometric effects, as well as external factors (e.g. diet and food acquisition), will also contribute towards functional needs. The evolutionary history of a group represents a combination of these functional–developmental factors and factors imposed by the group's ancestry.

Moles are a diverse group with complex phylogenetic history. Here we consider the question of whether shape variation occurs to different extents in the mole dentary, in order to discriminate whether shape and size have been influenced by phylogenetic factors and whether other factors (e.g. functional and size differences) may be predominant. We will also examine questions related to the existence and extent of intraclade functional convergence and/or phylogenetic unity within the overall dentary structure.

Material and methods

Specimens collection

We analyzed a total of 306 mandibles belonging to 36 species (see Supplemetary Appendix 1 to Chapter 2 for specimens list and localities). Our sample accounts for the entire variability of the extant Talpidae, as we have representatives from all the 17 genera reported as valid (Hutterer, 2005). Unfortunately, with the exception of *Proscapanus sansaniensis*, we did not have the possibility to include fossil specimens in the sample. The moles mandible is a very brittle skeletal element and, when found in fossil assemblages, it inevitably presents fractures in the distal part of the horizontal ramus and in the ascending ramus.

Geometric Morphometrics

The mandibles have been photographed in labial view. We digitized 12 landmarks and 26 semi-landmarks on the mandible (Figure 2.2).

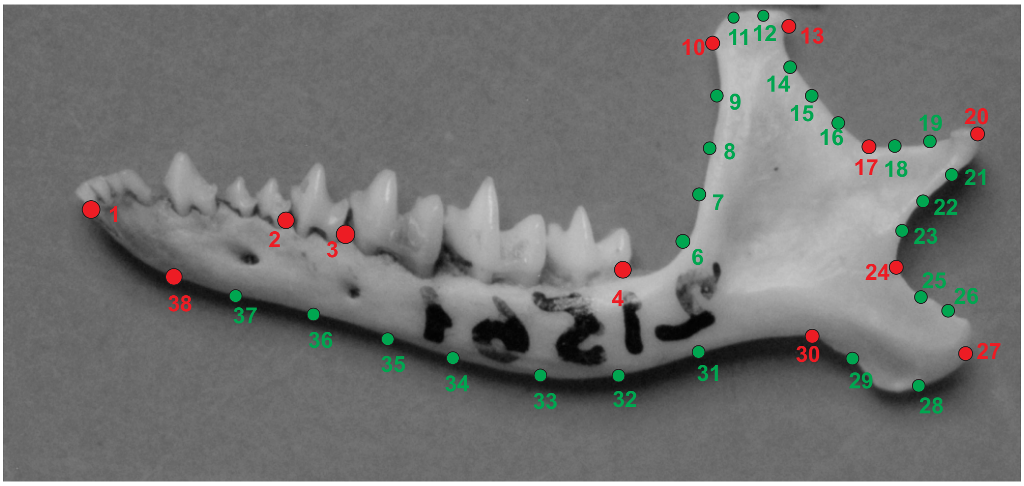

Figure 2.2. Landmarks (red points) and semi-landmarks (green points) digitized on the mandible. 1) Anterior tip; 2) anterior and of p4; 3) anterior end of m1; 4) posterior end of m3; 5-7) anterior profile of the coronoid process; 10-13) profile of the condyle of coronoid process; 14-17) posterior profile of the coronoid process; 18-24) condylar process; 25-30) profile of the angular process; 31-38) profile of the orizontal ramus.

Results

Shape and size analyses

The bgPCA performed on the per-species averaged aligned procrustes coordinates (Figures 2.3A and 2.3B) show a good degree of separation between the fully fossorial clades and the non-fossorial clades. In particular along the PC1 (51.22% of the total variance) Condylurini, Talpini and Scalopini (negative values) are well separated from Urotrichini, Uropsilini, Neurotrichini and Desmaninae (positive values). At negative values of the PC1 the mandible shows a reduced coronoid process, an enlarged condylar process, an angular process that is shifted in a parallel position in respect to the horizontal ramus and a slender tip of the mandible. At positive values of the PC1 we observe an expanded coronoid process, a reduced condylar process and the angular is placed on the same line of the horizontal ramus, the last is thickened in correspondence of the antemolar teeth row. Along the PC2 (14.47% of the total variance) the separation between the Condylurini (positive values) and all other clades (negative values) it is clearly evident. At positive values the mandible shows a more slender horizontal ramus, a thin coronoid process, a hooked and enlarged condylar process and a very thin angular process. At negative values the mandibular shape shows a broad coronoid process, a straight shaped condylar process and a broad angular process. Along the PC3 (10.5% of the total variance) all the clades are well superimposed it is possible to separate only the Condylurini at positive values. The shape changes associated with the PC3 separates Condylurini by almost the same features described along the PC2.

PerMANOVA returned an highly significant difference (p-value < 0.001) between clades. Significant size (averaged per-species CS) variations (perANOVA p-value < 0.001) have been found between clades. The pairwise perMANOVA, performed on the per-species averaged shape variables, revealed no significant differences between

Condylurini and the other clade, but returned significant difference between Talpini and Scalopini (see Table 2.1). The boxplot computed for the CS (Figure 2.4) showed the Desmaninae, Scalopini and Talpini having the largest size, while Neurotrichini, Urotrichini and Uropsilini are the smallest. Pairwise perANOVA (Table 2.2) returned significant results between Talpini and Uropsilini, between Scalopini and Uropsilini and between Talpini and Desmaninae.

	Uropsilinae	Desmaninae	Urotrichini	Neurotrichini	Condylurini	Scalopini	Talpini
Uropsilinae	NA	0.0589	0.0729	0.220	0.202	0.0019	0.0009
Desmaninae	NA	NA	0.3246	0.323	0.341	0.0259	0.0019
Urotrichini	NA	NA	NA	0.674	0.307	0.0329	0.0039
Neurotrichini	NA	NA	NA	NA	NA	0.2557	0.0579
Condylurini	NA	NA	NA	NA	NA	0.1238	0.0589
Scalopini	NA	NA	NA	NA	NA	NA	0.0009
Talpini	NA	NA	NA	NA	NA	NA	NA

Table 2.1. Results of pairwise perMANOVA test.

	Uropsilinae	Desmaninae	Urotrichini	Neurotrichini	Condylurini	Scalopini	Talpini
Uropsilinae	NA	0.0609	0.1518	0.2117	0.222	0.0053	0.0009
Desmaninae	NA	NA	0.3366	0.6693	0.652	0.1263	0.0289
Urotrichini	NA	NA	NA	1	0.307	0.0469	0.0109
Neurotrichini	NA	NA	NA	NA	NA	0.2577	0.1028
Condylurini	NA	NA	NA	NA	NA	0.3896	0.4635
Scalopini	NA	NA	NA	NA	NA	NA	0.2557
Talpini	NA	NA	NA	NA	NA	NA	NA

Table 2.2. Results of the paiwise perANOVA test.

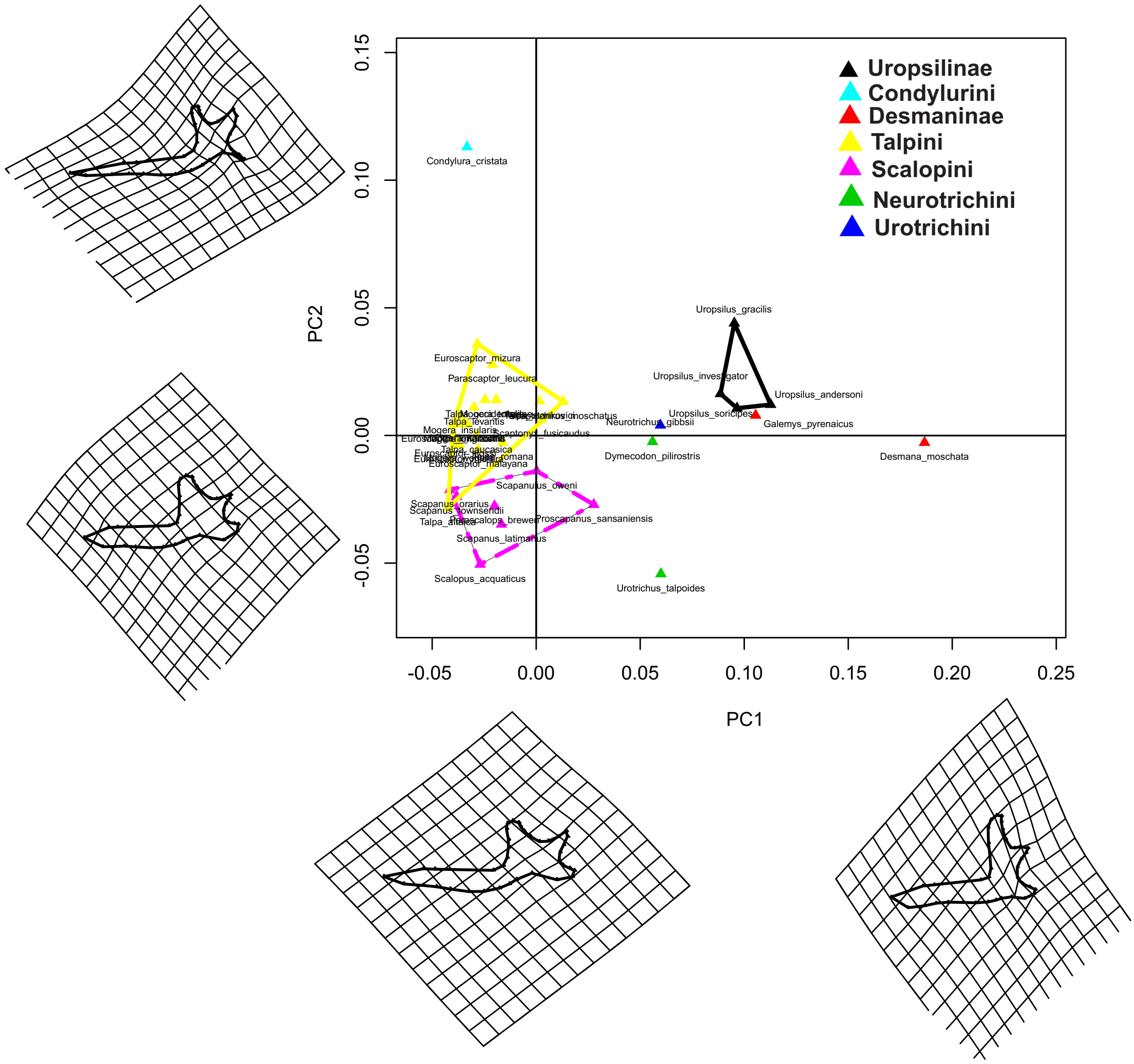

Figure 2.3A. Scatterplot of the first two axes of the PCA. Deformation grids refer to axes extremes (positive and negative values).

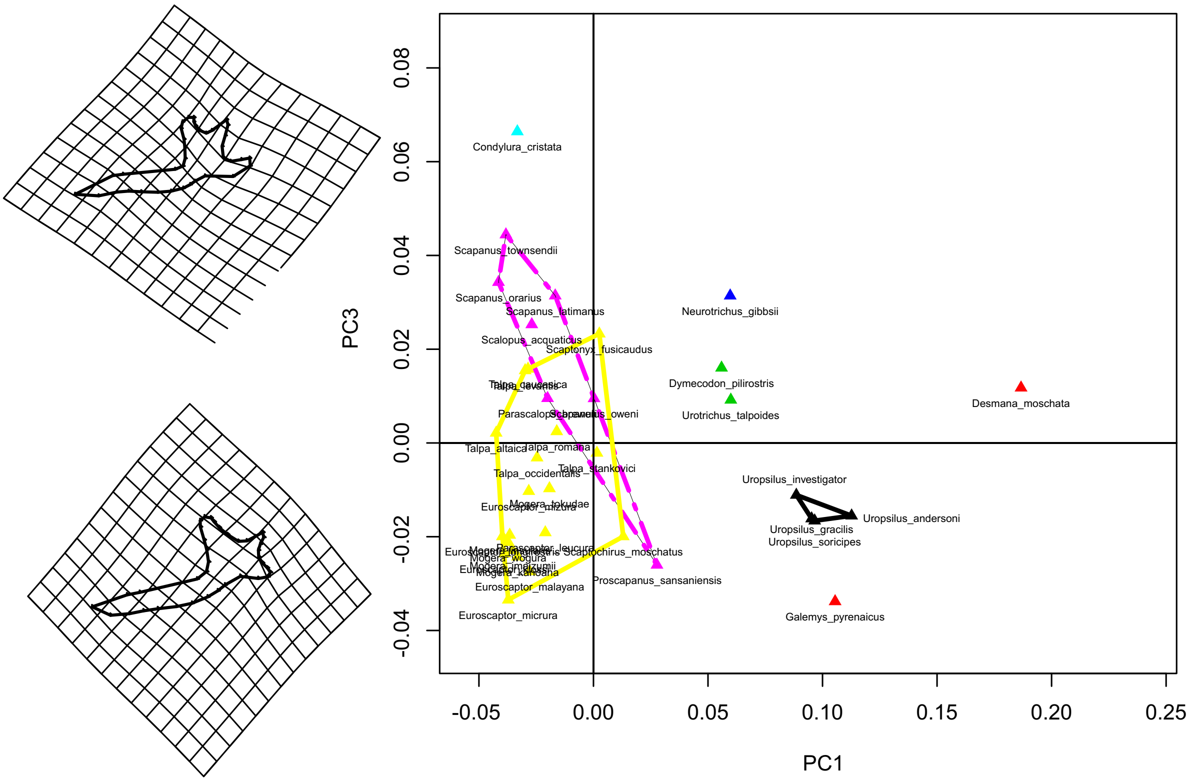

Figure 2.3B. Scatterplot of the first and third axes of PCA. Deformation grids refer to axes extremes (positive and negative values).

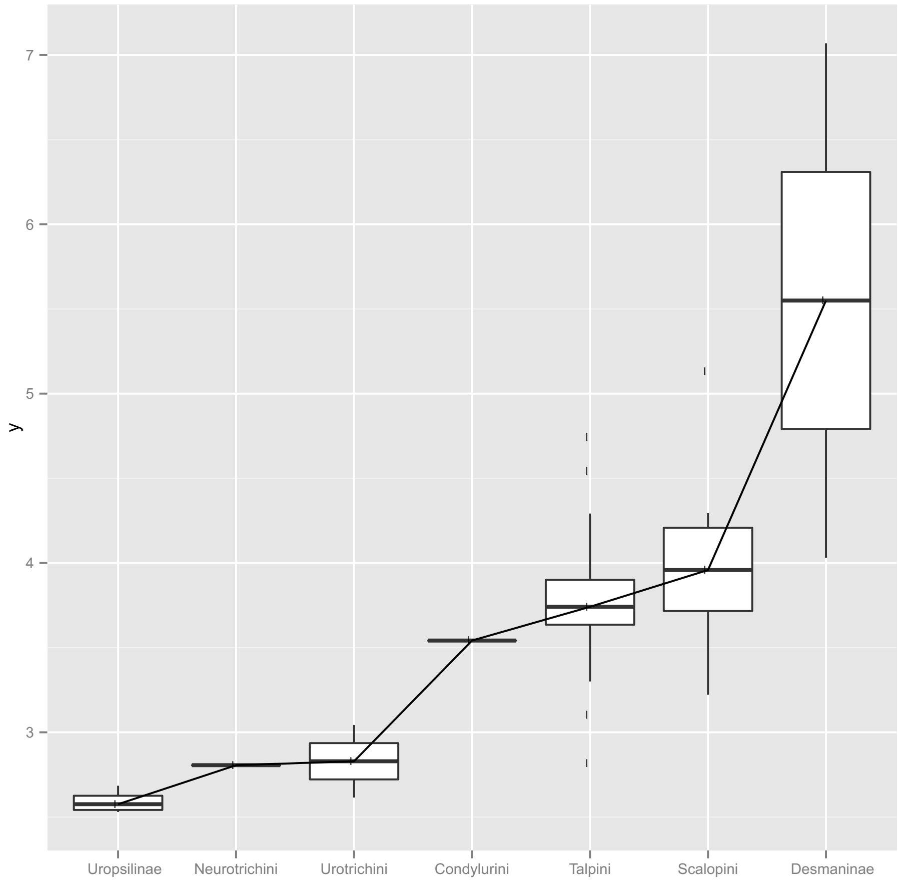

Figure 2.4. Boxplot of the centroid sizes. Bottom and top of the boxes are the first and third quartiles, the horizontal solid black lines represent the median, the whiskers represent the minimum and maximum values.

Allometry

Multivariate regression of per-species shape averaged variables on per-species averaged CS returned a non significant result (p-value = 0.11). Separate per-clade multivariate regressions returned non-significant results for all clades.

Inclusion of phylogeny

Phylogenetic signal

The Mantel test, performed on the shape and size variables, returned highly significant results (p-value = 0.001 and p-value < 0.001). The analysis of single components of the shape variation revealed the presence of a phylogenetic structure in the first eight PCs (accounting for more than 95% of the total variance) with the exception of the sixth and the seventh. The phylosig function returned a highly significant result also for CS (p-value = 0.002, K = 0.28).

The function physignal() returned a significant result for the shape variables (p-value = 0.004; K value = 0.54). Figure 2.5A shows the ancestral character estimation for size along the phylogenetic tree, with phylogenetically nearest species having similar CS values. Figure 2.5B shows the ancestral character estimation for the shape vaiables along the phylogenetic tree, with the phylogenetically related species having similar shapes.

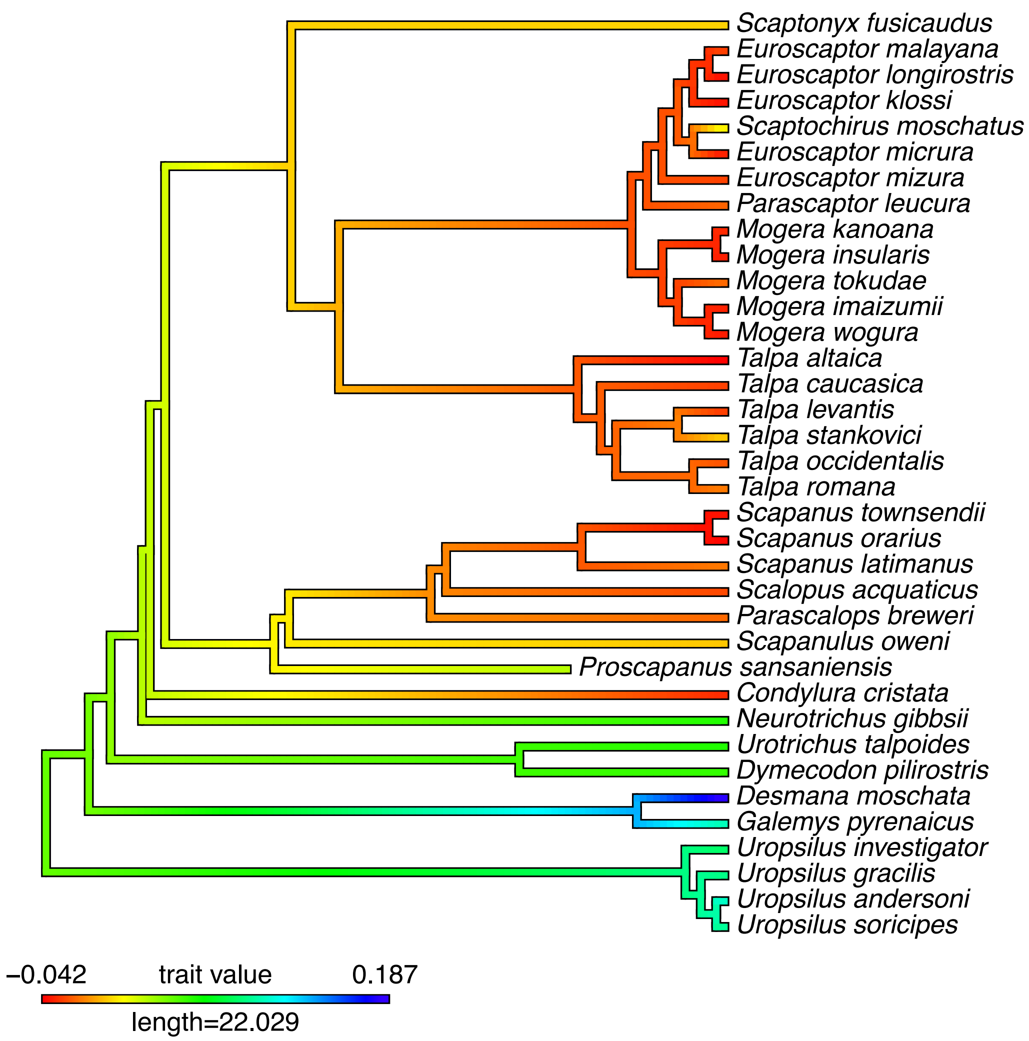

Figure 2.5A. Plot of the PC1 trait on the phylogeny.

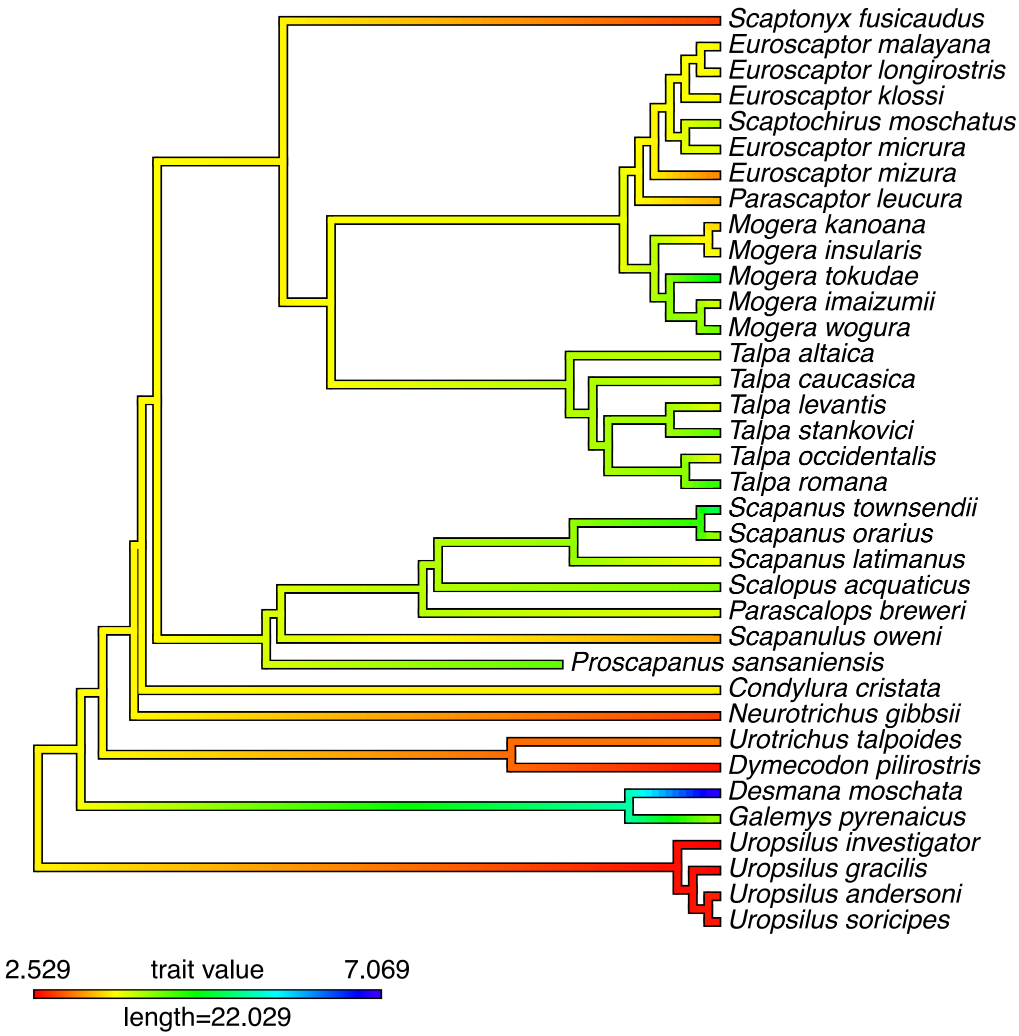

Figure 2.5B. Plot of the CS trait mapped on the phylogeny.

Phylogenetic non-independence

Phylogenetic MANOVA computed on the shape variables returned a significant result (p-value = 0.014), while phylogenetic ANOVA computed on the CS rerevealed a non-significant result (p-value = 0.53). The PGLS returned a significant interaction between the shape variables and the CS when taking the phylogeny into account (p-value <0.001).

Evolutionary rates

We found that the rate of the mandible morphology evolution in Talpidae was different from Brownian motion (p-value < 0.001). The evolutionary rates were significantly different between clades (p-value = 0.001). Desmanini and Uropsilini possess higher ML rates (6.3 and 1.8 respectively), while Scalopini, Urotrichini and Talpini have similar lower rate. The evolutionary rates were different between clades (p-value = 0.001). We found positive shifts in correspondence of Desmaninae and of *Scaptochirus moschatus*, while we found a neat negative shift in correspondence of *Uropsilus* spp. (figure 2.6). When performing the same analyses on CS we found that the presence of the large sized *Desmana moschata* significantly influenced the rates values. In fact we found an evident positive shift in correspondence of the Russian desman (ML rate = 206.4).

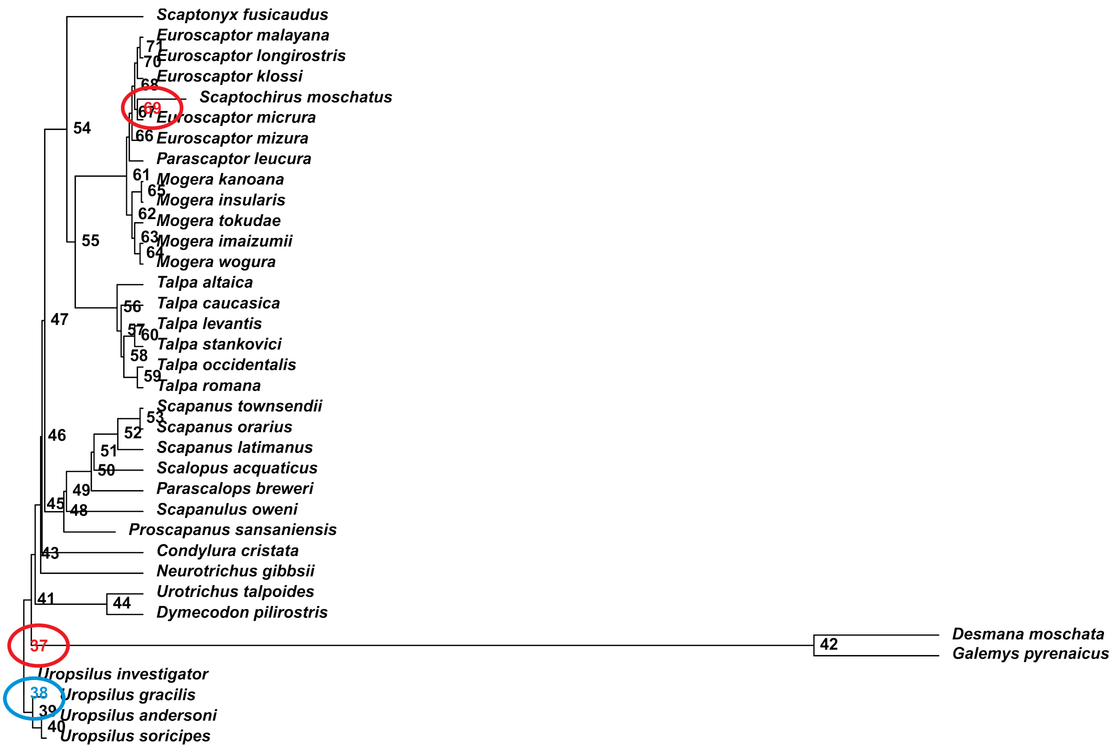

Figure 2.6. Plot of the multivariate shift found for the evolutionary the shape variables. Red circles represent the positive shifts; cyan circle indicate the negative shift.

Morphological and size disparity

The betadisper analysis returned a non significant result (*p*-value = 0.11) when computed for the shape variables, Desmaninae have the highest average distance to median, while Uropsilini have the lowest. The CS disparity resulted to be significant as revealed by the Levene's test (*p*-value = 0.005), with Urotrichini having the highest average distance to mean. The morphological disparity through time was higher than expected under Brownian motion. In fact the dtt() function (figure 2.7A) returned a positive MDI (MDI = 0.13). The dtt() function returned a positive MDI (MDI = 1.02) also for the CS, again suggesting a deviation from a constant pace of evolution (figure 2.7B). The node-height test returned non significant results for the first 3 PCs (*p*-values = 0.82; 0.6; 0.85, respectively). The node-height test performed on the CS returned again a non significant result (*p*-value = 0.22).

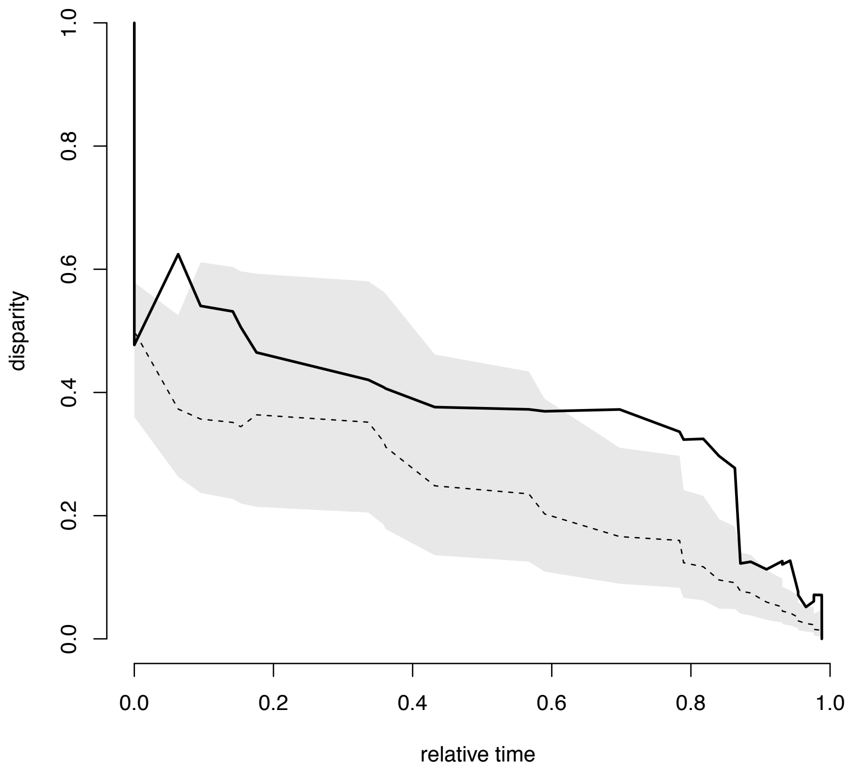

Figure 2.7A. Plot of the dtt() function performed on the shape variables. The solid line represent the empirical data, the dotted line represent the simulated data under Brownian motion.

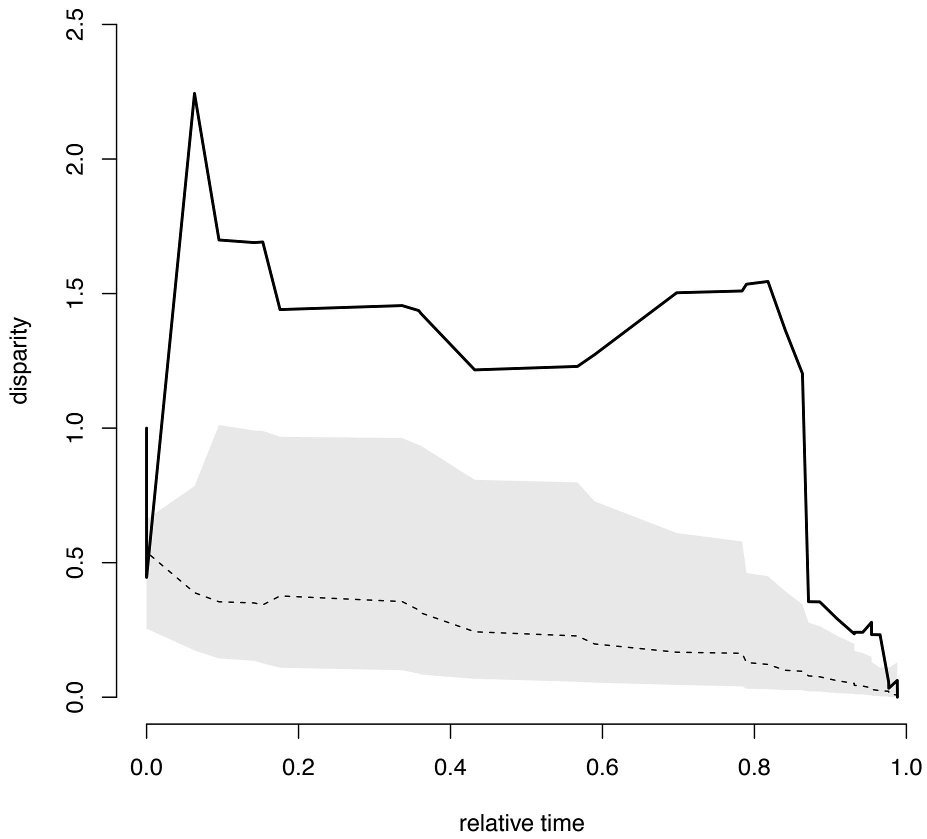

Figure 2.7B. Plot of the dtt() function performed on the CS. The solid line represent the empirical data, the dotted line represent the simulated data under Brownian motion.

"Surface" analysis, search for no a priori local optima

The surface analysis revealed that no convergence occurred in the talpids mandible shape. While we found convergence in *Desmana moschata* and *Scapanus townsendii* mandible size. We found the presence of 7 shifts under OU model for the shape variables, while we found 3 shifts under OU model for the CS.

Discussion

The continuous mandible shape variation evidenced a neat separation between the highly fossorial clade and the non-fossorial ones (see figure 2.3A). Talpini, Scalopini and Condylurini have a slender antemolar region of the horizontal ramus when compared with desmans and shrew-moles. Shape of the horizontal ramus is mostly affected by tooth development (Cheverud, 1996). There are also important distinctions in the antemolar formulae among talpids (Ziegler, 1971) and differences, such as the number of antemolar teeth or their relative sizes, appear to determine the depth and curvature of the horizontal ramus (Barrow and Macleod, 2008). Dentition differences coincide with horizontal ramus shapes found among genera in this study. In *Desmana* and *Galemys* the first two incisor teeth are large (particularly the second incisor) relative to the rest of the antemolar dentition and the anterior region of the horizontal ramus is deep. Similarly, *Urotrichus* and *Dymecodon* have an enlarged second incisor (the first is missing in this genus; Ziegler, 1971) and a corresponding deep anterior region of the horizontal ramus. In *Uropsilus* spp. the number of antemolar teeth is also reduced and the molars occupy the majority of the space along the horizontal ramus. Talpini are all characterized by an enlarged first premolar tooth and small incisor and canine teeth, unlike Scalopini. *Scapanus* and *Parascalops*, within the Scalopini, have largely unspecialized and uniform antemolar dentition. These differences appear to be correlated with the shape of the anterior region of the horizontal ramus. The reduced number of antemolar teeth and enlarged second incisor in *Scalopus* distinguish it from the other two Scalopini genera. We moreover found that *Neurotrichus* horizontal ramus shape was more similar to *Dymecodon* than to Scalopini as pointed out by Barrow and Macleod (2008). Differences in the ascending ramus were mostly related to the coronoid process. We found that highly fossorial moles were characterized by a reduced coronoid process, while it was higher and expanded in non-fossorial clades. In particular *Desmana moschata* was found at extreme positive values of PC1 having a very high coronoid process, while *Galemys* closely resemble *Uropsilus* spp. The coronoid process plays a more dominant functional role in the mole dentary than in the rodent dentary (Barrow and Macleod, 2008). Among moles, movements are mostly governed by the temporalis muscle pulling on the relatively large coronoid process. Desmans are a clearly monophyletic group (Crumpton and Thompson, 2013), nevertheless, differences among their dentaries were found and may result from a number of factors during a separate evolutionary history of several million years. Although size variation was excluded from this analysis, *Desmana* is clearly larger than *Galemys*. Size could be constraining some aspects of the desman dentary.

Along the PC2 and PC3 it was striking the separation of *Condylura cristata* from all other taxa. *Condylura*, the star-nosed mole, differs from other moles in that it has 22 fleshy appendages on its muzzle used for navigation and food location (Catania, 2002). A unique shape also characterizes its dentary, which is more elongated and slender than those of other talpids, moreover its premolar row is gapped (Sanchez-Villagra et al., 2006). The foraging apparatus is thought to have been maximized for exploiting large quantities of small prey at high speed (Catania and Remple, 2005). It appears that development of a unique nasomaxillary articulation and nasolabial musculature associated with the starry-nose relates to the evolution of the long proboscis. This has shifted the plane of the anterior teeth, lengthened the mandibular ramus and weakened the masticatory mechanism (including a reduced size of the temporalis and masseter muscles) compared with other talpids (Grand et al., 1998).

Correspondingly, our results show that the *Condylura* dentary also displays unique shapes for each part of the dentary.

We found a strong phylogenetic structure in both shape and size variables. When we mapped the two phenotypes on the phylogeny we found that closely related species were also very similar in both traits. Phylogenetic ANOVA revealed as the size differences were related to phylogeny (non-significant result). We did not found a significant interaction between size and shape, nevertheless we found a significant correlation when taking into account phylogeny, revealing the presence of an evolutionary allometry between clades. It is possible that shared ancestry influenced the size-shape relationship differently than ecological factors.

We found a neat acceleration in the mandible shape evolutionary rates in correspondence of desman and of *Scaptochirus moschatus*, while we found a slowdown in correspondence of Uropsilinae. Uropsilinae are the most basal subfamily; in this framework we suggest that the dentary shape of *Uropsilus* spp. did not changed substantially through time (Sanchez-Villagra et al., 2006), and reached a functional optimum early in their evolution. Desmans are semiacquatic mammals, we hypothesize that the higher morphological evolutionary rates could be related with the different feeding adaptation in the acquatic environment. Russian desmans are reported to have seasonal preference in preys, and fishes are also often found in stomach contents, while acquatic invertebrates are abundant as well as molluscs (Borodin, 1962; Oparina et al., 2013). Desmaninae are also more disperse in the morphorspace, when compared with other taxa, as evidenced by the betadisper analysis.

The morphological disparity through time was found to be slighty higher than that expected under Brownian motion model (figure 2.7A), suggesting a deviation from constant evolution. We found a similar pattern for the mandible size, where again Desmaninae proved to have the higher variance. We found no convergence for the shape variables, while the "SURFACE" analysis evidenced as only *Desmana moschata* and *Scapanus townsendii* were convergent in size. The mandible morphology discriminate all clades and Geometric Morphometrics revealed pattern of variation according with previous analysis (Barrow and Macleod, 2008). Our results showed that morphological variation occurs to different extents in individual parts of the dentary. The condylar process shape showed least variation between clades, the coronoid process shapes showed greatest variation between highly fossorial moles and non-fossorial moles, as well as the horizontal ramus.

In conclusion the dentary shape was mainly influenced by phylogeny and mandible proved to be a conservative skeletal element. Major modifications could be related with the evolution of fossoriality in highly fossorial taxa and to the particular feeding habits of desman.

Further investigation should be aimed to testing the integration and modularity between the different regions of the dentary (here investigated as a whole).

THE MOLES LOWER M1

Introduction

Butler (1961) revolutionized our understanding of how mammalian molar teeth evolve, stressing that functional integration between occluding teeth channels evolutionary change. Cusps, cingulae, and basins of tribosphenic molars interlock in a complicated, threedimensional manner related to masticatory trajectories. Each upper molar has three major cusps: paracone, protocone, and metacone that fit into spaces among the five major cusps of the lower molars paraconid, protoconid, metaconid, entoconid, and hypoconid. As teeth come into contact during mastication, the mandible moves up and medially, sliding occlusal facets of the lower cheek teeth against corresponding facets on the uppers until the teeth reach the centric position. As the cycle continues, the mandible moves medially and downwards, sliding a second set of facets against one another (Crompton and Hiiemae, 1970; Kay and Hiiemae, 1974). Each set has, coarsely speaking, its own common direction of orientation parallel to mandibular movement during the phase of contact. Each pair of upper and lower facets shares a common plane of orientation with one axis parallel to mandibular movement. This system of facets integrates the cusps, cingulae, and basins so that evolutionary change in any one of the structures of the occlusal region must therefore be accompanied by corresponding changes in functionally adjacent ones.

Butler's functional approach has critically shaped our understanding of the diversification of therian mammals. Experimental studies extended the integration paradigm, providing the basis for dietary and masticatory inferences to be made from the morphological structure of cheek teeth (Mills, 1966; Crompton and Hiiemae, 1970; Rensberger, 1995; Kay and Hiiemae, 1974; Hiiemae, 2000). Phylogenetic studies have used the functional perspective to infer evolutionary transformations in the dentition during early mammalian diversification (Clemens, 1968; Crompton, 1971; Mills, 1971; Seligsohn and Szalay, 1974; Fox, 1975; Clemens and Lillegraven, 1986; Signogneau-Russell and Ensom, 1998; Kielan-Jaworowska et al., 2002). More recently, evolutionary constraints imposed by functional integration have been viewed as important factors for explaining the taxonomic diversity of higher-level clades of mammals (Hunter and Jernvall, 1995; Jernvall et al., 1996; Hunter, 1998; Asher and Sànchez-Villagra, 2005).

Morphological data do sometimes reflect intraspecific variation (Berry, 1977; Patton and Smith, 1989; Martin, 1993; Lister, 1995; Thorpe et al., 1995), although traits that are both phylogenetically informative at the population-level and commonly preserved in the fossil record may be difficult to find. Mammalian molars are good candidates for the role of morphological population markers because they are complex morphological structures that are well represented in the fossil record because of their durability and small size. Molar structure evolves so quickly that even isolated teeth can often be assigned to a particular species. Finally, palaeontologists are often able to recognize the species identity of a mammal from its molar form, which is thought to have a higher genetic component than other skeletal elements because teeth do not remodel after mineralization. For molar shape to be useful for studying Talpidae evolution, several questions must be answered: Can clades, species, or populations of Talpidae being statistically differentiated based on molar shape? Are quantitative differences in mean molar shape and size correlated with phylogenetic divergence? Are evolutionary rates different in different Talpidae clades? Can molar shape analysis allow us to interpret the fossil record of the Talpidae in terms of convergence and parallelism? Are Talpidae molar phenotypes channeled by evolutionary allometry? In this section we will answer to these question by using Geometric morphometrics and comparative methods.

Material and methods

Specimens collection

We analyzed a total of 389 molars belonging to 68 extant and extinct species (see Supplemetary Appendix 2 to Chapter 2 for specimens list and localities). Our sample encompasses the entire talpid variability as it includes representatives from all the Talpidae subfamilies and tribes. We choose to include in our sample only young adult individuals with relatively unworn first lower molar.

Geometric Morphometrics

Molar shape was measured using twelve two-dimensional landmarks from the crown of the first lower molar (Figure 2.8). Only relatively unworn teeth were included because wear can change the apparent shape of the crown. Specimens were oriented in ‘functional view’ with the tooth positioned with its vertical shearing blades parallel to the line of sight and to the angle of mandibular movement during ‘phase one’ occlusion (Butler, 1961). This position was more replicable than others and minimized shape distortion caused by wear. Error in orientation and landmark placement can be significant so each specimen was imaged three times and then averaged (Polly, 2003).

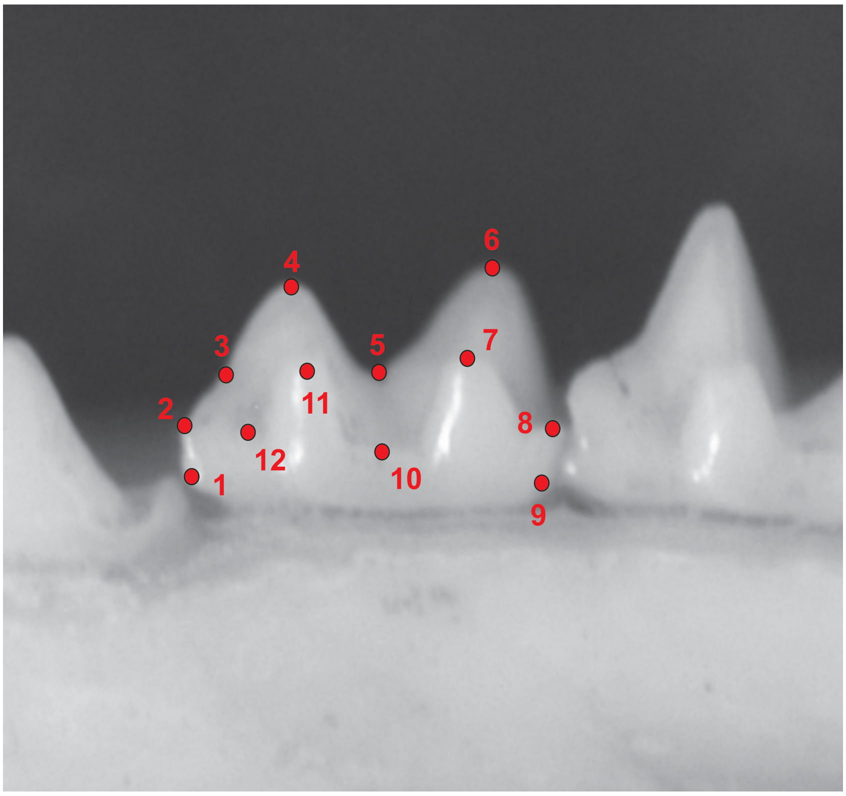

Figure 2.8. Landmarks digitized on the m1. 1) anterior base of the crown; 2) Paraconid; 3) Paracristid notch; 4) Protoconid; 5) cristid oblique notch; 6) Hypoconid; 7) Entoconid; 8) Entostylid; 9) posterior base of the crown; 10) Talonid notch; 11) Metaconid; 12) notch between Metaconid and Paraconid.

Results

Shape analysis

The bgPCA on Procrustes aligned coordinates showed that all the clades have a very similar dispersion in the morphospace (figure 2.9A and 2.9B). Along the PC1 (31.3% of the total variance) it is possible to separate the Scalopini from Uropsilini. It is also worth to note as the Condylurini occupies a separate position in correspondence of negative values of the PC1. At negative values of the PC1 the m1 morphology shows a hypoconid shifted posteriorly, a low protoconid, a shallow paracristid notch, a shallow talonid notch, a low metaconid and an overall larger and lower tooth crown. At positive values the m1 shape shows an anteriorly shifted hypoconid, a high protoconid, a deep paracristid notch, a deep talonid notch, an high metaconid and an overall shorter and higher tooth crown. Along the PC2 (19.3% of the total variance) all the clades have a high degree of overlap. At negative values of the PC2 the m1 shape show a narrow and high hypoconid, an anteriorly shifted entoconid, a shallow talonid notch and a smaller paraconid. At positive values of the PC2 the m1 morphology show a wider and lower hypoconid, a posteriorly shifted Entoconid, a deep talonid notch and a larger paraconid. Along the PC3 (12.03% of the total variance) it is possible to discriminate Condylurini (negative values) from all other clades. At negative values the m1 morphology show an anterior shift of the protoconid, a posterior shift of the entoconid, a shallow talonid notch, a small entostylid and an overall low profile of the lingual cusps. At positive values the m1 shape show a posterior shift of the protoconid, an anterior shift of the entoconid, a deep talonid notch, a large entostylid and an overall higher profile of the lingual cusps.

The perMANOVA returned highly significant results (*p*-value < 0.001) for the shape variables. The pairwise perMANOVA (Table 2.3) evidenced significant differences between Uropsilini, Desmaninae and Scalopini. It is worth to note how Urotrichini resulted to be not different from both Talpini and Scalopini, while a significant difference occurred between Talpini and Scalopini. The perANOVA retuned highly significant results for the CS (*p*-value < 0.001). The boxplot (Figure 2.10) shows as the Desmaninae present the largest forms, followed by Talpini and Scalopini, while the non-fossorial clades possess the smallest size, with Neurotrichini having intermediate values. The pairwise perANOVA (Table 2.4) evidenced how Talpini and Scalopini were significantly different only from Uropsilini, and how Neurotrichini were not different from other clades.

	Uropsilinae	Desmaninae	Urotrichini	Neurotrichini	Scalopini	Talpini
Uropsilinae	NA	0.07	0.217	0.561	0.015	0.015
Desmaninae	NA	NA	0.200	0.561	0.015	0.015
Urotrichini	NA	NA	NA	0.561	0.510	0.198
Neurotrichini	NA	NA	NA	NA	0.217	0.510
Scalopini	NA	NA	NA	NA	NA	0.015
Talpini	NA	NA	NA	NA	NA	NA

Table 2.3. Results of pairwise perMANOVA analysis.

	Uropsilinae	Desmaninae	Urotrichini	Neurotrichini	Scalopini	Talpini
Uropsilinae	NA	0.015	0.434	0.208	0.015	0.015
Desmaninae	NA	NA	0.015	0.456	0.434	0.198
Urotrichini	NA	NA	NA	1	0.015	0.015
Neurotrichini	NA	NA	NA	NA	0.434	0.456
Scalopini	NA	NA	NA	NA	NA	1
Talpini	NA	NA	NA	NA	NA	NA

Table 2.4. Results of pairwise perANOVA analysis.

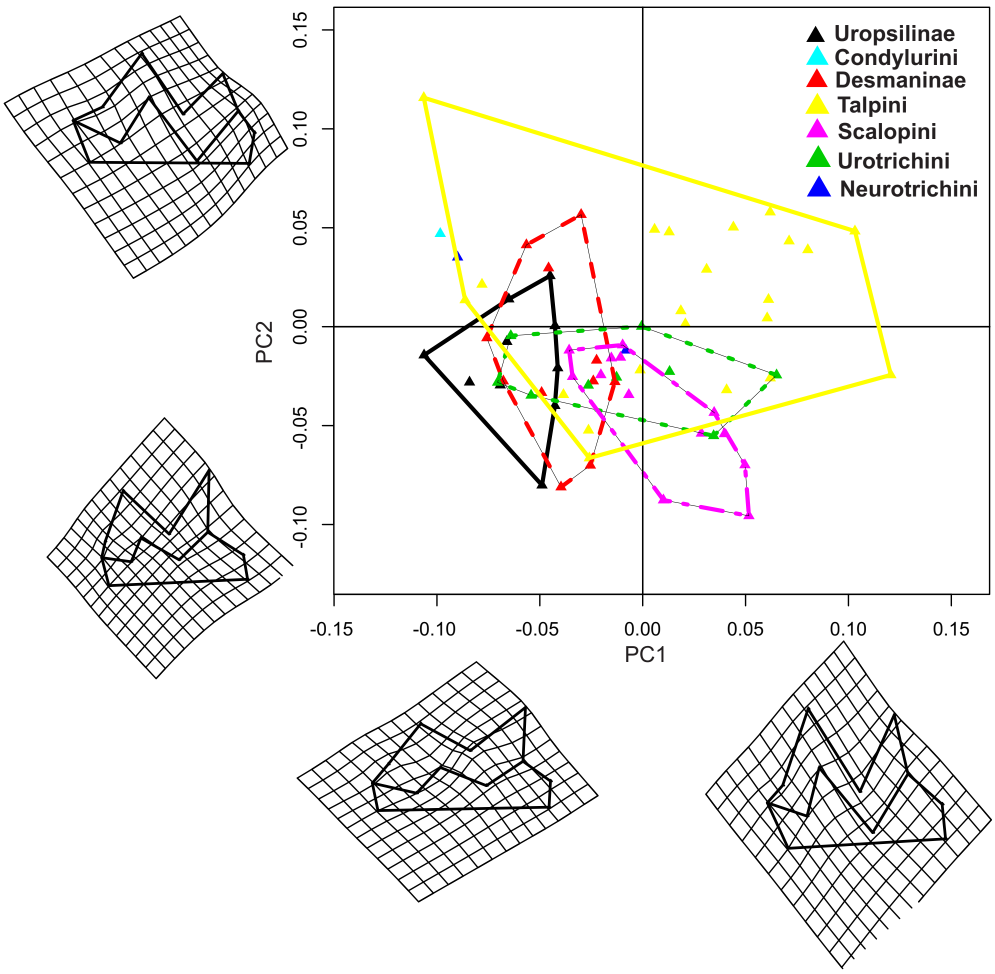

Figure 2.9A. Scatterplot of the first two axes of the bgPCA. Deformation grids refer to axes extremes (positive and negative values).

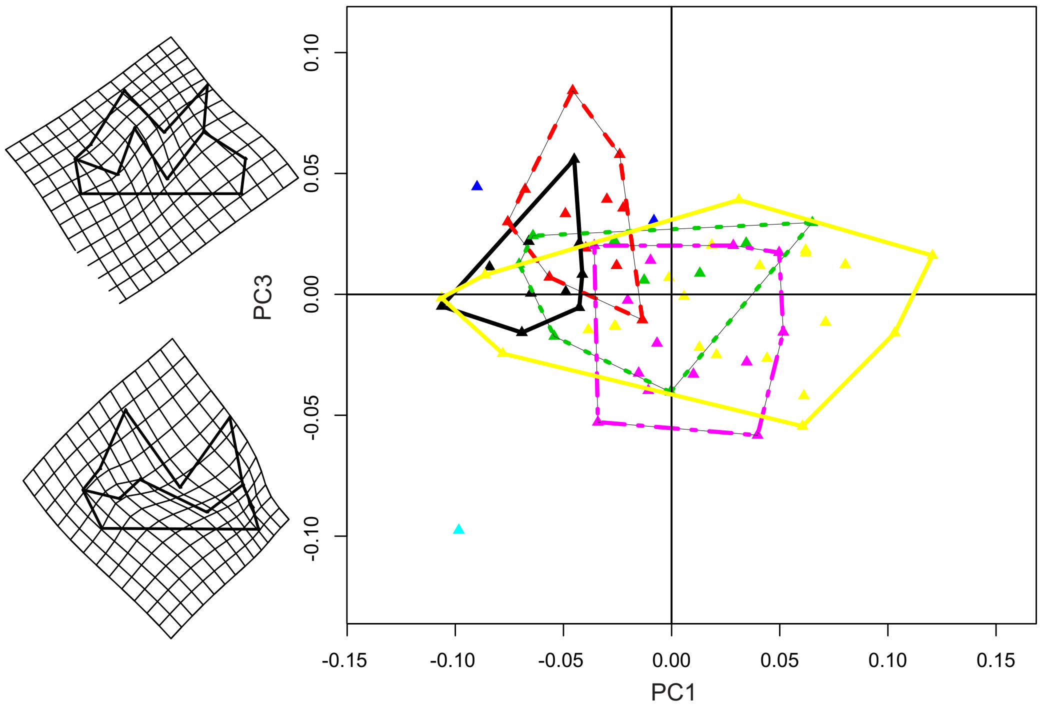

Figure 2.9B. Scatterplot of the first vs. third axes of the bgPCA. Deformation grids refer to axes extremes (positive and negative values).

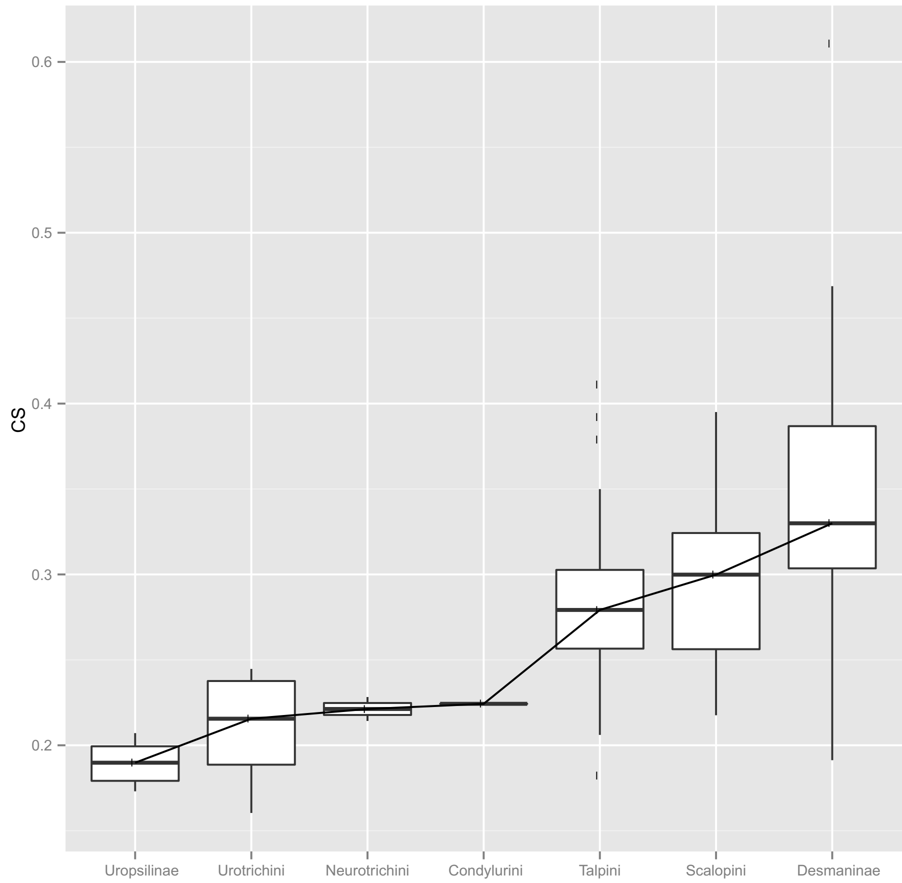

Figure 2.10. Boxplot of the centroid sizes. Bottom and top of the boxes are the first and third quartiles, the horizontal solid black lines represent the median, whiskers represent the minimum and maximum values.

Allometry

Multivariate regression of per-species averaged shape variables on per-species averaged CS returned a significant interaction (*p*-value = 0.002). However separate per-clade multivariate regressions returned significant results only for Talpini (*p*-value < 0.001). The perMANCOVA test returned a significant result (*p*-value = 0.045). The m1 shape shows very few changes when associated with CS (fig. 2.11). In particular at low CS values the labial cusps are slightly lower, the paraconid is lower and slightly displaced anteriorly.

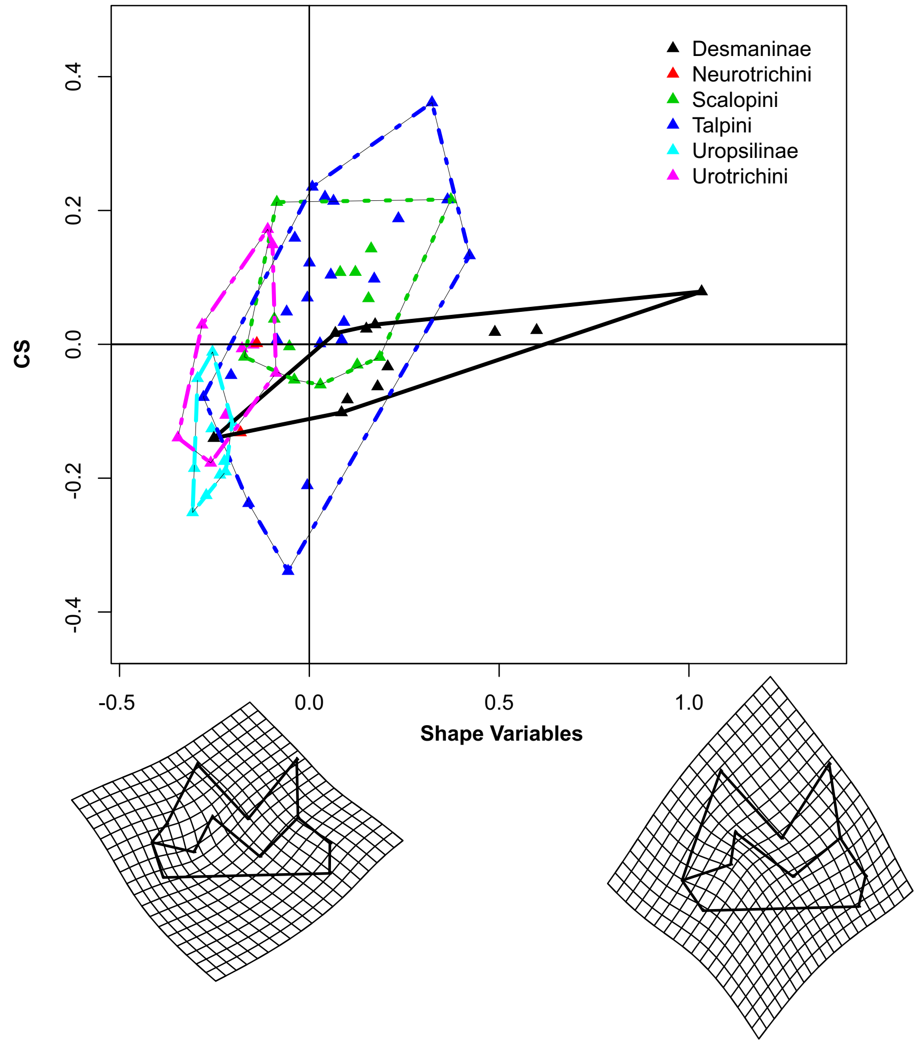

Figure 2.11. CCA scatterplot of shape on size. Deformation grids refer to positive and negative extremes.

Inclusion of Phylogeny

Phylogenetic signal

The Mantel test returned highly significant results for both shape and size variables (p-value < 0.001 and p-value = 0.001, respectively). The phylosig() function returned significant results when computed for the CS (p-value < 0.001, K = 0.377). The physignal() function returned a highly significant result (p-value = 0.004; K = 0.28).

The ancestral character estimation for both shape and size variables (figure 2.12A and 2.12B) along the phylogenetic tree, shows that the phylogenetically nearest species are also very similar in both shape and size.

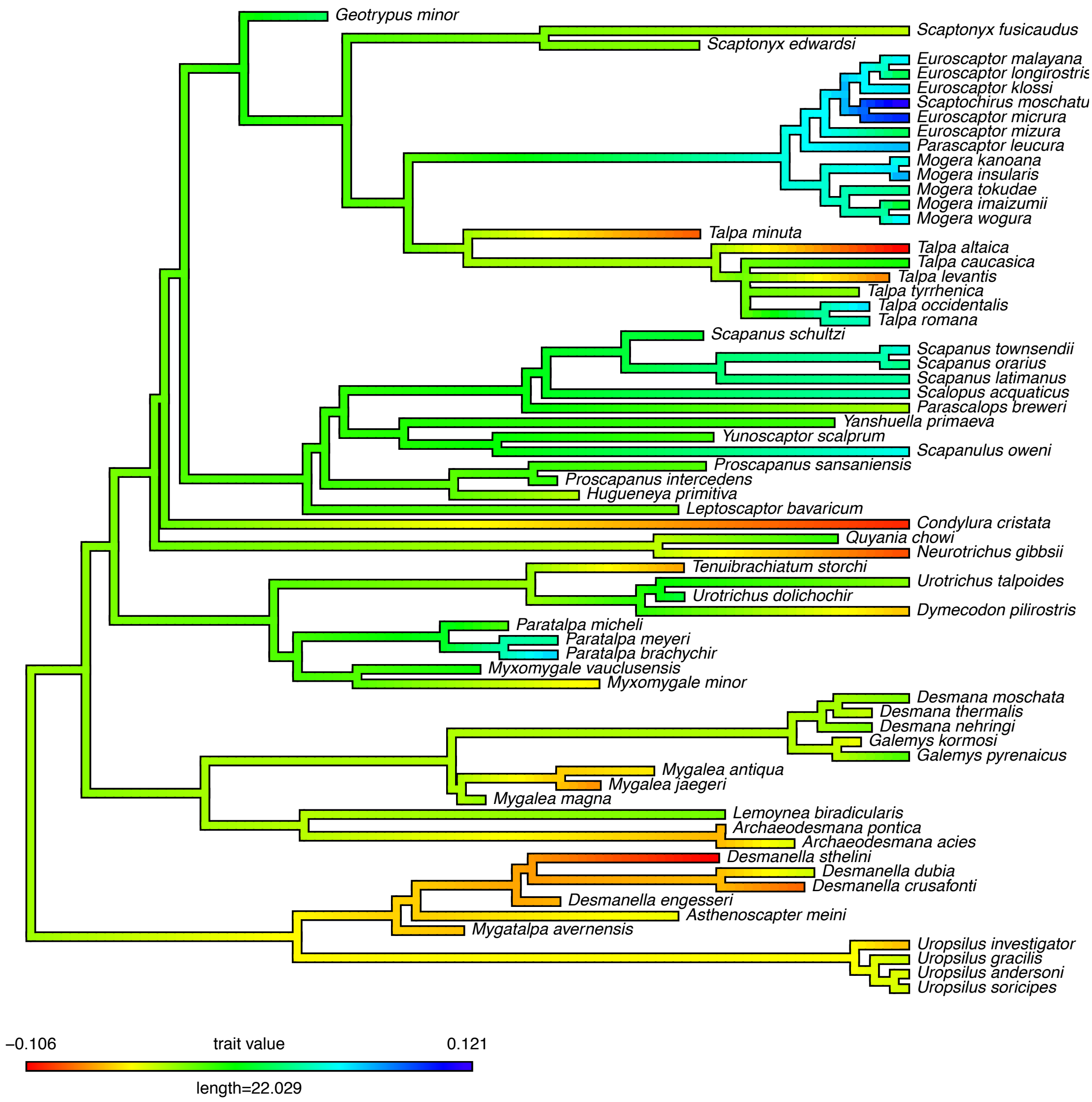

Figure 2.12A. Plot of the PC1 trait on the phylogeny.

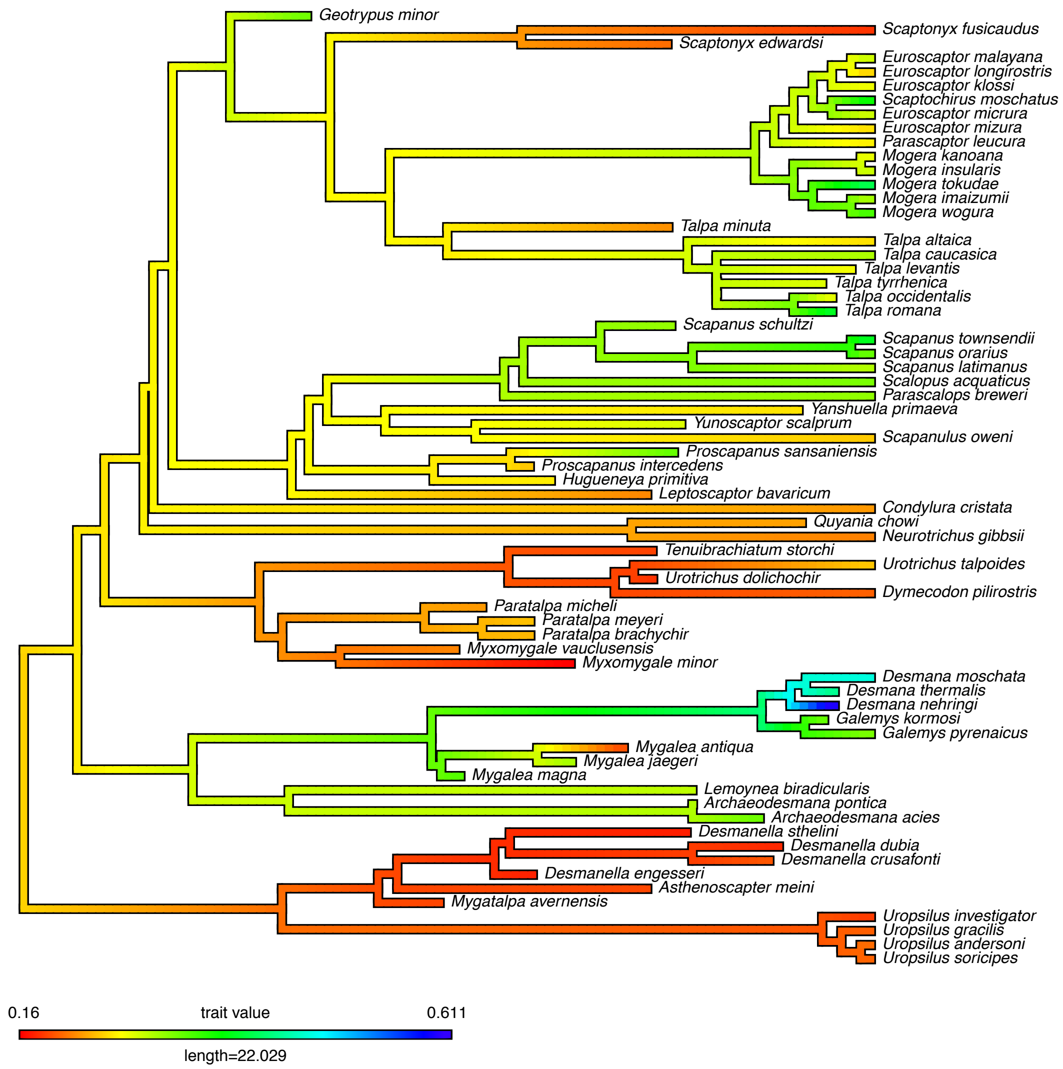

Figure 2.12B. Plot of the CS trait on the phylogeny.

Phylogenetic non-independence

The phyMANOVA and phyANOVA retuned non-significant results for the shape and size variables (p-value = 1, p-value = 0.55 respectively). The covariation between the shape and size variables resulted to be significant when performing the PGLS (p-value < 0.001).

Evolutionary rates

We found that Talpidae rate of morphological evolution is different from Brownian motion (p-value < 0.001). The evolutionary rates were significantly different between clades (p-value = 0.001). Talpini, Desmanini and Uropsilini possess similar ML rates (~3.5), while Scalopini and Urotrichini have a lower rate (~2) and Neurotrichini have the lowest rate (~1). We found positive shifts in correspondence of species *Uropsilus andersoni* and *Archaeodesmana acies* and in correspondence of the *Euroscaptor* + *Scaptochirus* spp. (fig. 2.13). When performing the same analyses on CS we found that the presence of the large-sized *Desmana moschata* and *Desmana nehringi* significantly influenced the rates values. In fact, we found an evident positive shift in correspondence of the desmans (ML rate = 903.4).

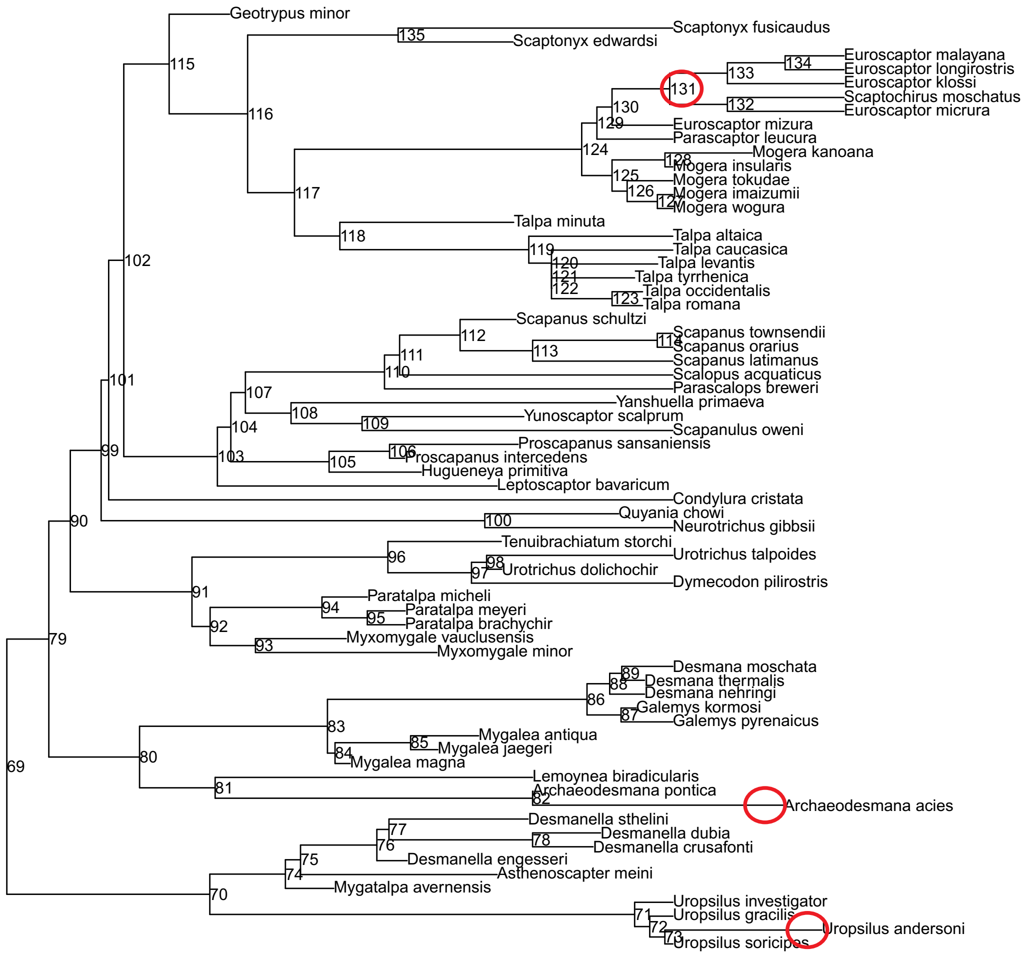

Figure 2.13. Plot of the shifts found for the evolutionary rates in the shape variables. Red circles represent the positive shifts.

Morphological and size disparity

The betadisper analysis returned significant results (p-value = 0.001) when computed for the shape variables. Talpini possess the higher average distance from mean, while Neurotrichini have the lower. The CS disparity resulted to be non-significant as revealed by the Levene test (p-value = 0.08).

The morphological disparity through time was higher than expected under Brownian motion. In fact the dtt() function (figure 2.14A) returned a positive MDI (MDI = 0.22). The dtt() function returned a positive MDI (MDI = 0.013) also for the CS, again suggesting a deviation from the gradualism (figure 2.14B). The node-height test returned significant values for the first 3 PCs (p-values = 0.001; 0.012; 0.001; respectively). The node-height test performed on the CS returned again an highly significant result (p-value = 0.002).

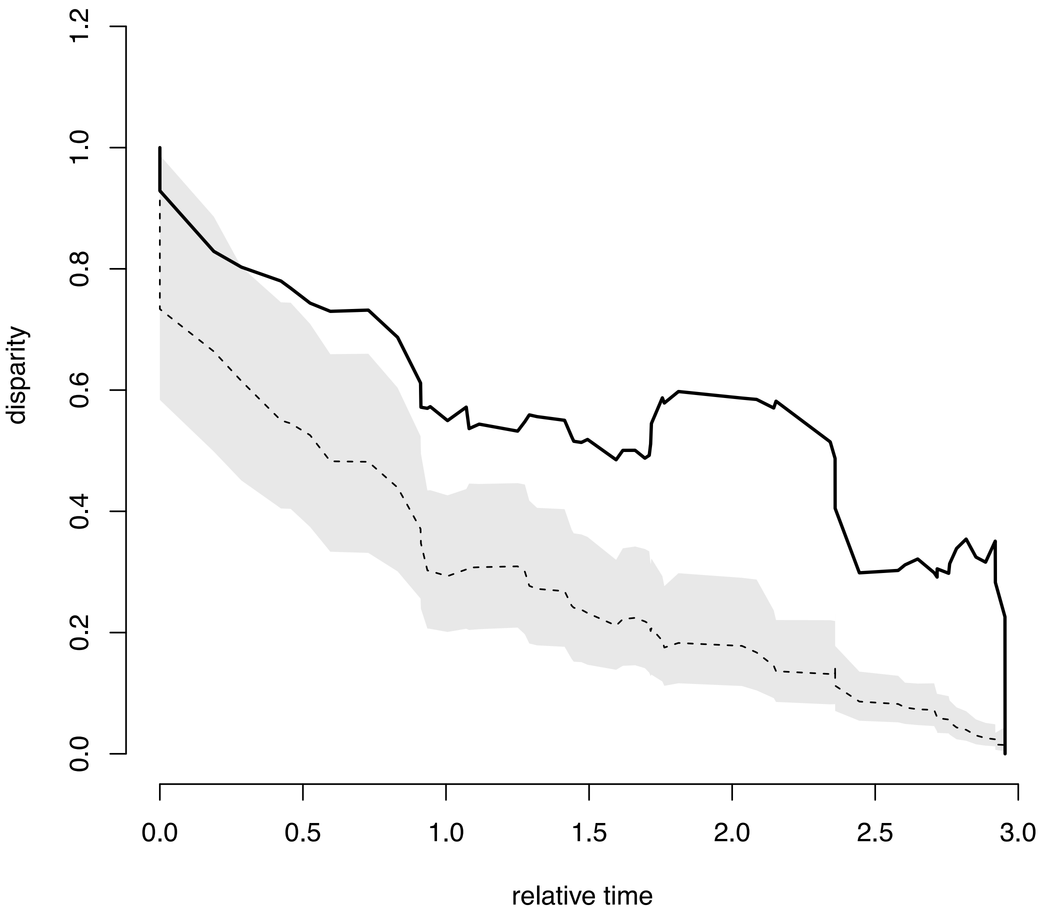

Figure 2.14A. Plot of the dtt() function performed on the m1 shape variables. The solid line represent the empirical data, the dotted line represent the simulated data under Brownian motion.

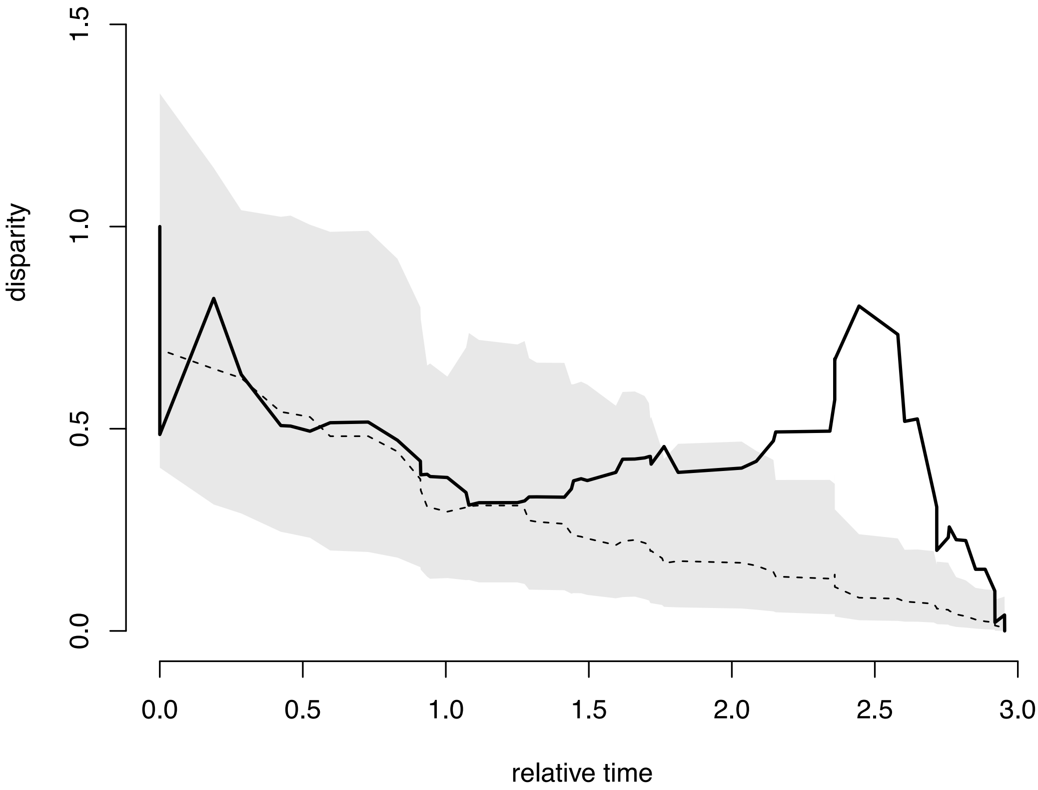

Figure 2.14B. Plot of the dtt() function performed on the m1 shape variables. The solid line represent the empirical data, the dotted line represent the simulated data under Brownian motion.

"Surface" analysis, search for no a priori local optima

The surface analysis revealed the absence of convergence in the talpids m1 shape. However, we found convergence in m1 size in *Talpa romana*, *Scaptochirus moschatus*, *Desmana moschata* and *Desmana nehringi*. We found the presence of 6 shifts under OU model for the shape variables, and 11 shifts under OU model for CS.

Discussion

The shape analysis performed on the m1 evidenced an overall superimposition of the different clades. Nevertheless along the PC1 (see figure 2.9A) it is possible to separate two m1 morphologies: brachyodont (negative values) and hypsodont (positive values). Uropsilinae, Desmaninae, Condylurini and Neurotrichini all have brachyodont m1, while Urotrichini, Talpini and Scalopini show some intra-clade differences. In particular, among Talpini, the Eastern Asian species present a high degree of hypsodonty, with *Scaptochirus moschatus* and *Euroscaptor* spp. positioned at the positve extreme of the morphospace. The European Talpini, instead, show a brachyodont configuration, with the exception of the western species *Talpa romana* and *Talpa occidentalis*. The latter species has been reported to live in more xeric environments than other representative of the genus (Niethammer, 1990; Loy, 2008). Among Scalopini, the European Miocene species show a brachyodont morphology, while the extant and extinct North-American species (including *Scapanulus oweni*) possess an hypsodont configuration. The *Paratalpa* species show a hypsodont morphology, while other Urotrichine shrew-moles have the brachyodont configuration. The hypsodont adaptation would allow moles to exploit an abrasive diet by allowing a longer tooth life, and potentially a longer animal longevity (Hutchinson, 1987). Uropsilinae cluster at the negative extreme of the morphospace, thus suggesting that the brachyodont configuration should be ancestral (Motokawa et al., 2003; Sanchez-Villagra et al., 2006). The hypsodont morphology probably evolved several times in different clades and could be related to abrasive dietary specializations. Along the PC3 *Condylura cristata* occupies a unique region of the morphospace (negative values). The star-nosed mole is distinct from all other clades by having a very deep cristid obliqua notch and very low lingual cusps. The particular molar shape of *Condylura* is, probably, due to the same factors that influenced the mandible morphology (see “The moles dentary” section).

The perMANOVA and perANOVA revealed significant differences between clades. However, when taking into account phylogeny, these analyses turned out to be non-significant, thus, suggesting a strong phylogenetic constrain in both phenotypes. In fact, shape and size variables bear a strong phylogenetic signal. The presence of a strong phylogenetic structure was evident when we mapped the two traits on the time calibrated tree, the closely related species were also very similar in both traits. Multivariate regression revealed the presence of an evolutionary allometry, even the PGLS confirmed this evidence. Despite this, we have to report that separate multivariate regressions revealed a significant interaction for Talpini only. As expected, minor shape changes were related to size.

The evolutionary rates were proven to be different with Talpini and Desmaninae having the higher rates. In particular it is worth to note that the major positive shift was found in correspondence of the *Euroscaptor* + *Scaptochirus* spp. As noted before these species share a highly hypsodont m1.

The disparity through time was higher than that expected under Brownian motion for both shape and size variables, indicating a deviation from gradualism toward punctualism (Slater et al., 2010; Slater et al., 2013). When we performed the node height test (Freckelton and Harvey, 2006; Slater et al., 2010) we obtained a positive correlation, suggesting an acceleration in evolutionary rates for both size and shape variables.

We did not find any convergence for the shape variables. The "SURFACE" analysis evidenced as only *Talpa romana*, *Scaptochirus moschatus*, *Desmana moschata* and *Desmana nehringi* were convergent in size, these species share the larger values in centroid size.

We often think of convergent evolution in terms of distantly related taxa that have evolved to become extremely similar in appearance. However, in many cases in which clades are very different in phenotype, natural selection may cause two species to become more similar to each other than were their ancestors, but this convergence is not of sufficient magnitude to obliterate the pre-existing differences that occur among clades (Losos, 2011). Herrel et al. (2004) refer to such examples as “incomplete convergence” and Stayton (2006) provides a geometric framework in which this is one type of convergent evolution. In this light, an alternative definition of convergent evolution might be “instances in which species independently evolve to become more similar to each other than were their ancestors” (Losos, 2011). In the moles case, evolutionary change could have occurred occurred in similar ways in species independently subject to the same selective conditions (Hutchinson 1987), but the resulting changes have not been great enough to override pre-existing interclade differences. In cases such as these, we may ask why species do not converge completely. Possible explanations are that the optimal phenotype with respect to a given selective context may differ depending on the other characteristics of the species, that selective environments are not identical, that constraints preclude some lineages from attaining the optimal phenotype, or that some species are still in the process of adapting (Stayton, 2006; Revell et al., 2007; Hansen et al., 2008).

In conclusion, the analysis of the m1 revealed a strong phylogenetic control on both shape and size. However, the GM analysis revealed that brachyodonty was the ancestral condition in talpids. We recognized different adaptations in the m1 shape, in particular among Talpini and Scalopini. Further investigations should be aimed to test how hypsodonty evolved in the highly fossorial clades, and how these phenotypes could have influenced the distribution in fossil and extant species.

THE HUMERAL MORPHOLOGICAL VARIATION

Introduction

The humerus is the bone of the shoulder girdle that experienced the most remarkable transformations in relation to the evolution of the fossosial lifestyle (Dobson, 1882; Freeman, 1889; Reed, 1951; Yalden, 1966; Sànchez-Villagra et al., 2004). In highly fossorial moles such bone is widened and flattened in response to intense burrowing adaptation, it presents an elliptically shaped, ventrally directed head of humerus, a heavily expanded proximal end, an enlarged teres major tubercle, a deep brachialis fossa, a large, hemicylindrical clavicular facet, an enlarged medial epicondyle bearing a deep fossa for the attachment of the Flexor digitorum profundus tendon-muscle (Hutchinson, 1968). The complexity of the humerus (Figure 2.15B) makes this bone a potentially rich source of phylogenetic characters. The humerus has experienced transformations at higher (Gregory, 1949) and lower levels of tetrapods phylogeny (Woodman et al., 2003) that are of taxonomic and systematic value. Since the talpids humerus has become uniquely specialized in a stepwise fashion, then it likely contain phylogenetically and adaptive useful informations. Moreover the highly autapomorphic status of the humerus has allowed many fossil taxa to be recognized on the humerus alone (McKenna and Bell, 1997; Van den Hoek Ostende, 1997; Ziegler, 2003; Sansalone et al., in press; among others). There are detailed studies on the morphology and functional adaptation of the humerus in several species (Edwards, 1937; Campbell, 1939; Yalden, 1966; Gambaryan et al., 2003; Sanchez-Villagra et al., 2004; Piras et al., 2012). However the humeral morphology and its evolution has not been investigated by means of modern comparative methods. The aim of this section is to investigate the patterns of the humeral morphological disparification through the talpids phylogeny; to measure and compare the rates of evolution between different clades; to test if and how allometry shaped the humeral morphology when related to size; to test if convergence or parallelism occurred among Talpidae.

Material and methods

Specimens collection

We analysed a total of 711 humeri belonging to 71 extant and extinct species (see Supplemetary Appendix 3 to Chapter 2 for specimens list and localities) encompassing all the morphological variation of Talpidae. Our sample includes representatives from all sub-families and tribes including fossils.

Geometric Morphometrics

We digitized 22 landmarks and 14 semi-landmarks on the humerus in caudal view (figure 2.15A).

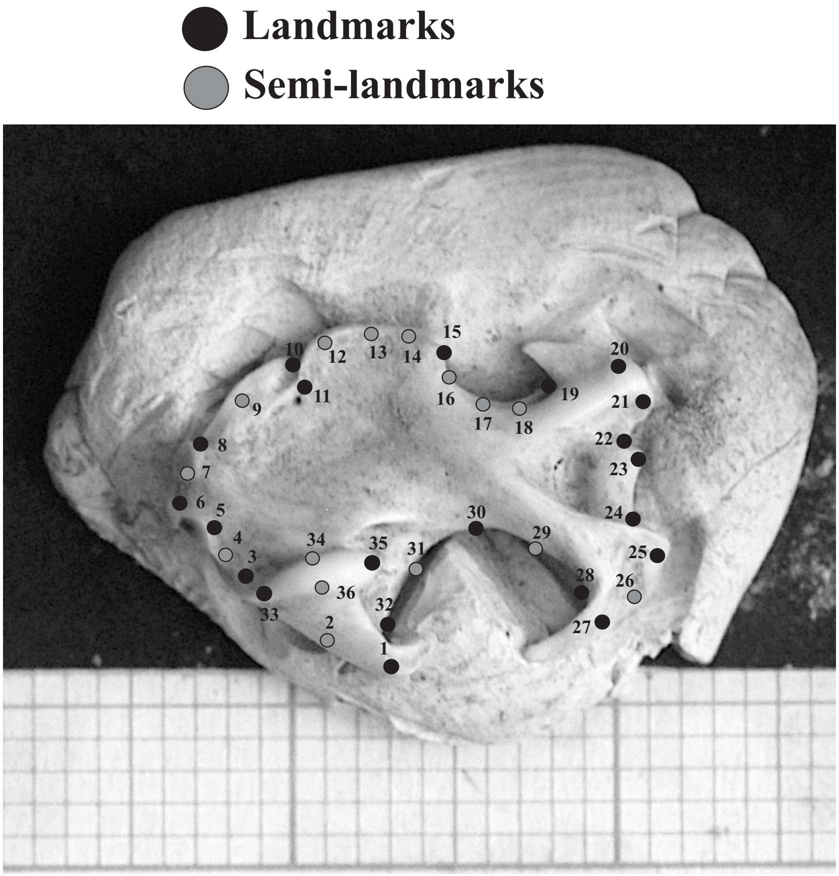

Figure 2.15A. Landmarks (black circles) and semilandmarks (white circles) digitized on the humerus in caudal norm: 1) lateral end of greater tuberosity; 2) articular facet for clavicula; 3) proximal edge of the articular facet for clavicula; 4) bicipital notch; 5) proximal end of lesser tuberosity; 6) medial edge of the minor tuberosity; 7) lateral edge of the lesser tuberosity; 8) bicipital ridge; 9) middle point of the bicipital tunnel; 10) lateral end of the scalopine ridge; 11) proximal end of the teres tubercle; 12-14) surface of the teres tubercle; 15) distal end of the teres tubercle; 16-18) minor sulcus; 19) posterior margin of the lateral epicondyle; 21-22) lateral epicondyle; 22-24) trochlear area; 25-27) medial epicondyle; 28) posterior margin of the medial epicondyle; 29-32) greater sulcus; 33-36) humeral head.

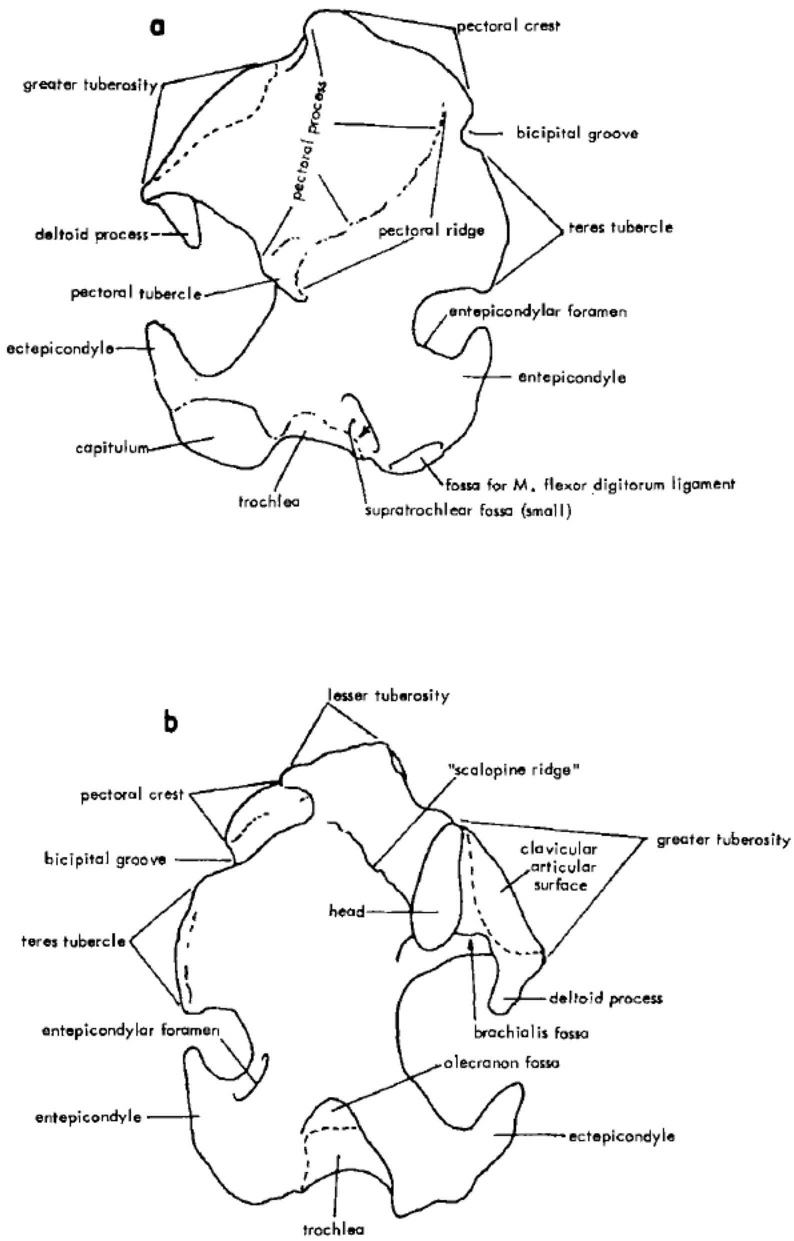

Figure 2.15B. Humeral terminology used here. Modified from Hutchinson (1974).

Results

Shape analysis

The bgPCA on Procrustes aligned coordinates showed that all the clades are well separated in the morphospace, a partial superimposition only occurs for Talpini and

Scalopini (figure 2.16A and 2.16B). In particular along the PC1 (80.3% of the total variance) it is possible to separate the highly fossorial moles (negative values) from the non-fossorial moles (positive values). At negative values the humeral shape have the typical robust configuration of the highly fossorial taxa, it shows an highly expanded distal region with highly expanded pectoral ridge, enlarged teres tubercle, enlarged medial and lateral epicondyles, expanded minor and greater tuberosities. At positive values the humerus show the typical slender and non-specialized configuration of the non-fossorial forms. The humerus have highly reduced teres tubercle and pectoral ridges, reduced medial and lateral epicondyle and reduced minor and greater tuberosities. Along the PC2 (6.8% of the total variance) it is possible to separate the Talpini (negative values) from the Scalopini (positive values). At negative values the humeral morphology show a longer but less expanded pectoral ridge and a more developed lesser tuberosity, while at positive values the humeral shape show a shorter but more expanded pectoral ridge and a reduced lesser tuberosity. Along the PC3 (2.8% of the total variance) it is possible to observe the neat separation of the *Geotrypus* spp. (negative values) from all other taxa. At negative values the humeral shape show a wider greater sulcus, a reduced and less developed pectoral ridge and a smaller and pointed teres tubercle, while at positive values it is possible to observe the robust humeral configurations typical of the highly fossorial moles. The perMANOVA test revealed a highly significant result (p-value < 0.001). The pairwise perMANOVA (Table 2.5) revealed how the highly fossorial moles (i.e. Scalopini and Talpini) were significantly different from all other taxa, while among the non-fossorial moles we found significant differences between Desmanini and Urotrichini. The perANOVA test returned a highly significant result (p-value < 0.001) when computed for the CS. The pairwise perANOVA revealed significant size differences between Talpini and Urotrichini (see Table 2.6). The boxplot (figure 2.17) showed the presence of outliers in many clades suggesting the presence of a high dispersion around the mean CS values.

	Desmaninae	Urotrichini	Neurotrichini	Condylurini	Scalopini	Talpini
Desmaninae	NA	0.036	0.024	0.152	0.015	0.015
Urotrichini	NA	NA	0.159	0.159	0.015	0.015
Neurotrichini	NA	NA	NA	0.159	0.015	0.015
Condylurini	NA	NA	NA	NA	0.075	0.028
Scalopini	NA	NA	NA	NA	NA	0.015
Talpini	NA	NA	NA	NA	NA	NA

Table 2.5. Results of the pairwise perMANOVA analysis.

	Desmaninae	Urotrichini	Neurotrichini	Condylurini	Scalopini	Talpini
Desmaninae	NA	0.182	0.209	1	1	1
Urotrichini	NA	NA	1	1	0.182	0.015
Neurotrichini	NA	NA	NA	1	0.230	0.015
Condylurini	NA	NA	NA	NA	1	1
Scalopini	NA	NA	NA	NA	NA	1
Talpini	NA	NA	NA	NA	NA	NA

Table 2.6. Results of the pairwise perANOVA analysis.

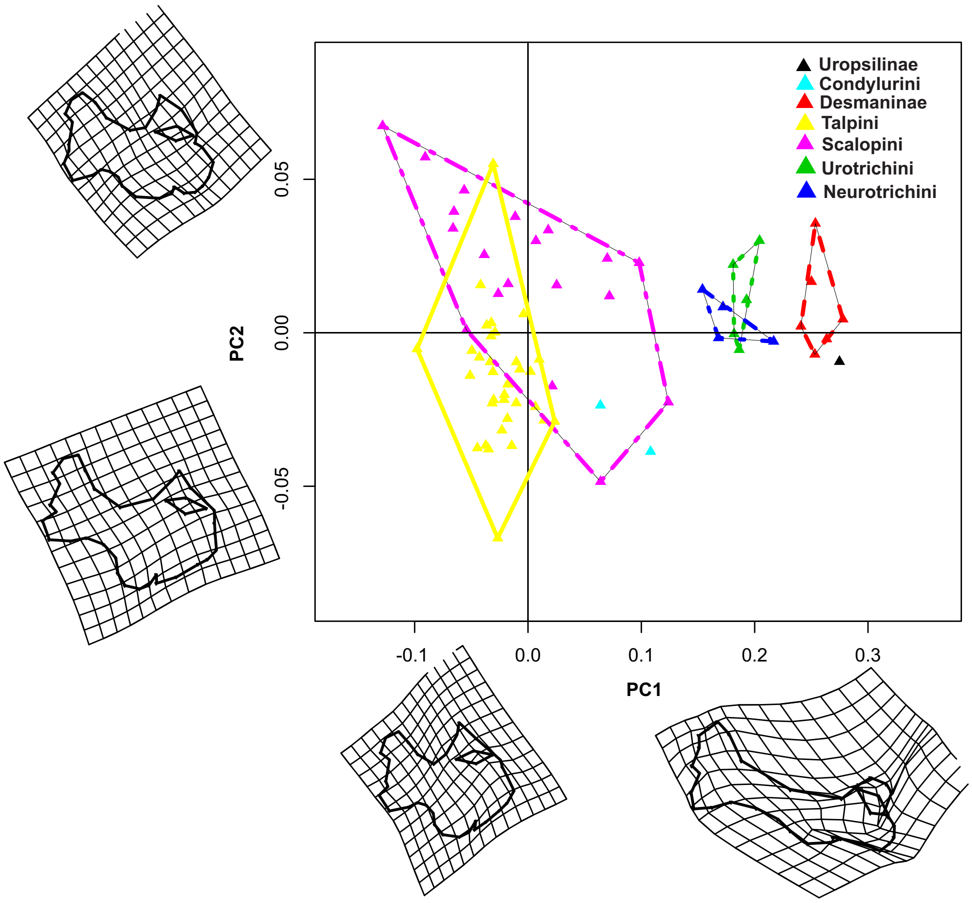

Figure 2.16A. Scatterplot of the first vs. second axes of the bgPCA on humeral shape variables. Deformation grids refer to axes extremes (positive and negative values).

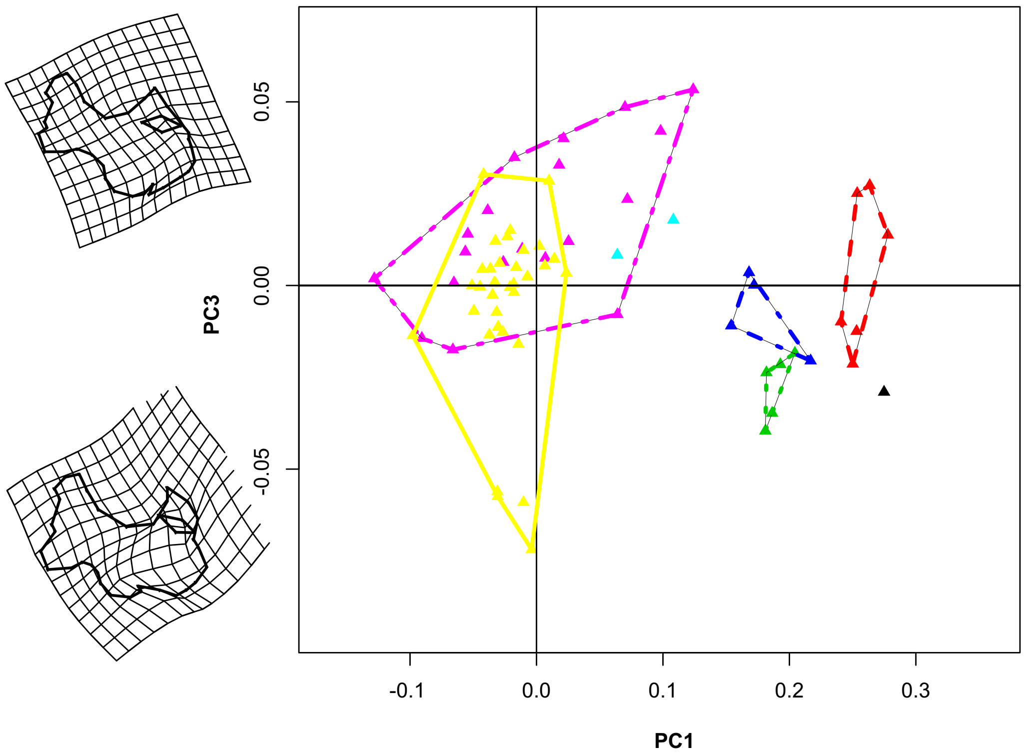

Figure 2.16B. Scatterplot of the first vs. third axes of the bgPCA on humeral shape variables. Deformation grids refer to axes extremes (positive and negative values).

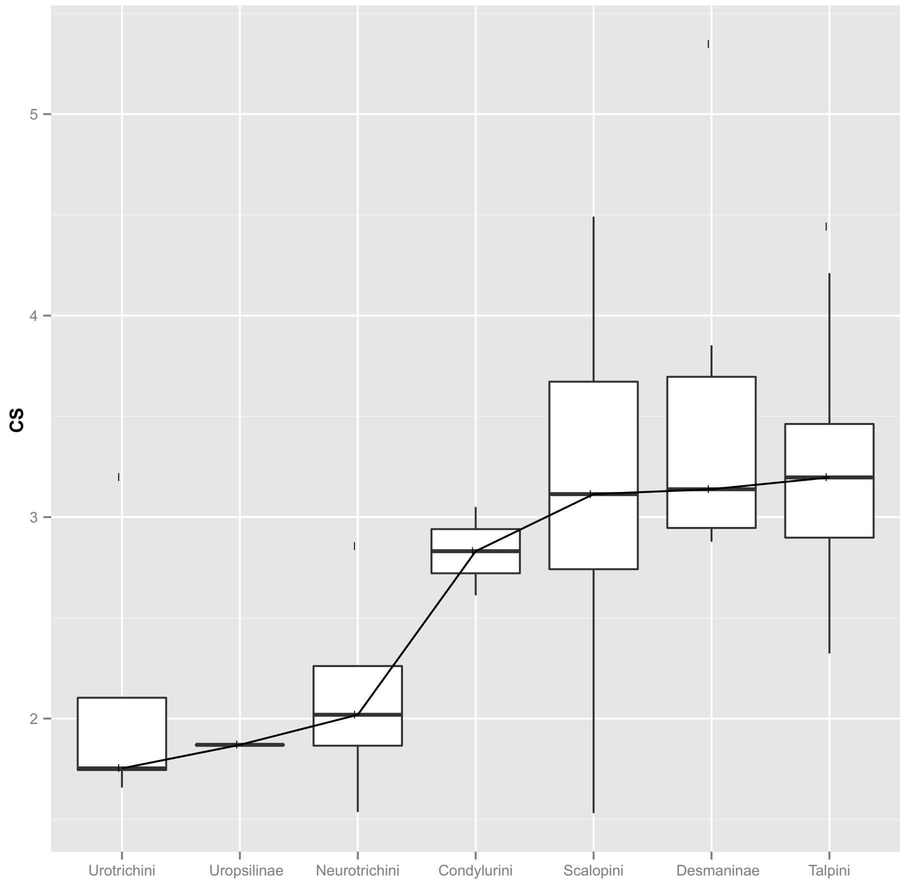

Figure 2.17. Boxplot of the centroid sizes. Bottom and top of the boxes are the first and third quartiles, the horizontal solid black lines represent the median, the whiskers represent the minimum and maximum values.

Allometry

The multivariate regression of shape on size returned a significant result (*p*-value = 0.002), with size accounting for 11% of the shape variables total variance. The separate per-clade multivariate regressions returned a significant interaction only inTalpini and Scalopini. The perMANCOVA test returned a significant result (*p*-value = 0.02). Low CS values are associated to a slender humeral configuration, while a large size is associated to a robust humeral configuration (figure 2.18).

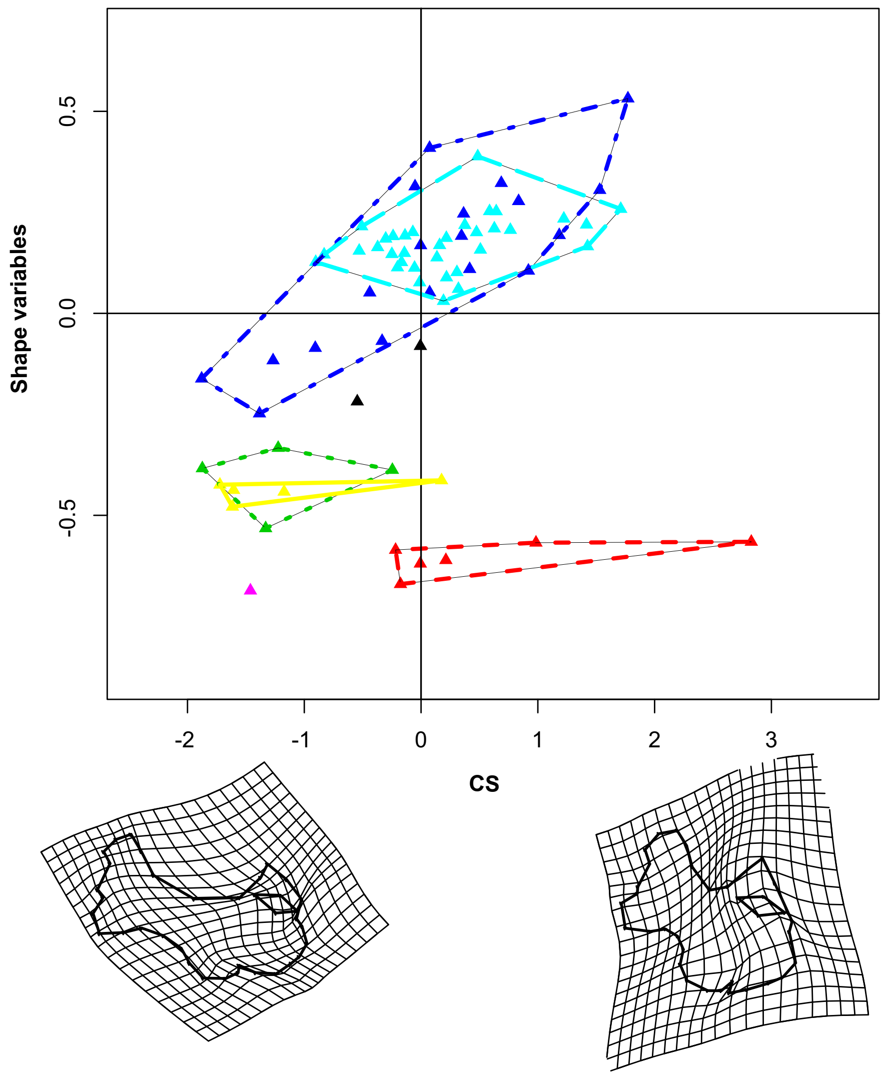

Figure 2.18. CCA scatterplot of shape on size. Deformation grids refer to positive and negative extremes.

Inclusion of phylogeny

The Mantel test returned highly significant results for both shape and size variables (p-value < 0.001 and p-value < 0.001, respectively). The phylosig() function returned significant results when computed for the CS (p-value < 0.001, K = 0.34). The physignal() function returned an highly significant result (p-value = 0.004; K = 1.38) when computed for the shape variables. The ancestral character estimation for both shape and size variables (figure 2.19A and 2.19B) along the phylogenetic tree, shows as the phylogenetically nearest species are also very similar in both shape and size.

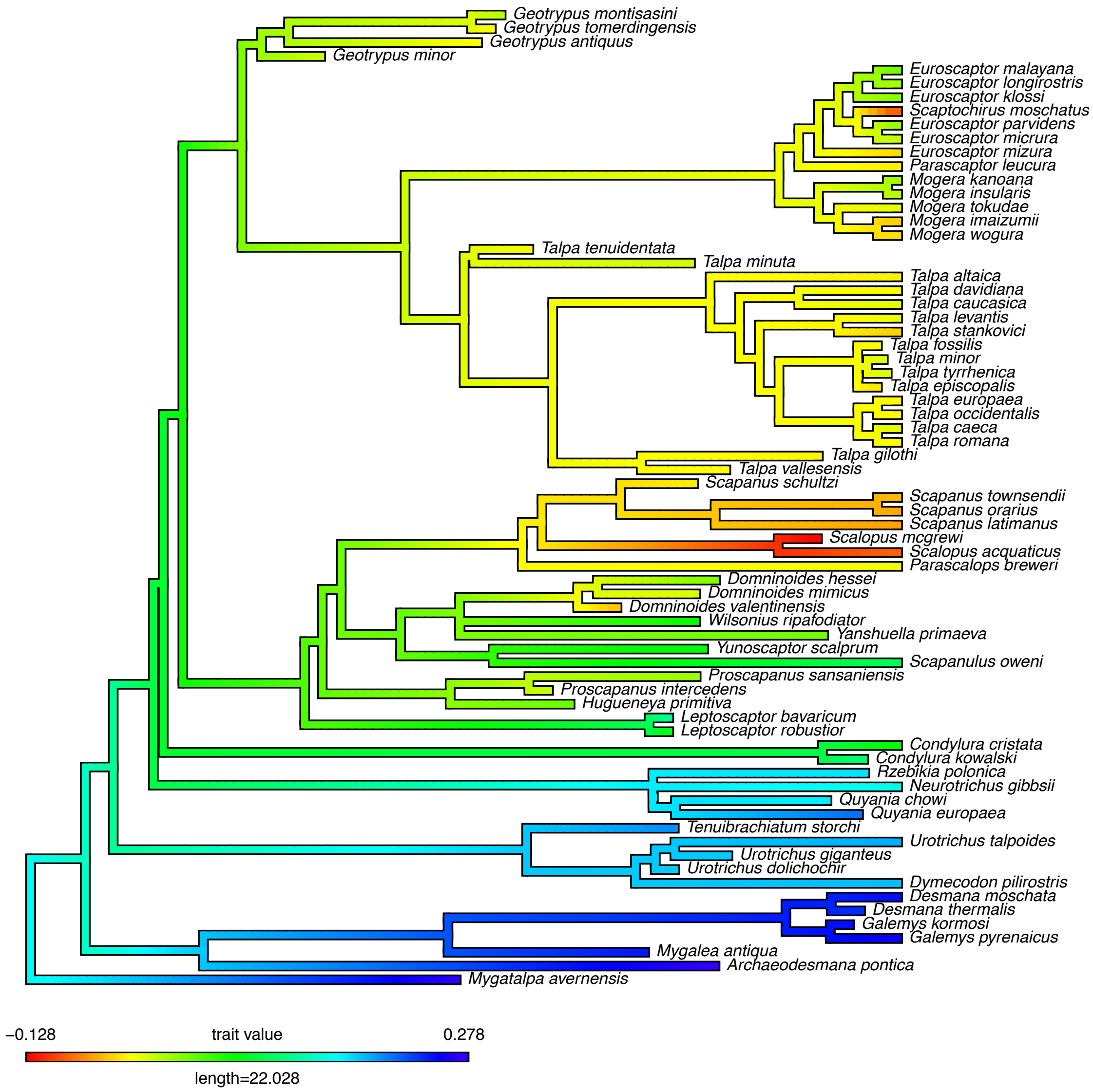

Figure 2.19A. Plot of the PC1 trait on the phylogeny.

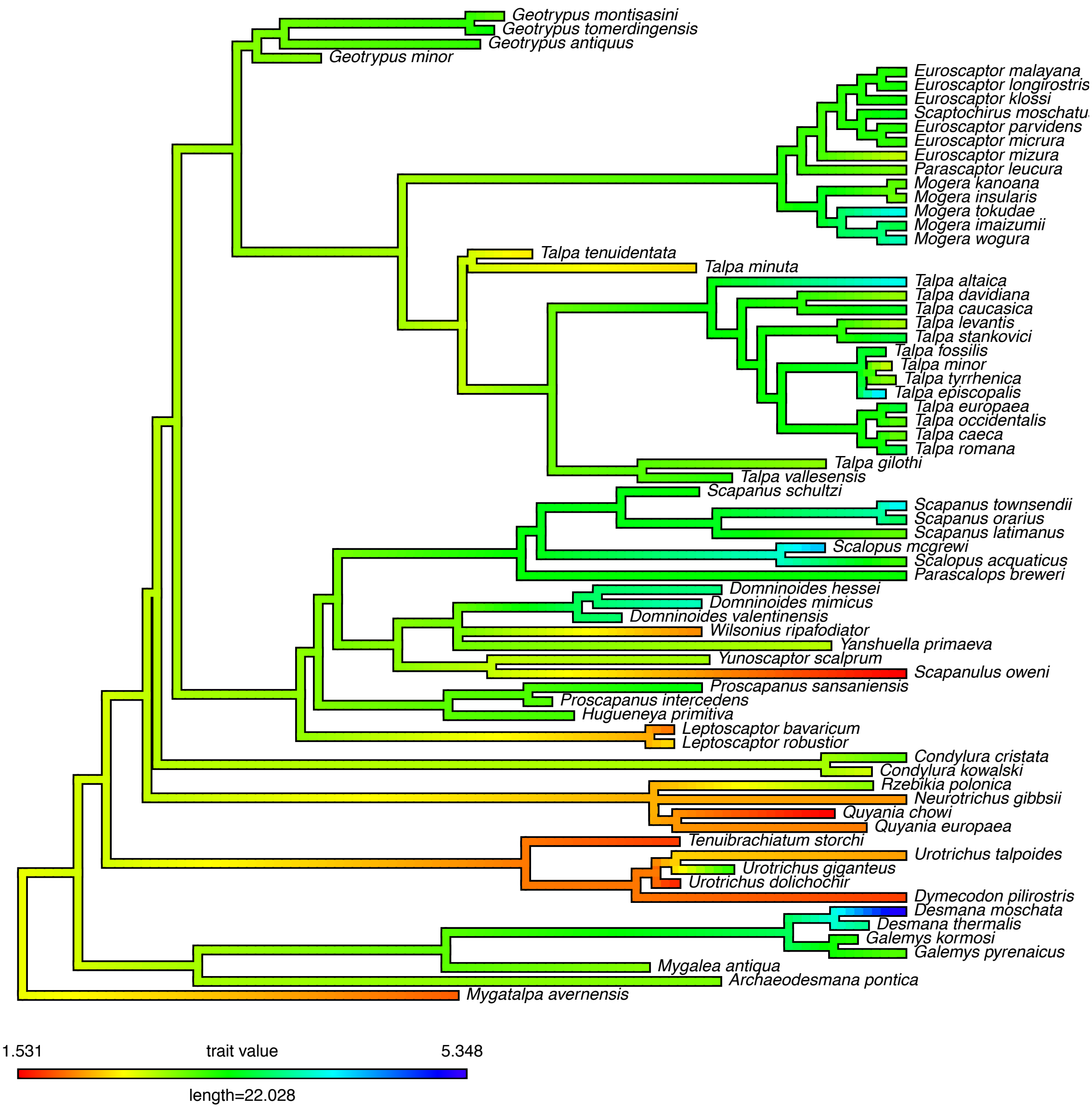

Figure 2.19B. Plot of the CS trait on the phylogeny.

Phylogenetic non-independence

The phyMANOVA returned a highly significant result (p-value = 0.013) for shape, while phyANOVA retuned non-significant results (p-value = 0.75) for size. The covariation between the shape and size variables resulted to be significant when performing the PGLS (p-value < 0.001).

Evolutionary rates

We found that Talpidae rate of morphological evolution is different from Brownian motion (p-value < 0.001). The evolutionary rates were significantly different between clades (p-value = 0.001). Desmaninae showed the highest ML rate (0.8), while Neurotrichini have the lowest (0.3). We found a neat acceleration in the evolutionary rates in correspondence of the highly fossorial moles (Condylurini, Talpini and Scalopini), while we found a negative shift in correspondence of the Uropsiline species *Mygatalpa avernensis* (figure 2.20).

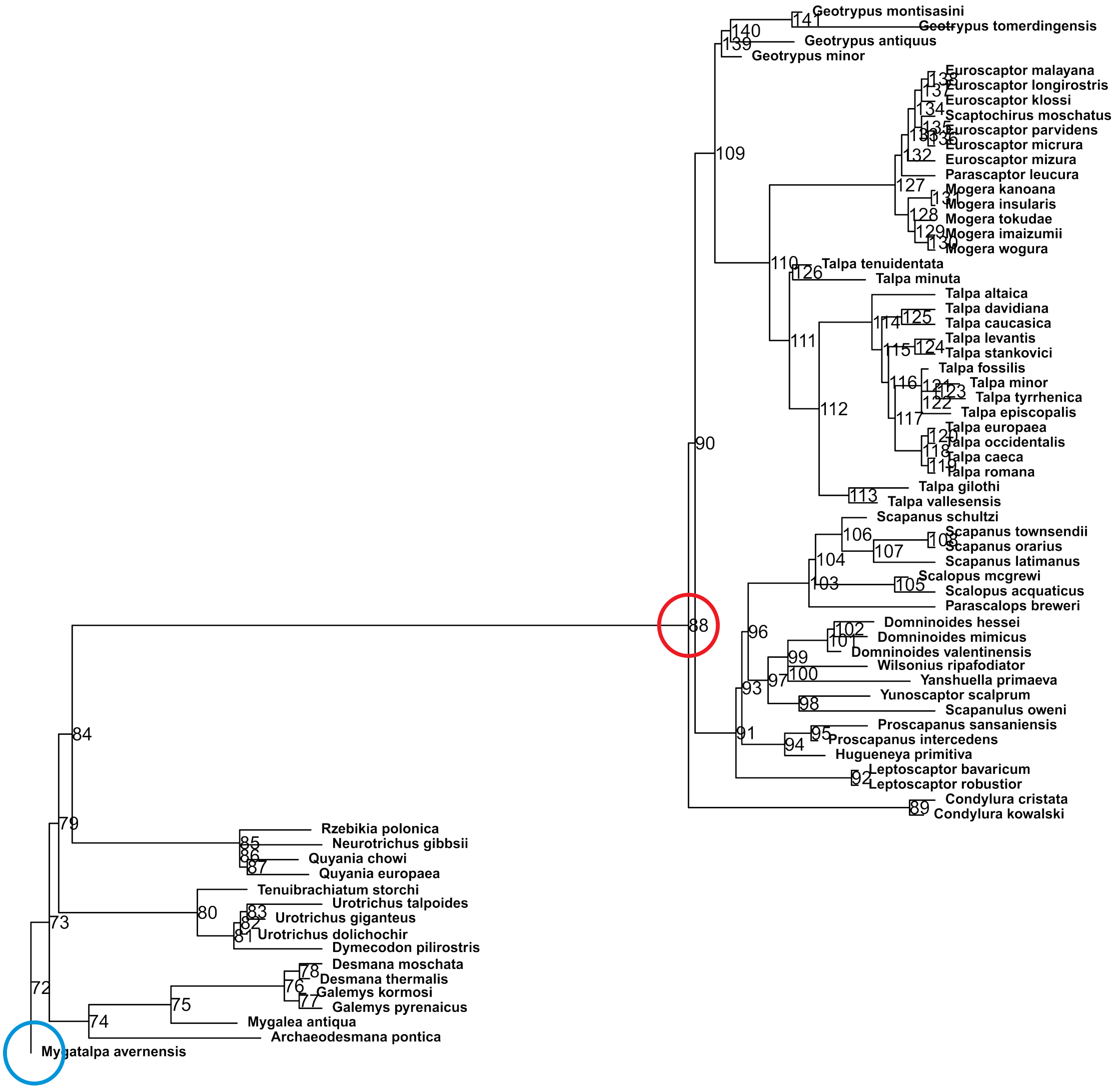

Figure 2.20. Plot of the shifts found for evolutionary rates in the shape variables. Red circles represent the positive shift, cyan circles indicate the negative shift.

Morphological and size disparity

The betadisper analysis returned significant results (*p*-value = 0.001) when computed for the shape variables. Scalopini showed the highest average distance from the mean, while Urotrichini have the lowest. The CS disparity resulted to be non-significant as revealed by the Levene's test (*p*-value = 0.17).

The morphological disparity through time was lower than expected under Brownian motion. In fact the dtt() function (figure 2.21A) returned a negative MDI (MDI = -0.22). The dtt() function returned a positive MDI (MDI = 0.33) the CS suggesting a deviation from the gradualism (figure 2.21B). The node-height test returned a negative significant correlation (*p*-values = 0.0086) for the first three PC (80.3% of the total variance). The node-height test performed on CS revealed a non significant result (*p*-value = 0.99).

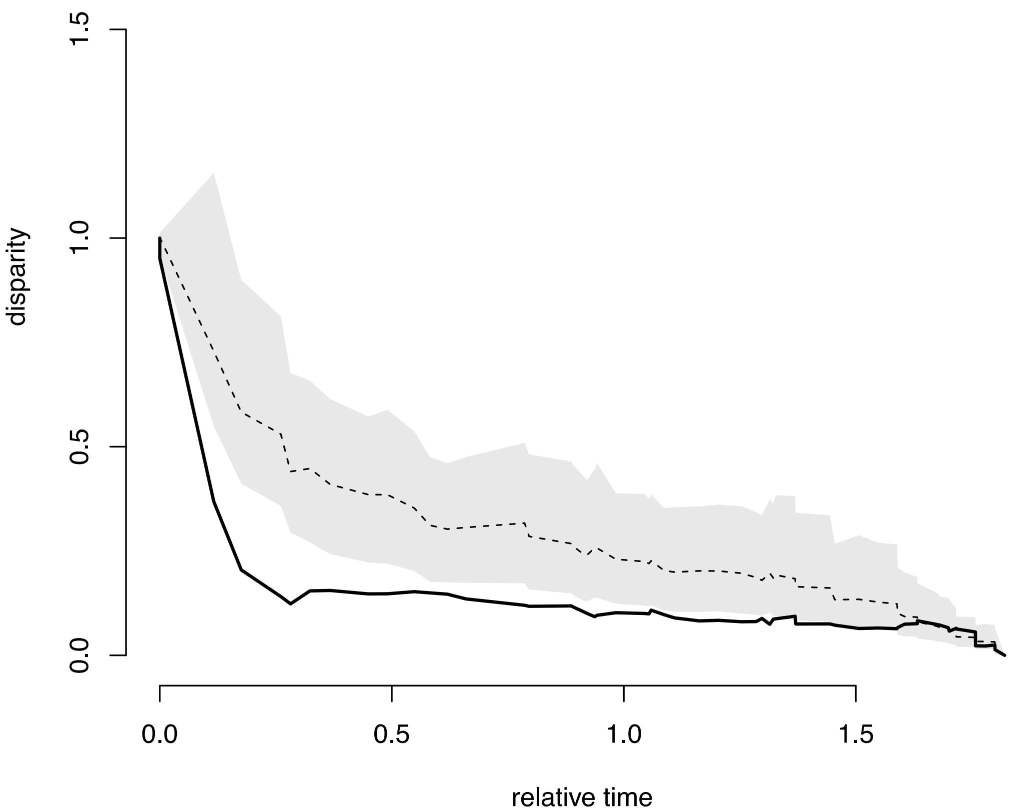

Figure 2.21A. Plot of the dtt() function performed on the humerus shape variables. The solid line represent the empirical data, the dotted line represent the simulated data under Brownian motion.

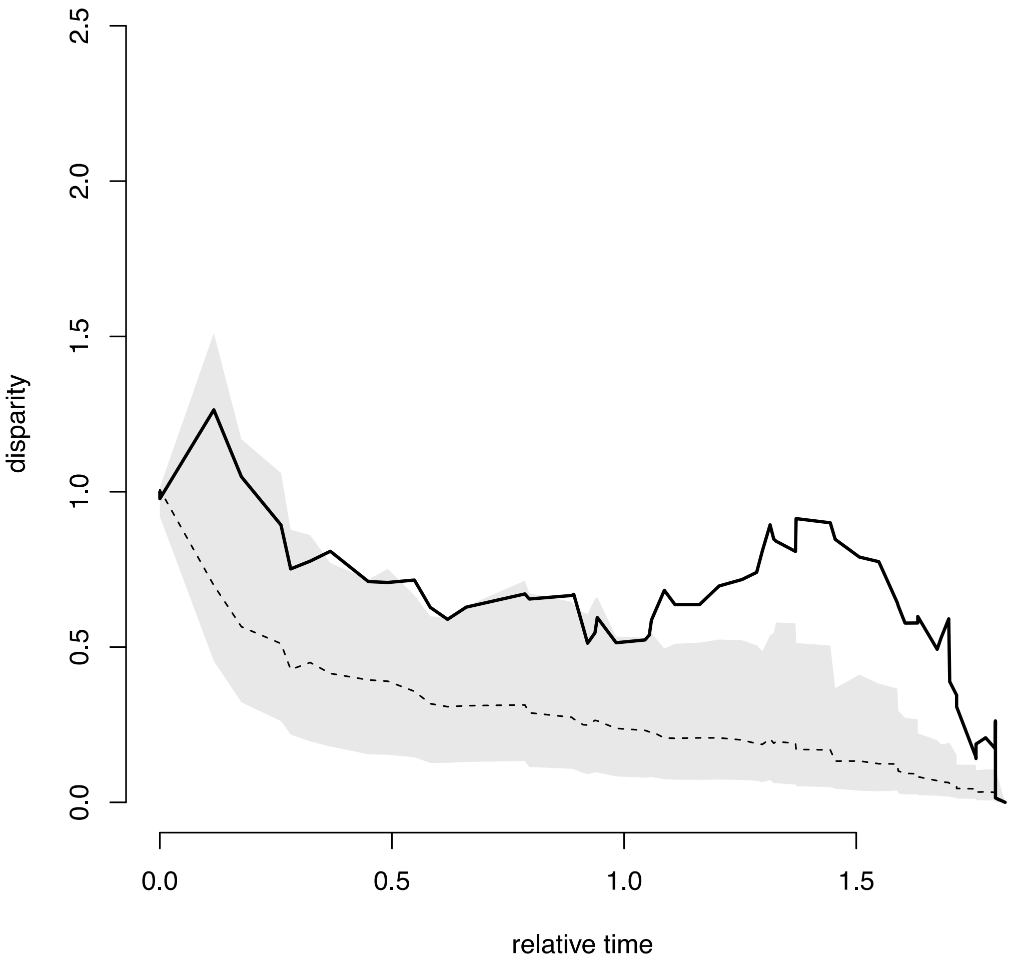

Figure 2.21B. Plot of the dtt() function performed on the humerus shape variables. The solid line represent the empirical data, the dotted line represent the simulated data under Brownian motion.

"Surface" analysis, search for no a priori local optima

The surface analysis (figure 2.22) revealed the presence of true convergence among the Scalopini and Condylurini humeral shape. In particular between *Condylura* spp. and *Wilsonius ripafodiator*, between the European Miocene Scalopini (with the exception of the slender species *Leptoscaptor bavaricum*) and between the *Scalopus* and *Scapanus* spp. We found the presence of 10 shifts under OU model for the shape variables. We found convergence in the CS for *Desmana moschata*, *Urotrichus* *giganteus* and *Scalopus mcgrewi*. We found the presence of 3 shifts under OU model for the size variable.

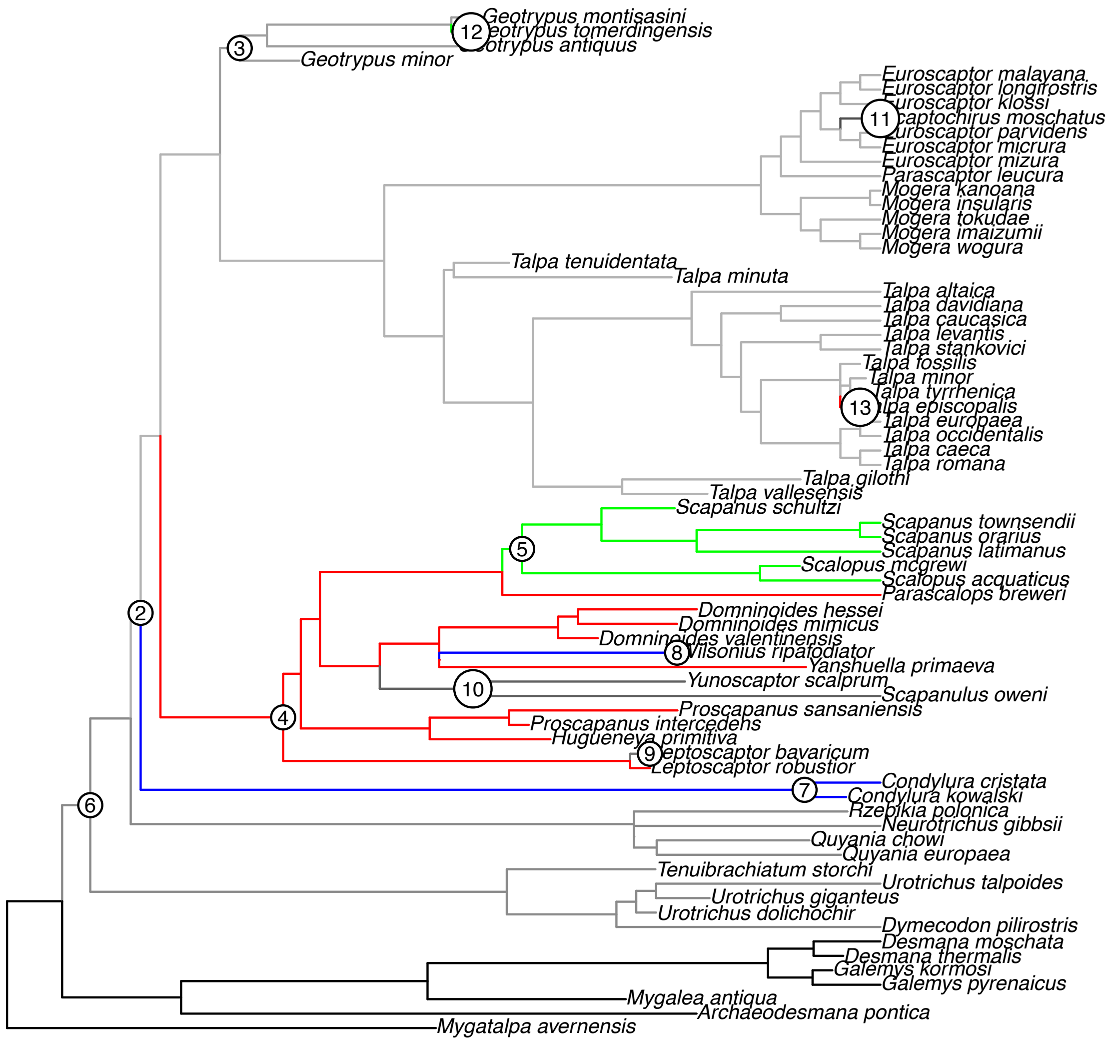

Figure 2.22. Plot of the "SURFACE" analysis on the humeral shape in different clades of Talpidae. The coloured branches represent convergence, while grey-scale indicates non-convergence. Numbers on branches indicate the order in which regime shifts were added during the forward phase.

Discussion

The shape analysis revealed a neat separation between the highly fossorial clades from the non-fossorial taxa. The humeral morphology shows dramatic changes shifting from the unspecialized slender from of the Uropsilinae to the highly specialized robust and round morphology of Talpini and Scalopini. The main modifications involved the anatomical regions directly related with the evolution of the fossorial lifestyle and digging performance (Gambaryan et al., 2003; Sanchez-Villagra et al., 2004; Sanchez-Villagra et al., 2006; Piras et al., 2012). The main derived features are: 1) the expansion of the teres tubercle where the Teres major and Latissimus dorsi muscles inserts; 2) the combined expansion of the pectoral ridge and of the minor tuberosity. During their expansion these two regions fuse and form the bicipital tunnel (see Chapter 5 for an extensive discussion on this autapomorphy). 3) The overall expansion of the distal region, here it is possible to observe an enlargement of the trochlear area and a modification of the medial epicondyle where the fossa for Flexor digitorum profundus tendon-muscle inserts (see Chapter 3 for an extensive discussion on the functional importance of this tendon-muscle). Along the PC3 was evident the differentiation of the *Geotrypus* spp., that show a peculiar humeral morphology by having a highly expanded pectoral ridge, a very reduced and pointed teres tubercle, a poorly developed lesser tuberosity and the presence of a marked bicipital notch. In this framework the *Geotrypus* spp. overall humeral morphology shows many primitive characters when compared with the other highly fossorial moles. The genus *Geotrypus* is considered by many authors to be basal to the Talpini clade (Sanchez-Villagra et al., 2004; Sanchez-Villagra et al., 2006; Schwermann and Martin, 2012; Ziegler, 2012).

The perMANOVA and perANOVA test revealed highly significant differences between clades. Differences in shape resulted to be significant even when taking into account the phylogeny, while the phylogenetic version of ANOVA on CS returned a non-significant result, suggesting a strong phylogenetic constraint on the moles humeral size. Both multivariate regression of shape on size and PGLS revealed a significant interaction, thus suggesting the presence of evolutionary allometry. However the separate per clade regressions revealed a significant interaction only for the Talpini and Scalopini clades. It is possible that evolutionary allometry significantly contributed to shape the humeral morphology only in the highly fossorial moles (see Chapter 4 for extensinve discussion about this topic). It is worth to note here how there was no interaction between shape and size in Desmaninae, despite their large size dispersion (see figure 2.17).

A neat positive shift in the humeral shape evolutionary rates was revealed in correspondence of the highly fossorial clades Talpini, Scalopini and Condylurini, while we found a slowdown in correspondence of Uropsilinae species. The disparity through time was lower than that expected under Brownian motion (negative MDI index), suggesting a slower mode of evolution (Slater et al., 2010). The negative significant correlation evidenced by the node height test also confirmed a slowdown in the shape evolutionary rates (Freckleton and Harvey, 2006; Slater et al., 2010, Slater and Pennell, 2013). We found a "kappa" value of 1.38 for the shape variables, according to Losos (2008) reported that value of "kappa" > 1 could be termed as "phylogenetic niche conservatism" (PNC; Harvey and Pagel, 1991). The existence of PNC suggests that some factor is causing closely related species to be more similar ecologically than would be expected by simple Brownian motion descent (Losos, 2008). PNC may occurs for two main reason: first, in the course of species proliferation, unused ecological space may be filled by members of the most ecologically similar species, which then diverge to become a distinct species. As a result, a tendency would exist for ecologically similar species to be closely related. This scenario has been elaborated by Price (1997) and Harvey and Rambaut (2000). Second, once the habitat is fully occupied, the presence of sympatric species, better adapted to using other aspects of the environment, may prevent a species, or its descendants, from departing from its ancestral niche (see also Lord et al., 1995; Patterson and Givnish, 2002). Habitat selection, in which members of a species prefer to remain in that part of the environment to which they are best adapted, reinforces this stabilizing selection (Ackerly, 2003). In other words, one would expect that related species should ecologically diverge through time. PNC is the observation that related species differ less ecologically than might be expected if ecological diversification had occurred in an unconstrained way. Our results strongly support this scenario. As described above the humeral morphology is strongly related to the digging performance and, indirectly, with lifestyle (Piras et al., 2012). Our results suggest that humeral morphology reached different functional optima early in Talpidae evolution (see also Piras et al., 2012) and, then, no significant changes occurred.

Finally we found true convergence between *Condylura* spp. and *Wilsonius ripafodiator*. The extant *Condylura cristata* is known to have a semi-acquatic lifestyle (Sanchez-Villagra et al., 2004), Hutchinson (1968) hypothesized a facultative semi-acquatic behavior for *Wilsonius*. A convergence between these two taxa could confirm the Hutchinson's hypothesis. We found convergence between the North-American and European Miocene Scalopini. Interpreting this evidence is challenging as it could reflect a common origin (shared ancestry) and similar ecological conditions as well. We also found convergence in the *Scapanus* and *Scalopus* spp. These two genera are easily distinguishable in their dentary features, but show closely resembling very robust humeri (Hutchinson, 1968).

The humerus proved to be one of the most interesting skeletal element in Talpidae. Our results showed how the humeral morphology is subject both to phylogenetic and adptive constraint. In the following chapters we will explore the potential of the humerus in order to understand how the fossoriality evolved among Talpidae.

CHAPTER III

STAIRWAY TO… UNDERGROUND

Testing convergence and parallelism in talpids humeral mechanical performance by means of Geometric Morphometrics and Finite Elements Analysis

Piras P., Sansalone G., Teresi L., Kotsakis T., Colangelo P., Loy A. 2012
Journal of Morphology, 273:696-711.

Introduction

Ever since Darwin (1859) the concept of adaptation has been a central topic in evolutionary biology. During the past thirty years it was the focus of many disputes (Gould and Lewontin, 1979) and of changes in semantics (Gould and Vrba, 1982). The term "adaptation" itself has many different definitions (Dobzhansky, 1956, 1970; Dobzhansky et al., 1968, Gould, 2002, among others). Patterns of shared adaptations among phylogenetically distant taxa are described in terms of either convergence or parallelism. Specifically, independently evolved similar character states could have originated through true adaptation (i.e. the function at the first appearance of a character and its current function coincide), exaptation (i.e. the current function is different from the original; Gould and Vrba, 1982), convergence (i.e. starting from different ancestral states, different taxa reach the same character state by means of opposite deviations relative to their original phenotypic states; Stayton, 2006) or parallelism (i.e. starting from different ancestral states, different taxa follow a parallel evolution toward the current phenotypic state by means of equal deviations relative to their original phenotypic states; Stayton, 2006).

A key aspect of these issues is to consider phylogenetic relationships as a central factor in explaining the above mentioned patterns. In some case, in fact, shared ancestry channels the phenotypes that, being adapted to a particular function, are positively selected (Revell et al., 2007).

Specific hypotheses about convergence and parallelism need specific tests that have been rarely applied in experimental studies (Stayton 2006, 2008; Revell et al., 2007; Adams and Collyer, 2009). Characters that are adapted to a particular function and are shared by different groups of taxa should be examined through their evolution, in order to assess the precise patterns underlying their evolutionary dynamics.

A caveat should be made here about the distinction between “true convergence” and “parallelism” (Stayton, 2006, fig. 3). In fact, while truly convergent pathways show opposite deviations from their starting points, parallel trajectories have equal deviations that unambiguously lead to the same current phenotypic state. For this reason, Stayton (2006) considered parallelism to be a special case within the broadly defined category of convergence (as in Simpson, 1961 and Gould, 2002).

As for the meaning of “adaptation” in biological structures, we adopt a narrow (and operative) definition, which is any inheritable trait that signifies a solution to a problem posed by environmental conditions and that appears simultaneously or soon after the new environmental condition sets in (after Arnold, 1994; cf. Gould and Vrba, 1982; Strömberg, 2006; Meloro et al., 2008; Raia et al., 2010; Piras et al., 2010). In this study, an example of adaptation is the complex architectural arrangement in the humerus of Talpidae, which is extremely well adapted to burrowing.

No other mammalian clade experienced such severe modifications in the humeral morphology as those observed in Talpoidea (including Proscalopidae, Talpidae and Dimylidae, families) in response to either fossorial (Talpidae) or aquatic (Dimylidae) adaptations (Reed, 1951). The lifestyle of the enigmatic clade Proscalopidae remains largely unknown.

This plastic phenotypic evolution represents a unique opportunity to study the dynamics of the adaptive process in different clades.

At present talpids are distributed in the Holartic ecozone. Modern talpids show a variety of lifestyles, from strictly subterranean, to semi-fossorial and semi-aquatic (Sánchez-Villagra et al., 2004, 2006). This distinction cannot easily be applied to extinct taxa. As many fossils were included in our analysis, we adopted a broader classification of lifestyle. Based on behavioural and ecological traits of extant species (thus avoiding circularity with humeral morphology) we divided extant taxa in complex tunnel diggers and non-complex tunnel diggers (see material and methods). Within Talpidae, the monophyletic clade Talpinae + *Condylura* includes exclusively complex tunnel digger species, while other complex tunnel digger taxa can be found in other branches on the Talpidae phylogeny (McKenna and Bell, 1997; Hutterer 2005). The strictly fossorial lifestyle is accompanied by modifications in the humerus but also (among other features) other skeletal modifications (carinate sternum, fused pelvis, etc), in visual performance, alteration of circadian rhythms, as well as in haemoglobin oxygen carrying capacity (Campbell et al., 2010). As fossils were included in phylogenetic comparative analyses, the use of morphological traits was the only way to determine different patterns of adaptation in a given clade. For this reason we analyzed the humeral morphology (described by means of Geometric Morphometrics) to estimate the mechanical performance (by means of Finite Element Analysis) in extant taxa Talpidae. We then assessed whether this performance was a good predictor of extant taxa lifestyle (ascertained through behavioural studies). Then, by means of specific comparative methods, we reconstructed the ancestral states of performance and lifestyle along the Talpidae phylogeny, including extinct taxa. We developed a specific strategy to describe the course of adaptation to digging in different clades, i.e. complex tunnel diggers belonging to Talpinae + *Condylura* clade and complex tunnel digger forms outside this clade. This allowed us to assess whether this course fits either convergence or parallelism. Moreover, we investigated whether the same sort of adaptive constraint affected complex tunnel diggers belonging to different clades in response to the same particular functional demand (intense digging). In fact, as pointed out by Schwenk (1995) and Gould (2002), adaptation to a particular physical environment requires specific performances that should not show broad ranges of variation. To answer this question, we examined how the evolutionary phenotypic rate of evolution was structured along talpids phylogeny, and if the phenotypic variance of complex tunnel diggers was significantly smaller than that of non complex tunnel diggers.

Finally, we also assessed if, (taking in to account their phylogenetic relationships), complex tunnel diggers belonging to different clades showed different humeral mechanical performances.

Our study was conducted at the genus level. According to Hutterer (2005) the family Talpidae includes about forty-two extant species, seventeen genera and three subfamilies, Talpinae, Desmaninae and Uropsilinae. Among the 17 extant genera, 12 of them are mono-specific (*Condylura*, *Parascalops*, *Scalopus*, *Scapanulus*, *Desmana*, *Galemys*, *Neurotrichus*, *Scaptonyx*, *Parascaptor*, *Scaptochirus*, *Dymecodon* and *Urotrichus*), while the remaining 5 genera (*Talpa*, *Scapanus*, *Euroscaptor*, *Mogera* and *Uropsilus*) include more than one species. Within the subfamily Talpinae the tribe Talpini includes strictly subterranean species, belonging to the polytypic genera *Talpa* (nine species), *Euroscaptor* (six species) and *Mogera* (eight species) and to the monotypic genera *Scaptochirus*, and *Parascaptor*.

More than one hundred extinct species of Talpidae belonging to 33 genera have been described to date. Talpidae diversity was higher in the past, especially in Europe (Mc Kenna and Bell, 1997; Ziegler, 2003; Loy et al., 2005).

There are no differences in lifestyles within the six extant polyspecific genera (Anthony, 1929; Stone, 1995; Loy, 2008; Kays and Wilson, 2009). Moreover, it is essential to note that humeral morphology of extinct species does not indicate the presence of intra-generic differences in their lifestyles as compared to their extant relatives. For instance, the humeral morphology of extinct species of genus *Talpa* (van Cleef-Roders and van den Hoek Ostende, 2001) suggests that all of them were well adapted to a subterranean lifestyle (i.e. complex tunnel diggers). This also applies to the four species of *Uropsilus* which show terrestrial lifestyles (i.e. they are non complex tunnel diggers), similar to soricid shrews, and to the three species of *Scapanus* that are almost exclusively fossorial, and so on. As no information on the behaviour and ecology of extinct species are available, we had to assume a similar pattern for intrageneric lifestyle diversity of extinct Talpidae. Therefore we assigned a unique lifestyle to extinct genera.

Material and Methods

Material

We digitized 19 landmarks and 31 semi-landmarks (Figure 3.1) on 32 humeri (one species for each genus) from published drawings and pictures in caudal norm, with the exception of *Talpa romana*, which was photographed by one of the authors (GS). All species were representative of the known extant genera of the family Talpidae (except the extant *Dymecodon, Parascaptor* and *Euroscaptor*) and of all extinct genera for which complete humeri were available in literature. Appendix I lists the genera and species as well as the primary literature references used for digitization.

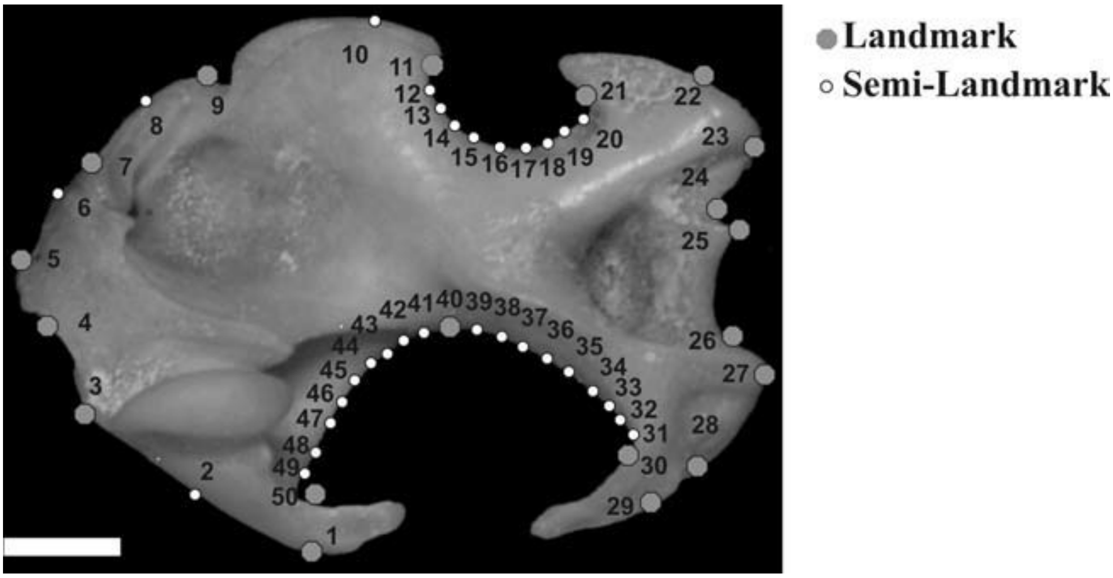

Figure 3.1. Landmarks digitized in humerus caudal norm. Landmark 1: lateral end of greater tuberosity; Semilandmark 2: articular facet for clavicula; landmark 3: proximal edge of the articular facet for clavicula; landmark 4: dorsal opening of the bicipital tunnel; landmark 5: proximal end of internal tuberosity; Semilandmark 6: medial lamina on the minor tuberosity; Landmark 7: edge of the medial lamina; Semilandmark 8: bicipital ridge; landmark 9: bicipital notch; Semilandmark 10: area of insertion of Teres maior and Latissimus dorsi muscles; landmarks 11 and 21: proximal and distal edges of the minor sulcus; Semilandmarks 12–20: internal surface of minor sulcus; landmarks 22 and 23: medial epicondyle; landmarks 24, 25, and 26: trochlea; landmarks 27, 28, and 29: lateral epicondyle; landmarks 30, 40, and 50; Semilandmarks 31–39 and 41–49: internal surface of greater sulcus. Scale bar equals 5 mm.

Geometric Morphometrics

Generalized Procrustes Analysis (GPA; Bookstein, 1991, Godall, 1991) implemented in tpsRelw software (Rohlf, 2006) was used to analyze different shapes among taxa. GPA rotates, aligns and scales landmark configurations to the unit centroid size (CS = the square root of the sum of squared distances of a set of landmarks from their centroid; Bookstein, 1986). Rotation of the scaled and translated landmark sets is achieved by comparison with a reference configuration (usually the first specimen in the dataset). Once rotation has been completed, a mean shape is calculated and the rotation process is repeated using the mean shape as the reference configuration for the sample (including the reference-specimen configuration). This mean-shape/rotation procedure is iterated in order to minimize rotation differences between subsequent iterations through a least-square procedure (Slice and Rohlf, 1990). The residual differences are to be ascribed to real shape differences plus measurement error. Principal component analysis (PCA) was performed on the shape residuals (Procrustes coordinates) to find orthogonal axes of maximum variation. This is a common procedure in geometric morphometric (GM) studies (Adams et al., 2004; Claude, 2008).

Semi-landmarks differ from landmarks because in addition to translating, scaling, and rotating landmarks optimally, these points are slid along the outline curve until they match as closely as possible the positions of the corresponding points along an outline in a reference configuration (Adams et al., 2004; Perez et al., 2006). Semi-landmarks are useful to depict the shape of curved lines where landmarks cannot be detected. Semi-landmarks assume the curves or contours are homologous from one specimen to the next, whereas individual points need not to be (Bookstein et al., 2002). According to the software requirements, a separate sliding semi-landmark file was prepared for tpsRelw to distinguish landmarks from semi-landmarks. tpsRelw performs the Relative Warp Analysis using the sliding-landmark information during computation (see software details at http://life.bio.sunysb.edu/morph/). Minimization of Bending Energy was used for semi-landmarks alignment.

Talpidae phylogeny

Building a synthetic phylogeny of Talpidae at the genus level was challenging. Some phylogenies of Talpidae were published in the past two decades (Shinoara et al. 2003, 2004; Cabria et al. 2006; Sánchez-Villagra et al., 2006; Colangelo et al., 2010).

Our efforts concentrated on exploring the literature regarding i) the taxonomic validity of all known extant and extinct genera; ii) their stratigraphic range; iii) the phylogenetic position of the genera recognized as valid. The resulting phylogenetic tree including 50 genera is shown in Appendix 2. In Figure 3.2 the phylogenetic tree (built in Mesquite 2.73) containing only the taxa used for our analyses is reproduced. Online Appendix III summarizes the literature *corpus* upon which we built the topology, branch length information for terminal taxa, and inner nodes. For extant taxa we followed the morphological cladistic analysis of Sánchez-Villagra et al. (2006) that is the sole phylogeny including all extant taxa, while for extinct taxa we used paleontological literature on their stratigraphic range and phylogenetic position.

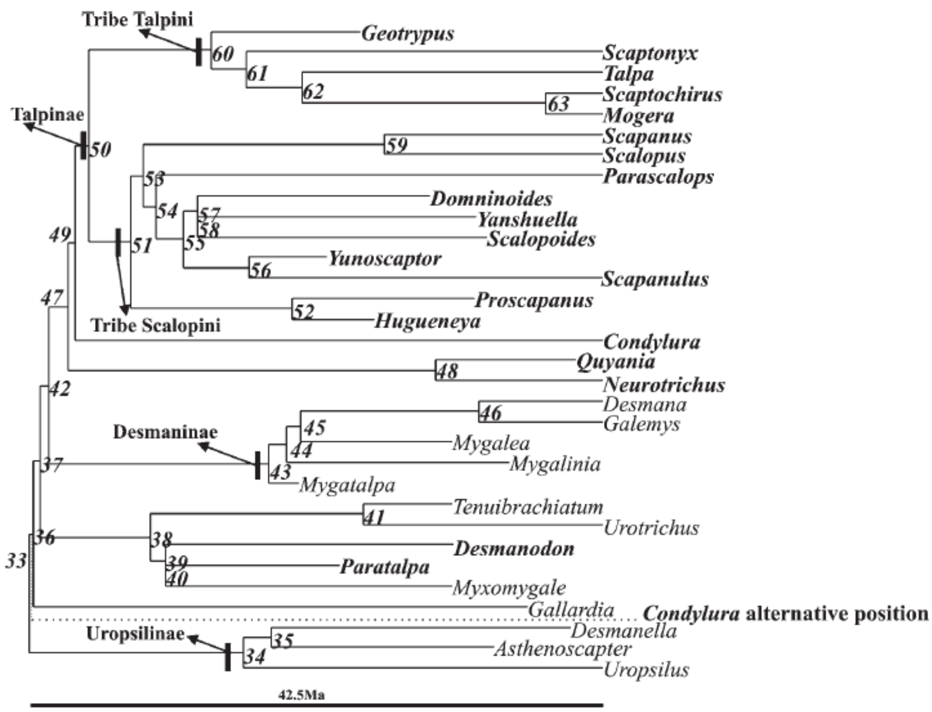

Figure 3.2. Phylogenetic tree containing only taxa used for comparative analyses. Branch lengths are proportional to geological time. Nodes labels are shown. See text and Appendix 1 and III for details about primary literature used for both full topology and ranges of taxa. In bold: complex tunnel diggers.

As no cladistic analysis was available for extinct taxa, we positioned the latter on the basis of qualitative considerations made from the various authors in literature. Polytomies in our tree represent divergent opinions among various authors.

We acknowledge that this approach has potential limitations due to uncertain affinities. However, we placed the taxa in agreement with the most robust and well supported evidence in literature. For instance, whenever possible, we used information on cranial and dental characters as reported by various authors.

One major difference between the topology of extant taxa adopted here and other previously published molecular phylogenies (Shinoara et al. 2003, 2004; Cabria et al. 2006) is the position of the genus *Condylura* which in the topology used here is a sister taxon of all Talpinae, whereas in the other topologies it is (unambiguously) the sister taxon of all Talpidae except Uropsilinae.

In order to test the impact of *Condylura* position, analyses were performed by taking into account both the main topology adopted here and the alternative topology suggested by other authors. Further details can be found in Appendix 1.

Finite element analysis-Humeral geometry reconstruction

In order to reconstruct humeral geometry, we used Procrustes coordinates as control points to generate a smooth, closed contour by spline approximation using a Matlab routine. A solid geometry was built in order to study the structural mechanics by means of Finite Element Analysis (FEA). FEA is a mathematical framework that is becoming popular within morphologists and bio mechanists in the study of the mechanical behaviour of biological structures (Rayfield, 2007, 2011). It provides a quantitative evaluation of the displacements within a structure with given material properties under appropriate applied loads and boundary conditions that mimic a particular functional or behavioural scenario.

These displacements are then used to calculate the stress and strain state, thus providing a thorough characterization of the mechanical state of the structure (see also Richmond et al., 2005; Zienkiewicz et al., 2005). A similar procedure, i.e. creating FE models starting from Geometric Morphometrics data, was successfully applied by Young et al. (2010), Pierce et al. (2008, 2009a, 2009b) and Stayton (2009) among others.

It is worth noting that FEA is used in a comparative fashion rather than in a validative one. In fact, one of the key questions in modern biologically-oriented FE studies is the reliability of simulation in comparison to real experimental studies. Many efforts (Ross et al., 2005; Strait et al. 2005; Kupczik et al., 2007; Farke, 2008; Gröning et al., 2009; Rayfield, 2011) focused on this problem demostrating that the incorporation of more precise approximations in FE simulations (anisotropic material properties, muscle activation data, etc.) improves the correlation between these simulations and the real experimental results. Aiming to compare FE models in the context of their phylogenetic relationships, in this study we applied the same approximations for all models. That is, isotropic material properties corresponding to haversian bone (Young modulus: 10 GPa, Poisson's ratio: 0.41, Rayfield et al., 2001) were applied to all FE models.

Based on the reconstructed 2D contours, 3D volumes were generated by extruding the 2D geometries along the orthogonal direction; the (homogeneous) thickness was chosen according to the maximum thickness measured at the humeral shaft. Unfortunately such a measure was only available for 8 of the 32 Operational Taxonomic Units (= OTUs; *Desmanella engesseri*, *Myxomygale gracilis*, *Mygalea magna*, *Talpa romana*, *Scalopoides sp.*, *Asthenoscapter meini*, *Mygatalpa arvernensis* and *Galemys pyrenaicus*) in our sample. In order to estimate humeral thickness for the other 24 OTUs, a linear regression between thickness (as dependent) and the maximum width of the proximal region (without condyles; as independent) were performed on the 8 OTUs for which both measures were available. As a significant correlation was found (thickness = maximum width*0.388+0.70; $p \ll 0.001$, $r = 0.95$). The regression coefficients were used to estimate the thickness in the other taxa. The 8 OTUs used in the regression encompass morphological extremes of the humeral morphology, thereby providing reasonably precise estimates. Given that the models were scaled to the same centroid size, thickness was also scaled according to regression coefficients.

Variations in thickness along each humerus were disregarded in the simulations. While this represents a simplification of humeral shape in lateral view, this allows a simpler Finite Element Analysis calculation in a comparative fashion. Moreover, we felt that taking into account thickness, even if homogeneous (statistically assessed, however), would have allows a more precise evaluation of solid mechanical behaviour than completely ignoring this dimension.

Thus, our 3D humerus appears to be an irregular cylindrical body with a smooth, curvilinear contour, as in Fig. 3.3A.

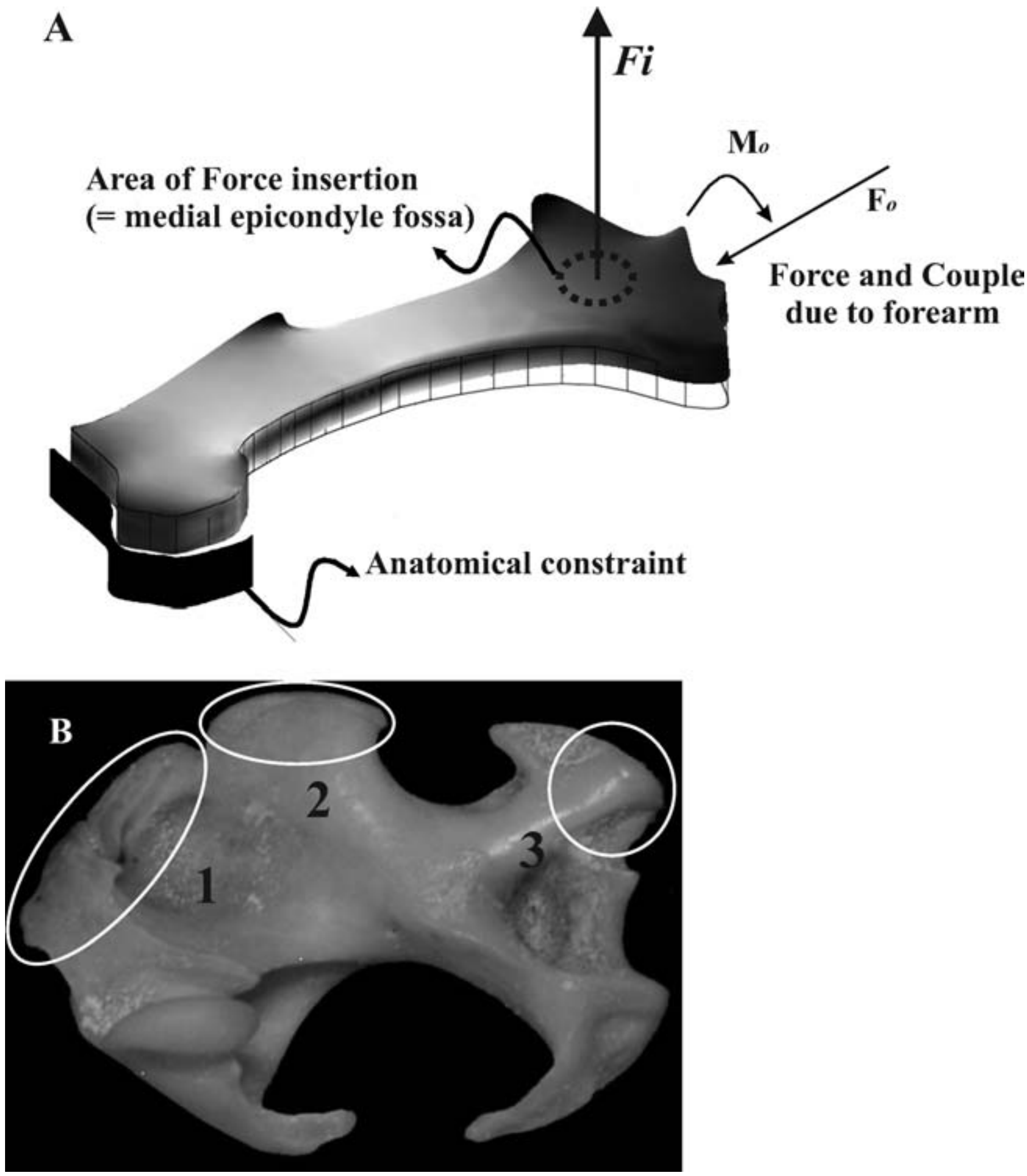

Figure 3.3. (A) Finite Element Model resulting from shape data and thickness estimation; (B) insertion areas of the main muscles involved in burrowing activity are indicated on the humeral morphology. 1: Pectoral ridge, where Pectoralis major and Subscapularis muscles are inserted. 2: Teres tubercle, into which the tendons of Teres major and Latissimus dorsi muscles are inserted. 3: Medial epicondyle, on it's posterior side is located the fossa where the tendon-muscle Flexor digitorum profundus arises.

Finite element analysis-Boundaries anatomy

To assign anatomically-based constraints on the humerus we considered the area corresponding to the clavicular facet (landmarks 1-3), that is the area lodging the

articulation between the humerus and the clavicle, and the area corresponding to the pectoral ridge (landmarks 4-9). In this latter the powerful muscles of the chest (Fig. 3.3B) perform two separate functions. First, they provide the necessary strength for the lateral thrust during digging. Secondly, they maintain the humerus in the correct anatomical position and prevent displacement. In fact, the humerus is in a deep position near the chest and is covered by pectoral muscles (Freeman, 1886).
An elastic constraint was applied rather than a fixed one in order to better mimic the compliance of the joint that is typical of moles.

Finite element analysis-Loadings

To evaluate the stress and strain states on the humerus we applied pressure loads, i.e. a force per unit area, acting in the orthogonal direction to the base (defined as the z direction), in the middle of the distal part of the humerus. This region corresponds to the trochlear area where the ulna is articulated. This simulated the same experimental anatomical design made by Scott and Richardson (2005), see Fig. 3.4A.
To test how different geometries react to the *same* loading the same resultant force Fi was applied to all specimens (Fi=22 N measured for *Talpa europaea*, a highly fossorial species (Gambaryan et al., 2003).
For each specimen i, the applied load s_i was computed as $s_i = Fi/A_i$, where A_i is the area of the medial epicondyle fossa. This area was used because it hosts the origin of the tendon-muscle *Flexor digitorum profundus* that counteracts the force generated by the digging muscles in order to prevent humerus displacement and pronation. In fact, the average pressure generated by the spade-like hands of the European mole *Talpa europaea* was evaluated in 2-3 kg, while the strength of the tendon of *M. flexor digitorum profundus* was estimated in 4-5 kg (Gambaryan et al., 2003). This area was

evaluated by measuring the medial epicondyle fossa on the 12/32 OTUs (*Myxomygale gracilis*, *Paratalpa brachychir*, *Geotrypus aff. montisasini*, *Scaptochirus primaevus*, *Desmanodon antiquus*, *Quyania chowi*, *Urotrichus talpoides*, *Scalopoides sp.*, *Asthenoscapter meini*, *Desmanella engesseri*, *Mygalea magna* and *Talpa romana*) for which medial epicondyle fossa pictures were available to measure. To estimate the fossa's diameter for taxa for which no humeral cranial norm pictures were available, a linear regression was performed between the fossa's diameter (as dependent) and the maximum width of the proximal region without condyles (as independent). As expected, this regression was significant (fossa diameter = maximum width*0.27+0.05; $p = 0.016$; $r = 0.65$). In more specialized talpids (i.e. highly fossorial species that are complex tunnel diggers), the diameter of the fossa becomes larger. The regression coefficients were used to estimate the fossa diameter for the other 20 taxa. Again, the 12 taxa used to estimate the regression coefficients encompass the morphological extremes of the humeral morphology of Talpidae.

In order to assess the mechanical response of the humerus, a two step procedure was followed. First, a one dimensional model of the forelimb was used to estimate the mechanical actions involved in digging. Then, a 3D model of the humerus was used for a more detailed stress analysis. Fig. 3.4A shows the one dimensional model of forces acting on the forelimb during digging (Scott and Richardson, 2005), with the ulna, the radius and the manus considered as a single complex. The resulting scheme of the levers mechanism consists of five parts (Fig. 3.4B, C, D and E): three levers – i.e. the scapula, the humerus, the forearm (the complex ulna+radius+manus) and two joints – i.e. the shoulder (the scapula-humerus joint) and the elbow (the humerus-forearm joint). The main actions on the levers mechanism are the force F_o, the reaction to the digging force exerted by the manus on the soil, and the force F_i, due to muscle contraction; in particular, F_i represents the resultant force exerted on the humerus by the *M. teres major* (operating very close to the elbow), *M. pectoralis*, *M. latissimus dorsi* and *M. subscapularis* (Gambarian et al., 2003).

Two further assumptions were made about the levers mechanism under this configuration: 1) the shoulder acts as a hinge, hence torque is zero and 2) the rotation with respect to the elbow is hampered by muscles, thus, a torque is present, see Fig. 3.4D and E. These assumptions imply that the balance of torques yield for the humerus is $L_i*F_i=M_o$, and for the forearm is $M_o=L_o*F_o$; it follows a simple relation for the muscle force and digging force: $F_o=L_i/L_o * F_i$.

L_0 represents the forearm length; in the model such a measure were estimated as twice the humeral length ($L_0 = L_i$ x 2). This arrangement was necessary because no forearm measurements for the majority of the extant taxa and for all of the extinct taxa were found in literature. The only extant OTUs for which this measure was available were *Talpa*, *Scalopus*, *Desmana* and *Galemys*. Basing on these four OTUs a L_0/L_I ratio of 1.8 was obtained (non complex tunnel diggers, walking species) and of 2.6 (complex tunnel diggers). Finite elements analyses were carried out with both ratios and an ANOVA analysis was performed on von Mises stress and elastic Energy so obtained with ratio category as factor. The ANOVA did not show significant statistical differences between structural values extracted from the two different ratios (Tukey's test p-value=0.99), so the ratio L_0/L_I =2 was used for all taxa. Forces F_o and F_i, and torque M_o were replaced by boundary loads for the unit area, acting on appropriately chosen parts of the boundary. In particular, the muscle force F_i was replaced by a pressure load with intensity $s_i=F_i/A_i$, where A_i is the area of the insertion zone, acting on the upper surface, as outlined above (black disk on Fig. 3.4B); the actions due to the force F_o and the torque M_o were replaced by a traction s_o acting on a portion of the mantle (grey disk; Fig. 4B, right), having the same resultant F_o and torque M_o. The shoulder was modelled as a compliant elastic, thus the boundary condition was assumed to be a surface traction s_k proportional to the boundary displacement: $s_k = K*u$, with K being the stiffness of the constraint and u being the displacement field.

Each specimen underwent the same numerical experiment (loading and boundary conditions) using Comsol Multiphsics software; due to the morphological differences, many different results were obtained. The mechanical response of different humeri was assessed by evaluating three global quantities. Let S and E be the stress and strain tensor, respectively, with components S_{ij}, E_{ij} :

Stored Elastic energy

$$E = \frac{1}{Vol(B)} \int_B \tfrac{1}{2} S \bullet E dV$$

Mean Von Mises stress or, equivalent tensile stress, a common measure of the yielding characteristics of materials

$$VM\_m = \frac{1}{Vol(B)} \int_B [S_{11}^2 + S_{22}^2 + S_{33}^2 - S_{11}S_{22} - S_{33}S_{22} - S_{11}S_{33} + 3(S_{12}^2 + S_{23}^2 + S_{13}^2)]^{1/2} dV$$

Mean vertical displacement of the bottom surface

$$W\_m = \frac{1}{Area(S)} \int_S w \, dA$$

These performance variables were subjected to a Principal Component Analysis in order to extract the axes summarizing the global mechanical behaviour of different humeri to be used in successive comparative analyses. The first principal component scores derived from PCA on the three performance variables were used as "stress data" in successive comparative analyses.

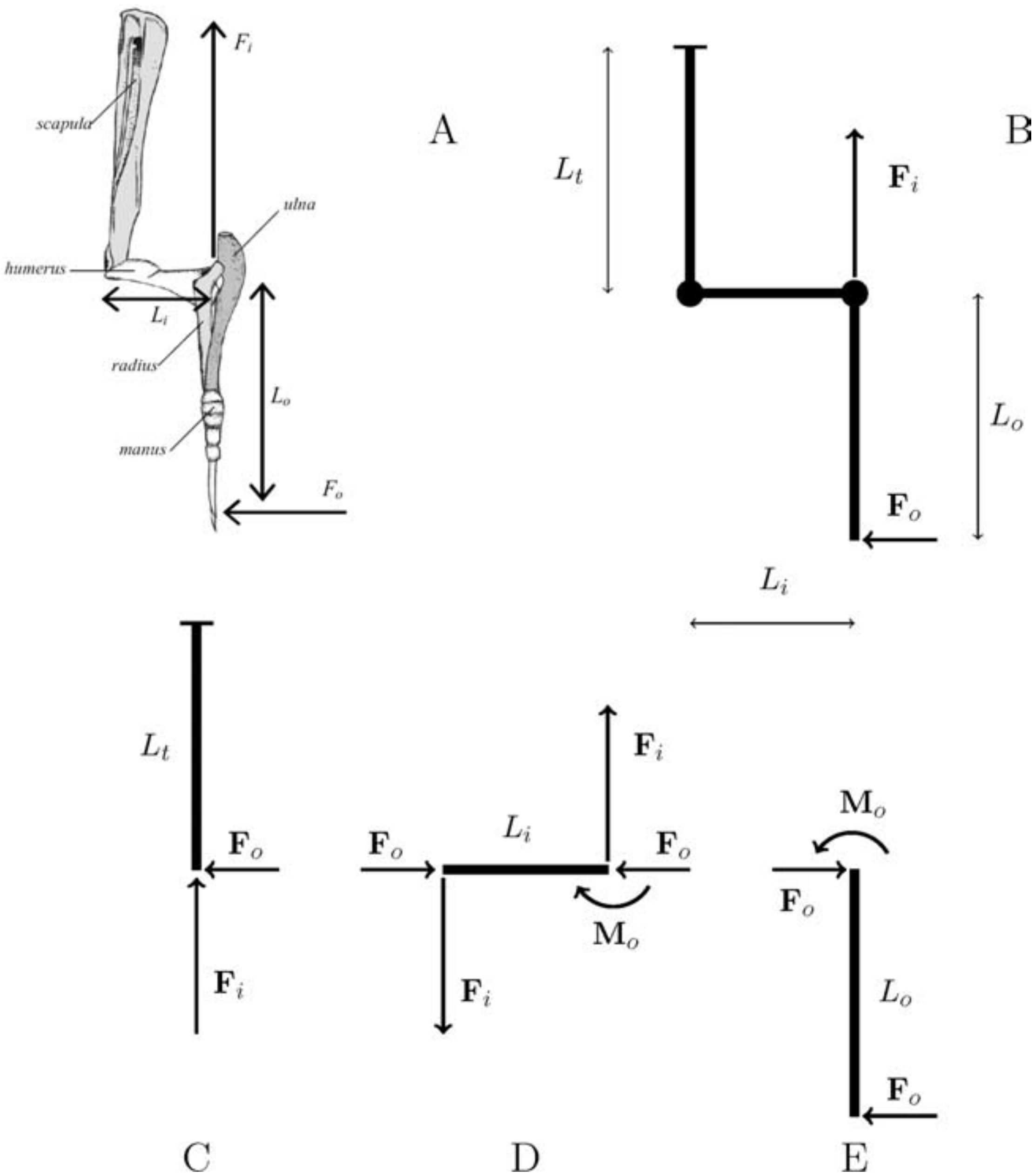

Figure 3.4. (A) Anatomical scheme of talpids forelimb. Redrawn from Scott and

Richardson (2005). (B) One-dimensional scheme illustrating the force acting on the whole model. (C–E) Forces acting on single elements of the whole model.

Lifestyle assignment and assumption validation

In order to circumvent circularity, any interference on the lifestyle of extinct and extant species from humeral morphology was avoided. The lifestyle of each extant species included in the clade Talpidae was derived from their known behavioral ecology (Table 3.1).

Taxa	Status	Lifestyle	References
Asthenoscapter meini	Extinct	NA	
Condylura cristata	Extant	1	Kays and Wilson (2009); Anthony (1929); Hickman (1983)
Desmana moschata	Extant	0	Tsytsulina et al. (2008); Stone (1995)
Desmanella engesseri	Extinct	NA	
Desmanodon antiquus	Extinct	NA	
Domninoides valentinensis	Extinct	NA	
Gaillardia thomsoni	Extinct	NA	
Galemys pyrenaicus	Extant	0	Cabral et al. (2005)
Geotrypus aff. montisasini	Extinct	NA	
Hugueneya aff. primitiva	Extinct	NA	
Mogera kanoana	Extant	1	Kawada et al. (2007)
Mygalea magna	Extinct	NA	
Mygalinia hungarica	Extinct	NA	
Mygatalpa arvernensis	Extinct	NA	
Myxomigale gracilis	Extinct	NA	
Neurotrichus gibbsii	Extant	1	Kays and Wilson (2009); Campbell and Hochachka (2000)
Parascalops breweri	Extant	1	Kays and Wilson (2009)
Paratalpa brachychir	Extinct	NA	
Proscapanus sp.	Extinct	NA	
Quyania chowi	Extinct	NA	
Scalopoides sp.	Extinct	NA	
Scalopus aquaticus	Extant	1	Edwards (1937)
Scapanulus oweni	Extant	1	Smith and Xie (2008)
Scapanus latimanus	Extant	1	Kays and Wilson (2009)
Scaptochirus primaevus	Extant	1	Smith and Xie (2008)
Scaptonyx fusicaudus	Extant	1	Chiozza (2008)
Talpa romana	Extant	1	Loy (2008)
Tenuibrachiatum storchi	Extinct	NA	
Uropsilus gracilis	Extant	0	Smith and Xie (2008)
Urotrichus talpoides	Extant	0	Abe and Ishii (2008)
Yanshuella primaeva	Extinct	NA	
Yunoscaptor scalprum	Extinct	NA	

0 = non-complex tunnel digger; 1 = complex tunnel digger; NA = Not applicable.

Table 3.1. Reference used for lifestyle assignment in extant taxa and extinct/extant status.

The specific interest was in the general burrowing performance rather than in other features, such as time spent underground, life cycle, habitat, or foraging. In order to distinguish taxa able to dig complex tunnel systems extant taxa were subdivided in two groups, "complex tunnel digger" (categorized as 1) and "non complex tunnel digger" (categorized as 0). We acknowledge that our categorization was rather broad, but dealing with extinct forms highly partitioned lifestyle subdivisions were not recommended, as extinct forms could had lifestyles with no extant homologous.

Table 1 reports the literature from where this distinction was inferred. For example, *Condylura cristata* (a semi-aquatic/semi-fossorial North-American species) was scored as 1 because it is able to burrow a *well developed* tunnel system similar to *Scalopus aquaticus*, a highly fossorial species, (Anthony, 1929; Hickman, 1983; Kays and Wilson, 2009). However, *Desmana moschata* (a semi-aquatic species from Russia) was scored as 0 because it is only able to dig, at the very best, a very short and simple tunnel (Stone, 1995). As mentioned in the Introduction, a broader classification was adopted in this study compared to more detailed subdivisions proposed in literature (semi-aquatic, semi-fossorial, subterranean, hypogeal, fully fossorial, etc.). Some taxa, such as those reported by Sánchez-Villagra et al. (2006) have lifestyles that are difficult to interpret e.g. *Scaptonyx*, considered "semi-fossorial" (Lunde et al., 2003) or even *Condylura* that, despite its evident fossorial adaptations is often found on the ground or in water (Hickman, 1983). Moreover, *Neurotrichus gibbsii* "although structurally less specialized for subterranean existence than other North American moles (Reed 1951), excavates *extensive* shallow underground galleries" (Campbell and Hochachka, 2000; p.578). On the other hand, *Urotrichus* as reported by Stone (1995, p.57) "…burrows just beneath the surface but has also been recorded foraging on the surface and even observed to climb low bushes". This taxon was then scored as 0, even if the same results were obtained when repeating our analyses by assigning to it the state "1".

In order to assign a lifestyle to the extinct taxa, a penalized Maximum Likelihood logistic regression was performed between stress data (as independent) and the lifestyle category (as dependent) on extant taxa solely. The coefficients of this regression were then used to estimate the lifestyle of extinct forms starting from their measured mechanical stress. State 1 was assigned to all taxa with predicted probabilities larger that 0.5 and state 0 for those having predicted probabilities smaller than 0.5. To account for covariance among observations due to phylogeny the logistic regression described above was performed in a comparative fashion using the Plogreg.M matlab routine (for technical details see Ives and Garland, 2010).

Phylogenetic signal and ancestral states reconstruction

A strategy similar to that used by Jones and Goswami (2010) was adopted to evaluate the amount of phylogenetic signal in humeral shape. Shape data being multivariate, Procrustes (Euclidean) distance matrix of shape data were correlated with the patristic distance matrix computed on the phylogeny presented above by means of Mantel test (using mantel.test function available in R package "ape").

Lifestyle was coded as a binary trait. In order to assess if lifestyle exhibits a phylogenetic signal, the new metric (*D*) for binary traits proposed by Fritz and Purvis (2010) was adopted, using "phylo.d" function available in R package "CAIC".

With regard to mechanical performance, the phylogenetic signal was assessed using the stress data as defined above. Several evolutionary models were tested using the "fitcontinuous" function in "geiger" R package (Harmon et al., 2008). This approach is only possible for univariate traits. The six possible models are Brownian motion, Ornstein-Uhlenbeck, Pagel's lambda, Pagel's kappa, Pagel's delta, ACDC model and white noise model when no phylogenetic signal is found for the trait. For details and model specifications see Harmon et al. (2009). The best model was chosen on the basis of Akaike Information Criterion (AIC). The original tree was transformed according to the parameter of the best model and on that transformed tree, a maximum likelihood optimization for stress data was performed in order to infer the ancestral character states for internal nodes. Coefficients of logistic regression, as described above, were then used to assign a lifestyle probability (from 0 to 1) to any node occurring in the tree, starting from their estimated stress value.

Testing convergence and parallelism: Evolutionary rates and ancestor-descendant trajectories

When testing for adaptational constraint, convergence or parallelism, three aspects of phenotypic evolution should be taken into account. First, if strong functional constraints due to a particular adaptation (complex tunnel digging) characterize a given clade (Talpinae + *Condylura*) including taxa sharing the same phenotypic state, a slowdown in rates of phenotypic evolution is expected in correspondence of their most recent common ancestor (MRCA). This means that, once a given phenotypic state has been reached, a character does not experience any significant additional change.

Secondly, if other taxa outside that clade show a similar adaptation, it must be proved that they reached their phenotypic condition by either convergence or parallelism. Even if this aspect seems trivial when considering adaptation to a particular lifestyle (such as fossoriality), this hypothesis deserves a specific statistical treatment.

Thirdly, as discussed in the Introduction, the variance of all taxa characterized by the same phenotypic state adapted to the function under study (humeral adaptation to burrowing) is expected to be significantly smaller than those taxa not sharing that adaptation. This allows to test if the adaptation to a particular function channels phenotypes (even in distantly related taxa), without allowing significant deviations from mean relatively to phenotypes not adapted to that function.

Evaluating evolutionary rates for measured traits is challenging. This topic has received particular attention in recent years and different methods were proposed (Schluter, 2000; Losos and Miles, 2002; Glor, 2010; Losos and Mahler, 2010; Mahler et al., 2010; Slater et al., 2010). O'Meara (2006), Thomas et al. (2006) and Revell (2008) proposed very similar methods for fitting two or more shifts in the evolutionary rates of continuous character evolution in *a priori* defined clades of a given phylogenetic tree. However, there is no reason to think that a major shift in the rate of morphological evolution should coincides with the node corresponding to the MRCA of an *a priori* defined groups. Following these considerations we adopted a different approach. We applied "evol.rate.mcmc" function in the R package "phytools" (Revell, 2011; Revell et al., 2011). This function looks for the major shift (acceleration or deceleration) in the phylogenetic tree for a univariate trait, *without assuming* any *a priori* defined group. This ensures that the largest shift (characterized by an increasing or decreasing rate) will only be found starting from the data and the phylogeny. The PC1 scores extracted from the stress variables were used as a continuous trait. This allowed highlighting how changes in rate of phenotypic evolution were linked to digging mechanical stress.

Once the major shift in rates of performance evolution on the tree are estimated, the ancestor-descendant phenotypic trajectories for the complex tunnel diggers in different clades can be calculated, i.e. those belonging to Talpinae + *Condylura* clade and those outside this clade. In order to track the course of evolution of fossoriality performance in different groups, we contrasted the evolutionary pathways of stress data of each group (starting from MRCAs of all OTUs of each group, up to the observed OTUs values) *versus* the corresponding nodes and OTUs depth (age in our case). Given *m* groups, *m* separate linear regressions were performed between the age of nodes and OTUs (selected as outlined above) *versus* their corresponding stress data. Fig. 3.5 shows an example of convergence of a single phenotypic trait in an ancestor-descendant morphospace.

The permutation procedure described in Adams and Collyer (2009), and Piras et al. (2010, 2011) was applied in order to assess whether the regression trajectories were convergent, parallel or divergent. This strategy is based on the computation of predicted values of *y* (i.e. stress data) at given small (i.e. oldest ancestral state age) and large (i.e. extant age) values of *x* (i.e. age). This way it was possible to assess whether the "fossoriality performance" between taxa belonging to different clades pointed toward a common value, thus suggesting a common optimum for the adaptive trait under study. Stayton (2008) proposed different methods to measure convergence in a given phylogenetic tree and a set of traits. These methods are variously related one to each other and measure the overall convergence in the whole phylogeny. It is argued here that the consideration of specific groups requires a different strategy, i.e. that similar to the Multidimensional Convergence Index proposed by Stayton (2006), based on the comparisons between sister taxa of putatively convergent taxa. However, we argue that once two taxa diverged from their MRCA, their evolution is formally *independent* and it makes little sense to consider the deviation of putatively convergent taxa from their *sister* taxa. On the contrary, this comparison should be made taking into account the *ancestral node values*. Taking into account deviations of nodes (including OTUs) in comparison to their direct ancestors is equivalent to perform a regression between nodes depth (including OTUs) and their phenotypes. Being based on the ancestral states reconstruction and topology, this procedure accounts for shared ancestry among OTUs. When the two groups under study are monophyletic, there is no ambiguity in choosing the nodes from where their phylogenetic phenotypic trajectories start. These nodes are just the two MRCAs of all of the taxa that belong to the two groups. A problem in interpretation arises if one group is monophyletic and the other is para- or polyphyletic (as with our case). In fact, for a para- (or poly-)-phyletic group, the MRCAs could reach the tree root. If the aim is to test evolutionary convergence or parallelism using phylogenetic phenotypic trajectories (when moving back towards the tree root), the ancestor estimates become more and more similar for any set of related taxa on the phylogeny. Thus, vector comparisons quite deep in the phylogeny may be spurious, depending on the ancestral state estimation approach. For this reason the Talpinae + *Condylura* (monophyletic) trajectory in Fig. 3.2 was started from node 49, i.e. their MRCA, while for complex tunnel diggers outside this clade (a polyphyletic group) it was necessary to start the trajectory from their MRCA more deeply in the tree (i.e. node 36 in Fig. 3.2). Obviously, different phylogenetic hypotheses could change some of the conclusions, because ancestral state optimizations, and consequently the estimates of phylogenetic phenotypic trajectories, are strongly dependent on the input topology. In fact, as mentioned in the "Talpidae phylogeny" section, this analysis was tentatively repeated by moving *Condylura* as basal to all Talpidae, with the exception of *Uropsilus*.

To evaluate variances a Levene test was performed on stress data (PC1) between non complex tunnel diggers *vs*. complex tunnel diggers pooled together (Talpinae + *Condylura* and other complex tunnel diggers forms outside this clade) in order to test whether the adaptation under study significantly constrains phenotypic variance relatively to non- complex tunnel diggers forms.

Standard and phylogenetic ANOVA and MANOVA

To test whether shapes and mechanical traits differed among complex tunnel digger taxa belonging to different clades, ANOVA and MANOVA were performed respectively on stress and shape data (all PCs explaining at least 95% of total variance) on complex tunnel digger taxa (i.e. those showing predicted probabilities of logistic regression higher than 0.5) belonging to the two groups as defined above (one monophyletic and one polyphyletic). These analyses were carried out both in their standard versions and in their comparative version (using “phy.anova” and “phy.manova” function implemented in GEIGER package, Harmon et al., 2008). They allowed to evaluate if differences in shape or performance were statistically supported even taking into account the phenotypic channelling due to shared ancestry.

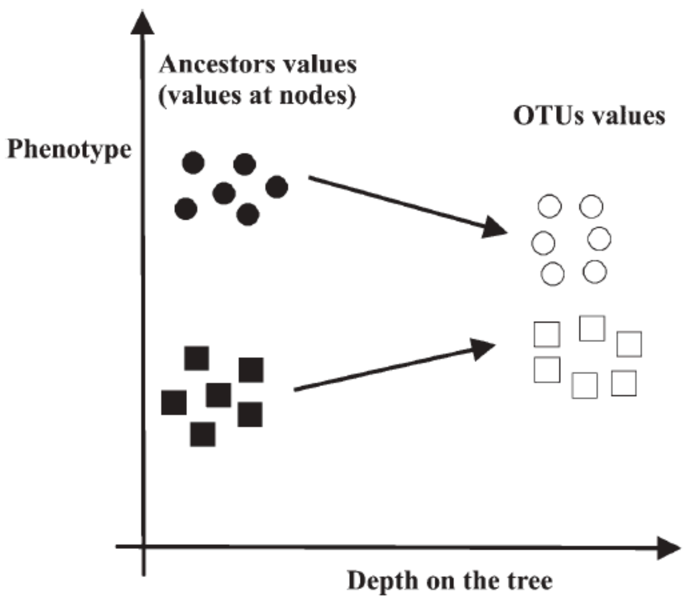

Figure 3.5. Hypothetical convergent phylogenetic phenotypic trajectories.

Results

Geometric morphometrics

Fig. 3.6 shows the deformation grids associated to the first two PCs, which explain about 75% of total variance. Points dimensions were set proportional to humeral size. Taxa on the negative PC1 extreme are characterized by a robust and wide humerus, with a huge expansion of the pectoral ridge and the greater tuberosity close to the proximal region. Teres major tubercle surface is also well developed and thick. Such morphology is present in the most specialized forms (i.e. *Talpa*, *Mogera*, *Scapanus*) classified as complex tunnel diggers. OTUs at the positive PC1 extreme are characterized by a more slender humerus, with the pectoral ridge heavily reduced, the greater tuberosity and the Teres major tubercle less developed and having a laminar aspect. This morphology is distinctive of the less specialized forms (i.e. *Asthenoscapter*, *Desmanella*), classified as non complex tunnel diggers. At the positive PC2 extreme the humerus proximal region is well developed but the minor and greater *sulcus* presents an elliptical shape. Such morphology belongs to the highly specialized forms (i.e. *Geotrypus*, *Scaptonyx*) classified as complex tunnel diggers. At negative values of PC2 the same region becomes less developed, the *Teres major* tubercle has a laminar aspect and it is placed near the middle of the humerus shaft. the pectoral ridge is reduced, as well as the greater tuberosity. This morphology corresponds to the less specialized forms (i.e. *Galemys*), classified as non complex tunnel diggers. The regression between shape and size returned non significant results (*p*-value: 0.38), suggesting that the lifestyle, as indicated by humeral shape modifications, is not associated to size variation. In fact, both small and large sized species can be found in both complex and non complex tunnel diggers forms.

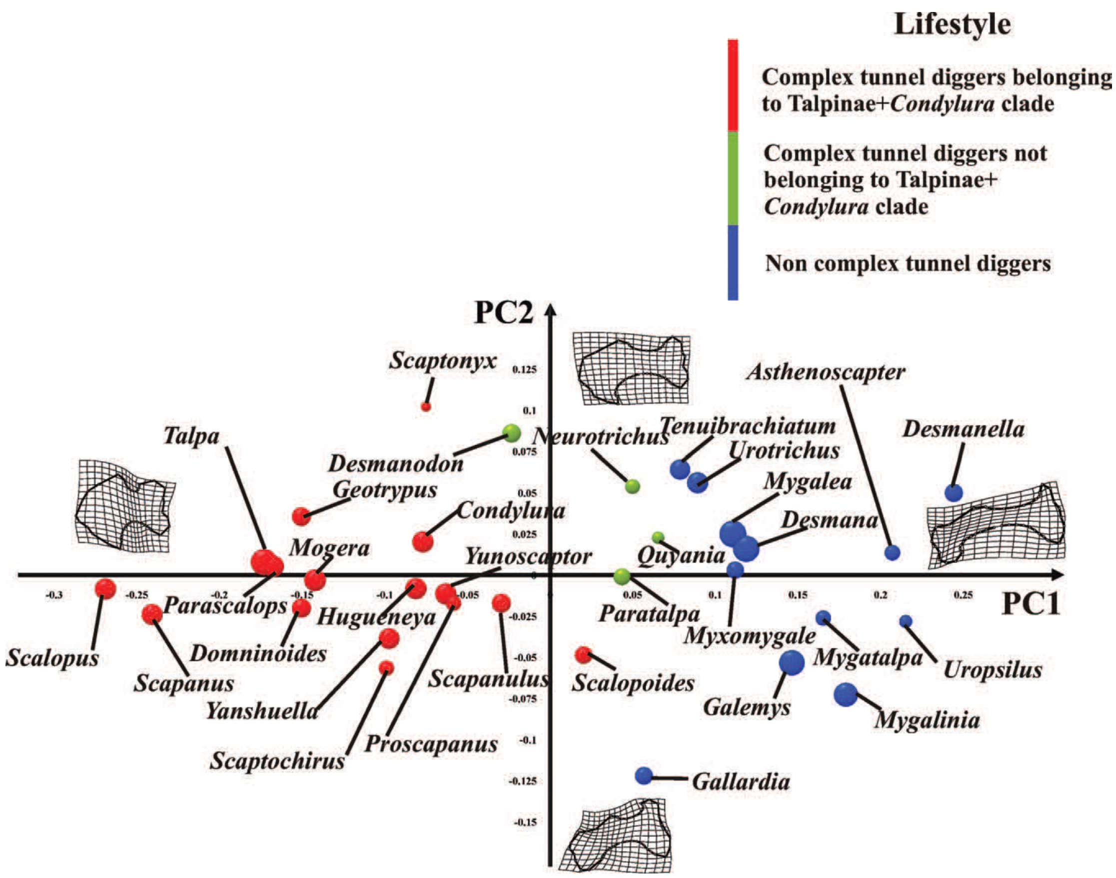

Figure 3.6. PC1/PC2 scatterplot of GM analysis showing the separation of the three groups identified by previous analyses. Points dimension is proportional to size. Deformation grids refer to axes extremes (positive and negative values).

Finite Element Analysis

Finite element analysis revealed, as expected, the strongest stress in the taxa possessing slender humerus and smallest thickness. In slender forms, stresses were concentrated all across the humeral shaft, suggesting the unsuitability of these forms for digging. Such forms belong to non-complex tunnel diggers. In particular, *Asthenoscapter*, *Desmanella* and *Uropsilus* (Uropsilinae) present the more stressed (as well as plesiomorphic) geometries. These taxa, relatively to the other non-complex tunnel diggers, still suffer stresses on the *teres* tubercle and to a lesser extent on the medial epicondyle.

The four taxa of complex tunnel diggers not belonging to Talpinae + *Condylura* clade show an intermediate stress pattern. They present a mix of primitive and derived features evidenced by a stressed slender shaft a non stressed expanded teres tubercle and medial epicondyle.

Differences in von Mises and elastic energy span more than one order of magnitude between slender and robust forms. FEA revealed that the more robust forms belonging to complex tunnel diggers present small pikes of evident stress. Robust forms reduced stress across the humeral shaft by expanding the area were pectoral muscles are inserted. Such modification allows an increase in stroke power and, at the same time, a powerful stabilization during digging. The same applies to the clavicular articular facet, which is more expanded in highly specialized forms. Furthermore, the more specialized forms (i.e. *Talpa*, *Mogera*, *Scalopus*, *Scapanus* and *Domninoides*), present smaller stress on the teres tubercle and on the medial epicondyle. The enlargement of the teres tubercle allows *Teres major* and *Latissimus dorsi* muscles to work on a more gainful lever arm, providing a more powerful stroke during burrowing. These features, together with the widening and thickening of the humerus, allow the humeral shaft to significantly reduce the stress loading.

It is worth noticing that *Geotrypus*, which is considered basal to the European moles lineage, possesses a relatively stressed geometry due to the presence of a plesiomorphic expanded greater sulcus. The same condition it is found in *Scalopoides* that keeps an overall slender shaft but possesses a well developed pectoral ridge as well as an enlarged teres tubercle and medial epicondyle.

The colour plates in Fig. 3.7 summarize the concentration of major solicitations in humeral Finite Element models. PCA performed on stress variables revealed that the PC1 explains 99.0% of total variance. The PC1 axis scores (“stress data”) were used as proxy of global mechanical behaviour of any model in the study for all successive comparative analyses.

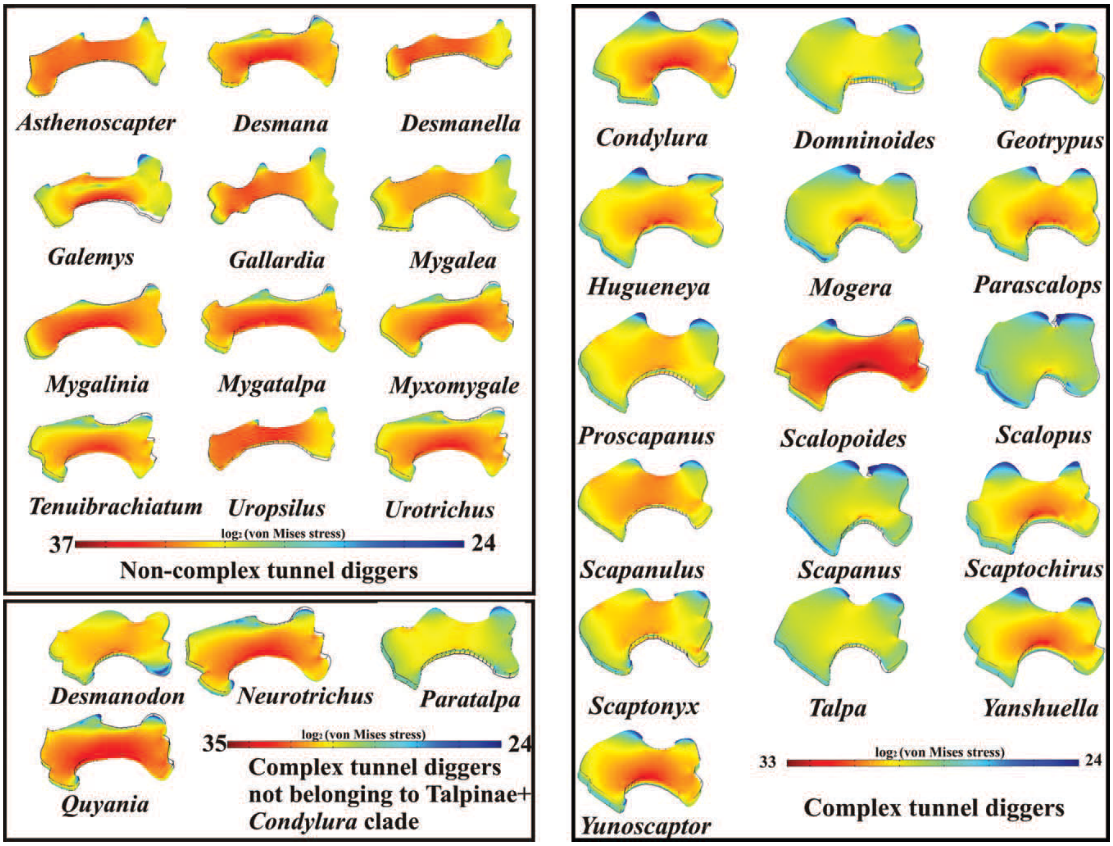

Figure 3.7. Finite element models in color showing both the intensity of stress experienced by different structures as well as the relative displacement as depicted by initial and final geometry positions. The three groups are depicted under the same stress scale calculated as logarithm of von Mises stress. Red colour indicates larger stress.

Logistic regression

Penalized Maximum Likelihood logistic regression was significant (LRT= 12.6; df=1; *p*-value: 0.0004). Regression coefficients were used to estimate extinct taxa lifestyle probabilities. Predicted probabilities for extinct taxa, extant taxa and internal nodes are specified in Table 2. Phylogenetic logistic regression was also significant (p-value <0.05).

OTUs and nodes (as numbered in Fig. 2)	Stress data (observed for OTUs, estimated for extinct taxa and nodes)	Predicted prob.	Lifestyle (observed for OTUs, estimated for extinct taxa and nodes)
Asthenoscapter meini	−32.83	0.27	0
Condylura cristata	27.24	0.95	1
Desmana moschata	−57.87	0.06	0
Desmanella engesseri	−40.15	0.19	0
Desmanodon antiquus	22.19	0.94	1
Domninoides valentinensis	29.98	0.96	1
Gaillardia thomsoni	−22.13	0.43	0
Galemys pyrenaicus	−56.04	0.007	0
Geotrypus aff. montisasini	26.42	0.95	1
Hugueneya aff. primitiva	28.40	0.96	1
Mogera kanoana	29.74	0.96	1
Mygalea magna	−30.35	0.31	0
Mygalinia hungarica	−47.27	0.12	0
Mygatalpa arvernensis	−57.55	0.07	0
Myxomigale gracilis	−52.07	0.09	0
Neurotrichus gibbsii	11.99	0.88	1
Parascalops breweri	28.67	0.96	1
Paratalpa brachychir	25.34	0.95	1
Proscapanus sp.	28.64	0.96	1
Quyania chowi	1.63	0.79	1
Scalopoides sp.	21.38	0.93	1
Scalopus aquaticus	31.02	0.96	1
Scapanulus oweni	27.50	0.96	1
Scapanus latimanus	30.75	0.96	1
Scaptochirus primaevus	28.60	0.96	1
Scaptonyx fusicaudus	28.59	0.96	1
Talpa romana	30.22	0.96	1
Tenuibrachiatum storchi	−24.94	0.39	0
Uropsilus gracilis	−53.58	0.08	0
Urotrichus talpoides	−39.39	0.19	0
Yanshuella primaeva	28.35	0.96	1
Yunoscaptor scalprum	27.51	0.96	1
33	−6.78	0.68	1
34	−29.74	0.31	0
35	−30.83	0.30	0
36	−6.26	0.69	1
37	−5.25	0.70	1
38	−5.01	0.71	1
39	−3.59	0.73	1
40	−3.59	0.73	1
41	−23.31	0.41	0
42	−4.25	0.72	1
43	−49.07	0.11	0
44	−47.85	0.12	0
45	−46.85	0.13	0
46	−54.33	0.08	0
47	2.64	0.80	1
48	5.72	0.83	1
49	4.88	0.82	1
50	8.79	0.86	1
51	16.93	0.91	1
52	25.46	0.95	1
53	18.77	0.92	1
54	20.09	0.93	1
55	22.48	0.94	1
56	25.42	0.95	1
57	23.11	0.94	1
58	23.11	0.94	1
59	27.10	0.95	1
60	20.44	0.93	1
61	22.34	0.94	1
62	24.39	0.95	1
63	28.67	0.96	1

Table 3.2. Stress data, lifestyle (observed forextant taxa), predicted lifestyle probabilities for extinct taxa and for nodes on the phylogeny based on sole extant logistic regression coefficients.

Phylogenetic signal and ancestral states reconstruction

Procrustes distances were significantly correlated with patristic distances (Mantel test z-statistics: 10912; permutation *p*-value: 0) as well as D metric (D: -0.15; *p*-value: 0), suggesting that both humeral shape and lifestyle are phylogenetically structured.

The best evolutionary model for stress data optimization (i.e. that one with the smallest Akaike Information Criterion) was the Brownian motion, thus suggesting that no branch length transformation is required before performing the Maximum Likelihood reconstruction at nodes. Reconstructed stress data values are specified in Table 3.2. Fig. 3.8A shows the tree with observed predicted probabilities for both taxa and internal nodes as predicted by sole-extant logistic regression coefficients.

Evolutionary rates and phylogenetic phenotypic trajectories

"evol.rate.mcmc" function identified the major shift in the rate of evolution in correspondence to node 49. This node is the MRCA of all Talpinae+*Condylura* clade. The inferred evolutionary rate (σ1) before the shift point was 0.37, while the inferred evolutionary rate after the shift point (σ2) was 0.017; suggesting a slowing down in the rate of evolution of the humeri in the Talpinae+*Condylura* clade.

When using the alternative phylogeny with *Condylura* in a more basal position, the shift was identified in correspondence of Talpinae clade.

Fig. 3.8 shows the original phylogenetic tree with the branch lengths scaled proportionally to their associated evolutionary rates.

In order to evaluate the phylogenetic phenotypic trajectory, the root node was excluded because all complex tunnel digger taxa not belonging to the clade Talpinae + *Condylura* can be traced back to node 36. The two trajectories are depicted in Fig.9. *Beta* coefficients (i.e. slopes) were significant (2.2e-9 and 0.02 respectively) and complex tunnel diggers not belonging to Talpinae + *Condylura* clade possessed a larger *beta* of than the Talpinae+*Condylura* clade (0.43 *vs*. 0.36). The permutated convergence test did not find significant differences (simulated p-value: 0.12) at beginning and end of the two trajectories, therefore indicating parallel pathways. However, if *Condylura* is moved to the position suggested by recent molecular topologies (i.e. Cabria et al. 2006; fig. 3.2) its status changes from belonging to a monophyletic complex tunnel diggers clade to the group defined here as "outside" this clade. Using this assignment, significantly convergent trajectories (p-value: 0.049) were found. Therefore, the phylogenetically labile *Condylura* position strongly influenced the interpretation of processes underlying Talpidae adaptation to the burrowing of complex tunnel systems. Variance of non complex tunnel diggers (169.19) resulted as significantly larger than that (50.79) of complex tunnel diggers (Levene's test p-value: 0.002).

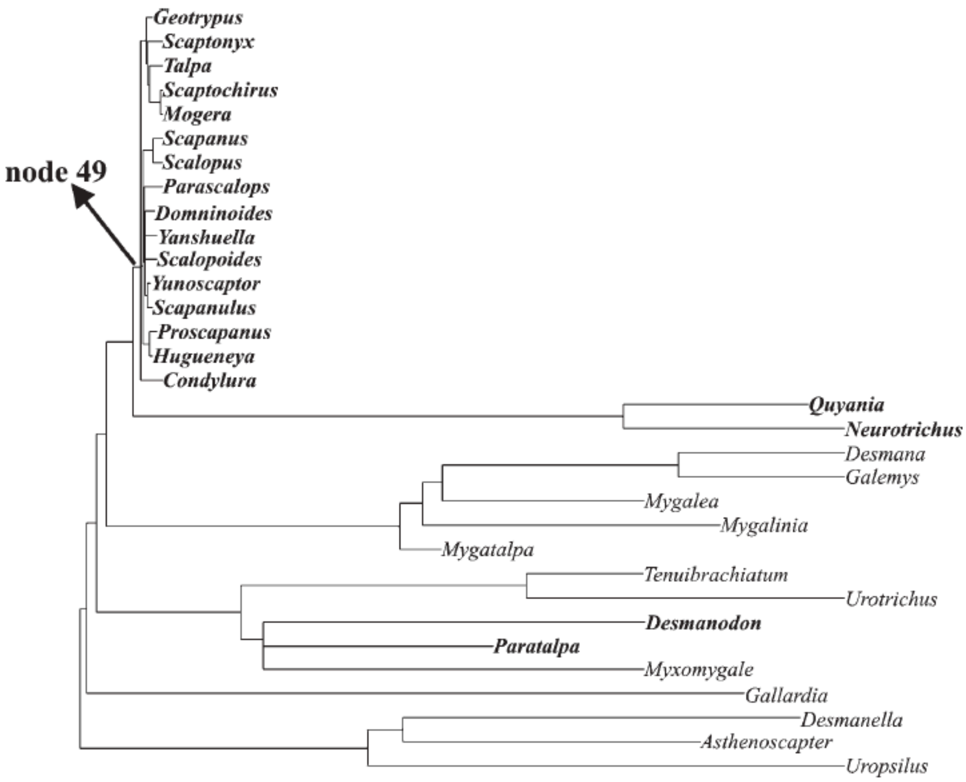

Figure 3.8. Our phylogenetic tree with branch lengths proportional to phenotypic evolutionary rates. A significant slowing was found in correspondence of node 49, that is, the MRCA of all Talpinae1Condylura clade. In bold: complex tunnel diggers.

Standard and phylogenetic ANOVA and MANOVA

With regard to shape, MANOVA produced significant results (p-value 0.007). However, phylogenetic MANOVA did not produce significant differences between the Talpinae + *Condylura* clade and the complex tunnel diggers not belonging to this clade, even moving *Condylura* to the above defined alternative position. These results indicate that the apparent morphological differences in the two groups are entirely due to phylogenetic covariance. Once this covariance is removed, the two groups did not differ in shape. ANOVA (p-value: 0.0005) was also significant for stress data. Phylogenetic ANOVA was still significant when using the main topology presented in Fig. 3.2. When moving *Condylura* toward the root, phylogenetic ANOVA was no longer significant.

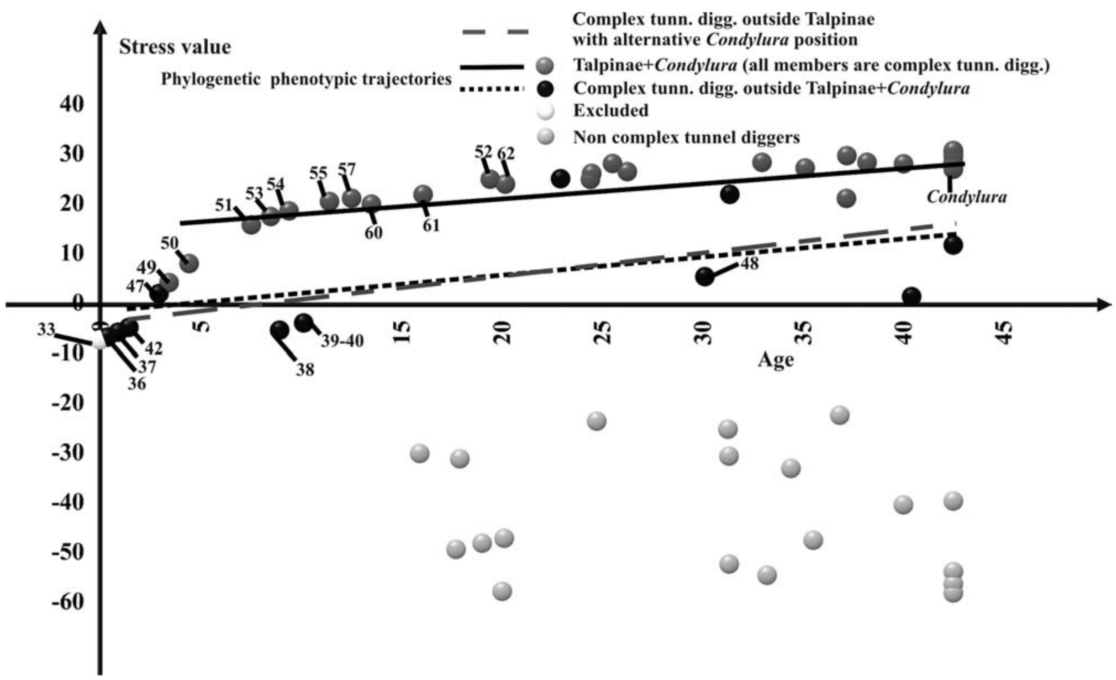

Figure 3.9. Evolutionary phenotypic trajectories computed for Talpinae + Condylura clade and complex tunnel digger forms not belonging to that clade. Numbers of internal nodes ancestral to the two groups and selected for the analysis are specified. See text for details about node selection. ''Age'' must be intended here as time from the tree root in Ma.

Discussion

Talpids humeral evolution has been the subject of previous phylogenetic and macroevolutionary analyses (Sánchez.Villagra et al., 2004; Sánchez-Villagra et al., 2006), although these were mainly based on osteological discrete characters. Our study is the first to use continuously distributed characters (combined with performance analysis) to reveal adaptation to digging during clade evolution, including both extinct and extant moles. Sole-extant logistic regression revealed a significant functional relationship between observed lifestyles and different humeral mechanical performances in moles. This evidence fully justified the use of humeral mechanical behaviour as a good predictor of underground lifestyle as defined in this paper (see above). Coefficients from the sole-extant logistic regression were used in order to establish their complex/non complex tunnel digger status. These coefficients were used for the first time to reconstruct the mechanical stress of extinct taxa. Two dimensional shape analyses revealed a neat separation between two main groups, i.e. the complex tunnel diggers (subdivided into those belonging to the Talpinae + *Condylura* clade and those not belonging to that clade), and non complex tunnel diggers. Evolutionary rate analysis revealed a neat deceleration in rates of phenotypic evolution in correspondence to the most recent common ancestor of the Talpinae + *Condylura* clade (node 49 in Fig. 3.2). This outcome suggests that, within the Talpidae, this clade achieved a functional optimum to respond to the intense burrowing functional demand. Once the taxa in this clade reached the optimal phenotypic status, their humerus did not undergo further morphological changes. Sánchez-Villagra et al. (2006) speculated about one or multiple occurrence of "fully fossorial" state in Scalopini and Talpini, considering *Scaptonyx* as semi-fossorial and hence invoking a reversal for the lifestyle status of this taxon.

In contrast with these authors the results of the present study suggest that the adaptation to complex tunnel digging within the Talpidae led to the same shape and mechanical performances through evolutionary parallelism (Stayton, 2006). Among the evidence that supports this hypothesis are 1) the significant slowing in evolutionary rate of stress data in the Talpinae + *Condylura* clade; 2) the parallel evolutionary phenotypic trajectories of Talpinae + *Condylura* clade and of the complex tunnel digger forms not belonging to this clade; 3) the smaller variance of complex tunnel diggers shapes compared to that of non complex tunnel digger forms; 4) the absence of significant differences in phylogenetic MANOVA of humeral shape between these two groups, suggesting that the overall differences were entirely is due to phylogenetic covariance. This interpretation switches to true convergence if *Condylura* is placed basal (as in Cabria et al., 2006).

As for phylogenetic ANOVA on stress data, different results were obtained depending on the position of *Condylura*. As this taxon was considered a complex tunnel digger, its phylogenetic position was crucial in the identification of phenotypic trajectories and group separation.

It was possible to distinguish between evolutionary parallelism and convergence *sensu latu* (Stayton, 2006) considering the topology presented in Fig. 3.2. In fact, when *Condylura* was moved to a deeper position in the phylogeny, evidence was found of true evolutionary convergence. This evidence made the analyses of evolutionary rates and of evolutionary phenotypic trajectories more coherent. In fact, the node depth was used as an independent age variable. Even if the null hypothesis of parallelism in the observed time interval can not be disregarded, the Talpinae+*Conylura* clade trajectory, having a smaller *beta* (i.e. slope), indicates that shape changes per unit time, i.e. evolutionary phenotypic rate, is smaller than in complex tunnel diggers not belonging to this clade. The results of this study suggest that, independently from convergence or parallelisms, when the same functional demands act on the same structure, the evolutionary pathway of its functional performance always points to the same phenotypic state. This has already been pointed out by Gould (2002) referring to Constructional Morphology theory (Seilacher, 1970). At least three factors were claimed to act on a given morphological trait; historical, functional and structural. In this view the monophyletic Talpinae + *Condylura* clade is expected to show a phylogenetic constraint in humeral morphology. Evidences of this constraint were suggested by both the phylogenetic MANOVA and evolutionary rates analysis. However, outside this clade some genera responded in the same way to the same functional demand, as evidenced by the Levene test in variance analysis, thus making irrelevant phylogenetic covariance. At family level, i.e. in more distantly related taxa, evolutionary pathways seem to be more influenced by strong functional constraints, such as those excised by the subterranean environment.

Adaptational constraints implied by intense burrowing activity in moles could lead to a functional shifting in the humerus of the genus *Condylura*, which is well adapted to swimming. As pointed out by Sánchez-Villagra et al. (2006), humeral propulsion for swimming in the star-nosed moles present similar selective forces to those for digging. It can be speculated, however, that this could be a clear case of exaptation (Gould and Vrba, 1982), because it could be difficult to hypothesize that the humerus of *Condylura* ancestors evolved for swimming performance rather than for digging.

Potential limitations of this study are mainly related to the phylogenetic hypothesis that, implying different character reconstructions, could also change the evaluation of evolutionary phenotypic trajectories. In fact, future cladistic analyses including extinct genera could provide better supported phylogenetic scenarios.

Moreover, some basal taxa (i.e. *Eotalpa*) included in the complete phylogeny (Appendix 2) were not included in comparative analyses because they are not represented by humeri in fossil record. New findings (new taxa or new humeri of already known extinct taxa) will likely allow the extension of these analyses, in order to better track the burrowing performance evolutionary pathway.

Appendices

Appendix 3.1. Entire literature *corpus* upon which we built the Talpidae phylogeny at the genus level. See Online Appendix II for resulting phylogenetic relationships.

Genus	**Stratigraphic Range**	**References for stratigraphic range**	**References for Phylogenetic position**
Geotrypus	MP 25 - MN 4 [29.0 - 18.0 my]	Crochet, 1995; Ziegler, 1999; Hoek Ostende, 2001	Ziegler, 1990; Hoek Ostende, 2001
Parascaptor	Only Recent	No fossils mentioned in the palaeontological literature	Sánchez-Villagra et al., 2006
Mogera	Nihewanian (= MN 17) - Recent [2.5 - 0 my]	Huang & Fang 1991; Kawamura, 1991; Qiu & Storch, 2005	Sánchez-Villagra et al., 2006
Euroscaptor	QM 4 - Recent [0.75 - 0 my]	Kawamura *et al.*,1989; Kawamura, 1991.	Sánchez-Villagra et al., 2006
Scaptochirus	MN 14/MN 15 - Recent [4.5 - 0 my]	Flynn & Wu, 1994; Qiu & Storch, 2005	Sánchez-Villagra et al., 2006
Talpa	MN 2 - Recent [22.5 - 0 my]	Ziegler, 1990, 1999	Sánchez-Villagra et al., 2006
Scapanoscapter	Barstovian 2 [15.0-13.0 my]	Gunnel *et al.*, 2008	Hutchinson, 1968
Scapanus	Barstovian 2 - Recent [15.0 - 0 my]	Gunnel *et al.*, 2008	Sánchez-Villagra et al., 2006
Scalopus	Clarendonian 2 - Recent [12.0 - 0 my]	Gunnel *et al.*, 2008	Sánchez-Villagra et al., 2006
Parascalops	Late Irvingtonian - Recent [0.5 - 0 my], (MN 14 - MN 15; 5.3 - 3.5 my)	Kurten & Anderson, 1980; Skoczen, 1993; Rzebik-Kowalska, 2005a	Sánchez-Villagra et al., 2006
Yanshuella	Late Tungurian - Late Baodean (= MN 8 - MN 16) [12.5 - 2.5 my]; Hemphillian 3 [8.0 - 5.0 my]	Storch & Qiu, 1983; Gunnel *et al.*, 2008; Qiu & Storch, 2005	Storch & Qiu, 1983; Gunnel *et al.*, 2008
Scalopoides	Arikarean 1 - Hemphillian 4 [30.0 - 5.3 my]	Gunnel *et al.*, 2008	Gunnell et al. 2008
Domninoides	Hemingfordian 2 - Hemphillian 4 [17.5 - 5.3 my]	Gunnel *et al.*, 2008	Reed 1962; Gunnell *et al.* 2008
Yunoscaptor	Middle Baodean (= MN11 - MN 12) [9.2 - 7.2 my]	Storch & Qiu, 1991; Qiu & Storch, 2005	Storch & Qiu, 1991, 1996
Scapanulus	Early Miocene (= MN 4) [18.0 - 0 my]	Storch & Qiu, 1983, 1996; Mein & Ginsburg, 1997	Sánchez-Villagra et al., 2006
Proscapanus	MN 4 - MN 10 [18.2 - 10.5 my]	Ziegler, 1999, 2006; Qiu & Storch, 2005; Ziegler &	Ziegler 1999

		Daxner-Höck, 2005	
Hugueneya	MN 1 - MN 4 [23.0 - 17.0 my]	Ziegler, 1999, 2006; Ziegler *et al.*, 2005	Ziegler 1999
Leptoscaptor	MN 7/MN 8 [12.5 - 11.2 my]	Ziegler, 2003	Ziegler, 2003
Tenuibrachiatum	MN 7/MN 8 [12.5 - 11.2 my]	Ziegler, 2003	Ziegler, 2003
Urotrichus	MN 5 - Recent [17.0 - 0 my]	Ziegler, 2003, 2006	Sánchez-Villagra et al., 2006
Dymecodon	QM 4 - Recent [0.75 - 0 my]	Kawamura *et al.*, 1989; Kawamura, 1991	Sánchez-Villagra et al., 2006
Myxomygale	MP 22? - MN 7/MN 8 [32.5 - 11.2 my]	Ziegler, 2003	Ziegler, 2003
Desmanodon	MN 2 - MN 8 [22.5 - 11.2 my]	Hoek Ostende, 1997; Prieto, 2010	Hoek Ostende 1997
Paratalpa	MP 29 -MN 2 [24.0 - 19.8 my]	Ziegler, 1990, 2003	Hugueney, 1972
Oreotalpa	Chadronian 3 [34.8-34.0 my]	Lloyd & Eberle, 2008	Lloyd & Eberle, 2008
Mongolopala	MP 21 - MP 23 [33.5 - 30.0 my]	Ziegler *et al.*, 2007	Ziegler *et al.*, 2007
Scaptonyx	Nihewanian (= MN 17) - Recent [2.5 - 0 my]	Qiu & Storch, 2005	Sánchez-Villagra et al., 2006
Mongoloscapter	Late Oligocene [26.0 - 24.0 my]	Lopatin, 2002	Lopatin, 2002; Ziegler, 2003
Quyania	Tungurian - Yushean (= MN 8 - MN 15) and MN 15 - MN 17 [12.5 - 2.0 my]	Storch & Qiu, 1983; Popov, 2004; Qiu & Storch, 2005	Carraway & Verts, 1991
Neurotrichus	Only Recent	Skoczen, 1980, 1993; Popov, 2004; Zijlstra, 2010	Sánchez-Villagra et al., 2006
Desmana	MN 11 - Recent [9.2 - 0 my]	Rümke, 1985; Ziegler & Daxner-Höck, 2005	Sánchez-Villagra et al., 2006
Galemys	MN 11 - Recent [9.2.0 - 0 my]	Ziegler & Daxner-Höck, 2005	Sánchez-Villagra et al., 2006
Archaeodesmana	MN 9 - MN 16 [11.2 - 2.5 my]	Ziegler, 1999; Ziegler, 2006; Minwer-Barakat *et al.*, 2008	Hoek Ostende *et al.*, 1989
Gerardstorchia	MN 6-MN 15 [15.2 - 3.5 my]	Dahlmann, 2001; Sabol, 2005; Ziegler, 2005, Ziegler *et al.*, 2005; Dahlmann & Dogan, 2010	Dahlmann, 2001
Mygalea	MN 2 - MN 7/8 [22.5 - 11.2 my]	Ziegler, 1999; Rzebik-Kowalska, 2005b; Ziegler *et al.*, 2005	Engesser, 2009
Mygalinia	MN 4/5 - MN 13 [17.0 - 5.3 my]	Gureev, 1964; Ziegler, 1999; Pita, 2005	Hutchison, 1974; Ziegler, 1999
Mygatalpa	MP 28 - MN 1 [24.8 - 22.5 my]	Remy *et al.*, 1987; Ziegler, 1999	Hutchison, 1974; Ziegler, 1999
Lemoynea	Hemphillian 1 - Hemphillian 2 [9.0 - 7.6 my]	Bown, 1980; Gunnel *et al.*, 2008	Bown, 1980
Condylura	Hemphillian 2 - Recent [7.6 - 0 my] my and MN 15 - MN 16 [4.2 - 2.5 my]	Scokzen, 1976, 1983; Kurten & Anderson, 1980; Gunnel *et al.*, 2008	Sánchez-Villagra et al., 2006
Achlyoscapter	Barstovian 2 - Late Blancan [14.8 - 2.5 my]	Gunnel *et al.*, 2008	Gunnell *et al.*, 2008
Gallardia	Barstovian 2 - Hemphillian 3 [14.8 - 5.8 my]	Gunnel *et al.*, 2008	Gunnell *et al.*, 2008
Mistypterus	Arikarean 1 - Clarendonian 3 [30.0 -10.1]	Gunnel *et al.*, 2008	Gunnell *et al.*, 2008
Asthenoscapter	MP 30 - MN 8 [23.2 -11.2 my] and "Middle" Baodean (= MN 11) [9.0 - 8.2 my]	Qiu & Wang, 1999; Ziegler, 1999; Engesser & Storch, 2008	Hoek Ostende, 2006; Engesser & Storch, 2008
Desmanella	MP 28 - MN 16 [24.8 - 2.5 my]	Ziegler 1999; Rzebik-Kowalska & Lungu, 2009	Hoek Ostende, 2001; Hoek Ostende & Fejfar, 2006
Uropsilus	Nihewanian (= MN 17) - Recent	Qiu & Storch, 2005	Sánchez-Villagra et al., 2006

	[2.5 - 0 my]		
Theratiskos	MN 1 - MN 3 [23.0 - 18.2 my]	Hoek Ostende, 2001	Hoek Ostende, 2001
Eotalpa	MP 17 - MP 21 [37.0 - 32.8 my]	Sigé *et al.*, 1977; Smith, 2007	Sigé *et al.*, 1977
Suleimania	MN 1 - MN 3 [23.0 - 18.2 my]	Hoek Ostende, 2001	Hoek Ostende, 2001
Quadrodens	Arikaerean 1 [30.0 - 28.0 my]	Gunnel *et al.*, 2008	Gunnell *et al.*, 2008
Nuragha	MN 2 [22.5 - 19.8 my]	Bruijn & Rümke, 1974	Bruijn & Rümke, 1974; Ziegler, 1999
Taxa ambiguously classified			
"*Scaptonyx*"	MN 4 - MN 9 [18.0 - 9.8 my]	Skoczen, 1980; Ziegler, 1999	Ziegler, 1999; Rzebik-Kowalska, 2005b
"Scapanulus" vel "Scalopoides"	MN 7/8 - MN 10 [12.5 - 9.2 my] and MN 14 - MN 17 [5.3 - 2.0 my]	Rzebik-Kowalska, 2005a; Ziegler *et al.*, 2005	Skoczen, 1980; Rzebik-Kowalska, 2005; Ziegler *et al.*, 2005
"Domninoides"	MN 7/8 [12.5 - 11.2 my]	Ziegler, 1999; Hoek Ostende & Furió, 2005	Ziegler, 1999; Hoek Ostende & Furió, 2005
Taxa synonymized			
Ruemkelia	*Archaeodesmana*		Hutterer, 1995; Rzebik-Kowalska & Lungu, 2009
Dibolia	*Ruemkelia, Archaeodesmana*		Rzebik-Kowalska & Pawlowski, 1994
Asioscalops	*Talpa*		Rzebik-Kowalska, 2007
Pseudoparatalpa	*Paratalpa*		Lopatin, 1999; Ziegler, 2003
Palurotrichus	*Myxomygale*		Ziegler, 1985; Hoek Ostende, 1989
Teutonotalpa	*Paratalpa*		Hutchison, 1974; Hoek Ostende, 1989
Nesoscaptor	*Mogera*		Abe *et al.*, 1991; Motokawa *et al.*, 2001
Galeospalax	*?Paratalpa*		Hutchison, 1974
Hyporyssus	*Nomen dubium*		Hutchison, 1974

Appendix 3.2. Complete phylogenetic tree with 50 genera, thicker line indicate observed stratigraphic range for taxa. Node numbers are not the same of Figure 3.2.

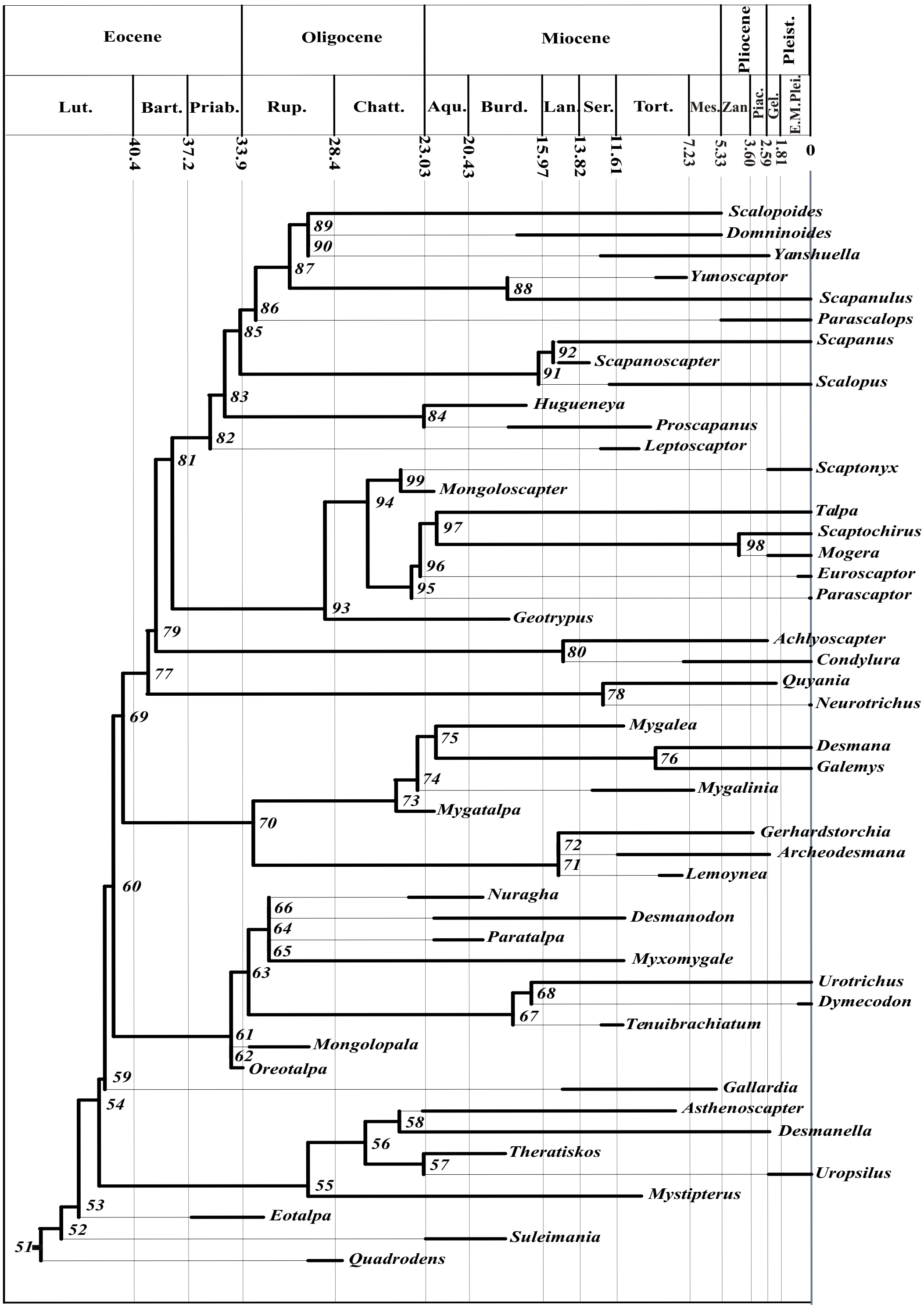
Eocene
Oligocene
Miocene
Pliocene
Pleist.
Lut.
Bart.
Priab.
Rup.
Chatt.
Aqu.
Burd.
Lan.
Ser.
Tort.
Mes.
Zan
Piac.
Gel.
E.M.Plei.
40.4
37.2
33.9
28.4
23.03
20.43
15.97
13.82
11.61
7.23
5.33
3.60
2.59
1.81
0
Scalopoides
Domninoides
Yanshuella
Yunoscaptor
Scapanulus
Parascalops
Scapanus
Scapanoscapter
Scalopus
Hugueneya
Proscapanus
Leptoscaptor
Scaptonyx
Mongoloscapter
Talpa
Scaptochirus
Mogera
Euroscaptor
Parascaptor
Geotrypus
Achlyoscapter
Condylura
Quyania
Neurotrichus
Mygalea
Desmana
Galemys
Mygalinia
Mygatalpa
Gerhardstorchia
Archeodesmana
Lemoynea
Nuragha
Desmanodon
Paratalpa
Myxomygale
Urotrichus
Dymecodon
Tenuibrachiatum
Mongolopala
Oreotalpa
Gallardia
Asthenoscapter
Desmanella
Theratiskos
Uropsilus
Mystipterus
Eotalpa
Suleimania
Quadrodens

CHAPTER 4

THEY DIG

Trajectories and evolutionary allometries constrain rates of evolution of humeral morphology within highly fossorial moles (Talpinae)

Sansalone G., Kotsakis T., Colangelo P., Loy A., Piras P. (in prep.)

Introduction

The subfamily Talpinae includes the highly fossorial moles and the most specialized forms of the Talpidae. This subfamily includes two tribes: the Eurasian Talpini and the North American Scalopini (with the exception of the endemic Gansu, China, *Scapanulus oweni*) whose most recent common ancestor traces back to the Late Eocene (Ziegler, 1999; Gunnel et al., 2008). Despite the strong phenotypic channel imposed by the subterranean environment (Nevo, 1979; Gorman and Stone, 1990), this subfamily is today the most diversified among Talpidae (Hutter, 2005). Representatives of Talpinae are also found well abundant in the fossil record, with several species described in the literature (Ziegler, 1999; Gunnel et al., 2008). Both North American and Eurasian origin have been proposed for this clade (Shinohara et al., 2003; Cabria et al., 2006). During the Neogene Talpinae spread across all the Palearctic (Ziegler, 1999; Gunnel et al., 2008). The humeral morphology of the entire subfamily is highly modified and adapted for complex tunnel digging. However, the two tribes still show morphological differences mainly related to the Teres tubercle, the bicipital tunnel and the pectoral crest. In this section we focus on this highly specialized clade in order to understand how the particular humeral shape evolved.

We will investigate the humeral shape variation by means of 2D Geometric Morphometrics. We will evaluate and test the difference (if any) in the humerus evolutionary rates. We will investigate the relationship between shape and size by means of comparison of the allometric trajectories. We will test the presence of convergence and/or parallelism in the humeral shape and size. Finally we will investigate the patterns of size and shape disparification through time.

Material and methods

Geometric morphometrics

We digitized 22 landmarks and 14 semi-landmarks on the humerus in caudal view (see figure 2.15). We analyzed a total of 623 humeri belonging to 19 Scalopini taxa and to 34 Talpini taxa (see Appendix 4.1), including both fossils and extant species. We include all the species for which at least one humerus was available from pictures or from pubblications.
The methods used in this chapter follow the scientific protocol described in chapter 2.

Results

Shape analysis

The bgPCA on Procrustes aligned coordinates showed that Talpini and Scalopini are well separated in the morphospace (figure 4.2A and 4.2B). Along the PC1 (43.86% of the total variance) it is possible to separate the slender Scalopini (*Wilsonius*, *Yanshuella*, *Yunoscaptor*, *Leptoscaptor bavaricum* and *Scapanulus*) at positive values from the robust Scalopini (*Scapanus* spp., *Scalopus* spp., *Domninoides* spp., *Leptoscaptor robustior*, *Hugueneya*, *Parascalops* and *Proscapanus* spp.) at negative values, while Talpini are well clustered and occupy a restricted region of the morphospace. Talpini species are near and partially superimposed with the Scalopini robust forms. At positive values the humerus show an overall slender configuration and a reduced teres tubercle and less expanded pectoral ridge, while at negative values the humerus show an overall more robust configuration with an enlarged teres tubercle and a more expanded pectoral ridge. Along the PC2 (22.6% of the total variance) it is possible to separate the Talpini (negative values) from Scalopini (positive values). At positive values the humerus show a longer teres tubercle and a shorter pectoral ridge, while at negative values the humerus show a shorter teres tubercle and a larger pectoral ridge. Along the PC3 Talpini and Scalopini are well clusterd in the same region of the morphospace (positive values), while at negative values the *Geotrypus* spp. are clearly discriminated. At positive values the humerus shows the typical robust configuration, while at negative values the humeral morphology shows a small and pointed teres tubercle, a very large pectoral ridge and an expanded minor tuberosity.

The perMANOVA test performed on the shape variables returned a highly significant result (p-value = 0.001), while the perANOVA test performed on the CS returned a non significant result (p-value = 0.618).

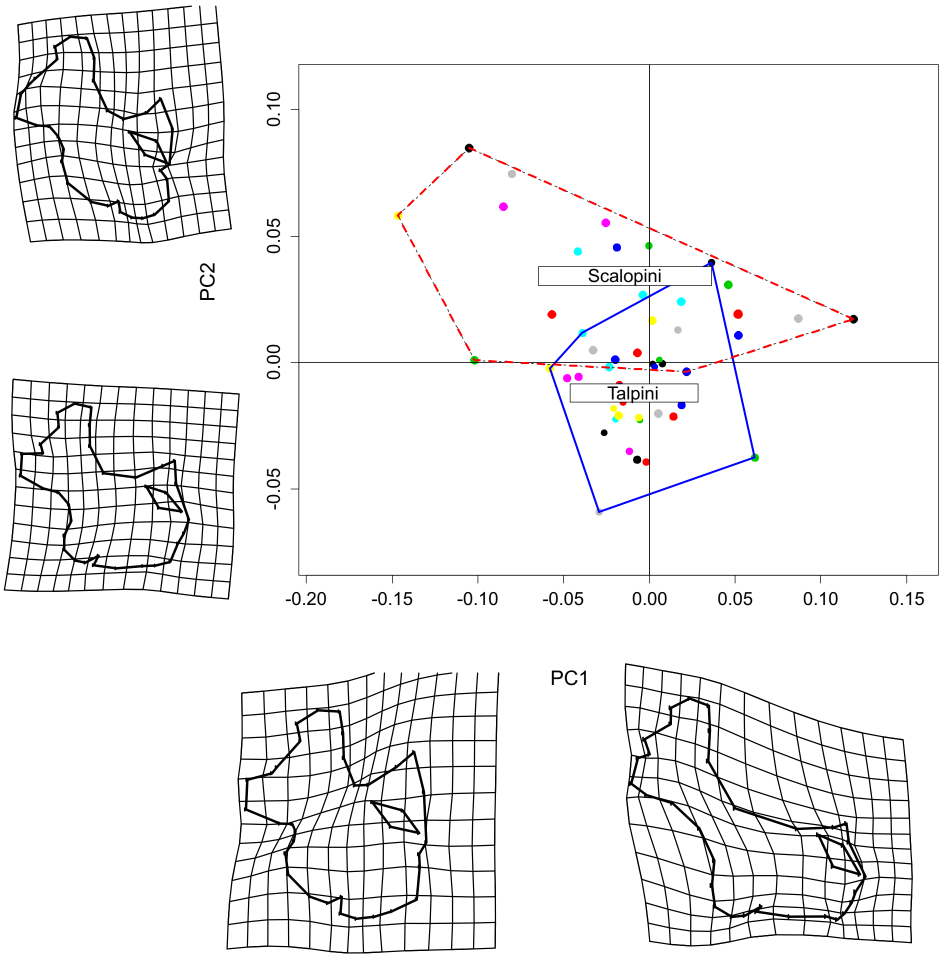

Figure 4.2A. Scatterplot of the first vs. second axes of the bgPCA on humeral shape variables. Deformation grids refer to axes extremes (positive and negative values).

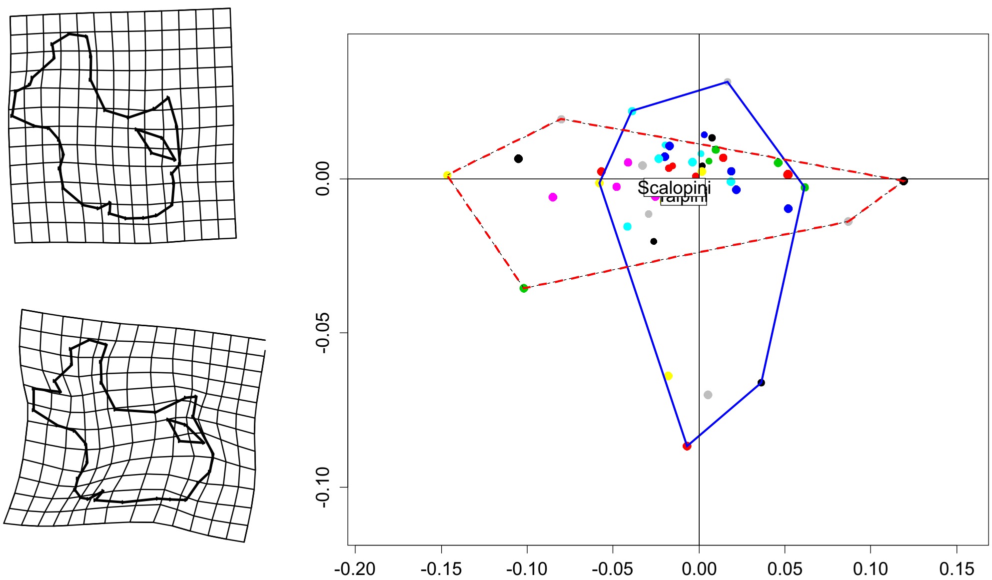

Figure 4.2B. Scatterplot of the first vs. third axes of the bgPCA on humeral shape variables. Deformation grids refer to axes extremes (positive and negative values).

Allometry

The multivariate regression of shape on size returned a highly significant result (*p*-value < 0.001). Multivariate separate per-clade regressions returned a significant result for both Talpini and Scalopini (*p*-value = 0.001, $r^2 = 0.10$; *p*-value < 0.001, $r^2 = 0.46$ respectively). The perMANCOVA test revealed that the slopes are significantly different (*p*-value = 0.001). The ontogenetic convergence test returned also a significant result (*p*-value = 0.019), revealing that the two trajectories were convergent (figure 4.3). In fact the Euclidean distances between the individuals predicted at small CS value (1.9) were greater than that between the individuals predicted at high CS value (4.49).

The shape changes associated with size showed that at low CS values the humerus have the slender configuration, while at high CS values it have the robust configuration (figure 4.4).

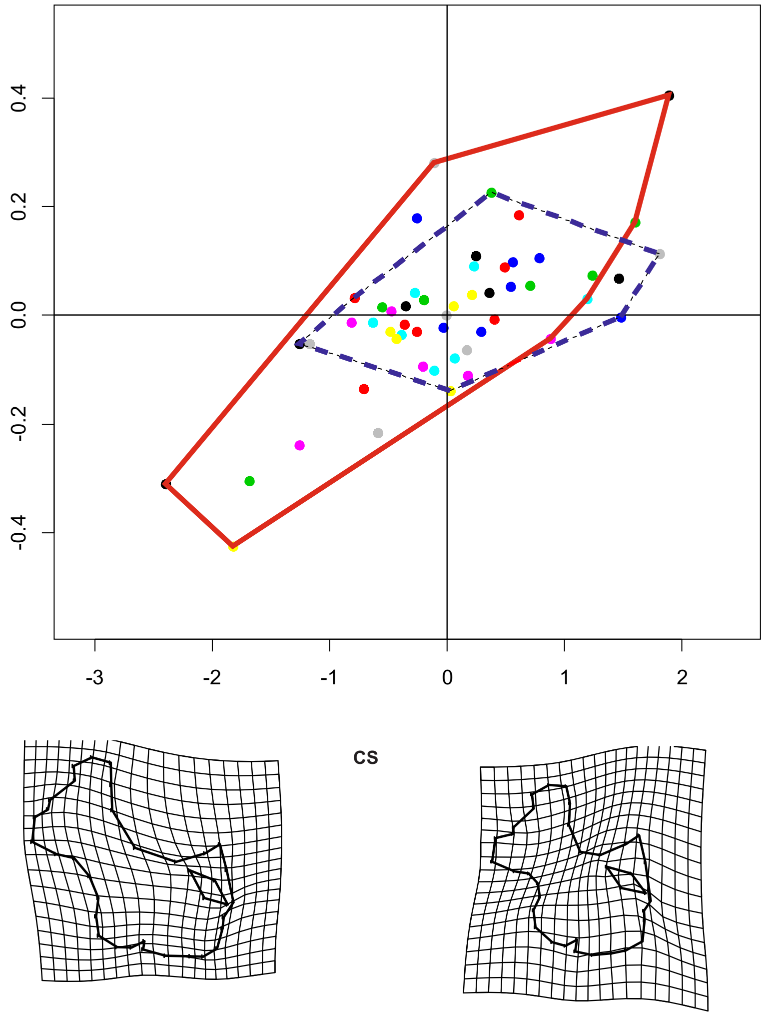

Figure 4.4. CCA scatterplot of shape on size. Deformation grids refer to positive and negative extremes.

Inclusion of phylogeny

Phylogenetic signal

Mantel test revealed significant result when computed for the shape variable (p-value < 0.001), while returned a non significant result when performed on the CS (p-value = 0.115). The phylosig() function returned also a non significant result for the CS (p-value = 0.97). The physignal() function returned a significant result when computed for the shape variables (p-value = 0.004, K=0.48). The ancestral character estimation for shape (PC1) showed as the phylogenetically nearest species share a similar shape configuration (figure 4.5A). When we mapped the ancestral character estimation for CS on the phylogeny it was evident as the closely related species were also significantly different in size (figure 4.5B).

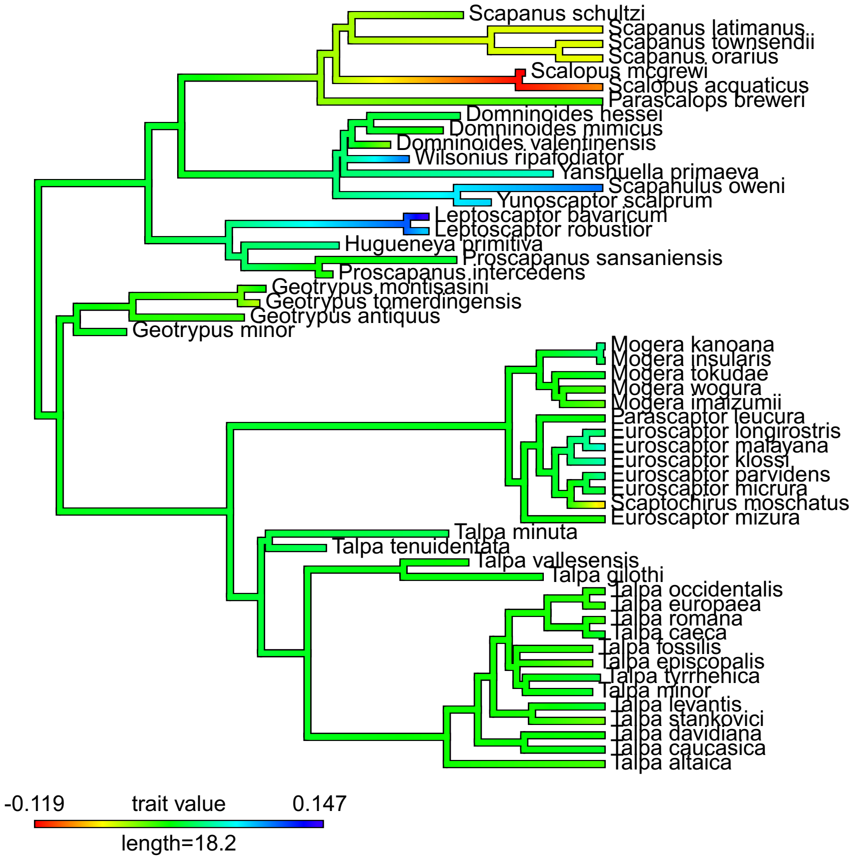

Figure 4.5A. Plot of the PC1 trait on the phylogeny.

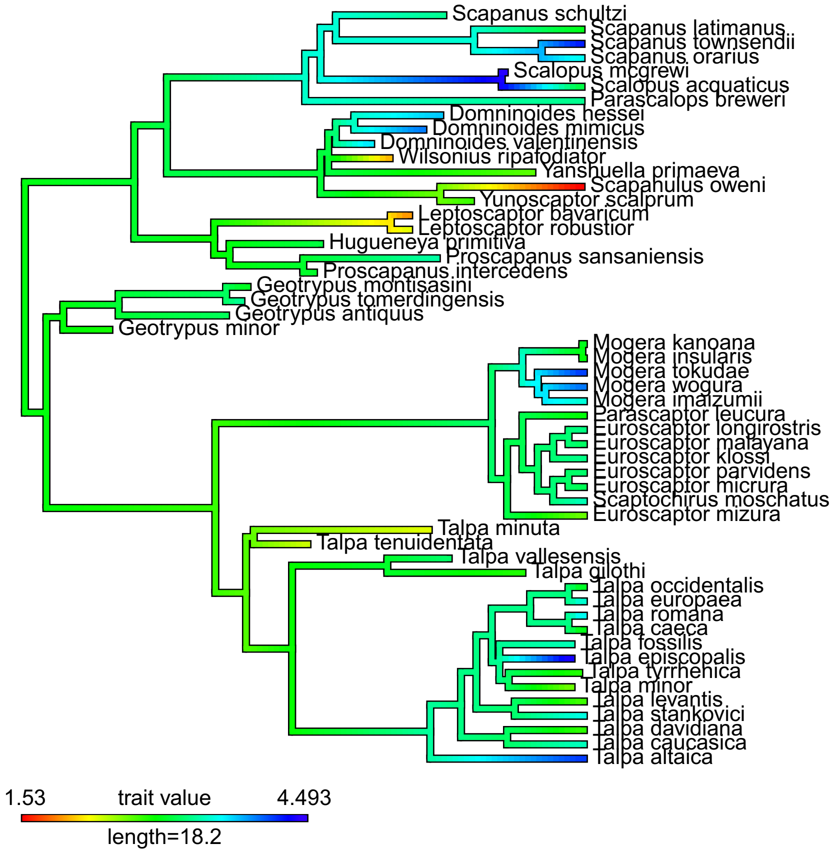

Figure 4.5B. Plot of the CS trait on the phylogeny.

Phylogenetic non independence

When taking into account phylogeny the phyMANOVA, performed on the shape variables, still returned a significant result (*p*-value = 0.029), while the phyANOVA returned a non significant result (*p*-value = 0.92). The PGLS revealed a significant interaction between shape and size in a phylogenetic context.

Evolutionary rates

We found that Talpinae rate of morphological evolution is different from Brownian motion (*p*-value < 0.001). The evolutionary rates were significantly different between the two tribes (*p*-value = 0.001). Talpini show the lowest ML rate (0.82), while

Scalopini have the highest (4.55). The ratebystate() function returned a non significant result (p-value = 0.33). We found a positive shift in correspondence of *Geotrypus* spp., while we found a neat slowdown in correspondence of the genus *Talpa* spp. (figure 4.6).

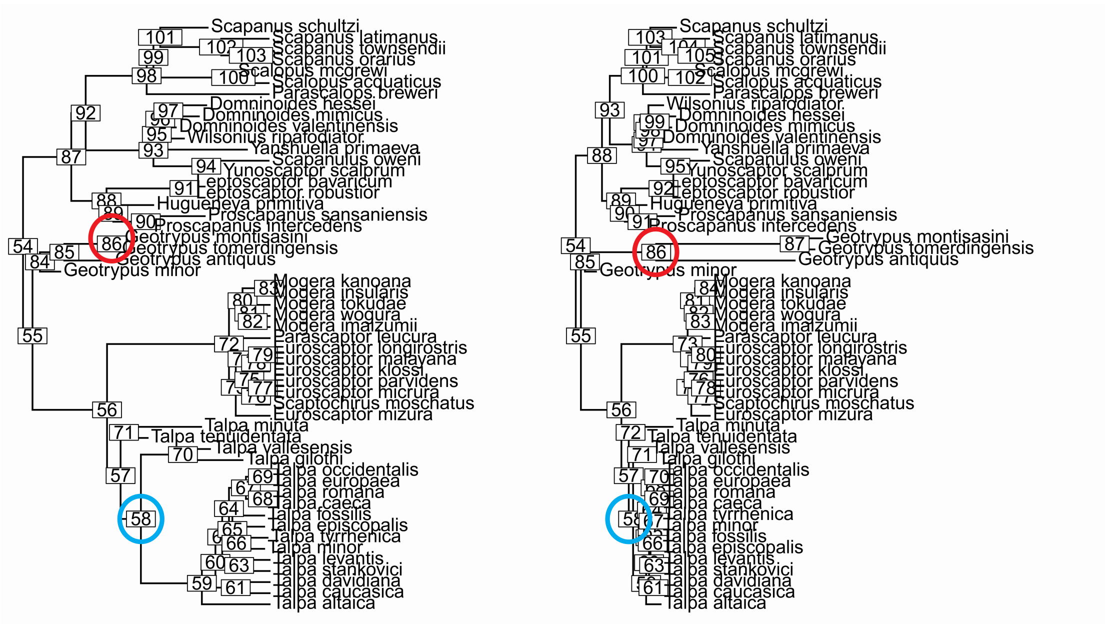

Figure 4.6. Plot of the shifts found for the shape variable. On the left is represented the original tree, on the right the tree branches are transformed according to evolutionary rates. The red circles indicate an acceleration, cyan circles indicate slowdown.

Morphological and size disparity

The betadisper analysis returned significant results (p-value = 0.001) when computed for the shape variables. Scalopini possess the highest average distance from mean (0.077), while Talpini have the lowest (0.044). The CS disparity resulted to be significant as revealed by the Levene test (p-value = 0.045), with Scalopini having the highest average distance to median (0.6) and Talpini the lowest (0.4).

The morphological disparity through time was higher than expected under Brownian motion. In fact the dtt() function (figure 4.7A) returned a positive MDI (MDI = 0.20). The dtt() function returned a positive MDI (MDI = 0.57) also for the CS, again suggesting a deviation from the gradualism (figure 4.7B). The node-height test returned non significant results for the first 3 PCs (see table x), also the robust regressions performed using the nh.test() function returned non significant results. The node-height test performed on the CS returned a significant result (*p*-value = 0.034), though the robust regression revealed a non significant interaction (*p*-value = 0.97).

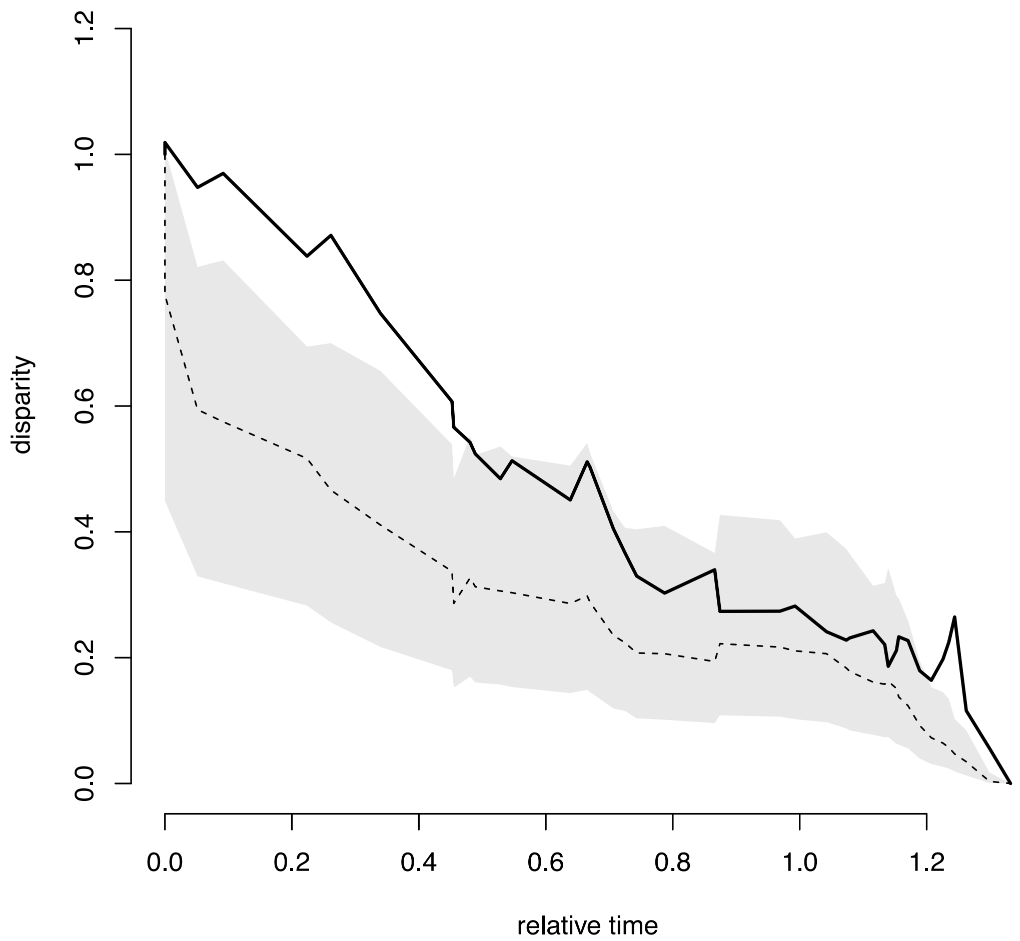

Figure 4.7A. Plot of the dtt() function performed on the humerus shape variables. The solid line represent the empirical data, the dotted line represent the simulated data under Brownian motion.

"Surface" analysis, search for no a priori local optima

The surface analysis (figure 4.8) revealed a convergence for the humeral shape in Miocene European Scalopini, and in the slender Scalopini. We found a convergence in size only for *Scapanulus oweni* and *Wilsonius ripafodiator*. We found the presence of 9 shifts under OU model for the shape variables, while we found 5 shifts under OU model for the CS.

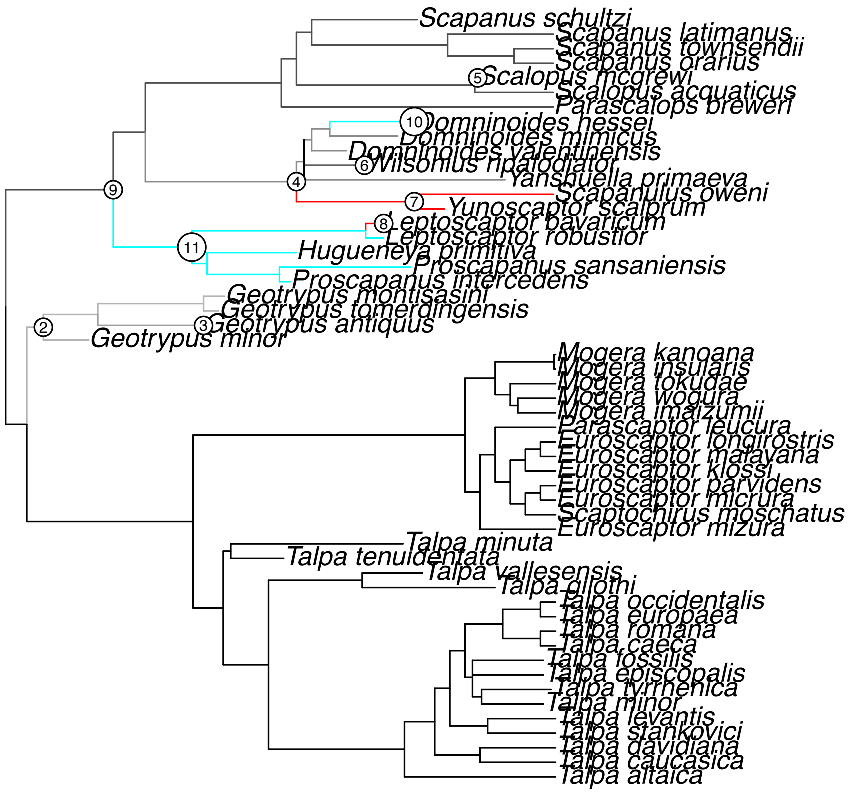

Figure 4.8. Plot of the "SURFACE" analysis on the humeral shape in different clades of Talpidae. The coloured branches represent convergence, while gry-scale indicates non-convergence. Numbers on branches indicate the order in which regime shifts were added during the forward phase.

Discussion

The shape analysis evidenced how also in the highly fossorial clades still significant differences exist. The major humeral modifications involve the proximal region, and in particular they are about the teres tubercle, the pectoral ridge and the minor tuberosity. As already pointed out in Chapter 2, along the PC3 it is evident the separation of *Geotrypus* spp. from all other taxa.

We do not found significant differences in size between the two clades even when controlling for shared ancestry. The size variable do not bear a phylogenetic signal. When we mapped the CS character on the phylogeny it was evident as the closely related species were also different in size. Following this evidence the size diversification in mole species could have occurred during the speciation processes of sister species in response to ecological constraints, such as inter-specific competition and the ability to exploit low productive soils (Loy et al., 1996; Loy, 2008). This pattern has been documentd extensively for genera *Talpa* and *Mogera* (Loy and Capanna, 1998; Shinohara et al., 2003; Sanchez-Villagra et al., 2006), and in general for many other Talpidae taxa (see Chapter 5). Size displacement between pairs of ecologically similar species is a common pattern in mammals (Simberloff and Boecklen, 1981; Dayan and Simberloff, 1998) and in moles it could provide a rapid response to intensive inter-specific competition.

The perMANOVA test returned a significant result even when performing the phylogenetic version. The shape variable beared a strong phylogentic signal and we measured a "kappa" value of 0.48. Also, the interaction between size and shape was highly significant even when taking into account the phylogeny, suggesting the presence of an evolutionary allometry. We found that the Talpini and Scalopini trajectories were convergent. This evidence suggests that evolutionary allometry channeled the humeral morphology in highly fossorial moles, in particular at large size. The CCA plot showed as the large sized Talpini and Scalopini also share the same phenotype. The Scalopini resulted to be more related with size than Talpini (greater r^2), in fact Scalopini includes also small sized species that show a slender humeral morphology.

As a result, the PCA and betadisper analysis revealed as the Scalopini, tough being less diversified (Hutterer, 2005), are more disperse than Talpini. Moreover the Scalopini were proved to have significantly higher evolutionary rates than Talpini. However when we searched for major evolutionary shift in the phylogenetic tree we found a neat acceleration in correspondence of the *Geotrypus* spp. and a slowdown in correspondence of the *Talpa* spp. As discussed in Chapter 3 the genus *Talpa* probably reached a functional optimum and did not experienced further structural changes.
The clades disparity through time was higher than that expected under Brownian motion, suggesting a deviation from gradualism, moreover the node height test was non significant and as reported before the “kappa” = 0.48. “Kappa” value lower than 1 are congruent with a mode of evolution that can be rapid and independent from time (Losos, 2008; Pearman et al., 2013). This pattern could be explained by the strong phenotypic channel imposed by evolutionary allometry combined with the lack of phylogenetic structure of size. In chapter 2 we described evolutionary patterns corresponding to those predicted by the “niche-filling” (Freckleton and Harvey, 2006; Slater et al., 2010). It is possible that highly fossorial moles, once the ecological niche was occupied, were able to diversify only by shifting in size (Slater et al., 2010).
We found convergence in the Miocene European Scalopini and in the Scalopini slender species.

CHAPTER 5

HUMERUS, GM AND SYSTEMATICS

AN AMERICAN MOLE IN POLAND?

New generic allocation for *Neurotrichus*? *polonicus* Skoczen, 1980 and *Neurotrichus*? *skoczeni* Skoczen, 1993 (Mammalia, Talpidae) via qualitative and quantitative shape analysis.

Sansalone G., Kotsakis T. and Piras P. In press. *Acta Paleontologica Polonica*.

Introduction

The Polish Plio-Plesitocene mammal bearing localities provided a huge amount of fossil talpid remains (Rzebik-Kowalska, 2005). Skoczen (1976; 1980; 1993) described five new species belonging to extant genera currently endemic of North America: *Condylura kowalskii* Skoczen, 1976, *Condylura izabellae* Skoczen, 1976, *Parascalops fossilis* Skoczen, 1993, *Neurotrichus*? *polonicus* Skoczen, 1980 and *Neurotrichus*? *minor* Skoczen, 1993. Storch and Qiu (1983) suggested the inclusion of *Neurotrichus*? *polonicus* in the genus *Quyania*, but, due to the lack of the upper and lower antemolar rows they maintained the generic status given by Skoczen (1980). They suggested that the Polish species is inserted in an ancestor-descendant lineage in relationship with *Quyania chowi* Storch and Qiu, 1983, hypothesizing a lineage characterized by a gradual reduction of the precingulid, the strenghtening of the upper molar protoconules and size increase. The description of the small species *Neurotrichus*? *minor* (Skoczen, 1993) raised the question by the large size as an advanced evolutionary character. Popov (2004), following the hypothesis of Storch and Qiu (1983), assigned the material from Varshets (Early Pleistocene, Bulgaria) to *Quyania* aff. *Q. polonica*. Popov (2004) considered the Polish species as more advanced than *Neurotrichus gibbsii* by having reduced precingulids and a humerus more adapted to a fossorial lifestyle. Rzebik-Kowalska (2005), maintained the original taxonomic identification provided by Skoczen (1980). Dalquest and Burgner (1941) described the extant North-American subspecies *Neurotrichus gibbsii minor* which is still considered valid. Therefore Zijlstra (2010) proposed the new name *Neurotrichus skoczeni*. Rzebik-Kowalska (2014) pointed out that the generic attribution of *Neurotrichus*? *polonicus* still represent an open question. Her revision showed that the Polish species displays characters shared by both genera *Neurotrichus* and *Quyania*. Rzebik-Kowalska (2014) left the generic attribution given by Skoczen (1980) considering the attribution to the genus *Quyania* as still immotivated. Although the generic attribution of these species has been questioned (Storch and Qiu, 1983; Popov, 2004; Rzebik-Kowalska, 2014), no new analyses or diagnoses have been provided up to now. Here we re-examined the material previously attributed to *Neurotrichus*? *polonicus* and *Neurotrichus*? *skoczeni* and provided a new generic diagnosis on the light of the most recent studies on talpid morphology and evolution (Gambaryan et al., 2003; Sánchez-Villagra et al., 2004, 2006; Piras et al., 2012). We also investigated the patterns of shape and size variation of the humerus by means of Geometric Morphometrics analysis. The humerus experienced the most remarkable transformations during talpid evolution (Dobson, 1882; Freeman, 1886; Reed, 1951; Yalden, 1966; Sánchez-Villagra et al., 2004; Piras et al., 2012). This skeletal element is usually found well preserved and abundant in fossil assemblages. It is thus widely used in systematics studies of extinct Talpidae (Ziegler, 2003) and, due to its abundance, allows the use of modern multivariate and univariate statistical methods.

Materials and Methods

Specimens collection

We analyzed a total of 48 left humeri belonging to *Urotrichus talpoides* Temminck, 1841 (n = 12), *Dymecodon pilirostris* True, 1886 (n = 8), *Urotrichus dolichochir* Gaillard, 1889 (n = 5), *Quyania chowi* Storch and Qiu, 1983 (n = 2), *Neurotrichus gibbsii* Baird, 1856 (n = 16), *Rzebikia polonica* gen. nov. Skoczen, 1980 (n = 6). We included in the analysis all the Late Neogene Neurotrichini and Urotrichini species for which complete humerus was available. See Appendix I for details about specimens codes, localities and collection storage.

Geometric Morphometrics

We digitized 22 landmarks and 14 semi-landmarks on the humerus in caudal view (figure 5.1).

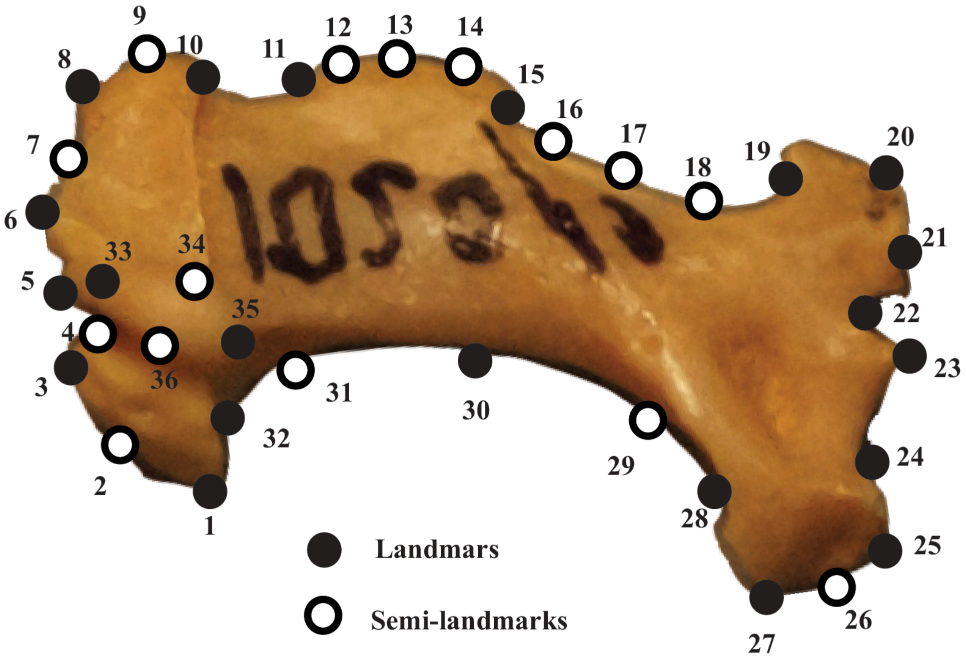

Figure 5.1. Landmarks (black circles) and semilandmarks (grey circles) digitized on the humerus in caudal norm: 1) lateral end of greater tuberosity; 2) articular facet for clavicula; 3) proximal edge of the articular facet for clavicula; 4) bicipital notch; 5) proximal end of lesser tuberosity; 6) medial edge of the minor tuberosity; 7) lateral edge of the lesser tuberosity; 8) bicipital ridge; 9) middle point of the bicipital tunnel; 10) lateral end of the scalopine ridge; 11) proximal end of the teres tubercle; 12-14) surface of the teres tubercle; 15) distal end of the teres tubercle; 16-18) minor sulcus; 19) posterior margin of the lateral epicondyle; 21-22) lateral epicondyle; 22-24) trochlear area; 25-27) medial epicondyle; 28) posterior margin of the medial epicondyle; 29-32) greater sulcus; 33-36) humeral head.

We excluded *Q. chowi* from all the pairwise permuted comparisons due to its small sample size (n = 2). The phenetic relationships among the taxa included in this study have been visualized performing an UPGMA on the Euclidean distance matrix computed on per-species mean shape variables.

Systematic paleontology

Class Mammalia Linnaeus, 1758

Order Eulipotyphla Waddel, Okada, Hasegawa, 1999

Family Talpidae Fischer, 1814

Subfamily Talpinae Fischer, 1814

Tribe Neurotrichini Hutterer, 2005

Genus *Rzebikia* nov.

Type species: *Rzebikia polonica* Skoczen, 1980 gen. nov.

Etymology: Dedicated to Prof. Barbara Rzebik-Kowalska.

Included species: *Rzebikia skoczeni* gen. nov.

Diagnosis

Humerus with moderate digging adaptations having a large teres tubercle separated by a marked notch from the pectoral ridge, partially unfused bicipital tunnel (the suture between the proximity of the pectoral ridge and the lesser tuberosity is present but not complete, see Fig. 2A), large minor sulcus, lesser tuberosity poorly developed toward the proximal end of the shaft. P_4 with straight metacristid and distinct entoconid separated from the protoconid by a furrow. The cingula are weakly developed with the M_1 having the precingulid extending only halfway it's width. The entoconids of both M_1 and M_2 are robust and displaced lingually making the lingual side of the lower molars concave. The M^1 and M^2 bear a strong paraconule. The M^2 lack precingulum and the parastyle is separated from the paracrista. The clavicle dorsal prominence of the manubrial articular facet is straight and the ventral process line is concave and possess two small spines.

Rzebikia polonica Skoczen, 1980 gen. nov.

1980 ?*Neurotrichus polonicus* Skoczen; Skoczen, 1980: p. 427-440, plates V-VI.

1983 ?*Neurotrichus polonicus* Skoczen; Storch and Qiu, 1983: p. 100-101, 105.

1993 *Neurotrichus polonicus* Skoczen; Skoczen, 1993: p. 133-134, fig. 4.

1994 "?*Neurotrichus polonicus*" Skoczeń; Rzebik-Kowalska, p. 80, 89, 90, 91.

1995 ?*Neurotrichus polonicus* Skoczeń; Doukas et al., p. 51.

2003 *Neurotrichus polonicus* Skoczen; Ziegler, 2003: p. 639.

2004 *Quyania polonica* (Skoczen); Popov, 2004: p. 71-75, fig. 6-8.

2005 *Neurotrichus* ? *polonicus*; Rzebik-Kowalska, 2005: p. 128-131.

2006 *Neurotrichus polonicus*; Ziegler, 2006: p. 139, 141.

2009 *Neurotrichus polonicus* Skoczen; Rzebik-Kowalska, 2009: p. 9, 22, 24, 25, 26, 51.

2014 ?*Neurotrichus polonicus* Skoczen; Rzebik-Kowalska, 2014: p. 9-11, fig. 2-3.

Etymology: From Poland.

Holotype: incomplete right mandible with with P_4–M_2 (MF/1016/1) from Kadzielnia (Skoczen, 1980: pl. VI).

Type locality: Kadzielnia, Poland.

Type horizon: Late Villanyian (MN17) or Pliocene/Pleistocene boundary.

Stratigraphic and Geographic range: Beside from the type locality, this species has also been recorded from the Early Villanyian (MN16) locality of Rębielice Królewskie 1A, Poland; from the Late Villanyan (MN17) locality of Kielniki 3B, Poland; from the Late Villanyan (MN17) locality of Zamkowa Dolna Cave A, Poland; from the Villanyan (MN17) locality of Varshets, Bulgaria.

Material: Rębielice Królewskie 1A, Poland: 1 P^4 (MF/1015/1); 3 M^1 (MF/1015/2-4), one right; right M^3 (MF/1015/5); incomplete premolar portion of the right mandible with P_3 (MF/1015/6); incomplete premolar portion of the right mandible with M_1 and M_2 (MF/1015/7); 2 middle fragments of left mandibles with M_1 and M_2 (MF/1015/8, 9); posterior part of left mandible with M_2 and M_3 (MF/1015/10); right M_1

(MF/1015/11); 3 M_2 (MF/1015/12-14); right and left M_3 (MF/1015/15, 16); 6 clavicles (MF/1015/17-22); 13 humeri (MF/1015/23-35); 1 ulna (MF/1015/36); 1 radius (MF/1015/37).

Zamkowa Dolna Cave near Częstochowa, layer C, Poland: 3 M^1 (MF/1017/1-3); right M^2 (MF/1017/4); right M_1 (MF/1017/5); right M_2 (MF/1017/6); right and left M_3 (MF/1017/7, 8); 1 right humerus (MF/1017/9).

Kadzielnia: 2 right mandible (MF/1016/1, 2), one with P_4-M_2 and other with M_1-M_2, 2 humeri (MF/1016/3, 4).

Kielniki 3B, Poland: 1 humerus (MF/1020/1).

Varshets, North Bulgaria: 3 fragments of mandible with M_1-M_3, 1 M_2 (V23: 4 – 5; V339), 3 humeri (V23: 1-3).

Diagnosis: Medium to large sized shrew-mole with moderate adaptation to digging. The humerus has an evident scalopine ridge and partially unfused bicipital tunnel (Fig. 2A). The protoconules are absent or vestigial. Lower molars have vestigial mesoconids.

Description: see Skoczen (1980; 1993), Popov (2004) and Rzebik-Kowalska (2014) for a complete and detailed description of the material.

Remarks: The material from Varshets (Popov, 2004) fit well in both size and morphological characters with that of *Rzebikia polonica* from Poland, so we ascribe the Bulgarian material to the Polish species.

Rzebikia skoczeni Zijlstra, 2010 gen. nov.

1993 *Neurotrichus minor* Skoczen; Skoczen, 1993: p. 130-133, fig. 4.

1994 *Neurotrichus minor* Skoczeń; Rzebik-Kowalska, p. 80, 88.

2004 *Quyania minor* Skoczen; Popov, 2004: p. 75.

2005 *Neurotrichus minor* Skoczen; Rzebik-Kowalska, 2005: p. 127.

2009 *Neurotrichus minor* Skoczeń; Rzebik-Kowalska, 2009: p. 9, 21.

2010 *Neurotrichus skoczeni*; Zijlstra, 2010: p. 1903.

2014 ?*Neurotrichus skoczeni* Zijlstra; Rzebik-Kowalska, 2014, p. 11, 12.

Etymology: the specific name honors Dr. Stanislaw Skoczen, the original describer of the species.

Holotype: right humerus ZPAL/M-2/2 (Skoczen, 1993: fig. 4)

Type locality: Weze 2, Poland.

Paratypus: isolated left M^1 (ZPAL/M-2/1)

Diagnosis: Small sized shrew-mole with moderate digging adaptation. The humerus have a well developed scalopine ridge and partially unfused bicipital tunnel, the pectoral tubercle is laterally displaced. The cingula of the M^1 weaker and reduced.

Description: see Skoczen (1993) for a complete and detailed description of the material.

Remarks: The humerus is very similar to that of *Rzebikia polonica*, it differs only for its smaller size and the laterally displaced pectoral tubercle. The M^1 is longer and narrower relative to that of *Rzebikia polonica* and differs for the shorter protoconus lacking a cingulum, the paraconus is narrower, the proto- and metaconuli are less prominent and the precingulum is markedly weak and short.

This species has been previously described as *Neurotrichus minor* by Skoczen (1993). Although we changed the generic attribution for this species we maintained the specific attribution of *skoczeni* because the name *minor* is a primary homonym and permanently invalid (ICZN 1999:art. 57.2; Zijlstra, 2010).

Stratigraphic and Geographic range: This species has been recorded from the Ruscinian/Villanyian boundary (MN 15, MN 16), locality of Weze 2, Poland (Skoczen, 1993).

Differential diagnosis

The following differential diagnoses are based on *Rzebikia polonica* gen. nov. because of the high similarity with the smaller species *Rzebikia skoczeni* gen. nov. and because of the most abundant material available for comparison.

Neurotrichus gibbsii. *Rzebikia polonica* gen. nov. shows many similarities in particular for the teeth (see Skoczen, 1980 for a detailed description) with the North American shrew mole, but differs by having reduced precingulids in M_1. It is distinct from *N. gibbsii* in the morphology of the humerus which is clearly less adapted to fossoriality by having:

– a partially unfused bicipital tunnel
– a more conspicuous scalopine ridge
– a shorter teres tubercle
– a longer greater sulcus
– the lesser tuberosity is less expanded in proximal direction

Urotrichus talpoides. *Rzebikia polonica* gen. nov. is different in many features from the Japanese greater shrew mole in particular by having:

– a partially unfused bicipital tunnel
– a longer teres tubercle

– a lesser distance between the teres tubercle and the lesser tuberosity

– the presence of the scalopine ridge

– metacristid of the P_4 in stright line

– less robust mandible

– presence of the P_3

– presence of the talonid notch

Urotrichus dolichochir. This species present clear Urotrichine affinity. It resembles the recent species *Urotrichus talpoides* in both size and shape of the humerus. *Urotrichus dolichochir* presents some primitive humeral features compared with extant Urotrichini such as an even small teres tubercle, open bicipital tunnel and a more slender shaft of the humerus. *Rzebikia polonica* gen. nov. differs from this species mainly for the same characters expressed for *U. talpoides*.

Dymecodon pilirostris. *D. pilirostris* has been considered for long time as a congeneric member of *Urotrichus* because of the strong similarities in their morphology (Kawada and Obara, 1999). *Rzebikia polonica* gen. nov. is different from the lesser Japanese shrew mole by the same features of *U. talpoides*.

Quyania chowi. *Rzebikia polonica* gen. nov. resembles *Q. chowi* in many features (see Storch and Qiu, 1983 for a detailed description) whereas it is distinct from the Chinese species by having:

– a more rounded and larger teres tubercle

– a partially unfused bicipital tunnel

– a shorter distance between the teres tubercle and the lesser tuberosity

– a weaker development of the cingula

– unbent lingual side of the lower molars

– more conspicous protoconules of the M^1 and M^2

– parastyle of the M^2 separated from the paracrista

Quyania europaea Rzebik-Kowalska, 2014. *Rzebikia polonica* gen. nov. differs from the European species of *Quyania* by having:

- more robust shaft of the humerus
- larger teres tubercle
- more evident and straight scalopine ridge
- partially unfused bicipital tunnel
- the presence of vestigial mesoconids
- mental foramen situated under the P_3

Neurotrichus columbianus Hutchinson, 1968. According with Storch and Qiu (1983) and Popov (2004), *Neurotrichus columbianus* should be related to the genus *Yanshuella* Storch and Qiu, 1983 and does not belong to Neurotrichini tribe at all.

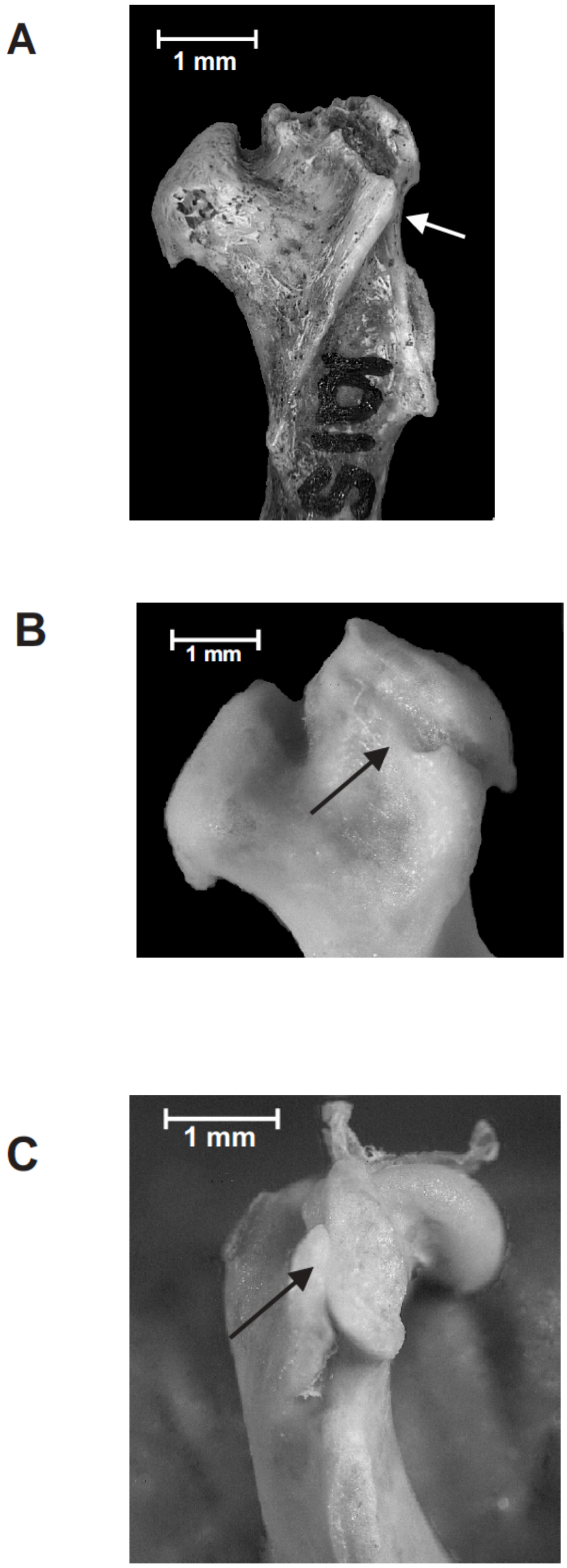

Figure 2. Pictures showing the different conditions of the bicipital tunnel. Arrows indicate the bicipital tunnel. **A)** *Rzebikia polonica* gen. nov. (frontal view) with partially unfused bicipital tunnel. **B)** *U. talpoides* (frontal view) with completely open bicipital tunnel. **C)** *N. gibbsii* (lateral view) with completely fused bicipital tunnel.

Results

Shape and size analyses

bgPCA performed on the procrustes coordinates shows a neat separation between the urotrichine and neurotrichine shrew moles in particular across the PC1 (Fig. 3A). At positive values of the PC1 (62.80% of the total variance) the humeral shape shows an enlargement of the teres tubercle, an enlargement of the medial epicondyle and an expansion of the greater tuberosity, while at negative values the humerus shows a contraction of these regions. Along the PC2 (17.56% of the total variance) it is possible to observe a separation between *Neurotrichus gibbsii* and *Rzebikia polonica* gen. nov. At positive values the humeral morphology shows a reduction of the teres tubercle, a lengthening of the greater sulcus and a contraction of the lesser tuberosity, while at negative values the humerus shows an enlargement of the teres tubercle and of the lesser tuberosity while the greater sulcus becomes shorter. Along the PC3 (10.84% of the total variance) it is possible to appreciate the separation between *Urotrichus talpoides* and *Dymecodon pilirostris* (Fig. 3B). At positive values the humeral shape shows an enlargement of the medial epicondyle and an increase of the greater tuberosity, while at negative values it is possible to observe a contraction of the regions previously described.

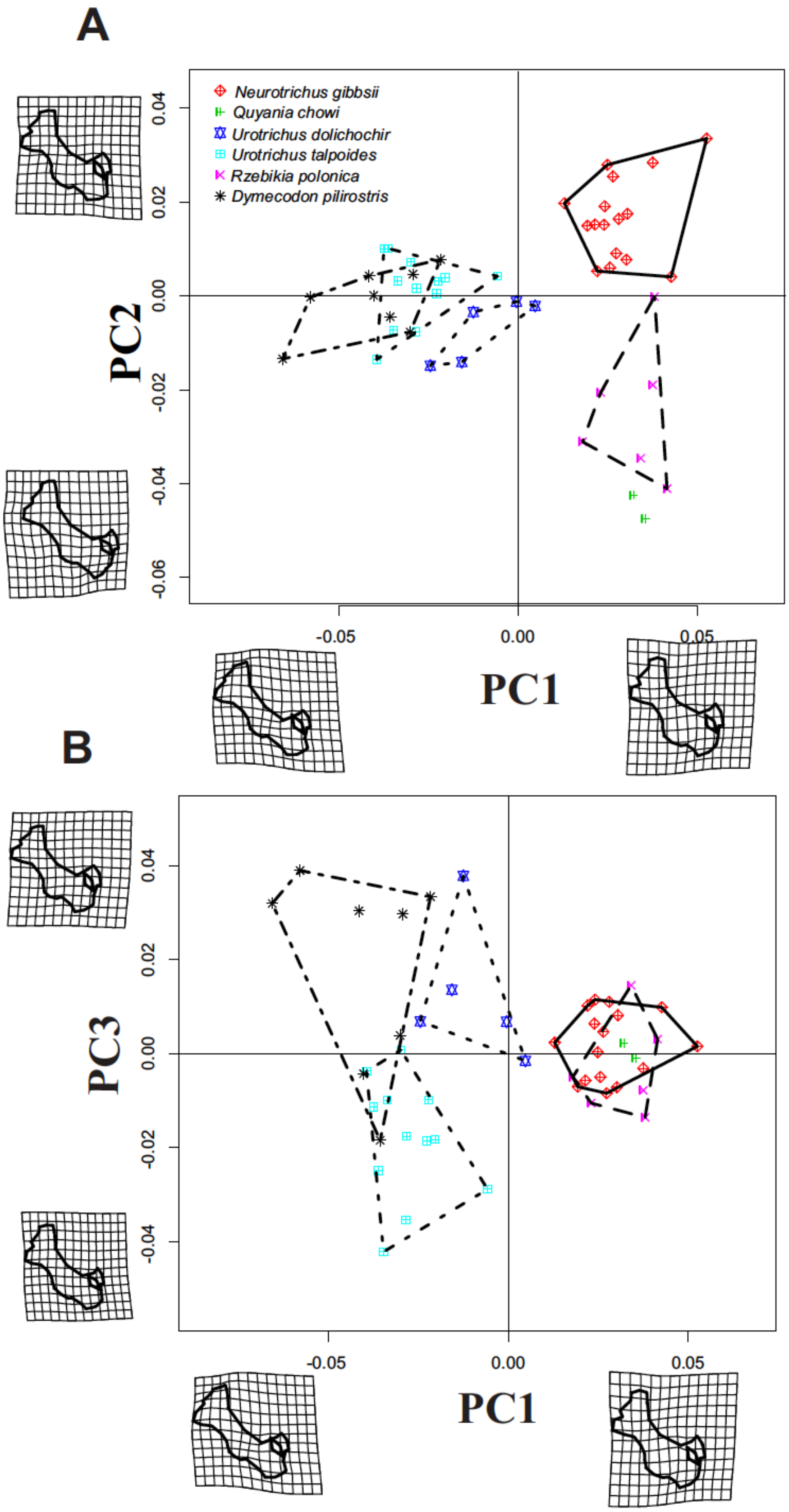

Figure 3. A) Scatterplot of the first two axes of the bgPCA. Deformation grids refer to axes extremes (positive and negative values). **B)** Scatterplot of the first and third

axes of bgPCA Deformation grids refer to axes extremes (positive and negative values).

Permutational MANOVA returned an overall highly significant difference (p-value < 0.001) among species and pairwise permutation MANOVA returned significant values (Table 1) for all the comparisons.

	Neurotrichus gibbsii	*Urotrichus dolichochir*	*Urotrichus talpoides*	*Rzebikia polonica*	*Dymecodon pilirostris*
Neurotrichus gibbsii		0.0009	0.0009	0.0009	0.0009
Urotrichus dolichochir			0.0019	0.0045	0.0134
Urotrichus talpoides				0.0009	0.0019
Rzebikia polonica					0.0019
Dymecodon pilirostris					

Table 1. Pairwise permuted MANOVA results. All p-values are corrected using "Holm" correction.

The boxplot computed for the CS (Fig. 4) showed a significant size variation (permutational ANOVA p-value < 0.001) among species. *Rzebikia polonica* gen. nov. was significantly different from all other taxa by means of pairwise permuted ANOVA (Table 2).

	Neurotrichus gibbsii	*Urotrichus dolichochir*	*Urotrichus talpoides*	*Rzebikia polonica*	*Dymecodon pilirostris*
Neurotrichus gibbsii		0.00159	0.76802	0.00099	0.00559
Urotrichus dolichochir			0.00239	0.00779	0.40215
Urotrichus talpoides				0.00099	0.00159
Rzebikia polonica					0.00449
Dymecodon pilirostris					

Table 2. Pairwise permuted ANOVA results. All p-values are corrected using "Holm" correction.

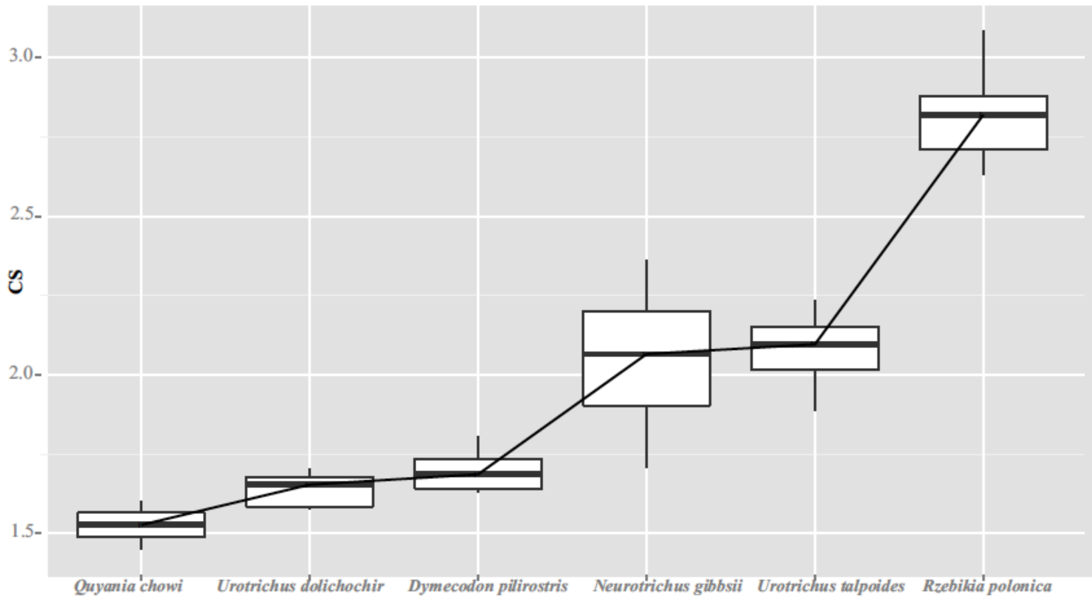

Figure 4. Boxplot of the centroid sizes. Bottom and top of the boxes are the first and third quartiles, the horizontal solid black lines represent the median, the whiskers represent the minimum and maximum values.

The UPGMA computed on the Euclidean distance matrix calculated on the shape variables (Fig. 5A) evidenced a neat morphological difference between the Urotrichini, where *U. talpoides* and *D. pilirostris* showed close similarities, and Neurotrichini, where *N. gibbsii* and *Rzebikia polonica* gen. nov. showed the closest morphological affinities.

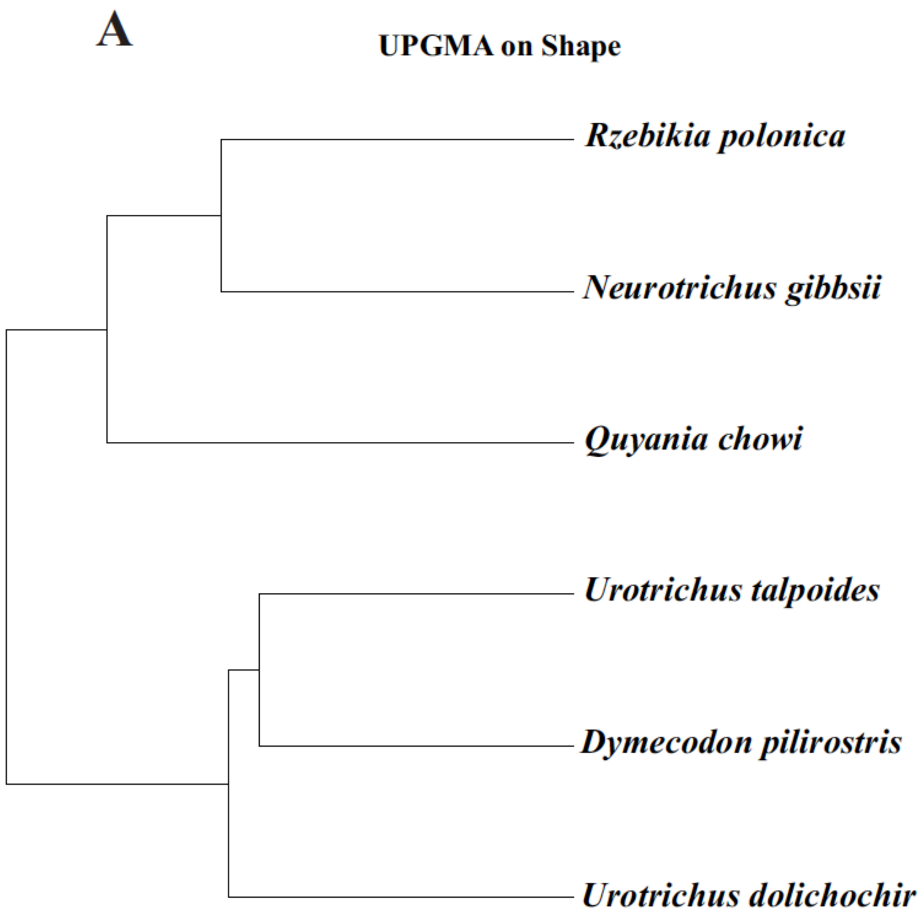

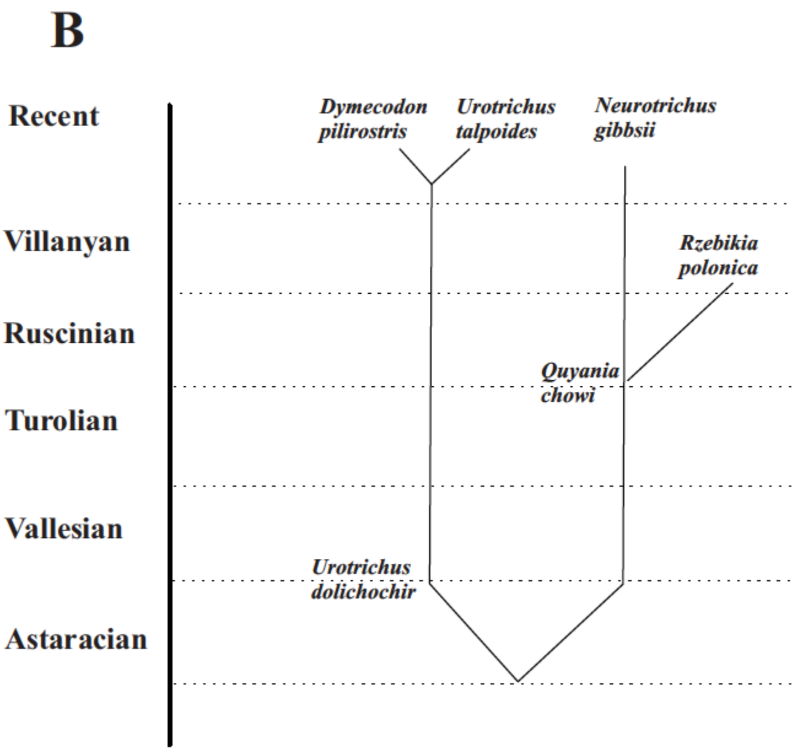

Figure 5. A) UPGMA calculated on the Euclidean distance matrix computed on the shape variables. **B)** Phylogenetic hypothesis proposed by Storch and Qiu (1983).

Discussion and concluding remarks

The continuous humeral shape variation evidenced by the GM analysis was congruent with the qualitative morphological differences observed in the specimens included in this study. In particular the neat separation between Urotrichini and Neurotrichini observed along the PC1 is due to major modifications of the regions mainly involved in the digging process (Gambaryan et al., 2003; Piras et al., 2012), such as the expansion of the teres tubercle. *Rzebikia polonica* gen. nov. has a partially unfused bicipital tunnel (Fig. 2A) while the Urotrichini have it open (Fig. 2B). Field observations on the extant *N. gibbsii* (Campbell and Hochachka, 2000; p.578; Stone, 1995; p.57) and recent Finite Elements Analysis (Piras et al., 2012) suggest that Neurotrichini are more adapted to a fossorial lifestyle than Urotrichini. The UPGMA (Fig. 5A) confirmed the distinction between Neurotrichini and Urotrichini. Rzebik-Kowalska (2014) pointed out that *Q. chowi* and *Rzebikia polonica* gen. nov. should be included in the Neurotrichini tribe. Our results support the inclusion of *Rzebikia polonica* gen. nov. in Neurotrichini tribe and exclude any Urotrichine affinity. Along the PC2 *Rzebikia polonica* gen. nov. discriminates from *N. gibbsii* and from *Quyania chowi*. According to Storch and Qiu (1983) and to Popov (2004), *Rzebikia polonica* gen. nov. descends from *Q. chowi*. In fact, the Polish genus has a more robust humerus, a bicipital tunnel showing a higher fusion degree between the pectoral crest and the lesser tuberosity, and a teres tubercle larger and more rounded. The phenetic relationships support *Rzebikia polonica* gen. nov. being more advanced than *Q. chowi* and hence justify its different generic allocation. Storch and Qiu (1983) hypothesized a parallel evolution of *N. gibbsii* and *Rzebikia polonica* gen. nov., suggesting that the

Polish species is more andvanced than *N. gibbsii* by having a relatively larger size. Popov (2004), following Storch and Qiu (1983), considered *Rzebikia polonica* gen. nov. as more advanced than *N. gibbsii*. Here we reject such hypothesis because *Rzebikia* gen. nov. shows many primitive features of the humerus when compared with the North American forms. The most striking features are the partially unfused bicipital tunnel (Fig. 2A), that is completely fused (Fig. 2C) in *N. gibbsii* (Reed, 1951; Sánchez-Villagra et al., 2004), the reduced teres tubercle, and the widened minor sulcus. The enlargement of the teres tubercle is an important character of talpids evolution (Gambaryan et al., 2003; Piras et al., 2012). This humeral region allows the insertion of the muscles Teres major and Latissimus dorsi, two of the main muscles involved during burrowing (Gorman and Stone, 1990; Gambaryan et al., 2003; Piras et al., 2012). A larger teres tubercle would allow the insertion of larger and more powerful digging muscles. *Neurtotrichus gibbsii* and *Rzebikia polonica* gen. nov. are separated along the PC2 and the humeral shape changes associated with this axis are in good agreement with our qualitative observations about the humeral morphological differences between these two taxa. Moreover, *N. gibbsii* and *Rzebikia polonica* gen. nov. are significantly different under pairwise permutational MANOVA. These evidences suggest that *N. gibbsii* is better adapted to digging than *Rzebikia polonica* gen. nov. and in a more derived evolutionary state. Nevertheless, *Rzebikia polonica* gen. nov. shows some derived features on teeth such as the reduced precingulid of M_1 and more pronounced protoconules (Storch and Qiu, 1983; Popov, 2004), not equally advanced in *N gibbsii*. Rzebik-Kowalska (2014) noted that, in *Rzebikia polonica* gen. nov., the protoconules are absent and vestigial only in one specimen. Moreover the upper and lower teeth of *Rzebikia polonica* gen. nov. are wider than those of *N. gibbsii* and more similar to those of *Quyania* (Rzebik-Kowalska, 2014). All of these evidences well support a new generic allocation. The UPGMA (Fig. 5A) shows close similarities with the phylogenetic hypothesis (Fig. 5B) proposed by Storch and Qiu (1983). We follow them in considering *Q. chowi* as the probable ancestor to *N. gibbsii, Rzebikia polonica* gen. nov. and *Rzebikia skoczeni* gen. nov. According to Storch and Qiu (1983) *Q. chowi* can be considered the ancestor of the neurotrichine lineage. *Neurotrichus gibbsii* could represent a derived form that colonized North America during the Early Pliocene, while one or two colonization events towards Eastern Europe could have occurred. The first colonization event could have involved the ancestor of *Q. europaea* during the Early Pliocene (another colonization wave from Asia, that involved the Urotrichini, during the Miocene-Pliocene boundary, is testified by the presence of *Urotrichus* sp. In Maramena locality, see Doukas et al., 1995) In this scenario it is possible to hypothesize *Rzebikia* gen. nov. being derived from the European *Q. europaea*. This represents the most parsimonious explanation, although we note that *Rzebikia* gen. nov. is more similar to *Q. chowi* (Storch and Qiu, 1983; Popov, 2004). If we consider *Rzebikia* gen. nov. directly derived from *Q. chowi* we should hypothesize a subsequent colonization event during the late Early Pliocene. *Quyania europaea* is clearly distinct from *Rzebikia* gen. nov. by its slender humerus and relative smaller size (Rzebik-Kowalska, 2014), suggesting a different digging capability and ecological adaptation. *Rzebikia skoczeni* gen. nov. and *Rzebikia polonica* gen. nov. are both larger than *Q. europaea* (Skoczen, 1993; Rzebik-Kowalska, 2014). *Rzebikia skoczeni* gen. nov. has been found in the MN15 locality of Weze 2 only (see Appendix III), where no other neurotrichine moles are present. *Rzebikia polonica* gen. nov. first appearence is in the MN16 Rębielice Królewskie 1A locality (see Appendix III). This species could be descended from *Rzebikia skoczeni* gen. nov. anagenetically by an increase in size. However, due to the scarcity of the

Rzebikia skoczeni gen. nov. fossil record it is not possible to test this hypothesis. *Rzebikia polonica* gen. nov. have been found in sympatry with *Q. europaea* (MN16 Rębielice Królewskie 1A and MN17 Kadzielnia localities). Size differences have been documented for sympatric species belonging to genera *Talpa* and *Mogera* (Abe, 1996; Loy et al., 1996; Loy and Capanna, 1998; van Cleef-Roders and van den Hoek Ostende, 2001; Yokohata, 2005; Bego et al., 2008; Loy, 2008), this phenomenon has been documented also in the extinct genus *Geotrypus* (van den Hoek Ostende, 2001). Moreover, we found a significant size difference between *U. talpoides* and *D. pilirostris* which has been reported to live in sympatry in Honshu and Shikoku regions (Abe, 1967). Following this evidence, the size displacement between *Rzebikia* gen. nov. *spp*. and *Q. europaea* could have occurred in response to eco-evolutionary constraints, such as inter-specific competition and the ability to exploit low productive habitats. Size character displacement between pairs of ecologically close and geographically overlapping species is a common pattern in mammals (Simberloff and Boecklen, 1981; Dayan and Simberloff, 1998) and could represent a rapid response to strong inter-specific competition in talpids (Loy and Capanna, 1998; Loy et al., 2001). Finally, recent contributions highlighted that humeral morphology possesses a taxonomic value at the genus level and in some cases at the species level as well (van den Hoek Ostende, 1997; Ziegler, 2003; Klietmann et al., 2014). In the present paper the highly significant values reported by pairwise permutational MANOVA confirm the chance to consider the humerus as a diagnostic element. Moreover, our results suggest that the landmark based shape analysis is useful in supporting systematics in palaeontological investigations where only skeletal elements are avilable.

Appendix I

List of the specimens used in the GM analysis. Abbrviations: IVPP: Institute of Vetebrate Paleontology and Paleonathropology, Beijing; ISEZ-PAN: Institute of Systematics and Evolution of Animals – Polish Academy of Sciences; UCMP: University of California Museum of Paleontology; LACM: Los Angeles County Museum;

Species	**Code**	**Museum**	**Locality**
Quyania chowi	6453.1.26, 6453.1.94	IVPP	Ertemte 2, China
Rzebikia polonica	MF/1015/23, MF/1015/24, MF/1015/25, MF/1015/26, MF/1017/9, MF/1018/24	ISEZ-PAN	Rębielice Królewskie 1A, Zamkowa Dolna Cave C, Kielniki 3B, Poland
Neurotrichus gibbsii	no code, 123766a, 123766b, 115.37.16, 115.37.17, 93940, 93942, 93943, 93944, 86880b, 86880c	UCMP; LACM	Lane County, Bodega Bay, USA
Urotrichus dolichochir	69136a, F-38, 69015, P6-1067, 69136b	Lyon Universitè; Augsburg NaturMuseum	La Grive, France; Petersbuch 6, Germany
Urotrichus talpoides	29116, 28206, 20661, 28207, 29456, 20169, 20690, 28208, 20618, 20623, 20620, 29455	National Museum of Nature and Science	Japan
Dymecodon pilirostris	27443, 27459, 27449, 27450, 27455, 29144, 20621, 29113	National Museum of Nature and Science	Japan

Appendix II

Measurements (mm) of the material of *Rzebikia polonica* and *Rzebikia skoczeni*. The measurements taken follow Skoczen (1980; 1993)

Locality	Material	N	Measure	Min	Mean	Max
Rębielice Królewskie 1A	P^4	1	L W1 W2		1.7 0.8 1.22	
Rębielice Królewskie 1A	M^1	3	L1 L2 L3 W1 W2	2.4 1.28 1.18 1.20 2.70	2.4 1.33 1.29 1.4 2.82	2.4 1.4 1.35 1.51 2.9
Rębielice Królewskie 1A	M^2	1	L1 L2 L3 W1 W2		2 1.48 1 2 2.45	
Rębielice Królewskie 1A	P_3	1	L W		0.91 0.60	
Rębielice Królewskie 1A	M_1	3	L1 L2 L3 W1 W2	1.85 0.9 0.85 0.97 1.22	1.92 0.96 0.99 1.07 1.26	1.95 1 1 1.1 1.3
Rębielice Królewskie 1A	M_2	9	L1 L2 L3 W1 W2	1.96 1 0.85 1.1 1.1	2.02 1.1 0.95 1.16 1.21	2.1 1.12 1 1.2 1.3
Rębielice Królewskie 1A	M_3	4	L1 L2 L3 W1 W2	1.7 0.96 0.5 0.9 0.8	1.75 1 0.7 0.97 0.84	1.82 1.1 0.77 1 0.9
Zamkowa Dolna Cave C	M^1	3	L1 L2 L3 W1 W2	2.2 1.12 1.1 1.1 2.42	2.33 1.14 1.27 1.2 2.58	2.49 1.18 1.4 1.3 2.68
Zamkowa Dolna Cave C	M^2	1	L1 L2 L3 W1 W2		1.8 1.26 0.92 1.78 2.45	
Zamkowa Dolna Cave C	M_1	1	L1 L2 L3 W1		1.71 1 0.71 0.88	

			W2		1.18	
Zamkowa Dolna Cave C	M_2	1	L1 L2 L3 W1 W2		1.91 1.11 0.8 1.07 1.1	
Zamkowa Dolna Cave C	M_3	1	L1 L2 L3 W1 W2		1.73 1.1 0.63 0.97 0.87	
Kadzielnia	P_4	1	L W		1.22 0.74	
Kadzielnia	M_1	2	L1 L2 L3 W1 W2	1.7 0.84 0.8 0.85 1.1	1.75 0.92 0.83 0.86 1.1	1.8 1 0.86 0.88 1.1
Kadzielnia	M_2	2	L1 L2 L3 W1 W2	1.85 1 0.85 1.1 1.1	1.87 1 0.87 1.1 1.1	1.9 1 0.9 1.1 1.1
Kadzielnia	M_3	1	L1 L2 L3 W1 W2		1.8 0.97 0.83 1 0.8	
Rębielice Królewskie 1A	Clavicle	6	L W	4.2 0.8	4.2 0.9	4.3 1.0
Rębielice Królewskie 1A	Radius	1	L W		8.8 0.9	
Rębielice Królewskie 1A	Humerus	8	L PW DW	8.4 3.9 4.3	8.6 4.1 4.6	9.1 4.4 4.8
Zamkowa Dolna Cave C	Humerus	1	L PW DW		8.3 4.1 4	
Kadzielnia	Humerus	1	L PW DW		7.8 3.9 3.8	
Varshets	Humerus	1	L PW DW		7.6 3.7 3.9	
Kielniki 3B	Humerus	1	L PW DW		8 4.1 4.2	
Rzebikia skoczeni						

Weze 2	Humerus	1	L PW DW		7.2 3.6 4	

Appendix III

List of the localities and relative ages where *Q. europaea*, *Rzebikia skoczeni* gen. nov. and *Rzebikia polonica* gen. nov. are present.

Locality	Age	*Q. europaea*	*Rzebikia skoczeni* gen. nov.	*Rzebikia polonica* gen. nov.
Podlesice	MN14	x	/	/
Weze 1	MN15	x	/	/
Weze 2	MN15	/	x	/
Rębielice Królewskie 1A	MN16	x	/	x
Kadzielnia	MN17	x	/	x
Kielniki 3b	MN17	/	/	x
Zamkowa Dolna Cave C	MN17	/	/	x
Varshets	MN17	/	/	x

TALPA FOSSILIS OR *TALPA EUROPAEA*, THAT IS THE QUESTION: GEOMETRIC MORPHOMETRICS AND ALLOMETRIC TRAJECTORIES OF HUMERAL REMAINS FROM HUNGARY.

INTRODUCTION

Ontogenetic, static, and evolutionary allometries are recognized depending on whether the relationship between shape and size is taken over the development of an individual, across individuals at a similar developmental stage within a population, or across separate evolutionary lineages (Cock, 1966; Gould, 1966; Cheverud, 1982). The allometric-constraint hypothesis (Voje et al., 2013; Firmat et al., 2014) state that the allometric slope remains stable at macroevolutionary level and its able to constrain the evolutionary diverngence in the morphospace along its specific trajectories (Voje et al., 2013, Pelabon et al., 2014; Firmat et al., 2014). Many recent comparative studies have provided evidences to account the constraining role of static allometry (Voje and Hansen, 2013; Voje et al., 2013; Firmat et al., 2014). However, very few studies investigated the evolution of ontogenetic, static or evolutionary allometry in the fossil record. The humerus of highly fossorial moles is well suited for this kind of investigations, as this skeletal element is often found abundant and well preserved in fossil assemblages. Here we re-investigated the *Talpa fossilis* and *Talpa europaea* humeral fossil material from several Hungarian localities and from Petersbuch 1 (see

Table 1). Hungarian localities provided a huge amount of fossil material belonging to the genus *Talpa*. The Late Pliocene-Middle Pleistocene *Talpa* material has been attributed to *T. fossilis* while the Late-Pleistocene specimens to *T. europaea* (Janossy, 1986). We provide a Geometric Morphometric analysis of the humerus (the most abundant and better preserved skeletal element) in order to quantitatively evaluate the differences (if any) in shape and size as well as in their relationship. We also investigated the static allometric trajectories occurring in the two taxa.

The name *Talpa fossilis* have been first used by Pomel (1848). He described a new species which was somewhat larger a robust and was differing from others by having some shape differences in the carpals. The description made by Pomel (1848) has gone unnoticed as *Talpa fossilis* is attributed to Petenyi (1864), that described *Talpa vulgaris fossilis* from the Hungarian fossil bearing locality of Beremend. Hereafter we report the original description translated by van Cleef-Roders and van den Hoek Ostende (2001): "*Talpa vulgaris fossilis* Petényi. The fossil bone material of this animal totally agrees with the corresponding bones of the recent common mole, both in morphology and size; thus this fossil mole does not differ from the recent mole on the specific level, if one does not take into account the only difference noted by me, viz. that in the modern mole the labial side of the mandible has only two foramina mentale, one under the second premolar, the other under the first molar, wheras in the fossil mole three of such foramina are found, one under the first premolar, but two - be it one of them very shallow - under the first molar." Following the original description of Petenyi (1864) *T. fossilis* could not be distinguished from *Talpa europaea* Linnaeus, 1758, and justify a distinction only at subspecific level. Despite this the middle-sized *Talpa* specimens from Middle-Late Pliocene to the Middle Pleistocene deposits are often attributed to *T. fossilis*, while in the more recent deposits are often classified as *T. europaea* (Janossy, 1986). Kormos (1930) described *Talpa praeglacialis* from the Early Pleistocene locality Püspokfürdo (Betfia 2), accounting for a larger number of foramina mentale than in *T. europaea*. Kretzoi (1938) placed *T. praeglacialis* in synonymy with *T. fossilis*. Von Koenigswald (1970) in its discussion on the *Talpa* specimens from the German locality Petersbuch 1 suggested that there were no differences in both size and morphology between *T. fossilis* and *T. europaea*. Rabeder (1972), in his discussion of the *Talpa* material from Hundsheim, suggested the presence of some slight morphological differences between *T. fossilis* and *T. europaea* such as the width of the M3 talonid and the number of the foramina mentale. Although he considered such differences indicative for a distinction at the subspecific level only. Robert (1983) proposed to retain the name *T. fossilis* as a chronospecies since she observed a gradual increase in size during the Pleistocene. However, van Cleef-Roders and van den Hoek Ostende (2001) pointed out that the material from Saint Seveaur could be referred to *T. caeca* s.l. because of the division of the mesostyle and the lack of humeri in the sample. They also questioned the evolutionary trend proposed by Robert (1983). Niethammer (1990) following Von Koenigswald (1970) considered *T. fossilis* as a stratigraphic species. van Cleef-Roders and van den Hoek Ostende (2001), reviewing the literature concerning *T. fossilis*, suggested the chance to consider *T. fossilis* as a junior synonym of *T. europaea*. However, they pointed out as including all the material belonging to *T. fossilis* into *T. europaea* would be probably misleading, thus suggesting a more accurate review of the fossil assemblages. From this brief review of the main contributions to this debate, emerge that the majority of the researchers tend to consider *T. fossilis* a subspecies or as a synonym of *T. europaea*. Despite these evidences, many authors (Sanchez-Villagra et al., 2004; Suarez and Mein, 2004;

Crochet et al., 2009; Colangelo et al., 2010; Rzebik-Kowalska, 2014 among others) still consider the distinction between the two species as valid. Moreover, many of the measures and of the morphological differences reported from several authors are statistically untested. We want to contribute to this debate by introducing the study of static allometric trajectories via modern shape analysis in order to unveil (if any) the potential different shape-size relationship within *T. fossilis* and *T. europaea*.

MATERIAL AND METHODS

Material

We analyzed a total of 113 left humeri belonging to *Talpa europaea* Linneus, 1758 (n = 67) and *Talpa fossilis* Petényi, 1864 (n = 46). See Table 1 for the specimens localities and their corresponding ages.

Table 1. List of the localities and corresponding ages where *T. fossilis* and *T. europaea* are present.

Locality	**Age**	*T. fossilis*	*T. europaea*
Osztramos 7	MN16	x	/
Villany 3	MN17	x	/
Betfia	Early Pleistocene	x	/
Puspokfurdo	Early Pleistocene	x	/
Beremend 15-16	Early Pleistocene	x	/
Somssich Hegy 2	Middle Pleistocene	x	/
Villany 8	Middle Pleistocene	x	/
Koversvarad	Middle Pleistocene	x	/
Tarkò	Middle Pleistocene	x	/
Brassò	Middle Pleistocene	x	/
Petersbuch 1	Middle Pleistocene	x	/
25-Fortuna Utca, Budapest	Middle Pleistocene	x	/
Istalloskò	Late Pleistocene	/	x
Bivak Barlang	Late Pleistocene	/	x
Kofulke	Late Pleistocene	/	x
Szelim Barlang	Late Pleistocene	/	x
Koszeg-Puskaporos	Late Pleistocene	/	x

Geometric Morphometrics

The humeri have been photographed in caudal view at a fixed distance of about 50 cm with a Nikon D100 camera with a Micro-Nikkor 105mm lens. We digitized 21 landmarks and 15 semi-landmarks (Figure 1) using the tpsDig2 software (Rohlf, 2006).

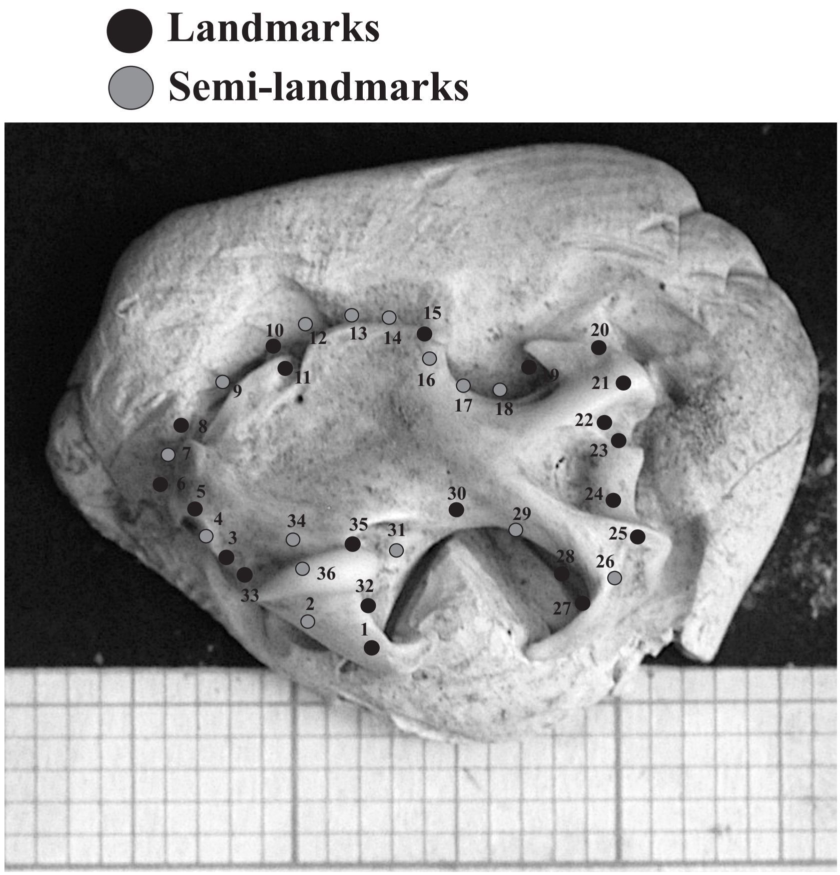

Talpa europaea

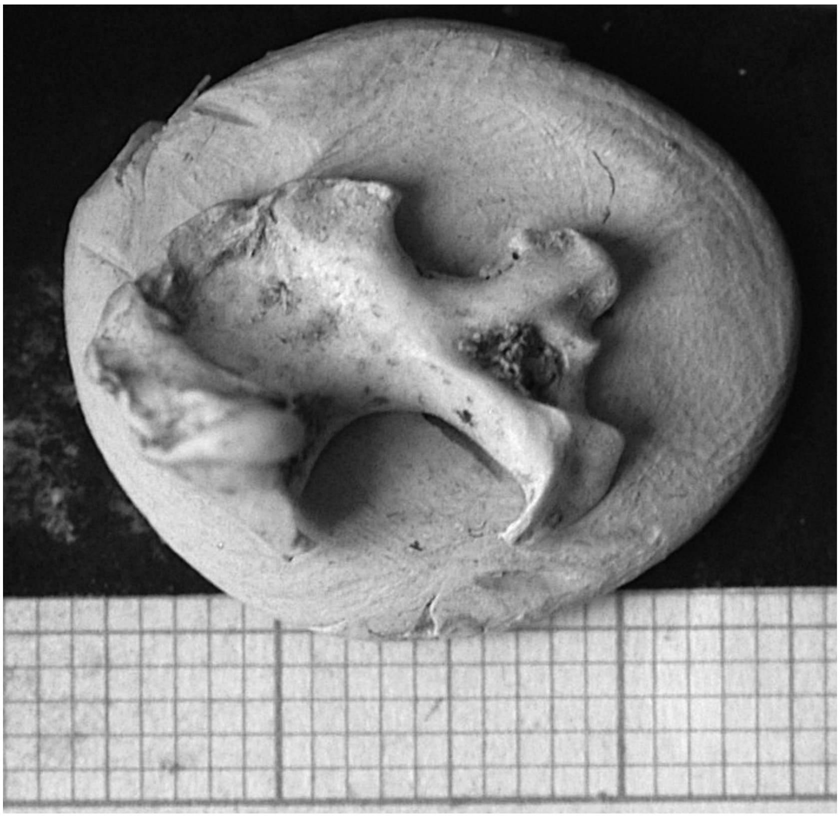

Talpa fossilis

Figure 6.1. Landmarks (black circles) and semilandmarks (white circles) digitized on the humerus in caudal norm: 1) lateral end of greater tuberosity; 2) articular facet for clavicula; 3) proximal edge of the articular facet for clavicula; 4) bicipital notch; 5) proximal end of lesser tuberosity; 6) medial edge of the minor tuberosity; 7) lateral edge of the lesser tuberosity; 8) bicipital ridge; 9) middle point of the bicipital tunnel; 10) lateral end of the scalopine ridge; 11) proximal end of the teres tubercle; 12-14) surface of the teres tubercle; 15) distal end of the teres tubercle; 16-18) minor sulcus; 19) posterior margin of the lateral epicondyle; 21-22) lateral epicondyle; 22-24) trochlear area; 25-27) medial epicondyle; 28) posterior margin of the medial epicondyle; 29-32) greater sulcus; 33-36) humeral head.

Static Allometry

As first we tested if shape and size variables were related to age. We regressed the species specific shape variables and CS against the average ages of localities where the different populations of *T. fossilis* and *T. europaea* have been found (see Table 6.1).

Table 6.1. List of the localities and corresponding ages where *T. fossilis* and *T. europaea* are present.

Locality	**Age**	*T. fossilis*	*T. europaea*
Osztramos 7	MN16	x	/
Villany 3	MN17	x	/
Betfia	Early Pleistocene	x	/
Puspokfurdo	Early Pleistocene	x	/
Beremend 15-16	Early Pleistocene	x	/
Somssich Hegy 2	Middle Pleistocene	x	/
Villany 8	Middle Pleistocene	x	/
Koversvarad	Middle Pleistocene	x	/
Tarkò	Middle Pleistocene	x	/
Brassò	Middle Pleistocene	x	/
25-Fortuna Utca, Budapest	Middle Pleistocene	x	/
Petersbuch 1	Middle Pleistocene	x	/
Istalloskò	Late Pleistocene	/	x
Bivak Barlang	Late Pleistocene	/	x
Kofulke	Late Pleistocene	/	x
Szelim Barlang	Late Pleistocene	/	x
Koszeg-Puskaporos	Late Pleistocene	/	x

The relationship between size (independent variable) and shape (dependent variable) was tested performing a multivariate regression of shape on size values averaged by species. All individuals analyzed in the present are adult or subadult basing on the ossification status of humeral epiphysis and diaphysis. Thus the allometric trajectories studied here belong to the category of static allometry. To test for differences in slopes among species we run a permutational multivariate analysis of covariance (perMANCOVA), using species as groups and size as covariate, (Zelditch et al., 2004, 2012). This analysis was performed using the function adonis(). If slopes do not differ significantly (in this case the species and size interaction of the MANCOVA is not statistically significant) it is possible to control for the allometric effect and compute size-corrected shape variables (Viscosi and Cardini, 2011; Viscosi et al., 2012; Zelditch et al., 2012). Just for the sake of visualization we performed a canonical correlation analysis (CCA), which determines an Y axis that represents the amount of Y (shape variables) that is best explained by the independent variable X (CS). As we were interested in studying interspecific shape differences too, we removed the intraspecific variation by performing separate per-species multivariate regressions between shape and size. Then, for each species, the residuals were added to species specific shapes predicted at maximum and minimum species specific size values. This procedure ensures elimination of intraspecific allometry while maintaining the interspecific size-shape differences due to evolutionary allometry (Piras et al., 2011, 2014). The differences between the predicted shape variables have been evaluated performing a perMANOVA using the function adonis(). This strategy, common in GM studies, allows the standardization of shape variables at determined size values (Zelditch et al., 2004, 2012). Finally, we plotted the Euclidean distances between shapes predicted at ten equal CS values for *T. fossilis* and *T. europaea* in order to visualize the course of interspecific morphological distances along the static allometry.

RESULTS

Shape and size analyses

The PCA performed on the aligned procrustes coordinates (Figures 2A and 2B) show a good degree of separation between *T. fossilis* and *T. europaea* in particular along the PC1 (17.18% of the total variance). At positive values of the PC1 the humeral morphology shows an enlargement of the pectoral crest and of the teres tubercle, an enlargement of the greater tuberosity and a medial shift of the humeral head, while at negative values it presents a contraction of the pectoral crest and a reduction of the teres tubercle, a reduction of the greater tuberosity and a lateral shift of the humeral head. At positive values of the PC2 (13.6% of the total variance) the humeral morphology shows an elongation of the teres tubercle and a shortening of the pectoral crest, while at negative values it can be seen a shortening of the teres tubercle and an elongation of the pectoral crest. At positive values of the PC3 (8.17% of the total variance) the humeral shape shows a contraction of the lateral epicondyle and an enlargement of the minor sulcus, while at negative values it shows an enlargement of the lateral epicondyle and a contraction of the minor sulcus.

1

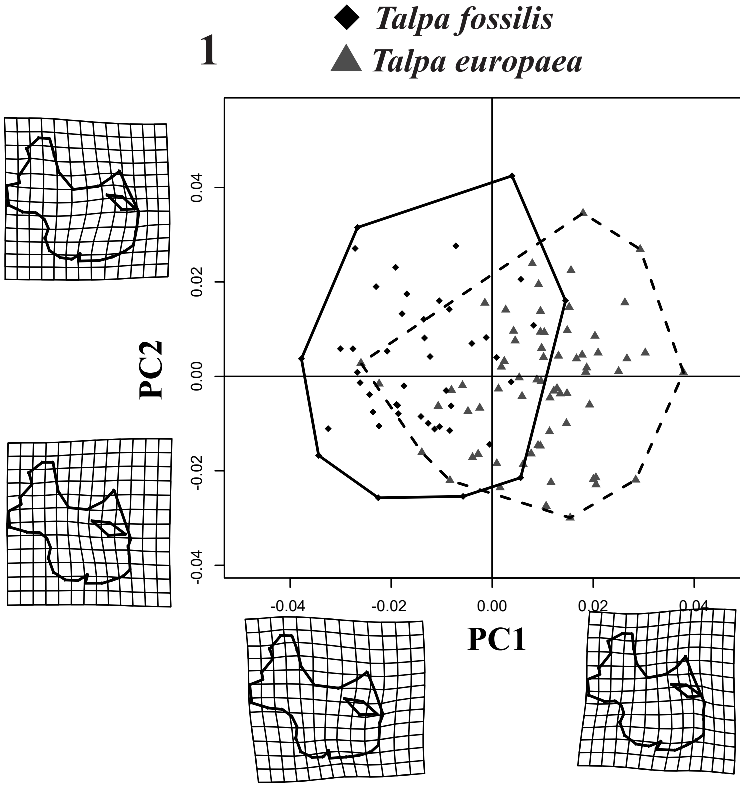

Talpa fossilis
Talpa europaea
PC2
PC1
0.04
0.02
0.00
-0.02
-0.04
-0.04
-0.02
0.00
0.02
0.04

2

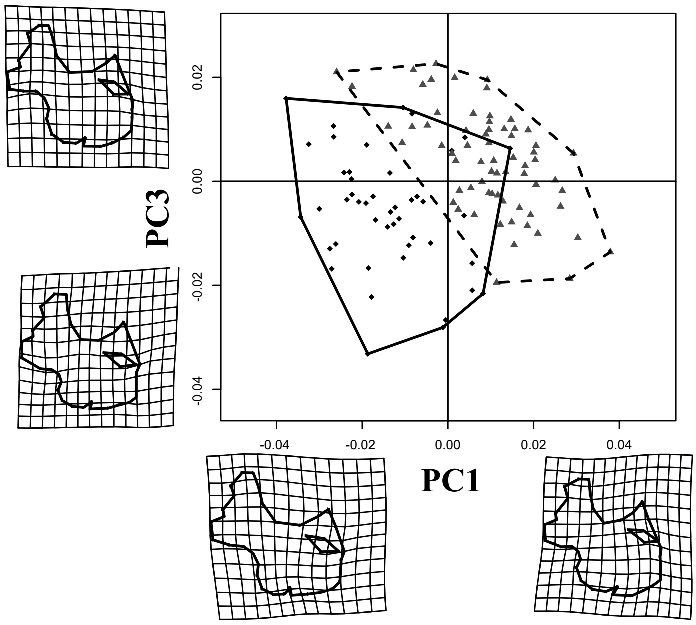

PC3
PC1
0.02
0.00
-0.02
-0.04
-0.04
-0.02
0.00
0.02
0.04

Figure 5.2. A) Scatterplot of the first two axes of the PCA. Deformation grids refer to axes extremes (positive and negative values). **B)** Scatterplot of the first and third axes of PCA. Deformation grids refer to axes extremes (positive and negative values).

PerMANOVA returned an highly significant difference (*p*-value < 0.001) between the two species. The boxplot computed for the CS (Figure 3) showed a significant size variation (perANOVA *p*-value < 0.001) between *T. europaea* and *T. fossilis* (see Table 2), with the first being larger than the latter.

Table 5.2. Table resuming the *p*-values computed from the different tests.

perMANOVA	**perANOVA**	**perMANCOVA**
<0.001	<0.001	0.0199
Multivariate Regression	**perMANOVA at min**	**perMANOVA at max**
<0.001	<0.001	<0.001

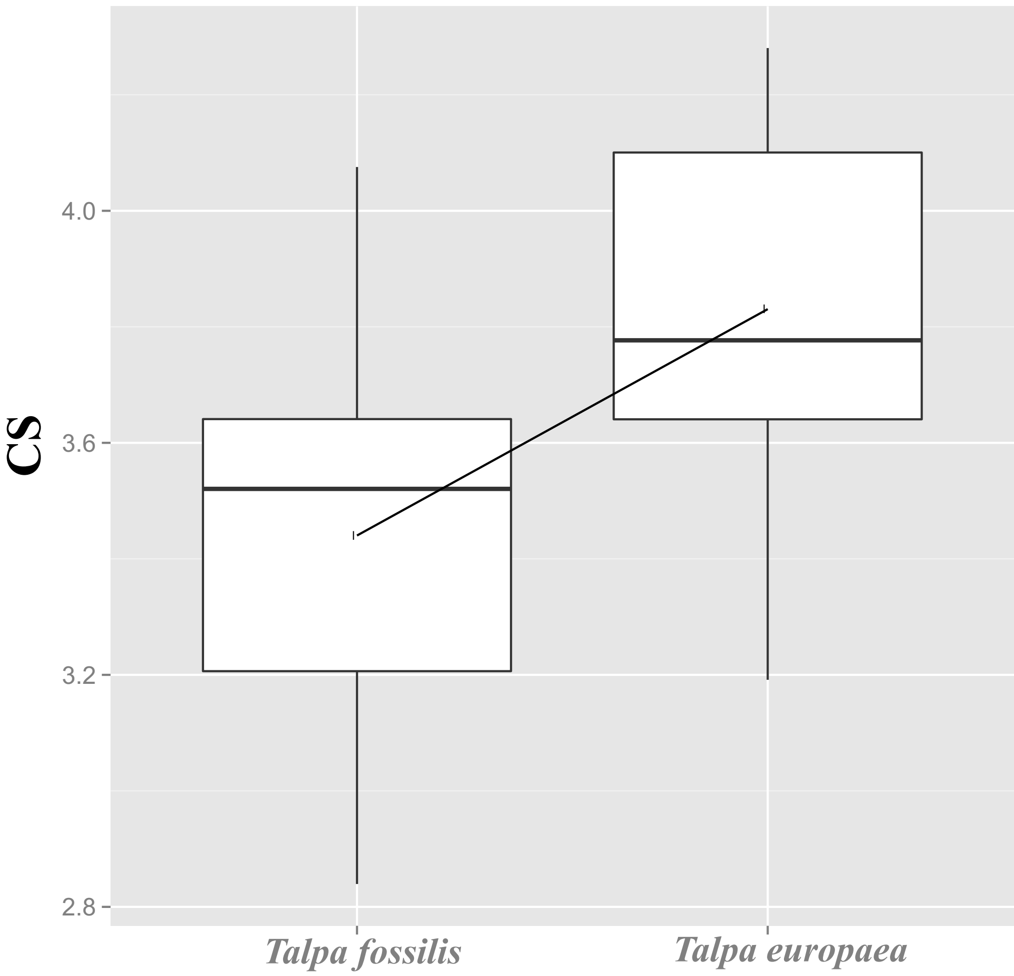

Figure 5.3. Boxplot of the centroid sizes. Bottom and top of the boxes are the first

and third quartiles, the horizontal solid black lines represent the median, the whiskers represent the minimum and maximum values.

Static Allometry

No significant relationships between species specific shape variables and CS with ages have been found (see Table 3).

Table 5.3. Table resuming the *p*-values of the species specific regressions of shape variables and CS against ages.

Species	**Shape Vs. Age**	**CS Vs. Age**
T. fossilis	0.44	0.12
T. europaea	0.07	0.16

According to the significant interaction (*p*-value = 0.0199) between species and size effects in the perMANCOVA, species allometric trajectories were proved to be non-parallel between the two species. Multivariate regression of shape data on size returned a significant result (*p*-value < 0.001), with size accounting for 6% of the total shape variance (Figure 4A). Separate multivariate regressions on *T. fossilis* and *T. europaea* returned significant results (*p*-value = 0.003, *p*-value < 0.001 respectively). PerMANOVA returned highly significant values for the standardized shapes variables both at maximum and minimum CS values (*p*-value < 0.001 and *p*-value < 0.001 respectively, see Table 3). Euclidean distances show a decrement toward the CS value of 3.3 (though not becoming zero), from that value they tend to augment (Figure 4B).

1

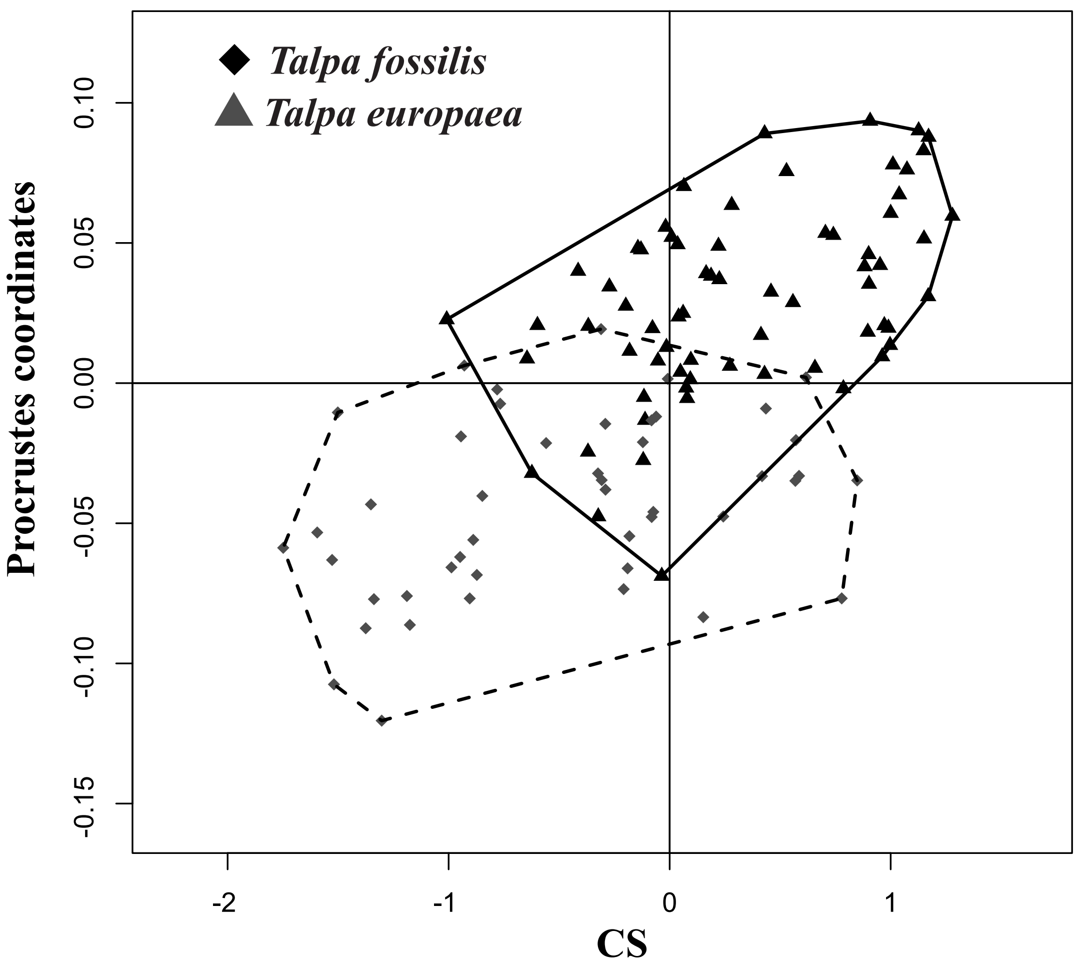

Talpa fossilis
Talpa europaea
Procrustes coordinates
0.10
0.05
0.00
-0.05
-0.10
-0.15
-2
-1
0
1
CS

2

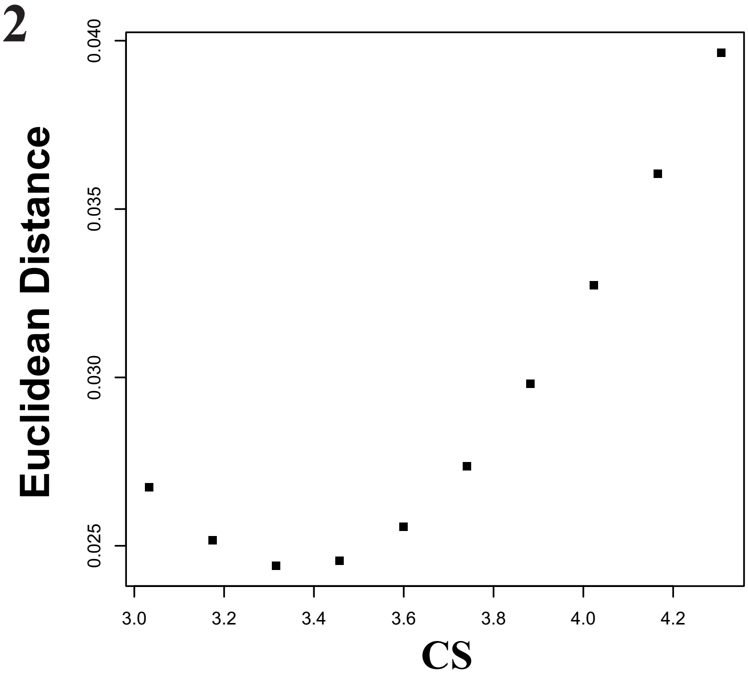

Euclidean Distance
0.040
0.035
0.030
0.025
3.0
3.2
3.4
3.6
3.8
4.0
4.2
CS

FIGURE 4. A) CCA Scatterplot of the shape and size variables. **B)** Plot of the Euclidean distances between the predicted shape values of *T. fossilis* and *T. europaea* against ten discrete CS intervals.

DISCUSSION AND CONCLUDING REMARKS

The separation between *T. fossilis* and *T. europaea*, observed along the PC1 (Figures 2A and 2B), is due to change in the Teres tubercle and in the pectoral ridge, two of the main humeral anatomical regions associated with the digging performance (Gambaryan et al., 2003; Piras et al., 2012). In particular *T. europaea* has the Teres tubercle and the pectoral ridge enlarged when compared with *T. fossilis*. On the Teres tubercle insert the Teres major and Latissimus dorsi muscles, while on the pectoral ridge inserts the Pectoralis Pars Sternalis muscle (Dobson, 1882; Freeman, 1886), two of the main muscles involved in the digging process (together they account for the 42,5% of the total digging muscles weight; Gambaryan, 2003). In this framework we suggest that *T. europaea* would be better adapted to burrowing by having larger area of insertion for the main digging muscles when compared with *T. fossilis*. The multivariate regression returned a significant interaction of the shape variable with the CS indicating the presence of an evolutionary allometry between *T. europaea* and *T. fossilis*, moreover the species-specific multivariate regressions were significant suggesting the presence of a static allometry in both the species. However the allometric trajectories have been proved to be non-parallel (perMANCOVA test significant). In particular the species-specific trajectories cross each other (see Figure 4B), in fact the Euclidean distances reduce in correspondence of the CS value 3.3 and rises in correspondence of higher CS values. This result suggests that the two trajectories have different starting and ending points, such evidence is confirmed by the significant shape differences found between *T. europaea* and *T. fossilis* even when the shape variables are predicted at the same CS value (see Table 3). In this scenario we suggest to consider *T. fossilis* as a distinct species in comparison to *T. europaea*. The two species proved to be different in both size and shape and moreover in their allometric patterns. In particular the last evidence would exclude the possibility to consider *T. fossilis* as a chronospecies, as already suggested by van Cleef-Roders and van den Hoek Ostende (2001), or a stratigraphic species (Rabeder, 1972). In this case we would expect to find very similar static allometric trajectories, as predicted by the allometric-constraint theory (Voje et al., 2013; Firmat et al., 2014). In particular when dealing with the humerus, a highly phenotypically channeled skeletal element (Nevo, 1979, Piras et al., 2012). Separating these two taxa would also fit with molecular data. According to Colangelo et al. (2010) the *T. europaea* basal split have a mean divergence time estimate of 0.7 my. The time estimate would be in agreement with the fossil record and the distinction usually present in literature (Sulimsky, 1959; Janossy, 1986). In this framework we hypothesize that *T. fossilis* originated from a different lineage in respect to *T. europaea*. The fossil record support the presence of four *Talpa* species since the early Miocene: *T. tenuidentata* (Ziegler, 1990), *T. minuta* (Ziegler, 1999), *T. vallesensis* (Villalta and Crusafont, 1944) and *T. gilothi* (Storch, 1978). It is possible that the *T. fossilis* lineage originated from an offshoot of the Miocene moles lineage, due to its primitive humeral features, and spread across Europe during the Plio-Pleistocene. According to Colangelo et al. (2010) the *T. europaea* lineage split occurred during the Early-Middle Pliocene. The intense climatic changes occurred during the Pleistocene could have influenced the actual distribution range of *T. europaea* (Colangelo et al., 2010). Probably this species found multiple refuge sites, both in European Peninsula and Eastern Europe, similar to many other small mammals (Jaarola and Searle, 2002; Koltlik et al., 2006; McDevitt et al., 2010), and thus was able to recolonize all those European areas covered by permafrost. Here we hypothesize that *T. europaea*, during its recolonization routes, could have come in contact with *T. fossilis* and replaced it by its larger size and better digging capability. Competition in moles is a well-known phenomenon and already described for genera *Talpa* and *Mogera* (Abe, 1996; Loy et al., 1996; Loy and Capanna, 1998; van Cleef-Roders and van den Hoek Ostende, 2001; Yokohata, 2005; Bego et al., 2008; Loy, 2008). Recent contributions highlighted that humeral morphology has a taxonomic value at the species level (van den Hoek Ostende, 1997; Ziegler, 2003; Klietmann et al., 2014). Our results suggest that the landmark based shape analysis is useful in supporting systematics in palaeontological investigations, in particular when morphological differences are not evident. Finally, following van Cleef-Roders and van den Hoek Ostende (2001), we highlight that considering *T. fossilis* as a distinct species from *T. europaea* does not mean that all the material previously assigned to *T. fossilis* should be separated from the recent species. But we suggest the need to review every assemblage separately.

CHAPTER 6

THE IMPORTANCE OF BEING *MESOSCALOPS*

Solving the enigma: the digging adaptation of *Mesoscalops montanensis* unveiled by Geometric Morphometrics and Finite Element Analysis

Piras P., Sansalone G., Teresi L., Moscato M., Profico A., Eng R., Cox T.C., Loy A., Colangelo P., Kotsakis T. In Press. *Journal of Morphology*.

Introduction

Since the origin of Mammals, the adaptation to digging has produced highly modified humeral morphologies in different mammalian clades (Puttick and Jarvis, 1977; Barnosky, 1981; 1982; Gasc et al., 1986; Sanchez-Villagra et al., 2006; Piras et al., 2012). Some extinct groups show very odd humeral shape. This is an evidence that adaptation process moulded humeral morphologies experimenting different solutions for the same function (Luo and Wible, 2005). One of the most enigmatic morphologies of this bone is that shown by the extinct family Proscalopidae (Mammalia, Talpoidea, Barnosky, 1981). Within this family, the species *Mesoscalops montanensis* from the Early Miocene of Montana (Barnosky, 1981) is represented by an exquisitely preserved skeleton with perfectly preserved humeri. Barnosky (1981) suggested that its morphology was adapted to burrowing even if no extant taxa show similar humeral shape. Barnosky (1981) qualitatively investigated the morpho-functional adaptations of this taxon by taking into consideration not only the humerus but also the entire skeleton, thus exploring functional interactions between all forelimb elements as well as the contribution of the skull movements during digging. He compared *M. montanensis* with extant taxa of Talpidae and Chrysochloridae. While in *M. montanenisis* some non-humeral structures (e.g., skull morphology: nuchal crest, deep basicranium; Barnosky, 1981) are more similar to chrysochlorids than to talpids, most of the humeral regions where muscles involved in digging insert are unique and hardly comparable to extant species. The humeral morphology of *Mesoscalops* (and all other proscalopids), instead, appears unique in the configuration of the main subregions involved in burrowing. The minor sulcus is absent and the Teres tubercle is larger in Proscalopidae than in non highly fossorial Talpidae. One of the most modified structures of Proscalopidae is the extremely developed lateral epicondyle that is reduced in both Talpidae and Chrysochloridae. Barnosky (1981) suggested that this peculiar morphology was probably suited for a mixed burrowing dynamic composed of both retraction (typical of Chrysochloridae) and rotation (typical of Talpidae). He additionally speculated that Proscalpidae dug with the contribution of head lift based on qualitative morpho-functional considerations of the cervical vertebrae and skull morphology (Barnosky, 1981). However, his original hypothesis was, and remains, quantitatively and comparatively untested. Here we test this hypothesis by evaluating the mechanical performance of the *Mesoscalops montanensis* humerus when contrasted with the humeral morphology and performance of both Chrysochloridae and Talpidae, including both extant and extinct species of the latter clade.

We tested the Barnosky's original hypothesis by analyzing both shape variation and mechanical performance of humeri from 22 species using three-dimensional CT scan data and geometric morphometrics (GM). Furthermore, we specifically tested the new hypothesis that the humeral shape and mechanical performance of *Mesoscalops* result from a convergence process identifiable by specific comparative methods on the phylogeny of the species analyzed in this study.

Many recent studies have focused on the relationships between shape, function, adaptation and convergence (for instance Alfaro et al., 2004, 2005; Young et al., 2010, among others). One important aspect in investigations aimed at comparing different taxa and their convergence upon similar phenotypes is identifying if similar morphologies result from adaptive or non adaptive constraints. Losos (2011) underlined that this is not always achieved via adaptation but also by means of other processes, such as genetic canalization, limited phenotypic evolvability or ontogenetic processes. In our case we set our numerical simulations under the assumption that the increase of forelimb use in digging underground plays a constraining role for species colonizing subterranean habitats. In this sense one should expect to observe humeri that are inevitably modified in order to achieve similar function. However, similar function can be attained via modification of different parts, a phenomenon called “many to one mapping” (Alfaro et al., 2005; Wainwrigth et al., 2005). Quoting Losos (2011) “for any phenotypic system in which parts interact to produce a function, then the same functional outcome may be produced by different combinations of trait values for the different parts”. In the case of a biomechanical investigation of a complex structure such as the humerus, we note that besides differences in pure morphologies, drastic variations exist in the arrangements and attachments of different muscles and in the articulation between humerus and the other pectoral girdle bones. When comparing distantly related groups, such as here, these arrangements could be interpreted in terms of phylogenetic inheritance rather than of adaptation to current conditions by means of comparative methods. For this reason it is imperative to account for phylogenetic relationships among species under study using appropriate comparative methods. Recently, Ingram and Mahler (2013) described a method to test convergence of continuous traits along phylogeny without identifying *a priori* different ecomorphs. They use the Ornstein-Uhlenbeck model of character evolution and information criteria to establish if one or more taxa exhibit similar phenotypes as result of convergent optima in the phylogeny/trait interaction. Here we use three-dimensional GM combined with finite element analysis (FEA) applied to CT-generated bone geometries to test the similarity of shape and stress behavior, under controlled mechanical simulations, to determine if and when *Mesoscalops* reached its functional digging performance by means of a true convergence process toward Chrysochloridae.

Materials and Methods

Taxon sampling and CTscan

In order to compare *Mesoscalops montanensis* with a relatively complete sampling of extant and extinct species encompassing the most extreme humeral adaptations to subterranean lifestyle among Eutheria, a considerable effort was made to collect data from CT scanning (see below). As Talpidae species present different lifestyles (Sanchez-Villagra et al., 2006), we included in our study both extant and extinct and extinct Talpidae, including species that occupy a highly fossorial, semi-fossorial-ambulatorial (shrew-moles), or semi-aquatic (desmans) niche. (Hutchison, 1976; Yates and Moore, 1990) in order to cover the entire humeral morphological variability of the group.

We also included four species of extant Chrysochloridae in order to test possible functional affinities of *M. montanensis* with this distantly related family of fossorial mammals. Australian Notoryctidae were not included in this study for their rarity and difficulty in being collected and because, being marsupial, they are really distantly related to the taxa analyzed here. Supplementary Table S1 lists all analyzed specimens and affiliated institutions where they are housed. All of these specimens, except for *Mesoscalops montanensis* and *Chrysochloris sthulmanni*, were scanned in Rome, Italy at the "Studio dentistico Moscato" using a Kodak 9000 3D Cone Beam Computed Tomography (CBCT) scanner. *M. montanensis* was scanned using a Skyscan 1076 microCT at the Small ANimal Tomographic Analysis Facility (SANTA) located in the Seattle Children's Research Institute, Seattle, Washington. *Chrysochloris sthulmanni* came from the digital collection of the digimorph database available at: http://www.digimorph.org/specimens/Chrysochloris_sp/whole/.

Post-processing of CT scan data

For each scan we obtained a set of stacked images composing humeral three-dimensional geometry for any species. At first we post-processed CT scan images using the open source FIJI software (Schindelin et al., 2012) in order to obtain final image datasets without noise that would produce a clean 3D surface mesh. We then imported the data into Amira 5.2 (Detlev et al., 2005) in order to generate corresponding geometries. All produced geometries were then saved in STL format after reducing all objects to approximately the same vertex resolution. Given the different resolution capabilities of the various CT scanners used to generate data for this study, we were obliged to find a comparable resolution suitable for numerical simulation without losing too much detail. We thus saved our STLs with a resolution of approximately 21000 tetrahedral elements. This compromise ensured relatively high fidelity to real geometry and the possibility of performing computationally intensive numerical simulations for all 22 specimens.

Phylogeny

We built our synthetic phylogeny depicted in Figure 6.1 in Mesquite 3.02 (Maddison and Maddison, 2015). 1 using species-specific references for both stratigraphic range and phylogenetic position. Supplementary Table S1 reports the entire literature corpus used for this purpose. As for *Mesoscalops montanensis*, we used the information provided by Gunnell et al. (2008) and Barnosky (1981). For extant taxa, recent molecular phylogenies (see Supplementary Table S1) were used in order to build a composite consensus topology. Branch lengths were set according to fossil evidence (see Supplementary Table S1). Tree root was set at the Early Paleocene reflecting the divergence time between Chrysochloridae and Talpidae (O'Leary et al., 2013).

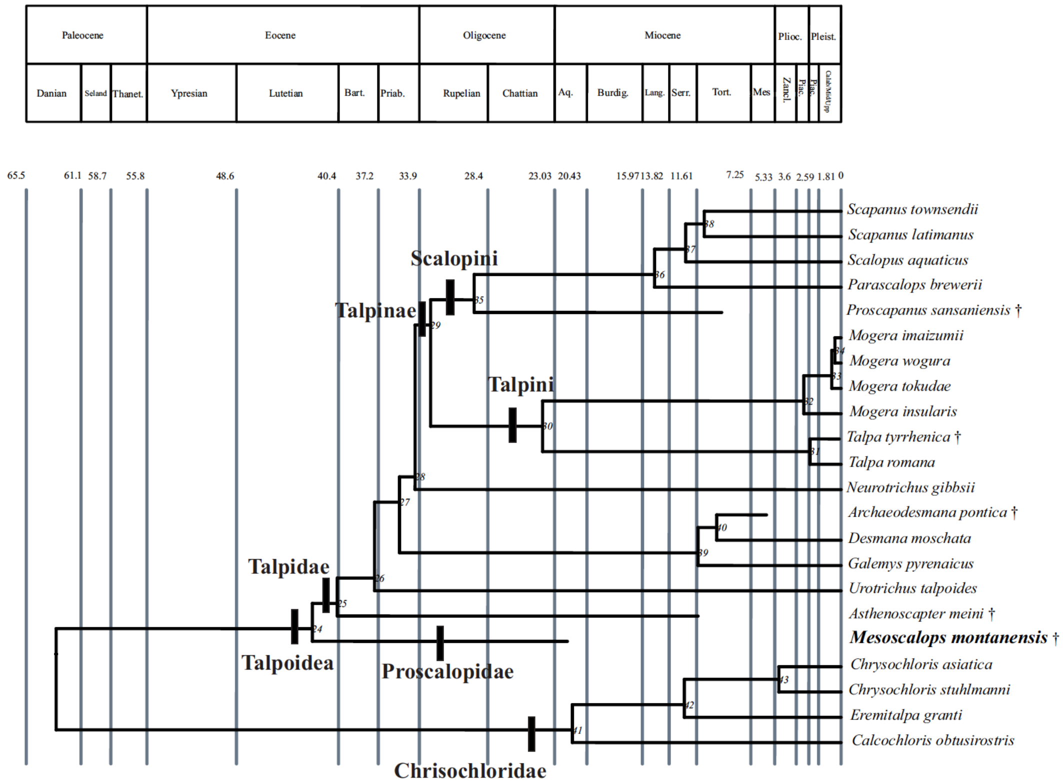

Figure 6.1. Time calibrated phylogeny; references used for tree building can be found in Supplementary Table S1. We depicted the relationships only for the taxa included in this study without adding any intermediate group (such as other Afrotheria or Boreotheria). † Symbol indicates extinct species.

Geometric morphometrics

We digitized 38 homologous landmarks on all geometries in Amira. Table 1 reports how these landmark configurations were defined and Supplementary Figure S1 shows, dynamically, landmarks on the *Neurotrichus gibbsii* mesh. Landmark configurations were built to accurately reflect the geometry. The three-dimensional coordinates were subjected to a Generalized Procrustes Analysis (GPA, Bookstein, 1991; Goodall, 1991). First, original coordinates are scaled to the same unit size by dividing any configuration by its proper Centroid Size (CS: square root of squared differences between landmark coordinates and Centroid coordinates). Next, they are successively translated by centering all centroids to the origin. Finally, configurations are rotated so as to minimize differences between configurations (i.e.,Procrustes distance: approximately, the square root of the sum of squared differences between the positions of the landmarks in optimally aligned configurations). The transformed coordinates are then subjected to Principal Component Analysis (PCA) in order to find axes of maximal variation. The PC scores are then used for linear models to test explicit hypotheses about trait evolution. Evolutionary allometry has been successively investigated by recovering the CS of GM analyses.

Table 1. Landmarks definition	
1	Distal end of the head of humerus
2	Distal half of the head of humerus
3	Proximal half of the head of humerus
4	Distal end of the head of humerus
5	Distal half of the medial side at the base of the head of humerus
6	Proximal half of the medial side at of the base of the head of humerus
7	Distal half of the lateral side of the base of the head of humerus
8	Proximal half of the lateral side of the base of the head of humerus
9	Distal border of the greater tuberosity
10	Middle point of the greater tuberosity
11	Proximal border of the greater tuberosity
12	Caudal end of the greater tuberosity
13	Frontal end of the greater tuberosity
14	Middle point of the Lesser tuberosity
15	Proximal border of the bicipital notch
16	Medial end of the distal border of the bicipital notch
17	Lateral end of the distal border of bicipital notch

18	Proximal part of the pectoral ridge
19	Distal part of the pectoral ridge
20	Proximal end of the teres tubercle
21	Middle point of the teres tubercle
22	Distal end of the teres tubercle
23	Lateral epicondyle
24	Lateral side of fossa for Flexor digitorum profundus
25	Medial side of fossa for Flexor digitorum profundus
26	Spine of the trochlea
27	Lateral side of the trochlear area
28	Distal end of the trochlear area
29	Medial side of the trochlear area
30	Medial side of the depression of the Trochlear area
31	Distal end of the medial epicondyle
32	Proximal end of the medial epicondyle
33	Posterior border of the process of the medial epicondyle
34	Lateral base of the deltoid process
35	Midpoint of humeral shaft in caudal view
36	Midpoint of greater sulcus
37	Midpoint of humeral shaft in frontal view
38	Midpoint of minor sulcus

Finite Element Modelling

Together with shape, we analyzed the phenotype “stress”, i.e. the von Mises stress, with appropriate comparative methods using a time-calibrated phylogeny (Figure 1). The von Mises stress, or equivalent tensile stress, is a common measure (Rayfield et al., 2001) of the yielding characteristics of materials (von Mises, 1913). We imported STLs from Amira into Comsol Multiphysics 4.5 (www.comsol.com). Using this software, we ran numerical simulations in order to assess the mechanical performance of different geometries. In the first instance, we set the Young modulus to 10 GPa and Poisson's ratio to 0.41 in all models consistent with haversian bone (Rayfield et al., 2001). To remove the size information as recommended for comparative biomechanical and shape analyses (Stayton, 2009) all simulations were made under a scale free framework by scaling all models to a unit volume: 0.82 cm^3. Then, we identified the functional types occurring in our sample. These types are illustrated in Figure 2A-C. Models are oriented in their natural anatomical position relatively to the ground. Figure 2A illustrates *Mesoscalops montanensis*. Figure 2B shows an extant chrysochlorid (*Chrysochloris asiatica*) with a typical quasi-columnar humeral position. Figure 2C is an extant talpid (*Talpa romana*) characterized by the highly rotated humeral position relatively to the ground plane. Then, each functional type presented above underwent different simulation experiments due to the different muscles involved in digging. We carefully followed detailed functional and anatomical studies (Puttick and Jarvis, 1977; Barnosky, 1981; Gasc et al., 1986; Gambaryan et al., 2003) in order to choose the main muscles involved in digging for the different taxa present in our sample. We simulated the action of these muscles according to experimentally measured forces (Gambaryan et al., 2003) and to available detailed anatomical descriptions (Edwards, 1937; Puttick and Jarvis, 1977; Barnosky, 1981; Gasc et al., 1986; Gambaryan et al., 2003; Sanchez-Villagra et al., 2006; Stayton, 2009). We did not simulate the entire bulk of muscles inserted or attached on the humerus (such as the supraspinatus and deltoideus) as they are not involved in digging but in different aspects of locomotion, such as recovery stroke. As detailed *in vivo* muscle force measurements exist only for *Talpa europaea* (Gambaryan et al., 2003), we did not set muscle force as an input. Instead, we set the same reaction force (22N, as measured in Gambaryan et al., 2003) on the trochlear area, where the ulna articulates, for all taxa. Given the comparative aim of this study, changing this reaction force would lead to the same results just scaled in intensity. It is important to note here that, in the real anatomy of the different functional types (hypothesized for *Mesoscalops*), muscles have different arrangements attachments and orientation, the articulations between bones are different and consequently the directions of loading and the distributions of constraints are not the same. Imposing the same loading scheme would therefore not respect the actual different anatomies and biomechanics of distantly related taxa. Consequently, our simulations were performed under different loading schemes corresponding to the real anatomies, an approach already applied in past studies aimed at comparing different taxa via FEA (Attard et al., 2011; Cox et al., 2011). Under such models, the larger the forces needed the lesser the adaptation to dig. We specified the number of nodes (i.e. tetrahedral vertices), area extensions (in terms of cm^2) and muscle loads of each model in Supplementary Table S2. Imposing the same reaction force is not, of course, realistic, but like the scaling to the same unit size, it allows comparison of humeri of different taxa.

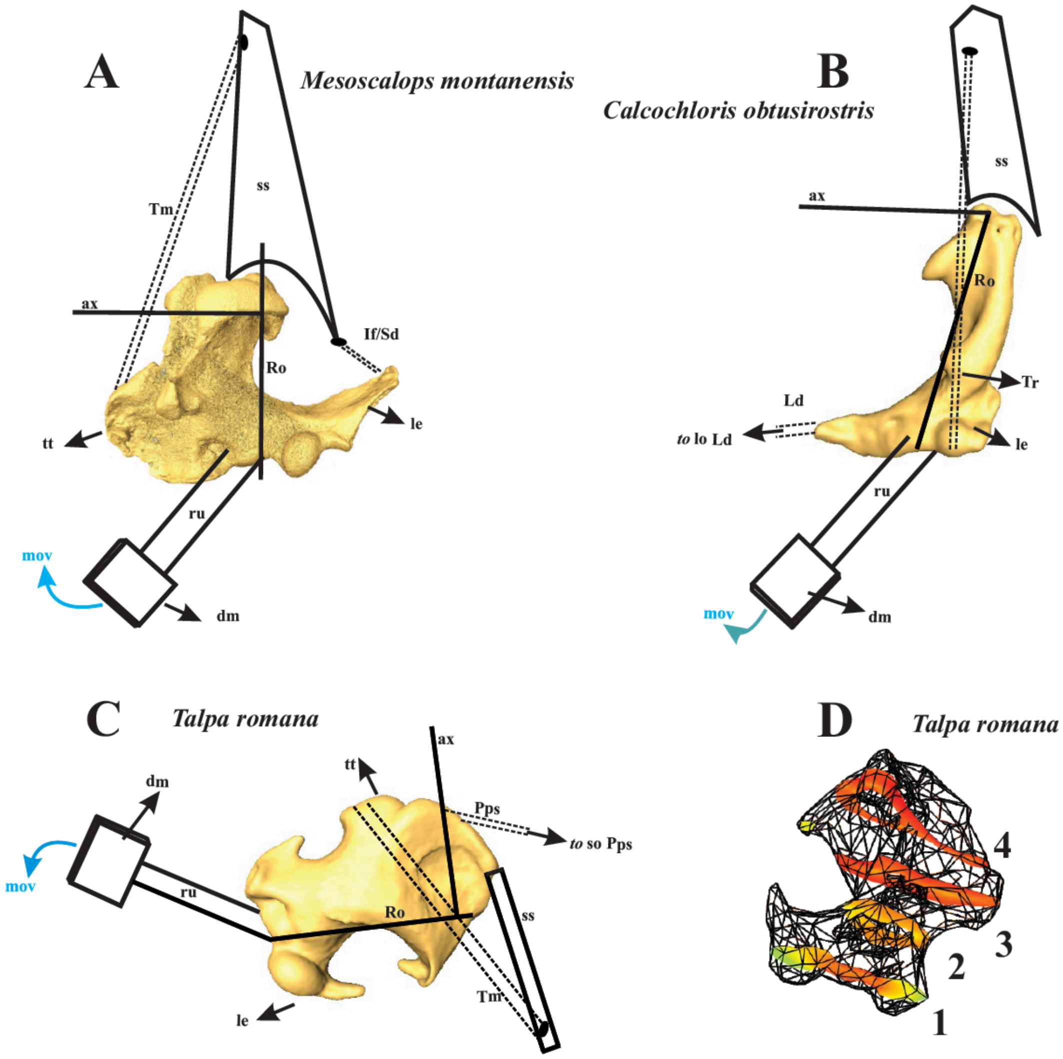

Figure 6.2. Functional contexts of the taxonomic sample under study. The three humeral functional types corresponding to the three different musculo-skeletal configurations occurring in (**A**) *Mesoscalops montanensis*, (**B**) a Talpidae and (**C**) a Chrysochloridae. (**D**) The position of the four slices in a humerus of *Talpa romana*. All elements are figured under their anatomical positions relatively to the ground. Abbreviations: **ax**: rotation axis for retraction; **dm**: dorsal surface of manus; **If/Sd**: m. Infraspinatus/ Spinodetoideus; **Ld**: m. Latissimus dorsi; **le**: lateral epicondyle; **lo Ld**: Lumbar origin of Latissimus dorsi. **mov**: direction of movement; **Pps**: m. Pectoralis pars sternalis; **ro**: Rotation axis for rotation; **ru**: radius and ulna; **so Pps**: Sternal origin of Pectoralis pars sternalis; **ss**: Scapula; **Tm**: m. Teres major; **tt**: teres tubercle; **Tr**: m. Triceps.

Anatomical constraints

Constraints are imposed on surfaces selected for each taxon separately. They are modeled as spring foundations acting along the three directions of the reference system. For Talpidae anatomical constraints were placed in correspondence of the humeral head and the clavicular facet. For Chrysochloridae and *Mesoscalops* they were placed only on the humeral head, as these latter taxa do not show any articulation between the humerus and clavicle (Puttick and Jarvis, 1977; Barnosky, 1981; Gasc et al., 1986).

Loadings

Similarly to the constraints, loads are applied on surfaces differently selected on each taxon. We assign a resultant force F (Newton) which is then transformed into a distributed load sigma (Newton/meter^2) acting on the loaded surface; the three components of the resultant force F are tuned separately in order reproduce as much as possible of the muscle line of action. For Talpidae, the loadings were placed in correspondence to insertion areas of the two main muscles used for digging, i.e. the m. Teres major and m. Pectoralis pars sternalis (Dobson, 1882; Freeman, 1886; Edwards, 1937; Gambaryan et al., 2003). For *Mesoscalops montanensis,* we selected faces of the STL geometry on anatomical regions where m. Teres major and independently either m. Spinodeltoideus or m. Infraspinatus were inserted (following Barnosky, 1981, fig. 28, p. 326). For Chrysochloridae, we selected areas of insertions of m. Latissimus dorsi and m. Triceps (Puttick and Jarvis, 1977; Gasc et al., 1986). In our experiments on Chrysochloridae, the Triceps and the Latissimus dorsi (the two main muscles involved in the digging stroke) were applied respectively on the lateral and medial epicondyles. Actually, in Chrysochloridae, these two muscles both insert on the olecranon of the ulna as depicted in Supplementary Figure S2. The olecranon process is a highly curved and very elongated structure that develops posteriorly to the distal region of the humerus (Gasc et al., 1986, fig 6, p. 22). Here the Triceps inserts on the part of the olecranon that is parallel to the lateral epicondyle and the Latissimus dorsi inserts on the part that is parallel to the medial epicondyle. As our simulated muscles possess the same direction of in vivo anatomy, our approximation represents a trustable solution for forces exerted by the Triceps and the Latissimus dorsi muscles on the humerus.

The orientation of muscles with respect to the humerus has been set on the basis of detailed anatomical descriptions illustrating the origin-insertion and direction (Dobson, 1882; Freeman 1886; Edwards, 1937; Yalden, 1966; Puttick and Jarvis, 1977; Barnosky, 1981; 1982; Gasc et al., 1986; Gambaryan et al., 2003; Scott and Richardson, 2005) for any muscle involved in our study.

Evaluation of stress

Von Mises stress values, calculated on all mesh tetrahedrals, were averaged (using arithmetic means) over the entire volumes and for four homologous coronal slices (trochlear area, distal humeral shaft, teres tubercle and humeral head) that account for specific critical anatomical districts that are functionally homologous among different species thus allowing a meaningful comparison of the stress state occurring in unambiguous functional regions (Figure 2D). We performed the global average of the four slices by calculating von Mises stress on all tetrahedral elements belonging to any slice and then by averaging them. We also used the averages of single slices that were obtained by averaging the von Mises stress values of tetrahedral elements belonging only to individual slices. The means calculated over the entire volumes and the means calculated over the four slices are highly collinear (r=0.96; *p*-value<0.00001). However, as stress concentration occurring on particular zones, such as tuberosities, condyles and hooked processes, is hardly comparable between distantly related taxa, we used the means of the individual slices in order to contrast, via UPGMA analyses, functionally homologous regions.

Linear models and Comparative methods

To assess the presence of phylogenetic signal in shape, size and von Mises stress, we used the phylosig() function in "phytools" R package (Revell, 2012) and evaluated the strength of the lambda parameter. Individual mapping on the phylogenetic tree for these variables was performed using the contMap() function in "phytools". Multivariate signal in shape (using the first 6 PC scores explaining 95% of total variance) was tested using the function physignal ("kmult" option) in the "geomorph" R package (Adams and Otarola-Castillo, 2013). We then proceeded to explore the best mode for evolution for the von Mises stress variable. We first fitted nine models (Brown, lambda, delta, kappa, ou, eb, trend, drift, white noise) allowed by the function fitContinuous() along the entire tree. However, this analysis does not account for local optima and does not guarantee that a single model is the most appropriate for trait evolution. To test for evolutionary convergence along the phylogeny we used our phylogenetic framework and the R package "surface" (Ingram and Mahler, 2013) to detect adaptive convergence shifts for both stress and multivariate shape, without placing *a priori* their position in the tree. We also subjected von Mises stress variable to a phenetic analysis via UPGMA cluster analysis (Sokal and Michener, 1958). Thus, we additionally performed supplementary analyses aimed at testing if models with multiple local optima performed better than single models using the Akaike

Information Criterion (AIC) as the decisive factor for model selection. Local optima were searched under the Ornstein-Uhlenbeck (OU) model. The advantage of this approach is that no *a priori* adaptive shift is requested, different from recently developed methods suited for similar purposes (Beaulieu et al., 2012). A maximum likelihood (ML) solution is fitted for different models in a stepwise fashion on the branches of the tree. Iteratively, the best model, together with its proper number of shifts and local optima values, is saved along with its AIC. Then, based on the AICs, the best model can be compared with single Brownian Motion and single OU models. Another advantage of the "surface" package is that it can handle multivariate data, such as PC scores of shape data.

Results

Geometric Morphometrics

3D GM shows a clear taxonomic signal with the clustering of Chrysochloridae on the negative side of PC1 and highly fossorial Talpinae (i.e. Talpini+Scalopini) on the positive side as illustrated in Figure 6.3A. At the negative extreme of PC1, the humeri show a very slender morphology with an extremely reduced teres tubercle, poorly developed proximal region and the absence of the clavicular articular facet, typical of chrysochlorids. At positive values of PC1 the humeral shape shows a very robust and round configuration with a highly expanded and medially displaced teres tubercle, a highly developed proximal region and the presence of a highly developed greater tuberosity bearing the clavicular articular facet, typical of highly fossorial moles. Slender Talpidae set apart from the highly fossorial species (Piras et al., 2012) and are positioned at the positive side of PC2, while *Mesoscalops montanensis* occupies a unique region of the morphospace at highly negative values of PC2. At positive values of the PC2 the humerus shows an overall slender morphology with a slight expansion of the proximal region and poor development of the teres tubercle. At highly negative values of PC2, the humeral morphology shows the peculiar features of *Mesoscalops montanensis* with the distally displaced teres tubercle, the broad distal region of the humerus and the extremely expanded, bladelike, lateral epicondyle. Figure 6.3B presents the morphological variation explained by the first two PC scores. Figure 6.3C shows, in a rainbow color map, the intensity of stress experienced by the various taxa. Supplementary Figures S3 shows in a dynamic pdf the space identified by the first three PC scores.

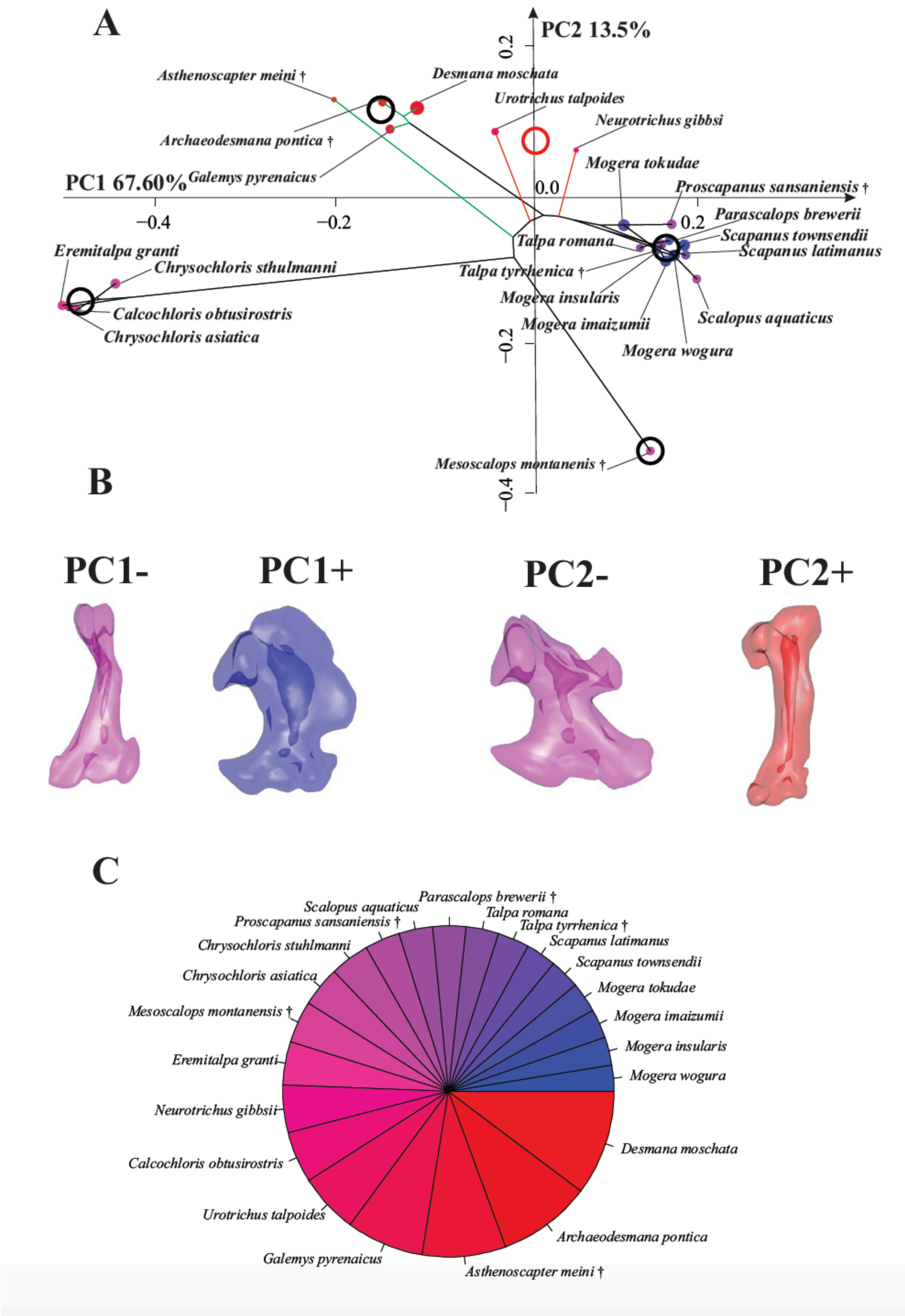

Figure 6.3. (**A**) Phylomorphospace related to the first two PCs. Points dimension is proportional to taxa centroid size. Points color is proportional to stress according to section B of this figure. Points are connected by the phylogeny branches. Red branches indicates shape convergence under surface analysis (see text), while green

branches indicate convergence for stress. Large empty circles represent the values of shape optima identified by the surface analysis. The red circle indicates the convergence between *Neurotrichus* and *Urotrichus*, the black circles indicate non-convergent optima.). † Symbol indicates extinct species. (**B**) Morphological expression of first two PC scores. Transparency allows appreciating inner medullary cavity. Colors refer to the rainbow scale presented in part C of this figure. **(C)** Rainbow color map showing the results of stress analysis. These color codes are used in successive figures showing PCA results. Red (=grey in printed version) indicates high stress while blue (dark grey in printed version) indicate low stress values. Similarly, the amplitude of any segment is proportional to stress value. Supplementary Figure S3 show the morphospace identified by the first three PC scores in colored dynamic 3D pdf and with meshes instead points.

Finite Element Analysis

When the highly different humeral shapes were subjected to FEA simulation according to realistic loading schemes focused on digging only, we found different stress magnitudes and distributions. Figure 6.4 shows the three-dimensional plot that adds the von Mises stress variable averaged over the four homologous slices to the PC1-PC2 plane. Supplementary Figure S4 show the same plot in a 3D dynamic pdf with meshes instead of points. Figure 6.5 and Supplementary Figures S5 summarize results of the FEA by mapping in a scale color the log transformed mean von Mises stress on the surface of individual meshes. Table 2 reports values of the von Mises stress of both single functionally homologous slices and of the means calculated over them for each taxon. Slender Talpidae, i.e. those species having elongated humeri (such as *Galemys* or *Asthenoscapter*), display the highest stress values that are concentrated in the humeral shaft region, while highly fossorial species are visibly less stressed in the same region. In particular, we observe less stress in correspondence of the main digging muscle insertions, i.e. Teres tubercle and pectoral ridge. Chrysochloridae, due to both different shape and muscle configuration relative to Talpidae, show a particularly stressed distal humeral region, e.g. the lateral and medial epicondyles, due to the direct Latissimus dorsi and Triceps insertions. In contrast, the proximal humeral region of Chrysochloridae is less stressed in comparison to Talpidae, as it is free of the muscles involved in digging (Puttick and Jarvis, 1977; Barnosky, 1982; Gasc et al., 1986). *Mesoscalops* showed a less stressed proximal region relative to Talpidae, while it has a more stressed teres tubercle due to its distally shifted position. It is worth noting that the lateral epicondyle, bearing the Infraspinatus/Spinodeltoideus, is particularly stressed. Figure 6.6A shows the von Mises stress averaged over the four critical coronal slices for four taxa belonging to the three functional types. Figure 6.6B shows the results of the UPGMA performed on the von Mises stress averaged over the four slices compared to UPGMA performed on PC scores of geometric morphometrics analysis. *Mesoscalops* falls within Chrysochloridae that cluster together along with Desmaninae and *Asthenoscapter*. *Mogera* spp. are clustered together along with Talpinae. UPGMA performed on shape places *Mesoscalops* basal to Talpidae thus in a very different position in comparison to functional similarities. Figure 6.7 shows the distribution of von Mises stress averaged over the four slices and that of individual slices with the relative UPGMA analyses. *Mesoscalops* possesses the lowest value for the 4^{th} slice followed by the chrysochlorids that in general present a very low stress in correspondence of the humeral head.

Table 2. Mean Values of von Mises stress $*10^{-6}$ resulted from FEA. † Symbol indicates extinct species.

	Mean over the 4 slices	Mean of slice 1	Mean of slice 2	Mean of slice 3	Mean of slice 4
Mogera wogura	1.69	1.10	0.77	1.46	3.56
Mogera insularis	1.81	0.91	0.95	2.12	3.26
Mogera imaizumii	1.88	0.96	0.77	2.15	3.35
Mogera tokudae	1.94	0.97	0.97	2.12	3.43
Scapanus townsendii	1.95	0.85	0.87	1.85	3.56
Scapanus latimanus	1.98	1.05	1.04	1.49	3.77
Talpa tyrrhenica †	2.05	0.78	0.72	2.38	3.61
Talpa romana	2.10	0.90	0.62	2.52	3.30
Parascalops brewerii	2.15	0.95	1.05	2.45	3.37
Scalopus aquaticus	2.17	0.76	1.35	1.81	3.41
Proscapanus sansaniensis †	2.27	1.10	0.94	2.20	3.62
Chrysochloris stuhlmanni	2.56	3.71	2.10	2.25	1.72
Chrysochloris asiatica	2.60	4.06	1.97	2.04	1.54
Mesoscalops montanensis †	2.71	2.78	3.87	2.67	0.54
Eremitalpa granti	2.80	3.97	2.66	3.24	1.72
Neurotrichus gibbsii	3.06	1.51	1.34	2.26	5.27
Calcochloris obtusirostris	3.32	4.68	2.72	2.75	2.17
Urotrichus talpoides	3.84	1.93	1.50	2.21	6.94
Galemys pyrenaicus	5.01	1.77	4.57	5.91	7.18
Asthenoscapter meini †	5.39	1.22	7.09	8.84	6.91
Archaeodesmana pontica †	6.03	2.29	5.21	5.67	9.10
Desmana moschata	6.79	2.57	4.10	6.85	10.04

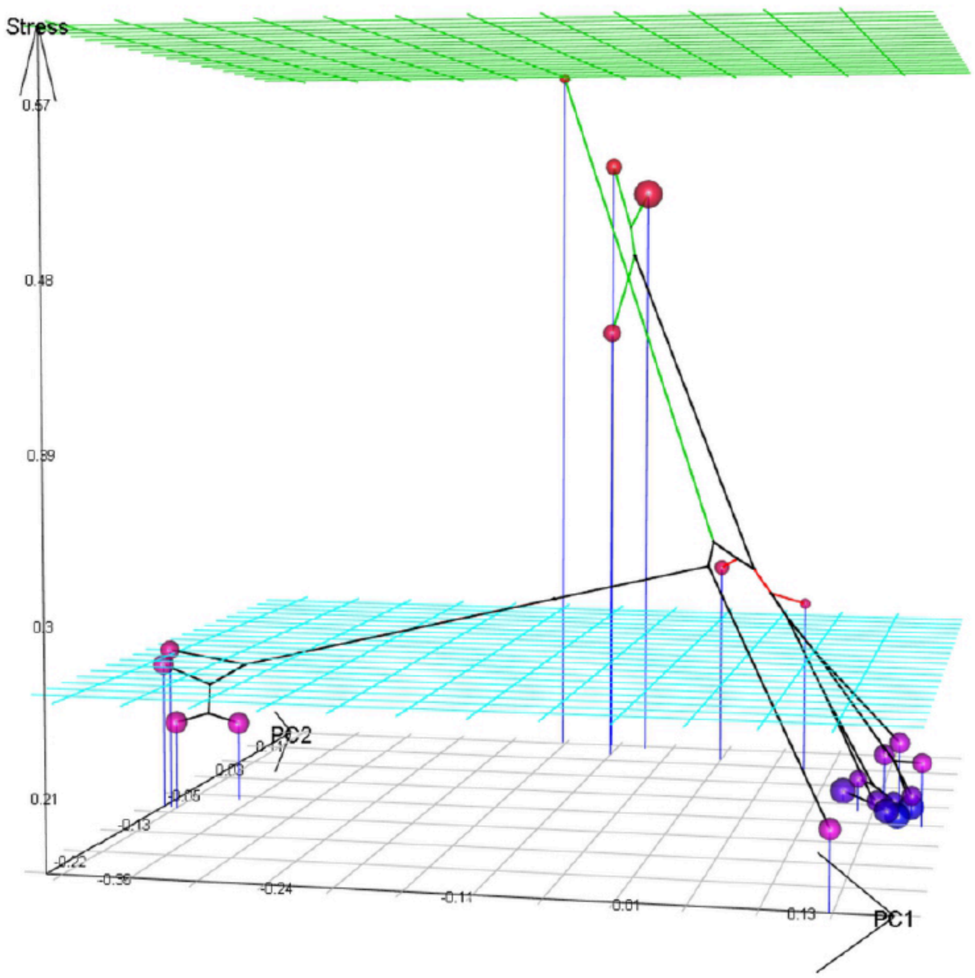
Stress
0.57
0.48
0.39
0.3
0.21
PC2
PC1
-0.36
-0.24
-0.11
0.01
0.13
-0.22
-0.13

Figure 6.4. Phylomorphospace of the first two PCs and stress*10^{-8} as vertical z-axis. Green plane indicates the value of the z-axis where convergence occurs, the cyan plane indicates the other non-convergent stress optimum found by the surface analysis. Size of points is proportional to the original species centroid size. Supplementary Figure S4 show the same morphospaces in colored dynamic 3D and with meshes instead points.

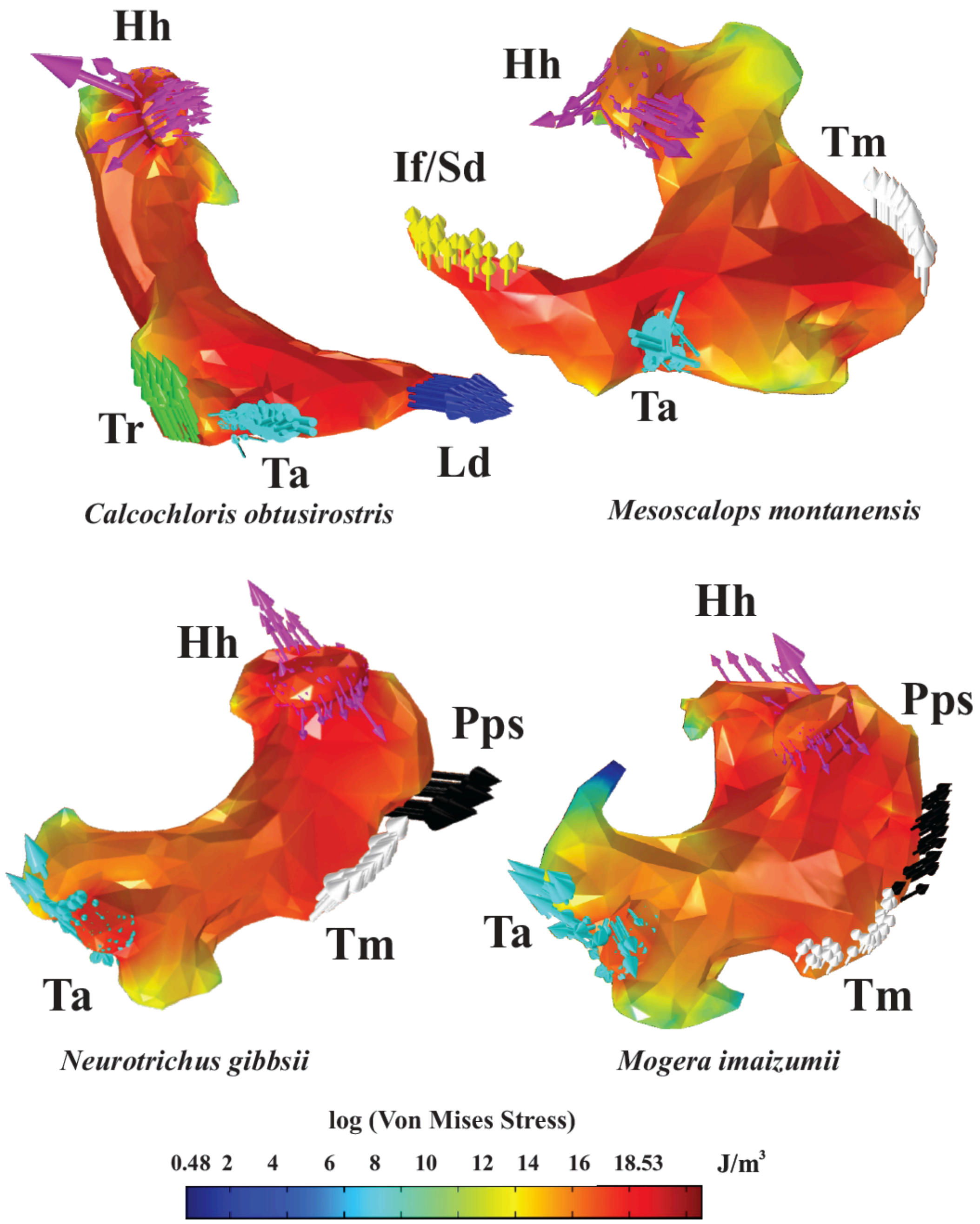

Figure 6.5. Details of FEA results in four taxa representative of the three functional types we defined in the present study. The entirety of FEA results for all taxa investigated in this study can be found in Supplementary Figure S5. In all taxa purple

arrows indicate reaction force on humeral head, while cyan arrows indicate reaction force on trochlear area. Green arrows in *Calcochloris* indicate m. Triceps loading, blue arrows that of m. Latissimus dorsi. Yellow arrows in *Mesoscalops* indicate m. Infraspinatus/Spinodeldoiteus, white arrows m. Teres major. In both *Neurotrichus* and *Mogera* black arrows indicate m Pectoralis pars sternalis, white arrows m. Teres major. Abbreviations: (**Hh**) humeral head, trochlear area (**Ta**), m. Latissimus dorsi (**Ld**), m. Triceps (**Tr**), m. Infraspinatus/Spinodeltoideus (**If/Sd**), m. Teres major (**Tm**) and m. pectoralis pars sternalis (**Pps**).

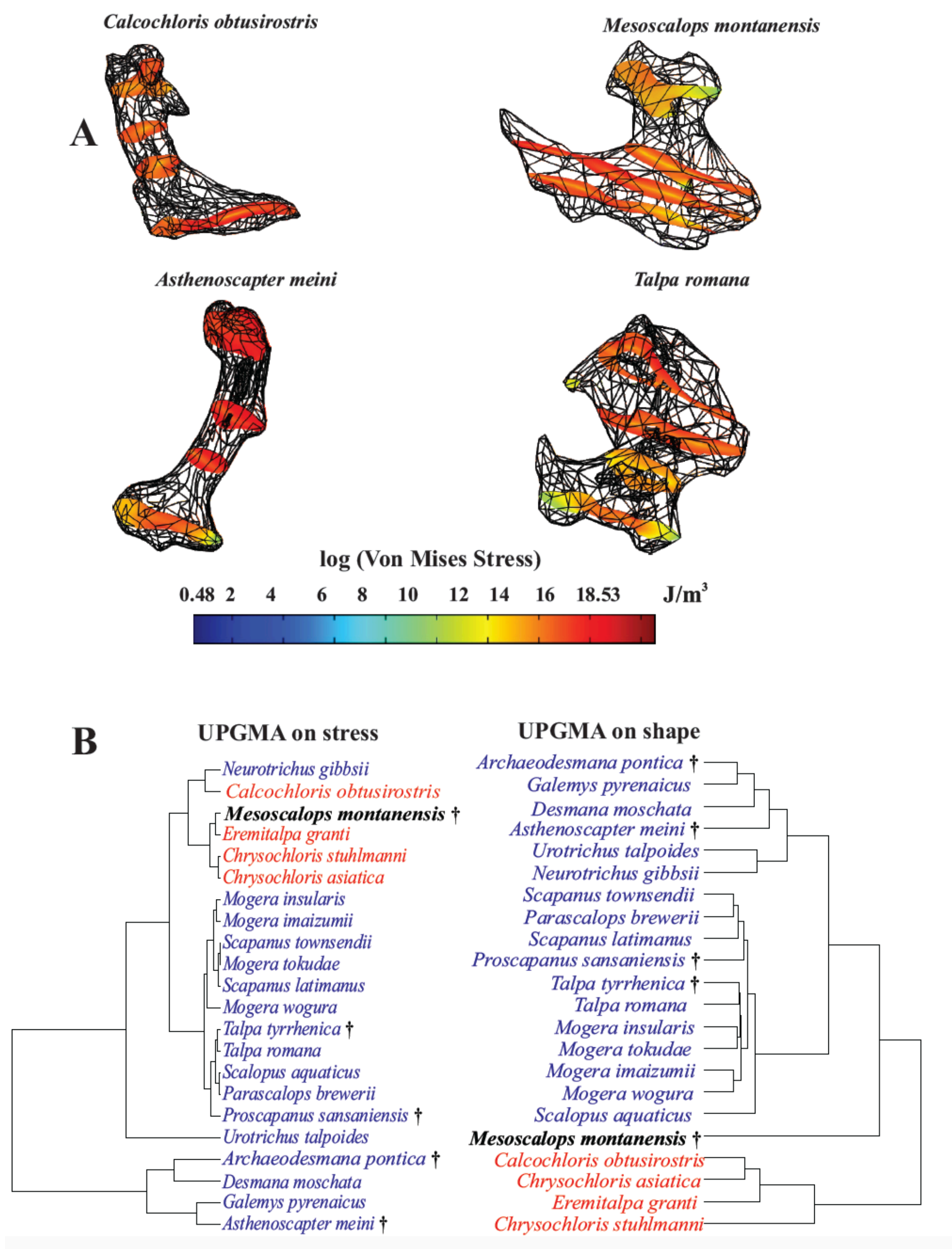

Figure 6.6. Similarity in stress and shape. (**A**) The four homologous coronal slices for

Mesoscalops montanensis and other three taxa representative of the main stress categories. (**B**) UPGMA analysis for stress values averaged, for any taxon, over the four homologous slices and UPGMA for shape data. In blue Talpidae, in red Chrysochloridae. † Symbol indicates extinct species.

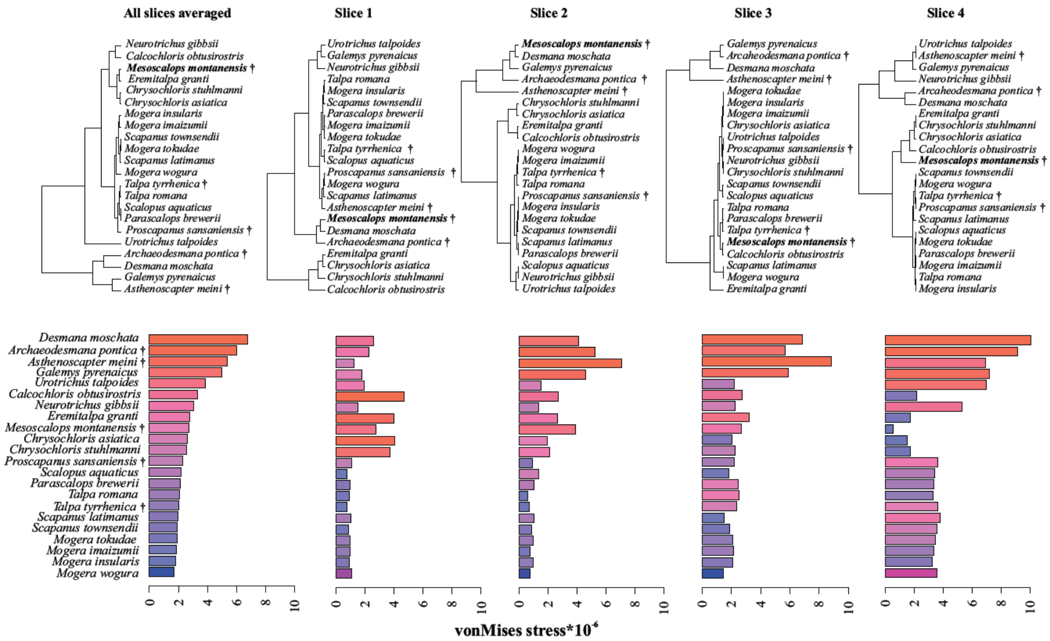

Figure 6.7. The comparison between UPGMAs performed on the von Mises stress averaged over the four slices and on individual slices. Barplots show, for any taxon, the variation of von Mises stress in the various slices. † Symbol indicates extinct species.

Linear models and comparative methods

In this analyses we used, as a stress proxy, the mean stress calculated over the four slices. No evolutionary allometry for shape or for stress was found under Ordinary Least Squares (OLS) or Phylogenetic Generalized Least Squares (PGLS) analyses. Regressing shape on stress data returned significant results under OLS but not under PGLS. This suggests a high conservatism of the two blocks of variables that is confirmed by the phylogenetic signal. Stress is individually significantly related to PC1 and PC2 of shape only. Multivariate shape shows a high phylogenetic signal: 01.35; *p*-value: 0.004. The first two PCs of shape possess, individually, a phylogenetic signal (lambda=0.99; *p*-value <0.001 and lambda=0.99; *p*-value <0.001, respectively). Size does not show a phylogenetic signal (lambda=0.63; *p*-value=1). Individual mapping of size, shape (PC1 and PC2) and stress on the phylogenetic tree are shown in Supplementary Figure S6. The stress variable exhibits a strong phylogenetic signal as computed using "phytools" R package (Revell, 2012). Exploring the best mode of evolution using the "geiger" R package (Harmon et al., 2014), we found that, globally, the evolution of this trait was better explained by a "trend" model with a slope parameter = -0.014 (thus close to Brownian motion). This means that the stress variable follows a model of evolution, along the tree, that only slightly deviates from Brownian diffusion with a light trend toward low values. Table 3 shows the details of fitContinuous analysis. The search for local optima on the phylogeny deserves particular attention. The relative phylomorphospace plot is shown in Figures 6.3 and 6.4 and, dynamically, in supplementary Figures S3 and S4 where the stress variable is added as the z-axis to PC1-PC2 space. Local optima values for shape are visualized in Fig. 6.3A and are indicated by the red branches and the red circle in the phylomorphospace graph. The sole convergence was found for *Neurotrichus* and *Urotrichus*, while the other optima did not represent convergence but unique phenotypic adaptations. The green branches indicate convergence for the stress variables better seen in Figure 6.4 where the vertical axis represents the von Mises stress. Figure 6.8A shows the different AICs for single shift and multiple shifts models for the stress variable. The two shifts model is the most supported solution. The theta values of the two shifts are indicated by the cyan and green planes in Figure 6.4 and are 2.71 and 7.0 respectively. The branches of the phylomorphospace colored in green indicate evolutionary convergence for the stress variable at theta = 7.0. *Mesoscalops montanensis* is close to the cyan optimum together with

Chrysochloridae, while slender species are close to the green optimum. Figure 6.8B shows the AIC results for multivariate shape (first six PC scores). The five optima are shown in Supplementary Figure S3 as spheres.

Table 3. Details of fitContinous() results for the von Mises stress variable. In bold the best model.

PARAMETER ESTIMATES

Brown	lambda	delta	kappa	ou	eb	**trend**	drift	White
NA	1	0.67669	1	6.22E-11	1.72E-11	**-0.0141**	-7.22E-05	NA

AKAIKE INFORMATION CRITERION VALUES

Brown	lambda	delta	kappa	ou	eb	**trend**	drift	White
56.16041	58.1604	57.9506	58.1604	58.1604	58.1604	**54.9843**	58.16041	82.5995

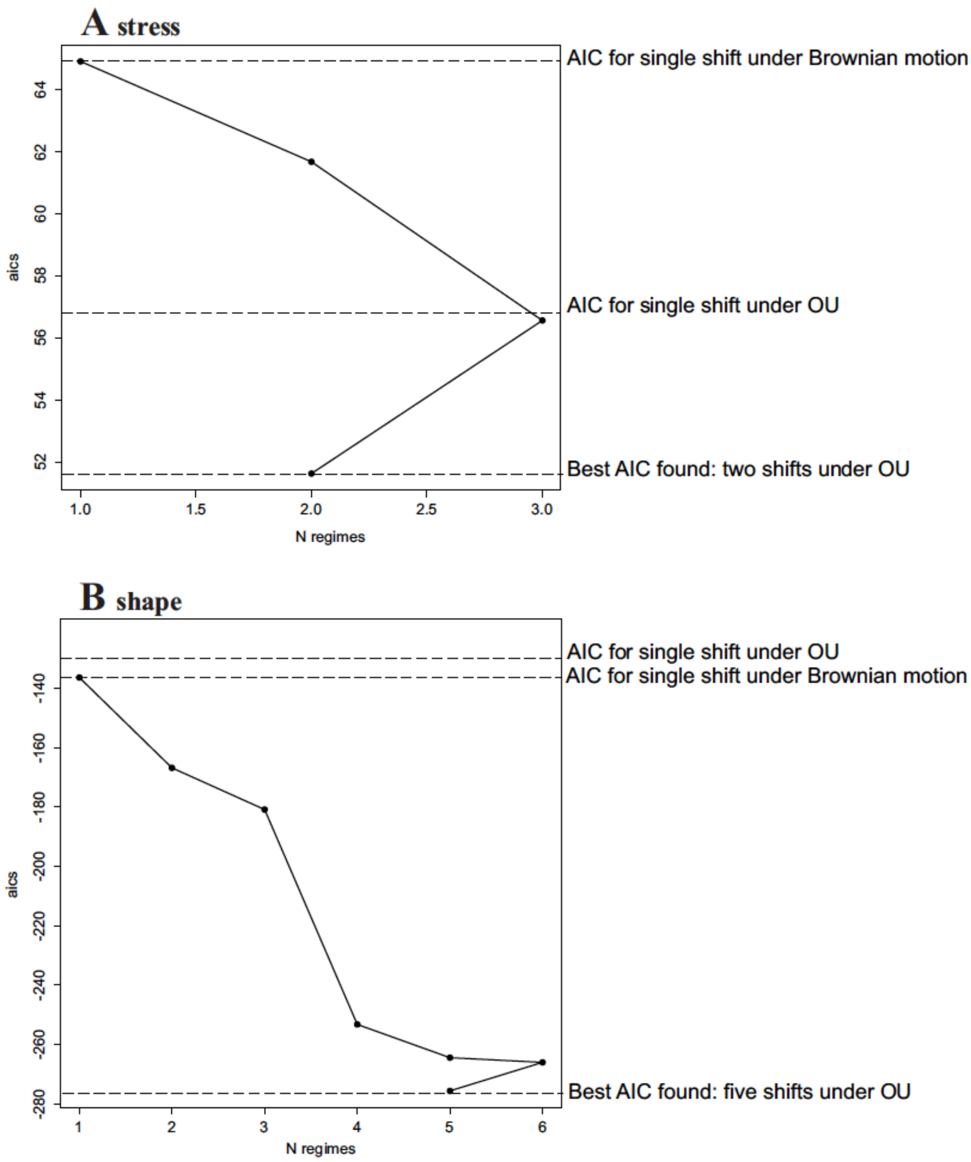

Figure 6.8. Results of surface analysis and corresponding AIC values for single and multiple optima regimes. (**A**) Analysis on stress. (**B**) Analysis on shape.

Discussion

Our results highlight that, despite a dramatic difference in shape and in muscular anatomy, *Mesoscalops montanensis* possessed humeral stress mechanics similar to those of Crysochloridae as previously suggested by Barnosky (1981, 1982). *Mesoscalops* showed the highest stress values in the distal region of the humerus, similar to Chrysochloridae, particularly in the lateral epicondyle where the m. Spinodeltoideus/Infraspinatus inserts, suggesting the presence of a powerful retraction movement during the burrowing process. Unfortunately, there is no way to identify if both these two muscles or one of them acted on the lateral epicondyle of *M. montanensis* because no extant taxa have this anatomical region developed in the same manner. Possibly, they could have acted together as happens in chrysochlorids where the m. Spinodeltoideus encloses m. Infraspinatus (Puttik and Jarvis, 1977). In talpids, the distal region of the humerus, i.e. slice 1, is less stressed when compared with chrysochlorids and with *M. montanensis*. In talpids the main digging muscles are positioned in the proximal region of the humerus (Gambaryan et al., 2003; Piras et al., 2012). All Talpidae, even slender forms, show an enlarged and low stressed distal region of the humerus (Sanchez-Villagra et al., 2004; Sanchez-Villagra et al., 2006). This condition is also found in the basal extinct *Asthenoscapter*, thus suggesting that it represents an ancestral condition in Talpidae family.

The presence, in *M. montanensis*, of a highly developed teres tubercle, where the m. Teres major inserts, also suggests the occurrence of an important rotational movement similar to Talpidae (Barnosky, 1981; 1982). The stress values on the third slice, that cuts the humerus in correspondence of the teres tubercle (Fig. 6), strongly support such evidence because *Mesoscalops* clusters with highly fossorial moles (Fig. 7, slice 3) for stress values on a substructure (teres tubercle) where muscle involved in rotation inserts (m. Teres major).

Highly fossorial moles and *M. montanensis* are very similar in the teres tubercle shape. In both *Mesoscalops* and highly fossorial moles the teres tubercle is enlarged and expanded, suggesting the presence of a large and powerful m. Teres major (Gambaryan et al., 2003). *Mesoscalops montanensis* and chrysochlorids show the smaller stress in the proximal region of the humerus, i.e. slice 4, when compared with talpids. This result reflects the different muscular position, humeral orientation and loading conditions. Talpids show a medially displaced humerus (Dobson, 1882; Freeman, 1886; Edwards, 1937; Reed, 1951; Gambaryan et al., 2003; Sanchez-Villagra et al., 2004; Sanchez-Villagra et al., 2006), while in chrysochlorids and *M. montanensis* it is in the typical position of other mammals (Hildebrand, 1985; Liem et al., 2001). Moreover, highly fossorial moles possess a short and cuboid shaped clavicle that articulates with the humerus on the clavicular facet, a flat surface on the greater tuberosity and contributes to avoid humeral dislocation during the power stroke (Freeman, 1886; Edwards, 1937; Reed, 1951; Yalden, 1966). These results evidence the unique combination of shape and stress state of *Mesoscalops* and suggest that the kinematics of this taxon was probably achieved via mixing retraction and rotation (Barnosky, 1981, 1982). This should of course be read by assuming that the loading scheme presented in Fig. 2 depicts the actual muscles arrangement and orientation in *Mesoscalops*.

UPGMA on global stress averaged over the four slices revealed that *Neurotrichus gibbsii* grouped with *M. montanensis* and chrysochlorids. The humerus of *Neurotrichus gibbsii*, though slender, shows an enlarged teres tubercle, a reduced minor sulcus and a completely fused bicipital tunnel (Sanchez-Villagra et al., 2004; Sansalone et al., in press). All of these features, also shared by the highly fossorial moles (Sanchez-Villagra et al., 2006), are likely to improve the digging performance. As a result, the *N. gibbsii* humerus, due to its peculiar morphology, shows a significantly less stressed configuration as for the mean of the four slices, when compared with other shrew-like moles as already argued by Sansalone et al. (in press), and presents a stress state similar to that of *M. montanensis* and chrysochlorids.

Our findings highlight that chrysochlorids and highly fossorial talpids likely represent two morphological extremes of adaptation to digging while other extinct forms, such as *Mesoscalops montanensis* could represent an "evolutionary experiment" that mixed different digging kinematics not shown by any extant species. It is possible that this condition played a role in the evolutionary history of Proscalopidae in relation to their extinction. In fact, Barnosky (1981) hypothesized that the arrival of talpids in North America during the Early Miocene (early Hemingfordian) represented the appearance of a highly competitive group in terms of subterranean locomotion and food search. Barnosky and Labar (1989) reported a Middle Miocene fossil fauna in Montana and Wyoming where Talpidae and Proscalopidae were found together thus suggesting a spatial overlap. However, recently, a new Talpidae genus, *Oreotalpa* (Lloyd and Eberle, 2008) from the Late Eocene of Colorado suggests that the first arrival of Talpidae in North America is more ancient than hypothesized before. Thus the temporal overlap of Proscalopidae and Talpidae has not been of small extent in absolute but there are no evidences of an important colonization or an adaptive radiation by Talpidae in North America since Eocene as happened during the Miocene. As a consequence, in order to falsify the hypothesis of competitive exclusion, more extinct Talpidae from Late Eocene and Oligocene of North America should be recorded.

Our results strongly support the greater kinematic efficiency of highly fossorial Talpidae in comparison to proscalopids. In fact, all Proscalopidae show (based on skeletal fragments) a humeral morphology very similar to that observable in *Mesoscalops montanensis* that is the sole taxon showing a complete humerus.

Comparing proscalopids digging kinematics to that of chrysochlorids is justified by the non complete lateral thrust movement of humerus during burrowing while in talpids digging kinematics implies a complete rotational movement.

However, this functional similarity should be considered in a phylogenetic context in order to assess what role shared history played in determining convergence (if any) between Proscalopidae and Chrysochloriadae. As stated in the introduction, the same function can be realized by different combinations of morphological features, as predicted by the "many to one" model (Wainwright et al., 2005). The case of humeral modifications for adaptation to digging could be included in this category because the distantly related groups studied here, even when showing humeri adapted to digging, present morphological changes in very different humeral sub-regions. Obviously, given the high taxonomic rank of observation, this is related to the phylogenetic relationship among species. For this reason the use of comparative methods was required for determining patterns of convergence. While data from a standard phenetic approach was consistent with an interpretation that *Mesoscalops* functional performance converges toward the Chrysochloridae character state (Fig. 7B), our surface analysis-based determination of morphological and functional optima of *Mesoscalops* provides strong evidence against such evolutionary convergence (Fig. 3 A). This is particularly interesting because, according to Losos (2011), in many cases in which clades are very distantly related and show very different morphologies, natural selection may cause two species to become more similar to each than were their ancestors from a functional point of view, but not be of sufficient magnitude to obliterate the preexisting morphological differences that occur among clades. On this basis, *Mesoscalops montanensis* (and all proscalopids) could be interpreted as an incomplete functional convergence due to the strong phylogenetic constraints linked to phylogenetic history that canalize morphological variation. This could explain the expression “evolutionary experiment” from a mechanistic point of view. It would be interesting to explore whether the patterns we found in this study represent parallel or convergent evolutionary trajectories in a broader phylogenetic context (Piras et al., 2012). For example other taxa covering higher level of phylogenetic relationships such as *Epoicotherium* (Paleanodonta, Rose and Emry, 1983), or even outside Eutheria such as extant Australian Notoryctidae, *Necrolestes* from the Early Miocene of Argentina (Rougier et al., 2012) or the very primitive mammal *Fruitafossor* from the Late Jurassic of Colorado (Luo and Wible, 2005), could be included in the present analysis. However, a more complete taxon sampling by means of CT scans should be available to test such hypothesis.

Supplementary material

Supplementary Table S1. Species list, specimen info and references for species stratigraphy and phylogeny for the sample under study.

Species	Institution	**Specimen code**	**Reference for species stratigraphy**	**Reference for species phylogeny**	**Ctscan**
Asthenoscapter meini	Lyon University	LGR69012	Qiu & Wang, 1999; Ziegler, 1999; Engesser & Storch, 2008	van den Hoek-Ostende and Fejfar, 2006; Engesser and Storch, 2008	Studio Dentistico Moscato
Calcochloris obtusirostris	Paris Museum of Natural History	MNHN-ZM-MO-1	Butler, 1984	Asher and Avery, 2010; Asher et al., 2010	Studio Dentistico Moscato
Chrysochloris asiatica	Paris Museum of Natural History	MNHN-ZM-MO-2	Butler, 1984	Asher and Avery, 2010; Asher et al., 2010	Studio Dentistico Moscato
Chrysochloris stuhlmanni	American Museum of Natural History	AMNH82372	Butler, 1984	Asher and Avery, 2010; Asher et al., 2010	Austin, Digimorph service

Desmana moschata	Wien Natural History Museum	NHMW61714	Harrison et al., 1988; Ziegler, 1999	Sanchez-Villagra et al., 2006	Studio Dentistico Moscato
Desmana pontica	Wien Natural History Museum	NHMW2014/0098/0001	Hoek Ostende & Furiò, 2005; Ziegler & Daxner Höck, 2005	Sanchez-Villagra et al., 2006	Studio Dentistico Moscato
Eremitalpa granti	Paris Museum of Natural History	MNHN-ZM-MO-3	Butler, 1984	Asher, 2010; Asher et al., 2010	Studio Dentistico Moscato
Galemys pyrenaicus	Patrimonio Cultural, Lisbon	PC1432	Agustì et al., 2010	Sanchez-Villagra et al., 2006	Studio Dentistico Moscato
Mesoscalops montanensis	Seattle Natural History Museum	UWBM54708	Gunnel et al., 2008	Gunnel et al., 2008	Seattle, SANTA service
Mogera imaizumii	Tsukuba Natural History Museum	SIK532	Kawamura; 1991	Shinohara et al., 2014	Studio Dentistico Moscato
Mogera insularis	Tsukuba Natural History Museum	SIK203	Qiu & Storch, 2005	Shinohara et al., 2014	Studio Dentistico Moscato
Mogera tokudae	Tsukuba Natural history Museum	SIK161	Kawamura; 1991	Shinohara et al., 2014	Studio Dentistico Moscato
Mogera wogura	Tsukuba Natural History Museum	SIK118	Kawamura; 1991	Shinohara et al., 2014	Studio Dentistico Moscato
Neurotrichus gibbsii	Los Angeles County Museum	LACM093944	Skoczen, 1980, 1993; Popov, 2004; Zijlstra, 2010	Sanchez-Villagra et al., 2006	Studio Dentistico Moscato
Parascalops brewerii	Wien Natural History Museum	NHMW62568	Kurten & Anderson, 1980; Skoczen, 1993; Ziegler, 1999, 2006; Qiu & Storch, 2005; Rzebik-Kowalska, 2005	Sanchez-Villagra et al., 2006	Studio Dentistico Moscato
Proscapanus sansaniensis	Lyon University	LGR6101	Ziegler & Daxner-Höck, 2005	Ziegler, 1999	Studio Dentistico Moscato
Scalopus aquaticus	Los Angeles County Museum	LACM67482	Gunnel et al., 2008	Sanchez-Villagra et al., 2006	Studio Dentistico Moscato
Scapanus latimanus	Los Angeles County Museum	LACM22981	Gunnel et al., 2008	Sanchez-Villagra et al., 2006	Studio Dentistico Moscato

Scapanus townsendii	Los Angeles County Museum	LACM30843	Gunnel et al., 2008	Crumpton et al., 2012	Studio Dentistico Moscato
Talpa romana	Comparative Anatomy Museum G. B. Grassi	CA22	Kotsakis et al., 2003	Colangelo et al., 2010	Studio Dentistico Moscato
Talpa tyrrhenica	Roma Tre University	U3-001	Abbazzi et al., 2004	Colangelo et al., 2010	Studio Dentistico Moscato
Urotrichus talpoides	Tsukuba Natural History Museum	SIK183	Ziegler, 2003, 2006	Sanchez-Villagra et al., 2006	Studio Dentistico Moscato

References for Supplementary Table S1.

L. Abbazzi *et al.,Rivista Italiana di Paleontologia e Stratigrafia* **110:** 681-706 (2004).
J. Agustì *et al*., *Quaternary International* **223-224**: 162-169 (2010).
R. J. Asher *et al*., *BMC Evolutionary Biology* **10**(69): 1-13 (2010).
R. J. Asher, D. M. Avery, *Paleontologia Electronica* **13**(1, 3A): 1-12 (2010).
P. M. Butler, *Palaeovertebrata* **14**: 117-200 (1984).
P. Colangelo, A. Bannikova, B. Kristufek *et al.*
Molecular Phylogenetics and Evolution 55:372–80 (2010).
N. Crumpton, R. J. Thompson, *Journal of Mammalian Evolution* **20**: 213-225 (2013).
B. Engesser, G. Storch, *Courier Forschungsinstitut Senckenberg* **260**: 185-251(2008)
G. F. Gunnel, T.M. Bown, J. H. Hutchinson, J. I. Bloch , Lipotyphla. In: Janis C.M., Gunnell G.F. & Uhen M.D. (Eds.), *Evolution of Tertiary Mammals of North America, Volume 2: Small Mammals, Xenarthrans, and Marine Mammals*, Cambridge University Press, Cambridge, 89-125. (2008).
Harrison D. L., Bates P. J. J., Clayden J. D. 1988. Vertebrate fauna. [In: P. L Gibbard, J. A. Zala-Siewicz (eds) – Pliocene – Middle Pleistocene of East Anglia. Field Guide. Quaternary Research Association, London, 178-179.
L. W. van der Hoek Ostende, O. Fejfar, *Beiträge für Paläontologie* **30**: 175-203 (2006).
L. W. van den Hoek Ostende, M. Furiò, Spain. In: Hoek Ostende L.W.van den, Doukas C.S. & Reumer J.W.F. (Eds.) – *The fossil record of the Eurasian Neogene insectivores (Erinaceomorpha, Soricomorpha, mammalian*). Part I. *Scripta Geologica*, Spec. Issue, **5**: 149-284 (2005).
T. Kotsakis *et al*., *Deinsea* **10**: 313-342 (2003).
Y. Kawamura, *The Quaternary Research (Japan)* **30**: 213-220 (1991).
B. Kurtèn, E. Anderson, *Pleistocene Mammals of North America*. Columbia University Press, New York, 443 p. (1980).
V. V. Popov, *Acta Zoologica Cracoviensia* **47**: 61-80 (2004).
Z. D. Qiu, G. Storch, China. In: Hoek Ostende L.W.van den, Doukas C.S. & Reumer J.W.F. (Eds.) *The fossil record of the Eurasian Neogene insectivores (Erinaceomorpha, Soricomorpha, mammalian)*. Part I. *Scripta Geologica*, Spec. Issue, **5**: 37-50 (2005)
Z. D. Qiu, X. M. Wang, *Vertebrata Palasiatica* **37**: 120-139 (1999).
B. Rzebik-Kowalska, Poland. In: Hoek Ostende L.W.van den, Doukas C.S. & Reumer J.W.F. (Eds.) *The fossil record of the Eurasian Neogene insectivores (Erinaceomorpha, Soricomorpha, mammalian)*. Part I. *Scripta Geologica*, Spec. Issue, **5**: 119-134 (2005).
A. Shinohara *et al*., *Journal of Mammalogy*, **95**: 455-466 (2014).
S. Skoczen. *Acta Zoologica Cracoviensia* **24**: 411-448 (1980).
S. Skoczen, *Acta Theriologica* **38**: 125-137 (1993).
M. R. Sanchez-Villagra, I. Horovitz, M. Motokawa, *Cladistics* **22**: 59-88 (2006).
R. Ziegler, Order Insectivora. In: Rössner G.E. & Heissig K. (Eds.), *The Miocene Land Mammals of Europe*, Verlag Dr. Friedrich Pfeil, München p. 53-74 (1999).
R. Ziegler, *Acta Palaeontologica Polonica* **48**: 617-648 (2003).

R. Ziegler, G. Daxner-Hock, Austria. In: Hoek Ostende L.W.van den, Doukas C.S. & Reumer J.W.F. (Eds.) – *The fossil record of the Eurasian Neogene insectivores (Erinaceomorpha, Soricomorpha, mammalian)*. Part I. *Scripta Geologica*, Spec. Issue, **5**: 11-29 (2005).
R. Ziegler, *Beiträge zur Paläontologie* **30**: 481-494 (2006).
J. S. Zijlstra, *Journal of Vertebrate Paleontology* **30**: 1903 (2010

CONCLUSIONS

The cladistics analysis, combined with the review of the literature about Talpidae, proved to be a very useful tool in order to understand the phylogenetic relationships among Talpidae. In particular the power of these analyses significantly improve when dealing with fossils. In this thesis we propose the most complete Talpidae phylogeny including almost all extant and extinct taxa.

The geometric morphometric approach, combined with modern comparative methods, was very useful in unveiling the complexity of the talpid morphological variation. The modern comparative methods revealed how the different anatomical regions followed different evolutionary patterns, in response to different phylogenetic or adaptive constraints.

The geometric morphometric approach, combined with qualitative observations, proved to be a powerful tool in detecting and solving systematic issues.

The Finite Elements Analysis revealed the dynamics undergoing the evolution of fossoriality. Moreover we were able to define subtle adaptive traits in the humeral morphology.

The biomechanichal analysis revealed the unique adaptation and digging capability of *Mesoscalops montanensis* and confirmed the systematic hypothesis proposed before.

As a conclusion we were able to answer to all the major aims proposed. However our results suggest that there are still some relatively not investigated fields and non tested hypothesis that will be the basis for further investigations.

ACKNOWLEDGEMENTS

We are particularly grateful to Dr. Lars van den Hoek Ostende from Naturalis Biodiversitat Center, Leiden, Netherland; Dr. Reinhard Ziegler from Staatliches Museum fur Naturkunde, Stuttgart, Germany; Prof. Barbara Rzebik-Kowalska from ISEZ-PAN, Krakow, Poland; Dr. Shin-Ichiro Kawada from Tsukuba Natural History Museum, Tsukuba, Ibaraki, Japan; for their useful suggestions during the manuscript preparation. We want to thank Dr. Christiane Bastos-Silvera from Museu de Historia Natural, Lisboa, Portugal; Prof. Zhuding Qiu from IVPP, Beijing, China; Dr. Paula Jenkins, Dr. Roberto Portella and Dr. Emma Bernard from NHM, London, UK; Dr. Emmanuel Robert from Lyon Universitè, Lyon, France; Dr. Michael Rummel From Augsburg Naturmuseum, Augsburg, Germany; Dr. Gertrud Roessner for BSPG, Munich, Germany; Dr. Ursula Goelich from Wien Natural History Museum, Wien, Austria; Dr. Jim Dines from LACM, Los Angeles, USA; Prof. Patricia Holroyd from UCMP, Berkeley, USA; Dr. Mihaly Gasparik from Budapest Natural History Museum, Budapes, Hungary; Prof. Laszlo Kordos from Budapest Geological Survey, Budapest, Hungary; Prof. Yukimitzu Tomida from Tokyo NHM, Tsukuba, Japan, they all allowed G. Sansalone visiting their collections and made his visits comfortable and pleasant.

REFERENCES

Abe, H. 1967. Classification and biology of Japanese Insectivora (Mammalia), I: Studies on variation and classification. *Journal of the Faculty of Agricolture, Hokkaido University* 55:191-265.

Abe, H. 1996. Habitat factors affecting the geographic size variation of Japanese moles. *Mammal Study* 21:71-87.

Abe H, Ishii N. 2008. *Urotrichus talpoides*. In: IUCN 2010. IUCN Red List of Threatened Species. Version 2010.04.00.

Ackerly, D.D. 2003. Community assembly, niche conservatism, and adaptive evolution in changing environments. *International Journal of Plant Sciences*, 163:165-184.

Adams, D.C. 2014. A generalized K statistic for estimating phylogenetic signal from shape and other high-dimensional multivariate data. *Systematic Biology*, 63:685-697.

Adams, D.C., Rohlf, F.J., Slice, D.E. 2004. Geometric morphometrics: Ten years of progress following the ''revolution''. *Hystrix, Italian Journal of Mammalogy* 71:5-16.

Adams DC, Collyer ML. 2009. A general framework for the analysis of phenotypic trajectories in evolutionary studies. *Evolution*. 63:1143-1154.

Adams, D.C. and Otarola-Castillo, E. 2013. geomorph: an R package for the collection and analysis of geometric morphometric shape data. *Methods in Ecology and Evolution*. 4:393-399.

Adams, D. C. 2014. A Generalized K Statistic for Estimating Phylogenetic Signal from Shape and other High-dimentional Multivariate Data. *Systematic biology*.

syu030.

Alfaro ME, Bolnick DI and Wainwright PC. 2004. Evolutionary consequences of redundant design in labrid fishes. *Integrative Computational Biology*, 44:514–514.

Alfaro ME, Bolnick DI and Wainwright PC. 2005. Evolutionary consequences of many - to - one mapping of jaw morphology to mechanics in labrid fishes. *The American Naturalist*, 165:140-154.

Anthony, H.E. 1929. Field Book of North American Mammals. Whitefish: Kessinger publishing. 748 p.

Arnold SJ. 1994. Is there a unifying concept of sexual selection that applies to both plants and animals? *The American Naturalist*. 114:1-12.

Asher, R.J., Sanchez-Villagra, M.R. 2005. Locking yourself out: Zalambdodonty as a key adaptation. *Journal of Mammal Evolution*, 12:265-282.

Attard MRG, Chamoli U, Ferrara TL, Rogers TL, and Wroe S. 2011. Skull mechanics and implications for feeding behaviour in a large marsupial carnivore guild: the thylacine, Tasmanian devil and spotted-tailed quoll. *Journal of Zoology*. 285:292–300

Atchley, W.R. 1993. Genetic and developmental aspects of variability in the Mammalian Mandible. In: Hanken J, Hall BK, eds. The vertebrate skull. Chicago: University of Chicago Press, pp. 207-247.

Atchley, W.R., Hall, B.K. 1991. A model for development and evolution of complex morphological structures. *Biological Review*, 66:101-157.

Atchley, W.R., Cowley, D.E., Vogl, C., McLellan, T. 1992. Evolutionary divergence, shape change, and genetic correlation structure in the rodent mandible. *Systematic Biology*, 41:196-221.

Badyaev, A.V., Foresman, K.R. 2004. Evolution of morphological integration. Functional units channel stress-induced variation in shrew mandibles. *American Naturalist*, 163:868-879.

Barnosky, A.D. 1981. A skeleton of Mesoscalops (Mammalia, Insectivora) from the Miocene Deep River Formation, Montana, and a review of the proscalopid moles: evolutionary, functional, and stratigraphic relationships. *Journal of Vertebrate Palaeontology*, 1:285-339.

Barnosky, A.D. 1982 Locomotion in moles (Insectivora, Proscalopidae) from the middle Tertiary of North America. *Science*, 216:183-185.

Barnosky AD, and Labar WJ. 1989. Mid-Miocene (Barstovian) environmental and tectonic setting near Yellowstone Park, Wyoming and Montana. *Bullettin of the American Geological Society*, 101.11: 1448-1456.

Barrow E., Macleod, N. 2008. Shape variation in the mole dentary (Talpidae, Mammalia). *Zoological Journal of the Linnean Society*, 153:187-211.

Beaulieu JM, Jhwueng DC, Boettiger C and O'Meara BC. 2012. Modeling stabilizing selection: expanding the Ornstein–Uhlenbeck model of adaptive evolution. *Evolution*, 66:2369–2383.

Bego, F., Kryštufek, B., Paspali, G. and Rogozi, E. 2008. Small terrestrial mammals of Albania: annoted list and distribution. *Italian Journal of Mammalogy* 19:83-101.

Bendukidze O., De Brujn H., Hoek Ostende, L.W. van den. 2009. A revision of Late Oligocene associations of small mammals from the Aral Formation (Kazakhstan) in the National Museum of Georgia, Tbilissi. *Paleodiversity*, 2:343-377.

Berry, R.I., 1977. Inheritance and Natural History. Collins, London.

Björklund, M., Merilä, J. 1993. Morphological differentiation in Carduelis finches: adaptive vs. constraint models. *Journal of evolutionary biology*, 6.3: 359-373.

Blomberg, S.P., Garland, T., Jr., Ives, A.R. 2003. Testing for phylogenetic signal in comparative data: Behavioral traits are more labile. *Evolution*, 57:717-745.

Bode, A. 1953. Die Insektenfauna des Ostniedersachsischen Oberen Lias. *Palaeontographica Abteilung A* 103:1-375.

Bookstein, F.L. 1986. Size and shape spaces for landmark data in two dimensions. *Statistical Sciences* 1: 181–222.

Bookstein, F.L. 1991. Morphometric tools for landmark data. 456 pp. Cambridge University Press, Cambridge.

Bookstein, F.L., Streissguth, A.P., Sampson, P.D., Connor, P.D., Barr, H.M. 2002. Corpus callosum shape and neuropsychological deficits in adult males with heavy fetal alcohol exposure. *Neuroimage*. 15:233–251.

Borodin, L.P. 1962. Russkaya vykhukhol (The Russian Desman), Saransk: Mordovsk. Knizh. Izd.

Boulesteix, A.L. 2005. A note on between-group PCA. *International Journal of Pure and Applied Mathematics* 19: 359–366.

Bown, T.M. 1980. The fossil Insectivora of Lemoyne Quarry (Ash Hollow Formation, Hemphillian), Keith County, Nebraska. *Transactions of the Nebraska Academy of Sciences*, 8:99-122.

Bruijn H. De, Rümke, C.G. 1974. On a peculiar mammalian association from the Miocene of Oschiri (Sardinia). *Proceedings of the Koninklijke Nederlandse Akademie van Wetenschappen*, ser. B, 77: 46-79.

Butler, P. M. 1961. Relationships between upper and lower molar patterns. In: International Colloquium on the Evolution of Lower and Non-Specialized Mammals I,G.Vandebroek, ed., pp. 117-126, Paleis der Academien, Brussels.

Butler, M. A., King, A. A. 2004. Phylogenetic Comparative Analysis: A Modeling Approach for Adaptive Evolution. *The American Naturalist*, 164:683-695.

Cabral, M.J., Almeida, J., Almeida, P.R., Dellinger, T., Ferrand de Almeida, N., Oliveira, M.E., Palmeiri m J.M., Queiroz, A.I., Rog ad o L., Santos-Reis, M. 2005. Livro Vermelho dos Vertebrados de Portugal [Red Book of Vertebrates of Portugal]. Lisbona: Instituto de Conservação da Natureza. 660 p.

Cabria, M.T., Rubines, J., Gomez-Molina, B., Zardoya, R. 2006. On the phylogenetic position of a rare Iberian endemic mammal, the Pyrenean desman (*Galemys pyrenaicus*). *Gene*. 375:1-13.

Campbell, K.L., Hochachka, W. 2000. Thermal biology and metabolism of the American shrew-mole *Neurotrichus gibbsii*. *Journal of Mammalogy* 81: 578–585.

Campbell, K.L., Storz, J.F., Signore, A.V., Moriyama, H., Catania, K.C., Payson, A.P., Bonaventura, J., Stetefeld, J.J., Weber, R.E. 2010. Molecular basis of a novel adaptation to hypoxic-hypercapnia in a strictly fossorial mole. *BMC Evolutionary Biology*. 10:214.

Catania, K.C. 2002. The nose takes a starring role. *Scientific American* 2002:54-59.

Catania, K.C., Remple, F.E. 2005. Asymptotic prey profitability drives star-nosed moles to the foraging speed limit. *Nature* 433:519-522.

Cheverud, J.M. 1982. Relationships among ontogenetic, static, and evolutionary allometry. *American Journal of Physical Anthropology*, 59:139-149.

Chiozza F. 2008. *Scaptonyx fusicaudus*. In: IUCN 2010. IUCN Red List of Threatened Species. Version 2010.04.00.

Claude, J. 2008. Morphometrics with R. New York: Springer Science+Business Media, LLC. 318 p.

Cleef-Roder, J.T. van, Hoek Ostende, L. van den. 2001. Dental morphology of *Talpa europaea* and *Talpa occidentalis* (Mammalia: Insectivora) with a discussion of fossil Talpa in the Pleistocene of Europe. *Zoologische Medelingen* 75: 51–68.

Clemens, W.A. 1968. Origin and early evolution of marsupials. *Evolution* 22:1-18.

Clemens,W.A., Lillegraven, J.A. 1986. New Late Cretaceous, North American advanced therian mammals that fit neither the marsupial nor eutherian molds. *Cont. Geology University of Wyoming*, 3:55–85.

Cock, A.G. 1966. Genetical aspects of metrical growth and form in animals. *The Quarterly Review of Biology*, 41:131-190.

Colangelo, P., Bannikova, A.A., Kryštufek, B., Lebedev, V.S., Annesi, F., Capanna, E. and Loy, A. 2010. Molecular systematics and evolutionary biogeography of the genus Talpa (Soricomorpha: Talpidae). *Molecular Phylogenetic and Evolution*, 35:372-380.

Cox PG, Fagan MJ, Rayfield EJ, and Jeffery N. 2011. Finite element modelling of squirrel, guinea pig and rat skulls: using geometric morphometrics to assess sensitivity. *Journal of Anatomy*. 219:696–709. doi: 10.1111/j.1469-7580.2011.01436.x.

Crochet J.Y. 1995. Le Garouilles et les sites contemporains (Oilgocène,MP 25) des Phosphorites du Quercy (Lot, Tarn−et−Garonne, France) et leurs faunes de vertébrés. 4. Marsupiaux et Insectivores. *Palaeontographica*, A, 236:39-75.

Crochet, J-Y., Welcomme, J-L., Ivorra, J., Ruffet, G., Boulbes, N., Capdevila, R., Claude, J. and Pickford, M. 2009. Une nouvelle faune de vertébrés continentaux, associée à des artefacts dans le Pléistocène inférieur de l'Hérault (Sud de la France), vers 1, 57 Ma. *Comptes. Rendus. Palevol.*, 8:725-736.

Crompton, A.W., Hiiemae, K.M. 1970. Molar occlusion and mandibular movements during occlusion, *Didelphis marsupialis*. *Zoological Journal of the Linnean Society*, 49:21-47.

Crumpton, N., and Thompson, R.S. 2013. The holes of moles: Osteological correlates of the trigeminal nerve in Talpidae. *Journal of Mammalian Evolution*. 20:213-225.

Dahlmann, T., Doğan, S., 2011. *Gerhardstorchia* nomen novum: a new name for *Storchia* Dahlmann 2001 (Mammalia: Lipotyphla: Talpidae: Desmaninae). *Paläontologische Zeitschrift* 85: 91.

Dalquest, W.W., Burgner, R.L. 1941. The shrew-mole of western Washington. *The Murrelet* 22:12-14.

Dalquest, W.W., Orcutt, D.R. 1942. The biology of the least shrew-mole, *Neurotrichus gibbsii minor*. *American Midland Naturalist*. 27:387-401.

Dalquest, W.W., Baskin, J.A., Schultz, G.E. 1996. Fossil mammals from a late Miocene (Clarendonian) site in Beaver County, Oklahoma. *Contributions in Mammalogy: A Memorial Volume Honoring Dr. J. Knox Jones, Jr. Museum of Texas Tech University*, 107-137.

Darwin, C.R. 1859. The origin of species. London: John Murray, Albemarle Street. 560 p.

Dayan, T., Simberloff, D. 1998. Size patterns among competitors: ecological character displacement and character release in mammals, with special reference to island populations. *Mammal Review* 28: 99–124.

Detlev, S., Westerhoff, M. and Hege, H.C. 2005. "Chapter 38, Amira: A Highly Interactive System for Visual Data Analysis". In Hansen CD, Johnson CR, The Visualization Handbook. Elsevier. pp. 749–767.

Dobson, G.E. 1882. A monograph of the Insectivora. 86-172. John Van Voorst, London.

Dobzhansky, T. 1956. What is an adaptative trait? *American Naturalist*. Vol. XC, NO. 855.

Dobzhansky, T., Ehrman, L., Kastritsis, P. 1968. Ethological isolation between sympatric and allopatric species of the obscura group of Drosophila. *Animal Behaviour*. 16:79-87.

Dobzhansky T. 1970. Genetics of the evolutionary process. New York: Columbia University Press. 505 p.

Doukas, C.S., Hoek Ostende, L.W. van den, Theocharopoulos, C.D., Reumer J.W.F. 1995. The vertebrate locality Maramena (Massedonia, Greece) at the Turolian-Ruscinian boundary (Neogene). 5. Insectivora (Erinaceidae, Talpidae, Soricidae, Mammalia). *Münchner Geowissenschaftliche Abhandlungen A* 28: 43-64.

Duarte, L.C., Monteiro, L.R., von Zuben, F.J., dos Reis, S.F. 2000. Variation in mandible shape in *Trichomys apereoides* (Mammalia: Rodentia): geometric analysis of a complex morphological structure. *Systematic Biology*, 49:563-578.

Edwards, L.F. 1937. Morphology of the forelimb of the mole (*Scalops aquaticus*, L.) in relation to its fossorial habits. *Ohio Journal of Science*. 37:20–41.

Engesser B., Storch G. 2008. Latest Oligocene Didelphimorphia, Lipotyphla, Rodentia and Lagomorpha (Mammalia) from Oberleichtersbach, Rhoen Mountains, Germany. *Courier Forschungsinstitut Senckenberg*, 260:185-251.

Engesser, B. 2009. The insectivores (Mammalia) from Sansan (Middle Miocene, south-western France). *Schweizerische Paläontologische Abhandlungen*, 128:1-91.

Farke, A.A. 2008. Frontal sinuses and head-butting in goats: a finite element analysis. *Journal of Experimental Biology*. 211:3084-3095.

Felsenstein, J. 1985. Confidence limits on phylogenies: an approach using the bootstrap. *Evolution*. 783-791.

Felsenstein, J. 1988. Phylogenies and Quantitative Characters. *Annual Review of Ecology and Systematics*, 19:445.

Filippucci, M.G., Nascetti, G., Capanna, E., Bullini, L. 1987. Allozyme variation and systematics of European moles of the genus *Talpa* (Mammalia, Insectivora). *Journal of Mammalogy*, 487-499.

Firmat, C., Lozano-Fernández, I., Agustí, J., Bolstad, G.H., Cuenca-Bescós, G., Hansen, T.F. and Pélabon, C. 2014. Walk the line: 600000 years of molar evolution constrained by allometry in the fossil rodent Mimomys savini. *Philosophical Transactions of the Royal Society B: Biological Sciences*, 369(1649), 20140057.

Flynn, L.J., Wu, W. 1994. Two new shrews from the Pliocene of Yushe Basin, Shanxi Province, China. *Vertebrata Palasiatica*, 32:73-86.

Fox, R.C. 1975. Molar structure and function in the early Cretaceous mammal *Pappotherium*: Evolutionary implications for Mesozoic Theria. *Canadian Journal of Earth Sciences*, 12:412-442.

Freckleton, R.P., Harvey, P.H. 2006. Detecting non-Brownian trait evolution in adaptive radiations. *PLoS Biology* 4, e373. (doi:10.1371/journal.pbio.0040373)

Freeman, R.A. 1886. The anatomy of the shoulder and upper arm of the mole (*Talpa europaea*). *Journal of Anatomy and Physiology* 20:201-219.

Fritz, S.A., Purvis, A. 2010. Phylogenetic diversity does not capture body size variation at risk in the world's mammals. *Procedings of the Royal Society B*. 277:2435-2441.

Gambaryan, P., Gasc, J.P., Renous, S. 2003. Cinefluorographical study of the burrowing movements in the common mole, *Talpa europaea* (Lipotyphla, Talpidae). *Russian Journal of Theriology* 1:91-109.

Garcìa-Alix, A., Furio, M., Minwer-Barakat, R., Martin-Suarez, E., Freudenthal, M. 2011. Environmental control on the biogeographical distribution of Desmanella (Soricomorpha, Mammalia) in the Miocene of the Iberian Peninsula. *Palaeontology*. 54:753-762.

Garland Jr, T., Ives, A.R. 2000. Using the past to predict the present: confidence intervals for regression equations in phylogenetic comparative methods. *The American Naturalist*, 155:346-364.

Gasc, J.P., Jouffroy, F.K., Renous, S. and von Blottnitz, F. 1986. Morphofunctional study of the digging system of the Namib Desert golden mole (*Eremitalpa granti namibensis*): cinefluorographical and anatomical analysis. *Journal of Zoology*, 208:9-35.

Gibert Clols, J. 1974. Études des Insectivores du miocène de Vallès-Penedès, Calatayud-Daroca et Rubielos de Mora. Thèse, Université Sabadell.

Gibert Clols, J. 1975. New Insectivores of the Miocene of Spain I and II. – *Proceedings of the Koninklijke Nederlandse Akademie van Wetenschappen*, Serie B 78:108-133.

Glor, R.E. 2010. Phylogenetic insights of adaptative radiation. *Annual Review of Ecology, Evolution and Systematics*. 41:251–70.

Goloboff, P. A., Pol, D. 2005. Parsimony and Bayesian phylogenetics.*Parsimony, phylogeny, and genomics*. 148-159.

Goodall, C. 1991. Procrustes methods in the statistical analysis of shape. *Journal of the Royal Statistical Society* 53: 285–339.

Gorman, M.L., Stone, R.D. 1990. *The natural history of the mole*. 138 pp. Christopher Helm, A. & C. Black, London.

Gould, S.J. 1966. Allometry and size in ontogeny and phylogeny. *Biological Review of the Cambridge Philosophical Society*, 41:587-640.

Gould, S.J., Lewontin, R.C. 1979. The spandrels of San Marco and the Panglossian paradigm: a critique of the adaptionist programme. *Procedings of the Royal Society London*. 205:581-598.

Gould, S.J., Vrba, E.S. 1982. Exaptation – a missing term in the science of form. *Paleobiology*. 8:4-15.

Gould, S.J. 2002. The structure of evolutionary theory. Harvard MA: Harvard University Press. 1433 p.

Grand, T., Gould, E., Montali, R. 1998. Structure of the proboscis and rays of the star-nosed mole, *Condylura cristata*. *Journal of Mammology*, 79:492–501.

Green, M. 1956. The lower Pliocene Ogallala-Wolf Creek vertebrate fauna, South Dakota. *Journal of Paleontology*, 30:146-169.

Gregory, W.K. 1949. The humerus from fish to men. *American Museum Novitates*, 1400:1-51.

Gröning F., Liu, J., Fagan, M.J., O'Higgins, P. 2009. Validating a voxel-based finite element model of a human mandible using digital speckle pattern interferometry. *Journal of Biomechanics*. 42:1224-1229.

Gunnel, G.F., Bown, T.M., Hutchinson, J.H. and Bloch, J.I. 2008. Lipotyphla. In: Janis CM, Gunnell GF & Uhen MD eds Evolution of Tertiary Mammals of North America, Volume 2: Small Mammals, Xenarthrans, and Marine Mammals, Cambridge University Press, Cambridge, pp. 89–125.

Gureev, A.A. 1964. Fauna of the USSR. *Zaiceobraznye (Lagomorpha)*, 3.10:1-224.

Hall, B.K. 2003. Unlocking the black box between genotype and phenotype. *Biology and Philosophy*, 18:219-247.

Hansen, T.F. 1997. Stabilizing Selection and the Comparative Analysis of Adaptation. *Evolution*, 51:1341-1351.

Hansen, T.F., Pienaar, J., Orzack, S.H. 2008. A comparative method for studying adaptation to a randomly evolving environment. *Evolution*, 62:1965-1977.

Harmon, L., Schulte, J., Larson, A., Losos, J. 2003. Tempo and mode of evolutionary radiation in iguanian lizards. *Science*, 301:961-964.

Harmon, L.J., Weir, J., Brock, C., Glor, R., Challenger, W., Hunt, G., Fitzjohn, R., Pennell, M., Slater, G., Brown, J., Uyeda, J. and Eastman, J. 2014. Package "geiger". *Bioinformatics* 24:129-131.

Harvey, P.H., Pagel, M.D. 1991. *The comparative method in evolutionary biology* (Vol. 239). Oxford: Oxford university press.

Harvey, P.H., Rambaut, A. 2000. Comparative analyses for adaptive radiations. *Philosophical Transactions of the Royal Society of London. Series B: Biological Sciences*, 355:1599-1605.

He, K., Shinohara, A., Jiang, X.L., Campbell, K.L. 2014. Multilocus phylogeny of talpine moles (Talpini, Talpidae, Eulipotyphla) and its implications for systematics. *Molecular Phylogenetics and Evolution*, 70:513-521.

Herrel, A., Vanhooydonck, B., Van Damme, R. 2004. Omnivory in lacertid lizards: adaptive evolution or constraint?. *Journal of evolutionary biology*, 17:974-984.

Hickman, G.C. 1983. Influence of the semiaquatic habit in determining burrow structure of the star-nosed mole (*Condylura cristata*). *Canadian Journal of Zoology*. 61:1688-1692.

Hildebrand, M. 1982. Analysis of vertebrate structure, 2nd edn. New York: John Wiley and Sons, Inc.

Hiiemae, K.M. 2000. Feeding inmammals. In: Feeding: Form, Function, and Evolution in Tetrapod Vertebrates, K. Schwenk, ed., pp. 411–448, Academic Press, New York.

Hoek Ostende, L. W. Van den. 1989. *The Talpidae (Insectivora, Mammalia) of Eggingen-Mittelhart (Baden-Württemberg, FRG) with Special Reference to the Paratalpa-Desmanodon Lineage: With 4 Tables*. Staatliches Museum für Naturkunde.

Hoek Ostende, L.W. van den. 1997. Insectivore faunas from the Lower Miocene of Anatolia. Part 4: The genus *Desmanodon* (Talpidae) with the description of a new species from the Lower Miocene of Spain. *Proceedings Koninklijke Akademie van Wetenschappen*. 100: 27–65.

Hoek Ostende, L.W. van den. 2001. Insectivore fauna from the Lower Miocene of Anatolia – part 5: Talpidae. *Scripta Geologica* 122:1-45.

Hoek Ostende, L.W. van den, Fejfar, O. 2006. Erinaceidae and Talpidae (Erinaceomorpha, Soricomorpha, Mammalia) from the Lower Miocene of Merkur-Nord (Czech Republic, MN 3). *Beiträge zur Paläontologie*, 30:175-203.

Huang, W.B., Fang, Q.R. 1991. The site of Wushan Man. China Ocean Press, Beijing: 229 pp.

Hugueney, M. 1972 Les talpidés (Mammalia, Insectivora) de Coderet-Bransat (Allier) et l'évolution de cette famille au cours de l'Oligocène supérieur et du Miocène inférieur d'Europe. Documents des Laboratoires de Géologie de la Faculté des Sciences de Lyon, 50:1-81.

Humphrey, L.T., Dean, M.C., Stringer, C.B. 1999. Morphological variation in great ape and modern human mandibles. *Journal of Anatomy*, 195:491-513.

Hunter, J.P. 1998. Key innovations and the ecology of macroevolution. *Trends in Ecology and Evolution*, 13:31-36.

Hunter, J.P., Jernvall, J. 1995. The hypocone as a key innovation in mammalian evolution. *Proceedings of the National Academy of Sciences U.S.A.*, 92:10718-10722.

Hutchinson, J.H. 1968. Fossil Talpidae (Insectivora, Mammalia) from the later Tertiary of Oregon. 120 pp. *Bullettin n°11 of the natural Hisory Museum of Oregon*.

Hutchison, J. H. 1974. Notes on type specimens of European Miocene talpidae and a tentative classification of Old World Tertiary Talpidae (Insectivora: Mammalia). *Geobios* 7.3: 211-256.

Hutchison, J. H. 1987. Moles of the Scapanus latimanus group (Talpidae, Insectivora) from the Pliocene and Pleistocene of California. *Contributions in science/Natural history museum of Los Angeles county*.

Hutterer, R. 2005. Order Soricomorpha. In: Wilson, D.E, Reeder, D.M. (Eds.), Mammals species of the world. A taxonomic and Geographic Reference, 3rd edition. The Johns Hopkins University Press, Baltimore, pp. 220-311.

Hylander, W.L. 2005. The functional significance of primate mandibular form. *Journal of Morphology*, 160:223–239.

Ingram, T. and Mahler, D.L. 2013. SURFACE: detecting convergent evolution from comparative data by fitting Ornstein-Uhlenbeck models with stepwise Akaike Information Criterion. *Methods in Ecology and Evolution*, 4:416-425.

International Commission for Zoological Nomenclature. 1999. International Code of Zoological Nomenclature, 4th edition. 306 pp. International Trust for Zoological Nomenclature, London.

Ives, R.A., Garland, T.Jr. 2010. Phylogenetic Logistic Regression for Binary Dependent Variables. *Systematic Biology*. 59:9-26.

Janossy, D. 1986. Pleistocene vertebrate fauna of Hungary. 207 pp. Elsevier, Amsterdam.

Jernvall, J., Hunter, J.P., Fortelius, M. 1996. Molar tooth diversity, disparity, and ecology in Cenozoic ungulate radiations. *Science*, 274:1489-1492.

Jin, C.Z., Liu, J.Y., 2009. Paleolithic Site e the Renzidong Cave, Fanchang, Anhui Province. Science Press, Beijing, pp. 1-439.

Jones, K.E., Goswami, A. 2010. Quantitative analysis of the influences of phylogeny and ecology on phocid and otariid pinniped (Mammalia; Carnivora) cranial morphology. *Journal of Zoology*. 280:297–308.

Kawada, S. and Obara, Y. 1999. Reconsideration of the karyological relationship between two Japanese species of shrew-moles, *Dymecodon pilirostris* and *Urotrichus talpoides*. *Zoological Science* 16: 167–174.

Kawada, S.I., Harada, M., Obara, Y., Kobayashi, S., Koyasu, K., Oda, S.I. 2001. Karyosystematic analysis of Japanese talpine moles in the genera *Euroscaptor* and *Mogera* (Insectivora, Talpidae). *Zoological Science*. 18:1003-1010.

Kawada, S. I. 2005. The historical notes and taxonomic problems of East Asian moles, Euroscaptor, Parascaptor and Scaptochirus, of continental Asia (Insectivora, Talpidae). *Mammal Study*. *30*: 5-11.

Kawada, S., Shinohara, A., Kobayashi, S., Harada, M., Oda, S., Liang-Kong, L. 2007. Revision of the mole genus *Mogera* (Mammalia: Lipotyphla: Talpidae) from Taiwan. *Systematics Biodiversity*. 5:223-240.

Kawada, S.I., Son, N. T., Ngoc Can, D. 2012. A new species of mole of the genus *Euroscaptor* (Soricomorpha, Talpidae) from northern Vietnam. *Journal of Mammalogy*. 93: 839-850.

Kawamura Y. 1991 Quaternary mammalian faunas in the Japanese islands. *The Quaternary Research (Japan)*, 30:213-220.

Kay, R.F., Hiiemae, K.M. 1974. Jaw movement and tooth use in recent and fossil Primates. *Journal of Physiatric Anthropology*, 40:227-256.

Kays, R.W., Wilson, D.E. 2009. Mammals of North America, 2nd edition. Princeton NJ: Princeton University Press. 248 p.

Kendall, D.G., Kendall, W.S. 1980. Alignments in two-dimensional random sets of points. *Advances in Applied Probability*, 12:380-424.

Kielan-Jaworowska, Z., Cifelli, R.L., and Luo, Z.-X. 2002. Dentition and relationships of the Jurassic mammal Shuotherium. *Acta Palaeontologica Polonica*, 47:479-486.

Klietmann, J. 2013. *Systematic and ecological analysis of Marsupialia and Eulipotyphla from Petersbuch 28 (Germany, Lower Miocene)* (Doctoral dissertation, uniwien).

Klingenberg, C.P., Mebus, K., Auffray, J.C. 2003. Developmental integration in a complex morphological structure: how distinct are the modules in the mouse mandible? *Evolution and Development*, 5:522-531.

Klingenberg, C.P. 2005. Developmental constraints, modules and evolvability. *Variation: A central concept in biology*, pp. 219-247.

Klingenberg, C. P., & Monteiro, L. R. 2005. Distances and directions in multidimensional shape spaces: implications for morphometric applications.*Systematic Biology*. 54.4: 678-688.

Klingenberg, C.P. 2011. MorphoJ. Faculty of Life Sciences, University of Manchester, UK. http://www.flywings.org.uk/MorphoJ_page.htm

Klingenberg, C.P., Gidaszewski, N.A. 2010. Testing and quantifying phylogenetic signals and homoplasy in morphometric data. *Systematic biology* 59:245-261.

Klietmann, J., Nagel, D., Rummel, M., Hoek Ostende, L.W. van den. 2014. A gap in digging: the Talpidae of Petersbuch 28 (Germany, Early Miocene). *Paläontologische Zeitschrift* 1-30.

Koenigswald, W. von. 1970. Mittelpleistozäne Kleinsäugerfauna aus der Spaltenfüllung Petersbuch bei Eichstätt. *Mitteilungen der Bayerischen Staatssammlung für Paläontologie und histor. Geologie*, 10:407-432.

Kormos, T. 1930. Diagnosen neuer Säugetiere aus des oberpliozänen Fauna des Somlyöberges, Püspokfürdo. *Annales Historico-Naturales Musei Nationalis Hungarici*, 27:237-246.

Kretzoi, M. 1938. Die Raubtiere von Gombaszög nebst einer Übersicht der Gesamtfauna. *Annales Historico-Naturales Musei Nationalis Hungarici*, 31:88-157.

Kretzoi, M., Kretzoi, M. 2000. Index generum et subgenerum mammalium. *Fossilium Catalogus Animalia* 137:1-433.

Krystufek, B., Spitzenberger, F., Kefelioglu, H. 2001. Description, taxonomy, and distribution of *Talpa davidiana*. *Mammalian Biology*, 66:135-143.

Kupczik, K., Dobson, C.A., Fagan, M.J., Crompton, R.H., Oxnard, C.E., O'Higgins, P. 2007. Assessing mechanical function of the zygomatic region in macaques: validation and sensitivity testing of finite element models. *Journal of Anatomy*. 210:41–53.

Li, Y., Zhang, Y., Li, J. 2013. Distribution of several Insectivora and the drying trend since the Pleistocene in North China. *Quaternary International* 313:240-247.

Liem KF, Bemis W, Walker WF and Grande L. 2001. Functional anatomy of the vertebrates: an evolutionary perspective. Thomson Brooks/Cole, Belmont, CA. 703 pp.

Lister, A., 1995. Sea-levels and the evolution of island endemics: the dwarf red deer of Jersey. *Geological Society Special Publication*, 96:151-172.

Liu, W., Wu, X., Pei, S., Xiujie, W., Norton, C.J., 2009. Huanglong Cave: A Late Pleistocene human fossil site in Hubei Province, China. *Quaternary International*, 211:29–41.

Lloyd, K.J., Eberle, J.J. 2008. A new talpid from the late Eocene of North America. *Acta Palaeontologica Polonica*, 53:539-543.

Lopatin, A.V. 2002. An Oligocene mole (Talpidae, Insectivora, Mammalia) from Western Kazakhstan. *Paleontological Journal*. 33:182-191.

Lopatin, A.V., 2004. Early Miocene small mammals from the North Aral Region (Kazakhstan) with special reference to their biostratigraphic significance. *Paleontological Journal* 38, supplement 3:217-323.

Lord, J., Westoby, M., Leishman, M. 1995. Seed size and phylogeny in six temperate floras: constraints, niche conservatism, and adaptation. *American Naturalist*, 349-364.

Losos, J.B., Miles, D.B. 2002. Testing the Hypothesis That a Clade Has Adaptively Radiated: Iguanid Lizard Clades as a Case Study. *American Naturalist*. 160:147-157.

Losos, J.B., Mahler, D.L. 2010. Adaptive Radiation: The Interaction of Ecological Opportunity, Adaptation, and Speciation. In . Evolution after Darwin: the first 150 years, eds Bell MA, Futuyma D, Eanes WF, Levinton JS. Chapter15. Sunderland Ma: Sinauer.

Losos, J.B. 2008. Phylogenetic niche conservatism, phylogenetic signal and the relationship between phylogenetic relatedness and ecological similarity among species. *Ecology Letters*, 11:995-1007.

Losos, J.B. 2011. Convergence adaptation and constraint. *Evolution*, 65:1827-1840.

Loy, A., Di Martino, S., Capolongo, D. 1996. Patterns of geographic variation of Talpa romana Thomas: preliminary results derived from a geometric morphometric approach. *Mammalia* 60:77–89.

Loy, A., Capanna, E. 1998. A parapatric contact area between two species of moles (genus Talpa): character displacement investigated through the geometric morphometric of skull. *Acta Zoologica Academiae Scientiarum Hungaricae* 44: 151–164.

Loy, A., Capula, M., Palombi, A., Capanna, E. 2001. Genetic and morphometric evidence of past introgression between Talpa europaea and Talpa romana along a parapatric contact zone. *Journal of Zoology* 254: 229–238.

Loy, A., Colangelo, P., Annesi, F., Capanna, E. 2005. Origin and evolution of Western European moles (genus *Talpa*, Insectivora, Mammalia): a multidisciplinary approach. *Mammal Study*. 30:13-17.

Loy, A. 2008. Famiglia Talpidae. In Amori, G., Contoli, L., Nappi, A. eds. Mammalia II. Erinaceomorpha, Soricomorpha, Lagomorpha, Rodentia. 437 pp. Fauna d'Italia, vol. XLIV Bologna: Edizioni Calderini de Il Sole 24 ORE Edagricole.

Luo, ZX and Wible, JR. 2005. A Late Jurassic digging mammal and early mammalian diversification. *Science* 308:103–107

Lunde, D.P., Musser, G.G., Truong Son, N. 2003. A survey of small mammals from Mt. Tay Con Linh II, Vietnam, with the description of a new species of *Chodsigoa* (Insectivora: Soricidae). *Mammal Study*. 28:31–46.

MacLeod, N. 2002. Geometric morphometrics and geological shape-classification systems. *Earth-Science Reviews*, 59:27-47.

Maddison, W.P., Maddison, D.R. 2010. Mesquite: a modular system for evolutionary analysis. Version 2.73.

Maddison, WP. and Maddison DR. 2015. Mesquite: a modular system for evolutionary analysis. Version 3.02 http://mesquiteproject.org

Mahler, D.L., Revell, L.J., Glor, R.E., Losos, J.B. 2010. Ecological opportunity and the rate of morphological evolution in the diversification of the Greater Antillean anoles. *Evolution*. 64:2731-2745.

Martin, R.A., 1993. Patterns of variation and speciation in quaternary rodents, pp. 226-280 in Morphological Change in Quaternary Mammals of North America, edited by RA. Martin & A.D. Barnosky. Cambridge University Press, Cambridge, England.

Martìn-Suárez, E., Mein, P. 2004. The late pliocene locality of saint-vallier (Drôme, France). Eleven micromammals. *Geobios*, 37:115-125.

Martín-Suárez, E., Bendala, N., Freudenthal, M. 2010. *Archaeodesmana baetica*, sp. nov. (Mammalia, Insectivora, Talpidae) from the Mio-Pliocene transition of the Granada Basin, southern Spain. *Journal of Vertebrate Paleontology*, 21:547-554.

McKenna, M.C., Bell, S.K. 1997. Classification of Mammals Above the Species Level. New York: Columbia University Press. 631 p.

McPeek, M.A. 1995. Testing hypotheses about evolutionary change on single branches of a phylogeny using evolutionary contrasts. *The American Naturalist*, 45:686-703.

Mein, P., Ginsburg, L. 1997. Les mammifères du gisement miocène inférieur de Li Mae Long, Thaïlande: systématique, biostratigraphie et paléoenvironement. *Geodiversitas*, 19: 783-844.

Meloro, C., Raia, P., Piras, P., Barbera, C., O'Higgins, P. 2008. The shape of the mandibular corpus in large fissiped carnivores: allometry, function and phylogeny. *Zoological Journal of the Linnean Society*, 154:832-845.

Mills, J.R.E. 1966. The functional occlusion of the teeth of Insectivora. *Zoological Journal of the Linnean Society*, 46:1-25.

Mills, J.R.E. 1971. The dentition of *Morganucodon*. In: Early Mammals, D.M. Kermack, K.A. Kermack, eds., pp. 29-63, The Linnean Society of London, London.

Minwer-barakat R., Garcia-alix A., Freudenthal M. 2008. Desmaninae (Talpidae, Mammalia) from the Pliocene of Tollo de Chiclana (Guadix Basin, southern Spain). Considerations on the phylogeny of the genus *Archaeodesmana*. *Geobios*, 41:381-398.

Mitteroecker, P., Bookstein, F. 2011. Linear discrimination, ordination, and the visualization of selection gradients in modern morphometrics. *Evolutionary Biology* 38: 100–114.

Monteiro, L.R., dos Reis, S.F. 2005. Morphological evolution in the mandible of spiny rats, genus *Trinomys* (Rodentia: Echimyidae). *Journal of Zoological Systematics and Evolutionary Research*, 43:332-338.

Monteiro, L.R., Bonato, V., dos Reis, S.F. 2005. Evolutionary integration and morphological diversification in complex morphological structures: mandible shape divergence in spiny rats (Rodentia, Echimyidae). *Evolution and Development* 7:429-439.

Motokawa, M. 2004. Phylogenetic relationships within the family Talpidae (Mammalia: Insectivora). *Journal of Zoology London*. 263:147-157.

Nevo, E. 1979. Adaptive convergence and divergence of subterranean mammals. *Annual Review of Ecology and Systematics*, 20:269-308.

Niethammer, J. 1990. Talpa. In: Niethammer, J. & F. Krapp (eds.) Handbuch der Säugetiere Europas. Bd. 3. Insektenfresser-Insectivora, Herrentiere-Primates. Wiesbaden: 93–161.

O'Leary MA, Bloch JI, Flynn JJ, Gaudin TJ, Giallombardo A, Giannini NP,. Goldberg SL Kraatz BP, Luo Z, Meng J, Ni X, Novacek MJ, Perini FA, Randall ZS, Rougier GW,. Sargis EJ, Silcox MT, Simmons NB, Spaulding M, Velazco PM, Weksler M, Wible JR, and Cirranello AL. 2013. The placental mammal ancestor and the post–K-Pg radiation of placentals. *Science* 339: 662-667.

O'Meara, B.C., Ané, C., Sanderson, M.J., Wainwright, P.C. 2006. Testing for different rates of continuous trait evolution using likelihood. *Evolution* 60:922–933.

Oksanen, J., Blanchet, F.G., Kindt, R., Legendre, P., Minchin, P.R., O'Hara, R.B., Simpson, G.L., Solymos, P., Henry, M., Stevens, H., Wagner, H. 2013. vegan: Community Ecology Package. R-package version 2.0-7. Available at http://CRAN.R-project.org/package=vegan.

Oparina, O.S., Filinova, I.E., Sonina E.E., Malinina, Y.A., Oparin, M.L. 2013. Current status of the Russian desman habitats in small rivers of the Don river basin in Saratov Oblast and the abundance of this species. *Biology Bulletin*, 40:854-861.

Pagel, M. 1997. Inferring evolutionary processes from phylogenies. *Zoologica Scripta*, 26:331-348.

Pagel, M. 1999. Inferring the historical patterns of biological evolution. *Nature*, 401:877-884.

Pashkov, A.V., Topachevsky, V.A. 1990. New representatives of the genus *Desmana* (Insectivora, Talpidae) from Late Pliocene deposits of Central Europe and south-west European part of the USSR. *Vestnik Zoologii,* 1990:25-34, 40.

Patterson, T. B., Givnish, T. J. 2002. Phylogeny, concerted convergence, and phylogenetic niche conservatism in the core Liliales: insights from rbcL and ndhF sequence data. *Evolution*, 56:233-252.

Patton, L., Smith, M.F. 1989. Population structure and thgenetic and morphological divergence among pocket gopher species (genus *Thomomys*), pp. 284-304 in Speciation and its Consequences, edited by D. Otte & J.A. Endler. Sinauer, Sunderland, Massachusetts.

Pearman, P.B., Lavergne, S., Roquet, C., Wüest R., Zimmermann, N.E., Thuiller, W. 2014. Phylogenetic patterns of climatic, habitat and trophic niches in a European avian assemblage. *Global Ecology and Biogeography*, 23:414-424.

Perez, S.I., Bernal, V., Gonzalez, P.N. 2006. Differences between sliding semi-landmark methods in geometric morphometrics, with an application to human cranio-facial and dental variation. *Journal of Anatomy* 208: 769-784.

Petényi, S.J. 1864. A beremendi mészköbánya természetrajz- és öslénytanilag leírva. *Hátrahagyott munkái*: 35–81.

Pierce, S.E., Angielczyk, K.D., Rayfield, E.J. 2008. Patterns of morphospace occupation and mechanical performance in extant crocodilian skulls: A combined geometric morphometric and finite element modeling approach. *Journal of Morphology*. 269:840–864.

Pierce, S.E., Angielczyk, K.D., Rayfield, E.J. 2009a. Morphospace occupation in thalattosuchian crocodylomorphs: skull shape variation, species delineation and temporal patterns. *Palaeontology*. 52:1057–1097.

Pierce, S.E., Angielczyk, K.D., Rayfield, E.J. 2009b. Shape and mechanics in thalattosuchian (Crocodylomorpha) skulls: implications for feeding behaviour and niche partitioning. *Journal of Anatomy*. 215:555–576.

Piras, P., Maiorino, L., Raia, P., Marcolini, F., Salvi, D., Vignoli, L., Kotsakis, T. 2010. Functional and phylogenetic constraints in Rhinocerotinae craniodental morphology. *Evolutionary Ecology Research*. 12:897-928.

Piras, P., Salvi, D., Ferrara, G., Maiorino, L., Delfino, M., Pedde, L. and Kotsakis, T. 2011. The role of post-natal ontogeny in the evolution of phenotypic diversity in *Podarcis* lizards. *Journal of Evolutionary Biology*, 24:2705-2720.

Piras, P., Sansalone, G., Colangelo, P., Teresi, L., Kotsakis, T., Loy, A. 2012. Testing convergent and parallel adaptations in talpids humeral mechanical performance by means of Geometric Morphometrics and Finite Element Analysis. *Journal of Morphology* 273: 696–711.

Piras, P., Buscalioni, A.D., Teresi, L., Raia, P., Sansalone, G., Kotsakis, T. and Cubo, J. 2014. Morphological integration and functional modularity in crocodilian skull. *Integrative Zoology*, 9:498-516.

Prieto, J. 2010. The Middle Miocene mole Desmanodon crocheti sp. nov.(Talpidae, Mammalia): the last representative of the genus in the North Alpine foreland basin. *Paläontologische Zeitschrift*, 84.2: 217-225.

Prieto, J., Gross, M., Böhmer, C., Böhme, M. 2010. Insectivores and bat (Mammalia) from the late Middle Miocene of Gratkorn (Austria): biostratigraphic and ecologic implications. *Neues Jahrbuch für Geologie und Paläontologie-Abhandlungen*. 258.1: 107-119.

Raia, P., Carotenuto, F., Meloro, C., Piras, P., Pushkina D. 2010. The shape of contention. Adaptation, history and contingency in ungulate mandibles. *Evolution*. 64:1489-1503.

Polly, P.D. 2003. Paleophylogeography of *Sorex araneus*: molar shape as a morphological marker for fossil shrews. *Mammalia*, 68:233-243.

Pomel, A. 1848. Étude sur les carnassiers insectivores. I Insectivores fossiles. II Classification des insectivores. *Archives des Sciences Physiques et Naturelles*, 9:159-165; 244-251.

Popov, V.V. 2004. Late Pliocene Erinaceidae and Talpidae (Mammalia: Insectivora) from Varshets (North Bulgaria). *Acta Zoologica Cracoviensia* 47:61-80.

Price, T. 1997. Correlated evolution and independent contrasts. *Philosophical Transactions of the Royal Society of London. Series B: Biological Sciences*, 352:519-529.

Puttick, G.M. and Jarvis, J.U.M. 1977. Functional anatomy of neck and forelimbs of Cape golden mole *Chrysochloris asiatica* (Lipotyphla Chrysochloridae). *Zoologica Africana*, 12(2):435–458.

Qiu, Zhuding and Storch, Gerhard, 2005: China. – In: van den Hoek Ostende, Lars W., Doukas, C.S. and Reumer, J.W.F. (eds.): The Fossil Record of the Eurasian Neogene Insectivores. (Erinaceomorpha, Soricomorpha, Mammalia), Part I. *Scripta Geologica* Special Issue 5:37-50.

Rabeder, G. 1972. Die Insectivoren und Chiropteren (Mammalia) aus dem Altpleistozän von Hundsheim (Niederösterreich). *Annalen des Naturhistorischen Museums in Wien*, 76:375-474.

Rayfield, E., Norman, D.B., Horner, C.C., Horner, J.R., Smith, P.M., Thomason, J.J. and Upchurch, P. 2001. Cranial design and function in a large theropod dinosaur. *Nature*, 4081033–1037.

Rayfield, E.J. 2007. Finite element analysis and understanding the biomechanics and evolution of living and fossil organism. *Annual Review of Earth Planet Science*. 35:541-576.

Rayfield, E.J. 2011. Strain in the ostrich mandible during simulated pecking and validation of specimen-specific finite elements model. *Journal of Anatomy*. 218: 47-58.

Reed, C.A. 1951. Locomotion and appendicular anatomy in three soricoid insectivores. *American Midland Naturalist* 45: 513–671.

Reed, K. M. 1962. *Two new species of fossil talpid insectivores*. Museum of Comparative Zoology.

Rees, R.W. 2005. Morphologic variation in the mandible of the white-tailed deer (*Odocoileus virginianus*): a study of populational skeletal variation by principal component and canonical analyses. *Journal of Morphology*, 128:113-130.

Remy J.A., Crochet J.-Y., Sigé B., Sudre J., De Bonis L., Vianey-Liaud M., Godinot M., Hartengerger J.-L., Lange-Badré B., Comte B. 1987. Biochronologie des phosphorites du Quercy: mise à jour des listes fauniques et nouveaux gisements de mammifères fossils. *Münchner Geowissenschaftliche Abhandlungen*, ser. A, 10:169-188.

Rensberger, J.M. 1995. Determination of stresses in mammalian dental enamel and their relevance to the interpretation of feeding behaviours in extinct taxa. In: Functional Morphology in Vertebrate Paleontology, J.J. Thomason, ed., pp. 151-172, Cambridge University Press, Cambridge.

Revell, L.J., Johnson, M.A., Schulte, J.A., Kolbe, J.J., Losos, J.B. 2007. A phylogenetic test for adaptive convergence in rock-dwelling lizards. *Evolution*. 61:2898–2912.

Revell, L.J., Mahler, D.L., Peres-Neto, P.R., Redelings, P.D. 2011. A new phylogenetic method for identifying exceptional phenotypic diversification. *Evolution*. doi: 10.1111/j.1558-5646.2011.01435.x.

Revell, L.J. 2012. phytools: an R package for phylogenetic comparative biology (and other things). *Methods in Ecology and Evolution*, 3(2):217–223.

Revell, L. J. 2013. Two new graphical methods for mapping trait evolution on phylogenies. *Methods in Ecology and Evolution*. 4.8: 754-759.

Richmond, B.G., Wright, B.W., Grosse, I., Dechow, P.C., Ross, C.F., Spencer, M.A., Strait, D.S. 2005. Finite element analysis in functional morphology. *Anatomical Records Part A*. 283: 259–274.

Robert, C. 1983. Recherches sur les Taupes (Talpa, Insectivora) de quelques gisements quaternaires de France. Thesis Université de Bordeaux I, 170 pp. 8 pl.

Rohlf, F.J., Slice, D.E. 1990. Extensions of the Procrustes method for the optimal superimposition of landmarks. *Systematics Zoology* 39: 40–59.

Rohlf, F.J. 2006. TpsDig 2.05. Department of Ecology and Evolution, State University of NY, Stony Brook, NY. Available at http://life.bio.sunysb.edu/morph/

Rose, KD and Emry, RJ. 1983. Extraordinary fossorial adaptations in the Oligocene palaeanodonts *Epoicotherium* and *Xenocranium* (Mammalia). *Journal of Morphology*, 175:33-56.

Ross, C.F., Patel, B.A., Slice, D.E., Strait, D.S., Dechow, P.C., Richmond, B.G., Spencer, M.A. 2005. Modeling masticatory muscle force in finite element analysis: Sensitivity analysis using principal coordinates analysis. *Anatomical Records Part A*. 283:288–299.

Rougier GW, Wible JR, Beck RMD, and Apesteguía S. 2012. The Miocene mammal *Necrolestes* demonstrates the survival of a Mesozoic nontherian lineage into the late Cenozoic of South America. *PNAS* 109: 20053–20058. doi:10.1073/pnas.1212997109

Rumke, C.G. 1974. New *Desmanella* species(talpidae,insectivore) from turolian of concud and los-mansuetos (prov of teruel-Spain). *Proceedings of the Koninklijke Nederlanlandse akademie van Wetenschappen series b-palaentology geology physics chemistry anthropology.* 77:359.

Rzebik-Kowalska, B. 1994. Pliocene and Quaternary Insectivora (Mammalia) of Poland." *Acta zoologica cracoviensia* 37(1).

Rzebik-Kowalska, B. 2005a: Erinaceomorpha and Soricomorpha (Mammalia) from the Miocene of Belchátow, Poland. IV. Erinaceidae Fischer von Waldheim, 1817 and Talpidae Fischer von Waldheim, 1817. – Acta Zoologica Cracoviensia, 48A (1-2): 71–91.

Rzebik-Kowalska, B. 2005b. Poland. In: Hoek Ostende, L.W. van den, Doukas, C.S. and Reumer, J.W.F. (Eds.) The fossil record of the Eurasian Neogene insectivores (Erinaceomorpha, Soricomorpha, Mammalia). Part I. *Scripta Geologica* Spec. Issue 5: 119–134.

Rzebik-Kowalska B. 2014. Revision of the Pliocene and Pleistocene Talpidae (Soricomorpha, Mammalia) of Poland. *Palaeontologia Electronica* 17: 1–26.

Sánchez-Villagra, M.R., Menke, P.R., Geisler, J.H. 2004. Patterns of evolutionary transformation in the humerus of moles (Talpidae, Mammalia): a character analysis. *Mammal Study* 29: 163–170.

Sánchez-Villagra, M.R., Horovitz, I. and Motokawa, M. 2006. A comprehensive morphological analysis of talpid moles (Mammalia) Phylogenetic relationship. *Cladistics* 22: 59–88.

Sandefur, M. 2008. Biomechanical Modeling of Forelimb Adduction in the Eastern Mole *Scalopus acquaticus*. Student honor theses, Western Kentucky University. 24 p. Available from: http://digitalcommons.wku.edu/stu_hon_theses/104.

Sansalone G., Kotsakis T., Piras P. In press. New systematic insights about Plio-Pleistocene moles from Poland. *Acta Palaeontologica Polonica*, http://dx.doi.org/10.4202/app.00116.2014

Schindelin, J., Arganda-Carreras, I., Frise, E., Kaynig, V., Longair, M., Pietzsch, T., Preibisch, S., Rueden, C., Saalfeld, S., Schmid, B., Tinevez, J.Y., White, D.J., Hartenstein, V., Eliceiri, K., Tomancak, P. and Cardona, A. 2012. Fiji: an open-source platform for biological-image analysis. *Nature Methods*, 9(7):676–682.

Schlager, S. 2014. Morpho: Calculations and visualisations related to Geometric Morphometrics. R-package version 2.0.3-1. Available at http://cran.r-project.org/web/packages/Morpho/index.html.

Schluter, D. 1996. Adaptive radiation along genetic lines of least resistance. *Evolution*, 50:1766-1774.

Schluter, D. 2000. The ecology of adaptive radiation. Oxford: Oxford University Press. 300 p.

Schwenk, K. 1995. A utilitarian approach to evolutionary constraint. *Zoology* 98:251-262.

Schwermann, A.H., Martin, T. 2012. A partial skeleton of Geotrypus antiquus (Talpidae, Mammalia) from the Late Oligocene of the Enspel Fossillagerstätte in Germany. *Paläontologische Zeitschrift*. 86:409-439.

Scott, R.G., Richardson, R.C. 2005. Realities of biologically inspired design with a subterranean digging robot example. *Robotics Applications*, 498:1-6.

Seligsohn, D., and Szalay, F. S. 1974. Dental occlusion and the masticatory apparatus in Lemur and Varecia: Their bearing on the systematics of living and fossil Primates. In: Prosimian Biology, R.D. Martin, G.A. Doyle, and A.C. Walker, eds., pp. 543–561, Duckworth, London.

Shinohara, A., Campbell, K.L., Suzuki, H. 2003. Molecular phylogenetic relationships of moles, shrew moles, and desmans from the new and old worlds. *Molecular Phylogenetics and Evolution*. 27:247–258.

Shinohara, A., Suzuki, H., Tsuchiya, K., Zhang, Y.P., Luo, J., Jiang, X.L., Wang, Y.X., Campbell, K.L. 2004. Evolution and biogeography of talpid moles from continental East Asia and the 72 Japanese Islands inferred from mitochondrial and nuclear gene sequences. *Zoological Sciences*. 21:1177-1185.

Shinohara, A., Kawada, S.I., Son, N.T., Koshimoto, C., Endo, H., Can, D.N., Suzuki, H. 2014. Molecular phylogeny of East and Southeast Asian fossorial moles (Lipotyphla, Talpidae). *Journal of Mammalogy*.

Sigé, B., Crochet, J.-Y., Insole, A. 1977. Les plus vieilles taupes. *Géobios,* Mém. Sp., 1:141-157.

Signogneau-Russell, D., Ensom, F. 1998. Thereuodon (Theria, Symmetrodonta) from the Lower Cretaceous of North Africa and Europe, and a brief review of symmetrodonts. *Cretaceous Resumes*, 19:445-470.

Simberloff, D., Boecklen, W. 1981. Santa Rosalia reconsidered: size ratios and competition. *Evolution* 1206–1228.

Smith, R. 2007. Présence du genre *Eotalpa* (Mammalia, Talpidae) dans l'Oligocène inférieur de Belgique (Formation de Borgloon, MP 21). *Bulletin de l'Institut Royal des Sciences Naturelles de Belgique, Sciences de la Terre*, 77:159-165.

Simpson, G.G. 1961. Principles of animal taxonomy. New York: Columbia University Press. 247 p.

Skoczeń, S. 1976. Condylurini Dobson, 1883 (Insectivora, Mammalia) in the Pliocene of Poland. *Acta Zoologica Cracoviensia* 21: 291–314.

Skoczeń, S. 1980. Scaptonychini Van Valen, 1967, Urotrichini and Scapolini Dobson, 1883 (Insectivora, Mammalia) in the Pliocene and Pleistocene of Poland. *Acta Zoologica Cracoviensia* 24: 411–448.

Skoczeń, S. 1993. New records of *Parascalops*, *Neurotrichus* and *Condylura* (Talpinae, Insectivora) from the Pliocene of Poland. *Acta Theriologica* 38: 125–137.

Slater, G.J., Price, S.A., Santini, F., Alfaro, M.E. 2010a. Diversity versus disparity and the radiation of modern cetaceans. *Procedings of the Royal Society B-Biological Sciences*, 277:3097-3104.

Slater, G.J., Figueirido, B., Louis, L., Yang, P., Van Valkenburgh, B. 2010b. Biomechanical Consequences of Rapid Evolution in the Polar Bear Lineage. *PLoS ONE* 5(11):e13870.

Slater, G.J., Pennell, M.V. 2014. Robust regression and posterior predictive simulation increase power to detect early bursts of trait evolution. *Systematic Biology*, in press.

Smith, R. 2007. Présence du genre Eotalpa (Mammalia, Talpidae) dans l'Oligocène inférieur de Belgique (Formation de Borgloon, MP 21). *Bulletin de l'Institut Royal des Sciences Naturelles de Belgique, Sciences de la Terre* 77: 159-165.

Smith, A.T., Xie, Y. 2008. A Guide to the Mammals of China. Princeton NJ: Princeton University Press. 576 p.

Sokal, R. and Michener, C. 1958. A statistical method for evaluating systematic relationships. *University of Kansas Scientific Bulletin*, 38:1409–1438.

Stayton, C.T. 2006. Testing the hypotheses of convergence with multivariate data: morphological and functional convergence among herbivorous lizard. *Evolution*. 60:824–841.

Stayton, C.T. 2009. Application of thin-plate spline transformations to finite elements models, or, how to turn a bog turtle into a spotted turtle to analyze both. *Evolution*, 63:1348–1355.

Stone, R.D. 1995. IUCN Species Survival Commission, Insectivore, Tree-Shrew and Elephant-Shrew Specialist Group; Sultanate of Oman, Sir Peter Scott IUCN/SSC Action Plan Fund; Chicago Zoological Society; National Wildlife Federation; English Nature; WWF Gland: IUCN.

Storch, G. 1978. Die turolische Wirbeltierfauna von Dorn-Dürkheim, Rheinhessen (SWDeutschland). 2. Mammalia: Insectivora. *Senckenbergiana lethaea*, 58:421-449.

Storch, G., Qiu, Z.D. 1983. The Neogene mammalian faunas of Ertemte and Harr Obo in Inner Mongolia (Nei Mongol), China. - 2. Moles – Insectivora: Talpidae. *Senckenbergiana Lethaea* 64:89-127.

Storch, G., Dahlmann, T. 2000. *Desmanella rietscheli*, ein neuer Talpide aus dem Obermioän von Dorn-Dürkheim 1, Rheinhessen. (Mammalia, Eulipotyphla). *Carolinea* 58: 65–69.

Strait, D.S., Wang, Q., Dechow, P.C., Ross, C.F., Richmond, B.G., Spencer, M.A., Patel, B.A. 2005. Modeling elastic properties in finite-element analysis: How much precision is needed to produce an accurate model? *Anatomical Records Part A*. 283:275–287.

Strömberg, C.A.E. 2006. Evolution of hypsodonty in equids: testing a hypothesis of adaptation. *Paleobiology*. 32:236-258.

Sulimski, A. 1959. Pliocene Insectivores from Weze. *Acta Palaeontologica Polonica*, 4:119-177.

Terry, C.J. 1981. Habitat differentiation among threespecies of *Sorex* and *Neurotrichus gibbsi* in Washington. *American Midland Naturalist*. 106:119–125.

Thomas, G.H., Freckleton, R.P., Székely, T. 2006. Comparative analyses of the influence of developmental mode on phenotypic diversification rates in shorebirds. *Procedings of the Royal Society of London B*. 273:1619-1624.

Thomas, G.H., Freckleton, R.P. 2012. MOTMOT: models of trait macroevolution on trees. *Methods in Ecology and Evolution*, 3:145-151.

Thorpe, RS., Malhotra, A., Black, H., Daltry, J.E., Wiister, W. 1995. Relating geographic pattern to phylogenetic process. *Philosophical Transactions of the Royal Society of London Ser. B,* 349: 61-68.

Topachevsky, V.A., Pashkov, A.V. 1990. New representatives of the genus *Desmana* (Insectivora, Talpidae) from Eopleistocene deposits of the south European USSR. *Vestnik Zoologii*, 1990:28-38.

Tsytsulina, K., Formozov, N., Sheftel, B., Zagorodnyuk, I. 2008. *Desmana moschata*. In: IUCN 2010. IUCN Red List of Threatened Species. Version 2010.04.

Tu, F., Fan, Z., Murphy, R. W., Chen, S., Zhang, X., Yan, C., Yue, B. 2014. Molecular phylogenetic relationships among Asiatic shrewlike moles inferred from the complete mitogenomes. *Journal of Zoological Systematics and Evolutionary Research*. 1:17.

Villalta Comella, J.F. De and Crusafont Pairó, M. 1944. Nuevos insectivoros del Mioceno Continental del Vallés-Panadés. *Notas Commissiones Institutos de Geologia y Mineralogia de Espagna*, 12:41-65.

Viscosi, V. and Cardini, A. 2011. Leaf morphology, taxonomy and geometric morphometrics: a simplified protocol for beginners. *PLoS One*, 6(10), e25630.

Viscosi, V., Antonecchia, G., Lepais, O., Fortini, P., Gerber, S. and Loy, A. 2012. Leaf shape and size differentiation in white oaks: assessment of allometric relationships among three sympatric species and their hybrids. *International Journal of Plant Science*, 173:875-884.

Voje, K.L. and Hansen, T.F. 2013. Evolution of static allometries: adaptive change in allometric slopes of eye span in stalk-eyed flies. *Evolution*, 67:453-467.

Voje, K.L., Hansen, T.F., Egset, C.K., Bolstad, G.H. and Pèlabon, C. 2014. Allometric constraints and the evolution of allometry. *Evolution*, 68:866-885.

Wainwright, PC, Alfaro ME, Bolnick DI and Hulsey CD. 2005. Many-to-one mapping of form to function: a general principle in organismal design? *Integrative Computational Biology*, 45:256–262.

Whidden, H. P. 2000. Comparative myology of moles and the phylogeny of the Talpidae (Mammalia, Lipotyphla). *American Museum Novitates* : 1-53.

Wilson, R. L. 1968. Systematics and faunal analysis of a lower Pliocene vertebrate assemblage from Trego County, Kansas.

Woodman, N., Cuartas-Calle C.A., Delgado, V.C.A. 2003. The humerus of *Cryptotis colombiana* and its bearing on the species phylogenetic relationships (Soricidae, Soricomorpha). *Journal of Mammalogy*. 84:832-839.

Yalden, D.W. 1966. The anatomy of mole locomotion. *Journal of Zoology* 149: 55–64

Yates, T. L., D. W. Moore. 1990. Speciation and evolution in the family Talpidae (Mammalia: Insectivora). *Progress in clinical and biological research* 335 : 1.

Yokohata, Y. 2005. A brief review of the biology on moles in Japan. *Mammal Study* 30: 25–30.

Young, M.T., Brusatte, S.L., Ruta, M., De Andrade, M.B. 2010. The evolution of Metriorhynchoidea (mesoeucrocodylia, thalattosuchia): an integrated approach using geometric morphometrics, analysis of disparity, and biomechanics. *Zoological Journal of the Linnean Society*. 158:801–859.

Zelditch, M.L., Swiderski, D.L., Sheets, H.D. and Fink W.L. 2004. Geometric Morphometrics for Biologists: A Primer. 437 pp. Elsevier, Academic Press. San Diego, CA.

Zelditch. M.L., Swiderski, D.L. and Sheets, H.D. 2012. Geometric Morphometrics for Biologists: A Primer. 488 pp. 2nd ed. Elsevier, Academic Press. San Diego, CA.

Ziegler, A. C. 1971. Dental homologies and possible relationships of recent Talpidae. *Journal of Mammalogy*. 50-68.

Ziegler, R., Dahlmann, T., Storch, G. 2007: 4. Marsupialia, Erinaceomorpha and Soricomorpha. – In: Daxner-Höck, Gudrun (ed.), 2007: Oligocene-Miocene Vertebrates from the Valley of Lakes (Central Mongolia): Morphology, phylogenetic and stratigraphic implications. *Annalen des Naturhistorischen Museums Wien*, 108:53-164.

Ziegler R. 1985. Talpiden (Mammalia, Insectivora) aus dem Orleanium und Astaracium Bayerns. *Mitteilungen der Bayerischen Staatssammlung für Paläontologie und Historische Geologie*, 25:131-175.

Ziegler, R. 1990. Talpidae (Insectivora, Mammalia) aus dem Oberoligozan und Untermiozan Süd-deutschlands. *Stuttgarter Beitrage fur Naturkunde B*, 167:1-81.

Ziegler, R., 1998b. Marsupialia und Insectivora (Mammalia) aus den oberoligozänen Spaltenfüllungen Herrlingen 8 und Herrlingen 9 bei Ulm (Baden-Württemberg). *Senckenbergiana lethaea* 77:101-143.

Ziegler, R. 1999. Order Insectivora. In: Rössner, G.E. and Heissig, K. (Eds.), The Miocene Land Mammals of Europe, Verlag Dr. Friedrich Pfeil, München, p. 53-74.

Ziegler, R. 2003. Moles (Talpidae) from the late Middle Miocene of South Germany. *Acta Palaeontologica Polonica* 48: 617–648.

Ziegler, R. 2006: Insectivores (Eulipotyphla) and Bats (Chiroptera) from the Late Miocene of Austria. *Annalen des Naturhistorischen Museums in Wien* 107:93-196.

Ziegler, R. 2012. Moles (Talpidae, Mammalia) from early Oligocene karstic fissure fillings in south Germany. *Geobios*, 45:501-513.

Zijlstra, J.S. 2010. *Neurotrichus skoczeni*, new name for *Neurotrichus minor* Skoczen, 1993. *Journal of Vertebrate Paleontology*, 30:1903.

Zienkiewicz, O.C., Taylor, R.L., Zhu, J.Z. 2005. The finite elements method: its basis and fundamentals. Amsterdam: Elsevier. 733 p.

www.comsol.com

Modified from tnt 10

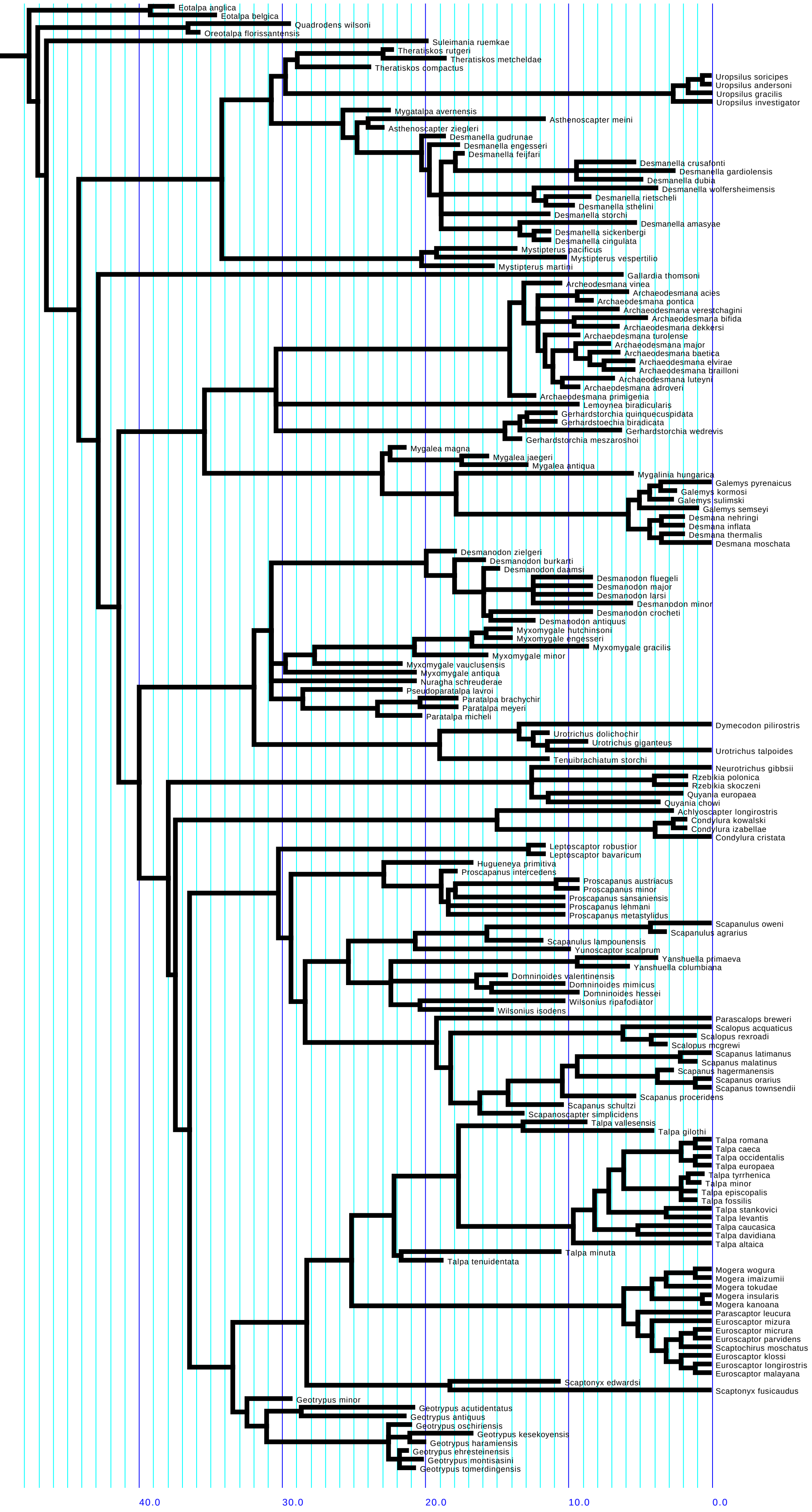

Modified from Imported tree 0

Species	cod
Urotrichus_talpoides	18199
Urotrichus_talpoides	18200
Urotrichus_talpoides	18201
Urotrichus_talpoides	18202
Galemys_pyrenaicus	12245
Parascaptor_leucura	69577
Parascaptor_leucura	69578
Desmana_moschata	2313
Galemys_pyrenaicus	116
Galemys_pyrenaicus	118
Galemys_pyrenaicus	119
Euroscaptor_klossi	95335_2
Mogera_insularis	1969545_3
Mogera_wogura	1854.4.29.2_2
Mogera_insularis	1899.7.21.1_3
Euroscaptor klossi	70.810_2
Urotrichus_talpoides	762
Urotrichus_talpoides	761
Condylura_cristata	1958.6
Scalopus_aquaticus	3117
Mogera_insularis	251
Mogera_insularis	252
Uropsilus_andersoni	118
Uropsilus_andersoni	128
Uropsilus_andersoni	127
Uropsilus_andersoni	131
Uropsilus_andersoni	130
Uropsilus_investigator	119
Uropsilus_investigator	115
Uropsilus_investigator	117
Uropsilus_investigator	118
Uropsilus_soricipes	55443
Uropsilus_soricipes	9812
Uropsilus_soricipes	419
Desmana_moschata	114
Desmana_moschata	111
Desmana_moschata	113
Desmana_moschata	112
Desmana_moschata	199
Desmana_moschata	122
Galemys_pyrenaicus	778
Galemys_pyrenaicus	947
Galemys_pyrenaicus	60559

Galemys_pyrenaicus	60603
Galemys_pyrenaicus	60600
Talpa_altaica	1212
Talpa_altaica	1211
Talpa_altaica	1213
Talpa_levantis	6512
Talpa_levantis	6514
Talpa_levantis	6511
Mogera_imaizumii	131
Mogera_imaizumii	132
Mogera_latouchei	1213
Mogera_insularis	110
Mogera_insularis	2513
Mogera_insularis	421
Mogera_wogura	221
Mogera_wogura	447
Euroscaptor_micrura	750
Euroscaptor_micrura	1620
Euroscaptor_micrura	2544
Euroscaptor_micrura	2540
Euroscaptor_micrura	2537
Euroscaptor_micrura	2535
Euroscaptor_micrura	2546
Euroscaptor_micrura	2536
Parascaptor_leucura	200933
Parascaptor_leucura	232
Parascaptor_leucura	638
Parascaptor_leucura	768
Parascaptor_leucura	711
Parascaptor_leucura	366
Parascaptor_leucura	50493
Parascalops_breweri	2641
Parascalops_breweri	126
Parascalops_breweri	2426
Parascalops_breweri	4583
Urotrichus_talpoides	5324
Urotrichus_talpoides	5336
Urotrichus_talpoides	128
Urotrichus_talpoides	236
Urotrichus_talpoides	486
Urotrichus_talpoides	473
Urotrichus_talpoides	449
Urotrichus_talpoides	126
Urotrichus_talpoides	482

Urotrichus_talpoides	456
Urotrichus_talpoides	458
Dymecodon_pilirostris	124
Dymecodon_pilirostris	8125
Dymecodon_pilirostris	8123
Condylura_cristata	174
Condylura_cristata	121
Condylura_cristata	252
Condylura_cristata	2659
Condylura_cristata	132
Condylura_cristata	2792
Condylura_cristata	1253
Condylura_cristata	172
Condylura_cristata	173
Condylura_cristata	2662
Euroscaptor_klossi	62712
Scapanus_townsendii	370
Scapanus_townsendii	375
Scapanus_townsendii	376
Scapanus_townsendii	374
Scaptochirus_moschatus	164
Scaptochirus_moschatus	162
Scaptochirus_moschatus	1468
Scaptochirus_moschatus	16114
Scaptochirus_moschatus	1116
Scaptonyx_fusicaudus	117
Scaptonyx_fusicaudus	112
Scaptonyx_fusicaudus	116
Scalopus_aquaticus	711
Scalopus_aquaticus	2019
Scalopus_aquaticus	2821
Scalopus_aquaticus	1233
Scalopus_aquaticus	2816
Scalopus_aquaticus	2819
Scalopus_aquaticus	1232
Scalopus_aquaticus	2473
Scalopus_aquaticus	1241
Scalopus_aquaticus	1239
Mogera_tokudae	1211
Euroscaptor_longirostris	124
Euroscaptor_longirostris	319
Euroscaptor_longirostris	148
Neurotrichus_gibbsii	3492
Neurotrichus_gibbsii	3484

Neurotrichus_gibbsii		982
Neurotrichus_gibbsii		3485
Neurotrichus_gibbsii		3481
Mogera_wogura		139
Mogera_wogura		330
Mogera_wogura		440
Mogera_wogura		391
Mogera_wogura		313
Mogera_wogura		2712
Scaptochirus_moschatus		531
Mogera_wogura		275
Talpa_levantis		6365
Euroscaptor_malayana		1418
Euroscaptor_klossi		20531
Euroscaptor_micrura		1280
Talpa_roamna		1128
Talpa_occidentalis		14552
Scapanulus_oweni		12853
Scaptonyx_fusicaudus		181
Uropsilus_andersoni		125
Uropsilus_gracilis		813
Uropsilus_investigator		116
Mogera_imaizumii		38369
Mogera_imaizumii		38797
Mogera_imaizumii		38130
Talpa_altaica		37112
Talpa_altaica		37102
Talpa_altaica		37120
Talpa_altaica		37091
Mogera_imaizumii		382
Urotrichus_talpoides	M8786	
Urotrichus_talpoides	M12545_5	
Urotrichus_talpoides	27300_4	
Urotrichus_talpoides	M3305_3	
Urotrichus_talpoides	M13918_9	
Urotrichus_talpoides	M19185_1	
Mogera_kanoana	M34007_1	
Mogera_kanoana	M33872_4	
Mogera_kanoana	M33871_9	
Mogera_kanoana	M33870_6	
Mogera_kanoana	M33867_5	
Mogera_kanoana	M33866_4	
Mogera_kanoana	M33865_4	
Mogera_kanoana	M33864_2	

Mogera_kanoana	M33863_4
Parascaptor_leucura	sik0903_4
Parascaptor_leucura	sik0904_4
Parascaptor_leucura	sik0901_4
Parascaptor_leucura	sik0909_7
Scapanus_orarius	sik0417_5
Euroscaptor_malayana	M34743_5
Mogera_tokudae	M14724_2
Mogera_tokudae	M147245_4
Dymecodon_pilirostris	M27444
Dymecodon_pilirostris	M27439
Dymecodon_pilirostris	M8764
Dymecodon_pilirostris	M10532
Dymecodon_pilirostris	M10533
Dymecodon_pilirostris	M27460
Dymecodon_pilirostris	M27459
Dymecodon_pilirostris	M12695
Dymecodon_pilirostris	M15837
Dymecodon_pilirostris	M14561
Condylura_cristata	M7999
Euroscaptor_malayana	M34738
Euroscaptor_malayana	M34379
Euroscaptor_malayana	M34740
Euroscaptor_malayana	M34744
Euroscaptor_klossi	M28453
Euroscaptor_mizura	M1543
Euroscaptor_mizura	M13367
Euroscaptor_mizura	M13332
Euroscaptor_mizura	M13340
Euroscaptor_mizura	M9502
Euroscaptor_mizura	M8476
Euroscaptor_mizura	M12475
Euroscaptor_mizura	M9801
Euroscaptor_mizura	M12319
Euroscaptor_mizura	M1514
Euroscaptor_mizura	M4275
Mogera_insularis	M13931
Mogera_insularis	M34010
Mogera_insularis	M34011
Mogera_insularis	M34009
Mogera_insularis	M34008
Mogera_insularis	M34012
Mogera_insularis	M34013
Mogera_insularis	M34014

Mogera_insularis	M34015
Mogera_etigo	M28713
Mogera_etigo	M28715
Mogera_etigo	M13209
Mogera_etigo	M28717
Mogera_etigo	M29389
Mogera_etigo	M29400
Mogera_etigo	M29392
Mogera_etigo	M29394
Mogera_wogura	M27884
Mogera_wogura	M27197
Mogera_wogura	M3576
Mogera_wogura	M17595
Mogera_wogura	M4723
Mogera_wogura	M4725
Mogera_wogura	M14091
Mogera_wogura	M5960
Mogera_wogura	M27303
Mogera_wogura	M5856
Mogera_wogura	M3574
Mogera_wogura	M21496
Mogera_tokudae	M15644
Mogera_tokudae	M15645
Mogera_tokudae	M9844
Mogera_tokudae	M14372
Mogera_tokudae	M14482
Mogera_tokudae	M14724
Mogera_tokudae	M14725
Mogera_tokudae	M13574
Mogera_tokudae	M13575
Mogera_tokudae	M13577
Mogera_tokudae	M13580
Mogera_tokudae	M16702
Mogera_tokudae	M16703
Mogera_imaizumii	M13801
Mogera_imaizumii	M1259
Mogera_imaizumii	M11829
Mogera_imaizumii	M1657
Mogera_imaizumii	M1652
Mogera_imaizumii	M1650
Mogera_imaizumii	M5915
Mogera_imaizumii	M5951
Mogera_imaizumii	SIK141
Mogera_imaizumii	SIK143

Mogera_imaizumii	SIK146	
Mogera_imaizumii	SIK403	
Mogera_imaizumii	SIK408	
Mogera_imaizumii	M17069	
Mogera_imaizumii	M10135	
Mogera_imaizumii	M10136	
Mogera_wogura	M1689	
Mogera_wogura	M5762	
Mogera_wogura	M2028	
Mogera_wogura	M2924	
Mogera_wogura	M4901	
Mogera_wogura	M5350	
Mogera_wogura	M4973	
Mogera_wogura	M4902	
Mogera_wogura	M3356	
Mogera_wogura	M19130	
Mogera_wogura	M9173	
Mogera_wogura	M9181	
Proscapanus_sansaniensis	LGR196	
Proscapanus_sansaniensis	LGR8178	
Scalopus_aquaticus		5973
Scalopus_aquaticus		3467
Scalopus_aquaticus		5972
Desmana_moschata		1887
Desmana_moschata	catB	
Desmana_moschata		20317
Desmana_moschata		6615
Desmana_moschata		26084
Galemys_pyrenaicus		11917
Galemys_pyrenaicus		11940
Galemys_pyrenaicus		1837
Galemys_pyrenaicus	D	
Galemys_pyrenaicus		1953
Euroscaptor_micrura		20831
Euroscaptor_micrura		20830
Parascalops_breweri		7257
Parascalops_breweri		21806
Condylura_cristata		10107
Condylura_cristata		7258
Condylura_cristata		92153
Neurotrichus_gibbsii		37020
Neurotrichus_gibbsii		86880
Neurotrichus_gibbsii		91130
Neurotrichus_gibbsii		91131

Neurotrichus_gibbsii	93840
Neurotrichus_gibbsii	93941
Neurotrichus_gibbsii	93942
Neurotrichus_gibbsii	93943
Scalopus_aquaticus	67481
Scalopus_aquaticus	28379
Scalopus_aquaticus	67482
Scalopus_aquaticus	4692
Scalopus_aquaticus	92162
Scalopus_aquaticus	6016
Scalopus_aquaticus	8956
Scalopus_aquaticus	7253
Scalopus_aquaticus	7254
Scalopus_aquaticus	7256
Scapanus_latimanus	39
Scapanus_latimanus	109
Scapanus_latimanus	159
Scapanus_latimanus	191
Scapanus_latimanus	43861
Scapanus_latimanus	22559
Scapanus_latimanus	22981
Scapanus_latimanus	43833
Scapanus_latimanus	60594
Scapanus_townsendii	30843
Scapanus_townsendii	2004
Scapanus_townsendii	4693
Scapanus_townsendii	92184
Scapanus_townsendii	92185
Scapanus_townsendii	4694
Scapanus_townsendii	3971
Scapanus_townsendii	3973
Scapanus_townsendii	3976
Scapanus_townsendii	3978
Scapanus_orarius	92178
Scapanus_orarius	18913
Scapanus_orarius	18914
Scapanus_orarius	18915
Scapanus_orarius	70376
Scapanus_orarius	4695
Scapanus_orarius	92179
Scapanus_orarius	27285
Neurotrichus_gibbsii	550
Scapanus_townsendii	3825
Scapanus_orarius	131169

Scapanus_orarius	2828
Uropsilus_soricipes	1
Desmana_moschata	2335
Condylura_cristata	62567
Parascaptor_leucura	2939
Talpa_stankovici	21561
Talpa_stankovici	21563
Talpa_altaica	19055
Talpa_altaica	19056
Talpa_altaica	19053
Talpa_caucasica	19944

institution	locality
Senckenberg	Japan
Senckenberg	Japan
Senckenberg	Japan
Senckenberg	Japan
Senckenberg	Spain
Senckenberg	NA
Senckenberg	NA
NHM_london	Russia
NHM_london	Spain
NHM_london	Spain
NHM_london	Spain
NHM_london	Saitong, Chiengmai, Thailand
NHM_london	Taipei, Hsien, Taiwan
NHM_london	Japan
NHM_london	Tasmin, Formosa
NHM_london	Doi Suthep, Thailand
NHM_london	Mt. Takao, Kanagawa
NHM_london	Mt. Takao, Kanagawa
NHM_london	Basswood Lake, Minnesota
NHM_london	Minnesota
NHM_london	Hainan
NHM_london	Hainan
NHM_london	Odung Valley
NHM_london	Odung Valley
NHM_london	Odung Valley
NHM_london	Odung Valley
NHM_london	Odung Valley
NHM_london	Yunnan
NHM_london	Yunnan
NHM_london	Yunnan
NHM_london	Yunnan
NHM_london	Szechuan
NHM_london	Szechuan
NHM_london	Szechuan
NHM_london	Russia
NHM_london	Russia
NHM_london	Russia
NHM_london	Russia
NHM_london	Russia
NHM_london	Russia
NHM_london	Burgos, Spain
NHM_london	Asturie, Spain
NHM_london	Ariege, ST girons, France

NHM_london	Ariege, ST girons, France
NHM_london	Ariege, ST girons, France
NHM_london	NA
NHM_london	NA
NHM_london	NA
NHM_london	NA
NHM_london	Turkey
NHM_london	NA
NHM_london	Chiba, Japan
NHM_london	Niigata, Japan
NHM_london	NA
NHM_london	NA
NHM_london	Formosa
NHM_london	NA
NHM_london	NA
NHM_london	Hondo, Japan
NHM_london	NA
NHM_london	NA
NHM_london	NA
NHM_london	NA
NHM_london	NA
NHM_london	Darjiling
NHM_london	NA
NHM_london	NA
NHM_london	India
NHM_london	NA
NHM_london	NA
NHM_london	NA
NHM_london	NA
NHM_london	NA
NHM_london	Burma
NHM_london	USA
NHM_london	USA
NHM_london	USA
NHM_london	USA
NHM_london	Japan
NHM_london	Japan
NHM_london	Japan
NHM_london	Japan
NHM_london	Japan
NHM_london	Japan
NHM_london	Japan
NHM_london	Japan
NHM_london	Japan

NHM_london	Japan
NHM_london	Japan
NHM_london	Japan
NHM_london	Japan
NHM_london	Japan
NHM_london	Labrador
NHM_london	Labrador
NHM_london	Ontario
NHM_london	NA
NHM_london	NA
NHM_london	NA
NHM_london	NA
NHM_london	NA
NHM_london	NA
NHM_london	NA
NHM_london	Pahang, Malaya
NHM_london	USA
NHM_london	USA
NHM_london	USA
NHM_london	USA
NHM_london	Shantung, China
NHM_london	Shantung, China
NHM_london	Beijing
NHM_london	Shantung, China
NHM_london	Shantung, China
NHM_london	Adung Valley, Burma
NHM_london	Adung Valley, Burma
NHM_london	Adung Valley, Burma
NHM_london	USA
NHM_london	USA
NHM_london	USA
NHM_london	USA
NHM_london	USA
NHM_london	USA
NHM_london	USA
NHM_london	USA
NHM_london	USA
NHM_london	USA
NHM_london	Sado, Japan
NHM_london	Omisan
NHM_london	Szechuan
NHM_london	Szechuan
NHM_london	USA
NHM_london	USA

NHM_london	USA
NHM_london	USA
NHM_london	USA
NHM_london	Japan
NHM_london	Japan
NHM_london	Japan
NHM_london	Haynai
NHM_london	Corea
NHM_london	Japan
NHM_london	NA
NHM_london	Japan
NHM_london	NA
NHM_london	NA
NHM_london	NA
NHM_london	NA
NHM_london	Ostia
NHM_london	La Granya
NHM_london	Gansu
NHM_london	Yunnan
NHM_london	Sychuan
NHM_london	NA
NHM_london	Yunnan
Tokyo NHM	Japan
Tokyo NHM	Japan
Tokyo NHM	Japan
Tokyo NHM	Ajendarovo, kemerobo, Russia
Tokyo NHM	Akademogorok, Novosibirsk; Russia
Tokyo NHM	Konovalovka, Novosibirsk
Tokyo NHM	Oriovoka, Novosibirsk
Tokyo NHM	Japan
Tokyo NHM	Japan
Tokyo NHM	NA
Tokyo NHM	NA
Tokyo NHM	NA
Tokyo NHM	NA
Tokyo NHM	NA
Tokyo NHM	Altshan, Chiayi, Taiwan
Tokyo NHM	Altshan, Chiayi, Taiwan
Tokyo NHM	Altshan, Chiayi, Taiwan
Tokyo NHM	Altshan, Chiayi, Taiwan
Tokyo NHM	Kenting, Pingtung, Taiwan
Tokyo NHM	Kenting, Pingtung, Taiwan
Tokyo NHM	Kenting, Pingtung, Taiwan
Tokyo NHM	Tatachia, yu-shan, nantou, taiwan

Tokyo NHM	Tatachia, yu-shan, nantou, taiwan
Tokyo NHM	Senchip, Mirozam, India
Tokyo NHM	Senchip, Mirozam, India
Tokyo NHM	Senchip, Mirozam, India
Tokyo NHM	Putao, Kachin, Myanmar
Tokyo NHM	Birch Bay, Washington, USA
Tokyo NHM	Boh estate
Tokyo NHM	Japan
Tokyo NHM	Japan
Tokyo NHM	Japan
Tokyo NHM	Japan
Tokyo NHM	Japan
Tokyo NHM	Japan
Tokyo NHM	Japan
Tokyo NHM	Japan
Tokyo NHM	Japan
Tokyo NHM	Japan
Tokyo NHM	Japan
Tokyo NHM	Japan
Tokyo NHM	USA
Tokyo NHM	Boh estate
Tokyo NHM	Boh estate
Tokyo NHM	Boh estate
Tokyo NHM	Boh estate
Tokyo NHM	Thailand
Tokyo NHM	Japan
Tokyo NHM	Japan
Tokyo NHM	Japan
Tokyo NHM	Japan
Tokyo NHM	Japan
Tokyo NHM	Japan
Tokyo NHM	Japan
Tokyo NHM	Japan
Tokyo NHM	Japan
Tokyo NHM	Japan
Tokyo NHM	Japan
Tokyo NHM	Hanpao
Tokyo NHM	Hanpao
Tokyo NHM	Hanpao
Tokyo NHM	Hanpao
Tokyo NHM	Hanpao
Tokyo NHM	Hanpao
Tokyo NHM	Hanpao
Tokyo NHM	Hanpao

Tokyo NHM	Hanpao
Tokyo NHM	Japan
Tokyo NHM	Japan
Tokyo NHM	Japan
Tokyo NHM	Japan
Tokyo NHM	Japan
Tokyo NHM	Japan
Tokyo NHM	Japan
Tokyo NHM	Japan
Tokyo NHM	Japan
Tokyo NHM	Japan
Tokyo NHM	Japan
Tokyo NHM	Japan
Tokyo NHM	Japan
Tokyo NHM	Japan
Tokyo NHM	Japan
Tokyo NHM	Japan
Tokyo NHM	Japan
Tokyo NHM	Japan
Tokyo NHM	Japan
Tokyo NHM	Japan
Tokyo NHM	Sado
Tokyo NHM	Sado
Tokyo NHM	Sado
Tokyo NHM	Sado
Tokyo NHM	Sado
Tokyo NHM	Sado
Tokyo NHM	Sado
Tokyo NHM	Sado
Tokyo NHM	Sado
Tokyo NHM	Sado
Tokyo NHM	Sado
Tokyo NHM	Sado
Tokyo NHM	Sado
Tokyo NHM	Japan
Tokyo NHM	Japan
Tokyo NHM	Japan
Tokyo NHM	Japan
Tokyo NHM	Japan
Tokyo NHM	Japan
Tokyo NHM	Japan
Tokyo NHM	Japan
Tokyo NHM	Japan
Tokyo NHM	Japan

Tokyo NHM	Japan
Tokyo NHM	Japan
Tokyo NHM	Japan
Tokyo NHM	Japan
Tokyo NHM	Japan
Tokyo NHM	Japan
Tokyo NHM	Japan
Tokyo NHM	Japan
Tokyo NHM	Japan
Tokyo NHM	Japan
Tokyo NHM	Japan
Tokyo NHM	Japan
Tokyo NHM	Japan
Tokyo NHM	Japan
Tokyo NHM	Japan
Tokyo NHM	Japan
Tokyo NHM	Japan
Tokyo NHM	Japan
Lyon	Lagrive
Lyon	Lagrive
Naturalis Leiden	Georgia
Naturalis Leiden	Miami
Naturalis Leiden	Georgia
Naturalis Leiden	Russia
Naturalis Leiden	Russia
Naturalis Leiden	Russia
Naturalis Leiden	Russia
Naturalis Leiden	Russia
Naturalis Leiden	Montfort
Naturalis Leiden	st girons
Naturalis Leiden	La motte
Naturalis Leiden	NA
Naturalis Leiden	NA
Naturalis Leiden	Taiwan
Naturalis Leiden	Taiwan
LACM	ohio
LACM	Massachussets
LACM	Harbor island
LACM	ohio
LACM	Pennsylvania
LACM	California
LACM	California
LACM	California
LACM	California

LACM	California
LACM	California
LACM	California
LACM	California
LACM	Florida
LACM	Florida
LACM	Florida
LACM	Georgia
LACM	Georgia
LACM	Lousiana
LACM	Michigan
LACM	ohio
LACM	ohio
LACM	ohio
LACM	California
LACM	California
LACM	California
LACM	California
LACM	California
LACM	California
LACM	California
LACM	California
LACM	California
LACM	Kent
LACM	Oregon
LACM	Oregon
LACM	Oregon
LACM	Oregon
LACM	Oregon
LACM	Kent
LACM	Kent
LACM	Kent
LACM	Kent
LACM	Washington
LACM	Washington
LACM	Washington
LACM	Washington
LACM	Washington
LACM	Oregon
LACM	Washington
LACM	Washington
UCMP	Oregon
UCMP	Oregon
UCMP	Humboldt county

UCMP	California
NHM Wien	China
NHM Wien	Russia
NHM Wien	Pennsylvania
NHM Wien	Dacca, Bangladesh
NHM Wien	Macedonia
NHM Wien	Macedonia
NHM Wien	Russia
NHM Wien	Russia
NHM Wien	Russia
NHM Wien	Kraj, Russia

Species
Lemoynea_biradicularis
Quyania_chowi
Quyania_chowi
Quyania_chowi
Quyania_chowi
Quyania_chowi
Quyania_chowi
Quyania_chowi
Quyania_chowi
Scaptochirus_moschatus
Scaptochirus_moschatus
Yanshuella_primaeva
Yanshuella_primaeva
Yanshuella_primaeva
Yanshuella_primaeva
Yanshuella_primaeva
Yanshuella_primaeva
Yanshuella_primaeva
Yanshuella_primaeva
Yanshuella_primaeva
Yanshuella_primaeva
Yunoscaptor_scalprum
Yunoscaptor_scalprum
Yunoscaptor_scalprum
Yunoscaptor_scalprum
Archaeodesmana_acies
Archaeodesmana_acies
Desmana_nehrigi
Desmana_nehrigi
Desmana_nehrigi
Desmana_nehrigi
Mygalea_magna
Parascalops_breweri
Parascaptor_leucura
Parascaptor_leucura
Paratalpa_cf_brachychir
Urotrichus_talpoides
Urotrichus_talpoides
Geotrypus_montisasini
Hugueneya_primitiva
Hugueneya_primitiva
Myxomygale_minor
Paratalpa_meyeri

Paratalpa_micheli
Desmana_moschata
Galemys_pyrenaicus
Galemys_pyrenaicus
Galemys_pyrenaicus
Euroscaptor_klossi
Euroscaptor_klossi
Mogera_wogura
Mogera_insularis
Mogera_insularis
Urotrichus_talpoides
Scalopus_aquaticus
Mogera_insularis
Mogera_insularis
Uropsilus_andersoni
Uropsilus_andersoni
Uropsilus_andersoni
Uropsilus_andersoni
Uropsilus_andersoni
Uropsilus_investigator
Uropsilus_investigator
Uropsilus_investigator
Uropsilus_investigator
Uropsilus_soricipes
Uropsilus_soricipes
Uropsilus_soricipes
Desmana_moschata
Desmana_moschata
Desmana_moschata
Desmana_moschata
Desmana_moschata
Galemys_pyrenaicus
Galemys_pyrenaicus
Galemys_pyrenaicus
Talpa_altaica
Talpa_altaica
Talpa_altaica
Talpa_levantis
Talpa_levantis
Talpa_levantis
Mogera_imaizumii
Mogera_latouchei
Mogera_insularis
Mogera_insularis

Mogera_wogura
Mogera_wogura
Mogera_wogura
Euroscaptor_micrura
Euroscaptor_micrura
Euroscaptor_micrura
Euroscaptor_micrura
Euroscaptor_micrura
Euroscaptor_micrura
Euroscaptor_micrura
Euroscaptor_micrura
Parascaptor_leucura
Parascaptor_leucura
Parascaptor_leucura
Parascaptor_leucura
Parascaptor_leucura
Parascaptor_leucura
Parascaptor_leucura
Parascalops_breweri
Parascalops_breweri
Parascalops_breweri
Parascalops_breweri
Urotrichus_talpoides
Urotrichus_talpoides
Urotrichus_talpoides
Urotrichus_talpoides
Urotrichus_talpoides
Urotrichus_talpoides
Dymecodon_pilirostris
Dymecodon_pilirostris
Dymecodon_pilirostris
Condylura_cristata
Condylura_cristata
Condylura_cristata
Condylura_cristata
Condylura_cristata
Condylura_cristata
Condylura_cristata
Condylura_cristata
Condylura_cristata
Condylura_cristata
Euroscaptor_klossi
Scapanus_townsendii
Scapanus_townsendii

Scapanus_townsendii
Scapanus_townsendii
Scaptochirus_moschatus
Scaptochirus_moschatus
Scaptochirus_moschatus
Scaptochirus_moschatus
Scaptochirus_moschatus
Scaptochirus_moschatus
Scaptonyx_fusicaudus
Scaptonyx_fusicaudus
Scalopus_aquaticus
Scalopus_aquaticus
Scalopus_aquaticus
Scalopus_aquaticus
Scalopus_aquaticus
Scalopus_aquaticus
Scalopus_aquaticus
Scalopus_aquaticus
Scalopus_aquaticus
Scalopus_aquaticus
Mogera_tokudae
Euroscaptor_longirostris
Euroscaptor_longirostris
Euroscaptor_longirostris
Neurotrichus_gibbsii
Neurotrichus_gibbsii
Neurotrichus_gibbsii
Neurotrichus_gibbsii
Neurotrichus_gibbsii
Mogera_wogura
Mogera_wogura
Mogera_wogura
Mogera_wogura
Mogera_wogura
Mogera_wogura
Scaptochirus_moschatus
Mogera_latouchei
Mogera_wogura
Talpa_levantis
Euroscaptor_malayana
Euroscaptor_klossi
Euroscaptor_micrura
Talpa_romana
Talpa_occidentalis

Urotrichus_talpoides
Scapanulus_oweni
Scaptonyx_fusicaudus
Uropsilus_andersoni
Uropsilus_gracilis
Proscapanus_sansaniensis
Myxomygale_vauclusensis
Myxomygale_antiqua
Myxomygale_antiqua
Talpa_tyrrhenica
Mogera_imaizumii
Mogera_imaizumii
Mogera_imaizumii
Talpa_altaica
Talpa_altaica
Talpa_altaica
Talpa_altaica
Talpa_altaica
Talpa_altaica
Mogera_imaizumii
Urotrichus_talpoides
Urotrichus_talpoides
Urotrichus_talpoides
Urotrichus_talpoides
Mogera_kanoana
Mogera_kanoana
Mogera_kanoana
Mogera_kanoana
Mogera_kanoana
Mogera_kanoana
Mogera_kanoana
Urotrichus_talpoides
Urotrichus_talpoides
Dymecodon_pilirostris
Dymecodon_pilirostris
Dymecodon_pilirostris
Dymecodon_pilirostris
Dymecodon_pilirostris
Parascaptor_leucura
Parascaptor_leucura
Parascaptor_leucura
Parascaptor_leucura
Dymecodon_pilirostris
Dymecodon_pilirostris

Dymecodon_pilirostris
Dymecodon_pilirostris
Scapanus_orarius
Condylura_cristata
Euroscaptor_malayana
Euroscaptor_malayana
Euroscaptor_malayana
Euroscaptor_malayana
Euroscaptor_klossi
Euroscaptor_mizura
Euroscaptor_mizura
Euroscaptor_mizura
Euroscaptor_mizura
Euroscaptor_mizura
Euroscaptor_mizura
Euroscaptor_mizura
Euroscaptor_mizura
Euroscaptor_mizura
Euroscaptor_mizura
Euroscaptor_mizura
Mogera_insularis
Mogera_insularis
Mogera_insularis
Mogera_insularis
Mogera_insularis
Mogera_insularis
Mogera_insularis
Mogera_etigo
Mogera_etigo
Mogera_etigo
Mogera_etigo
Mogera_etigo
Mogera_etigo
Mogera_etigo
Mogera_etigo
Mogera_wogura
Mogera_wogura
Mogera_wogura
Mogera_wogura
Mogera_wogura
Mogera_wogura
Mogera_wogura
Mogera_tokudae
Mogera_tokudae

Mogera_tokudae
Mogera_tokudae
Mogera_tokudae
Mogera_tokudae
Mogera_tokudae
Mogera_tokudae
Mogera_imaizumii
Mogera_imaizumii
Mogera_imaizumii
Mogera_imaizumii
Mogera_imaizumii
Mogera_imaizumii
Mogera_imaizumii
Mogera_imaizumii
Mogera_imaizumii
Mogera_imaizumii
Mogera_wogura
Mogera_wogura
Mogera_wogura
Mogera_wogura
Mogera_wogura
Mogera_wogura
Mygatalpa_avernensis
Scaptonyx_edwardsi
Scaptonyx_edwardsi
Proscapanus_sansaniensis
Urotrichus_dolichochir
Asthenoscapter_meini
Talpa_minuta
Proscapanus_sansaniensis
Proscapanus_sansaniensis
Proscapanus_sansaniensis
Proscapanus_sansaniensis
Proscapanus_sansaniensis
Proscapanus_sansaniensis
Proscapanus_sansaniensis
Proscapanus_sansaniensis
Proscapanus_sansaniensis
Proscapanus_sansaniensis
Proscapanus_sansaniensis
Scaptonyx_edwardsi
Proscapanus_sansaniensis
Mygalea_antiqua
Leptoscaptor_bavaricum

Leptoscaptor_bavaricum
Leptoscaptor_bavaricum
Talpa_minuta
Tenuibrachiatum_storchi
Tenuibrachiatum_storchi
Desmanella_sp
Desmanella_sthelini
Desmanella_sthelini
Desmanodon_sp
Proscapanus_sansaniensis
Proscapanus_sansaniensis
Proscapanus_sp
Paratalpa_micheli
Hugueneya_primitiva
Proscapanus_sansaniensis
Geotrypus_sp
Desmanella_engesseri
Desmanella_engesseri
Proscapanus_intercedens
Myxomygale_minor
Myxomygale_minor
Myxomygale_vauclusensis
Desmanella_engesseri
Desmanella_engesseri
Mygalea_jaegeri
Myxomygale_minor
Myxomygale_vauclusensis
Myxomygale_vauclusensis
Myxomygale_vauclusensis
Geotrypus_minor
Scalopus_aquaticus
Scalopus_aquaticus
Desmana_moschata
Desmana_moschata
Desmana_moschata
Desmana_moschata
Galemys_pyrenaicus
Galemys_pyrenaicus
Galemys_pyrenaicus
Galemys_pyrenaicus
Euroscaptor_micrura
Euroscaptor_micrura
Desmana_thermalis
Desmana_thermalis

Desmana_thermalis
Galemys_kormosi
Galemys_kormosi
Galemys_kormosi
Galemys_kormosi
Desmanella_dubia
Parascalops_breweri
Parascalops_breweri
Condylura_cristata
Condylura_cristata
Condylura_cristata
Neurotrichus_gibbsii
Neurotrichus_gibbsii
Neurotrichus_gibbsii
Neurotrichus_gibbsii
Neurotrichus_gibbsii
Neurotrichus_gibbsii
Scalopus_aquaticus
Scalopus_aquaticus
Scalopus_aquaticus
Scalopus_aquaticus
Scalopus_aquaticus
Scalopus_aquaticus
Scalopus_aquaticus
Scalopus_aquaticus
Scalopus_aquaticus
Scalopus_aquaticus
Scapanus_latimanus
Scapanus_latimanus
Scapanus_latimanus
Scapanus_latimanus
Scapanus_latimanus
Scapanus_latimanus
Scapanus_latimanus
Scapanus_latimanus
Scapanus_townsendii
Scapanus_townsendii
Scapanus_townsendii
Scapanus_townsendii
Scapanus_townsendii
Scapanus_townsendii
Scapanus_townsendii
Scapanus_townsendii
Scapanus_townsendii

Scapanus_townsendii
Scapanus_orarius
Scapanus_orarius
Scapanus_orarius
Scapanus_orarius
Scapanus_orarius
Scapanus_orarius
Scapanus_orarius
Mystipterus_sp
Scapanus_schultzi
Desmana_pontica
Desmana_pontica
Desmanella_crusafonti
Desmanella_crusafonti
Desmanella_crusafonti
Desmana_pontica
Desmana_pontica
Desmana_pontica
Desmana_pontica
Desmana_moschata
Condylura_cristata
Parascaptor_leucura
Talpa_altaica
Talpa_altaica
Talpa_altaica
Talpa_caucasica
Talpa_caucasica
Desmana_nehrigi
Desmana_nehrigi
Desmana_nehrigi
Galemys_kormosi
Desmana_pontica
Galemys_kormosi

cod	
FV1222	
6453_01	
6453_02	
6453_03	
6453_04	
6453_05	
6453_06	
6453_07	
6453_08	
V5416_01	
V5416_02	
6455_01	
6455_02	
6455_03	
6455_04	
6455_05	
6455_06	
6455_07	
6455_08	
6455_09	
6455_10	
9740_01	
9740_02	
9740_03	
9740_04	
	971009
	971010
SMF2692_01	
SMF2693_01	
SMF2692_02	
SMF2693_02	
SMF19877	
	43058
	69577
	69578
	19871
	18202
	18203
	44522
	44482
	44472
	45155
	44528

44482
2313
116
118
119
70810
95335
1854
1969545
1899
762
3115
4251
4252
11118
128
127
131
119
9119
115
117
118
55443
9812
419
114
113
111
199
122
60599
60603
60600
1212
1211
1213
6512
6514
6511
131
1213
12110
2513

1421
221
447
750
1620
2544
2540
2537
2535
2546
2536
200933
232
638
768
711
50493
366
2641
126
2426
4583
5336
128
236
486
473
449
124
8123
8125
174
121
252
2659
132
2792
1253
172
173
2662
62712
370
375

376
374
164
162
1468
114
163
1116
117
116
711
2019
2821
1233
2816
2819
1232
2473
1241
1239
81211
124
319
148
3492
3484
95982
3485
3481
1139
330
440
391
76313
2712
10531
171
275
6365
1418
20531
1280
1128
14552

	468
	12852
	181
	125
	813
M5369	
cast	
cast2	
JH010	
M16100	
	38369
	38797
	38130
	37112
	37092
	37102
	37110
	37120
	37091
	382
M8786	
M12545	
M3305	
M13918	
M34007	
M33872	
M33871	
M33870	
M33867	
M33866	
M33863	
M11582	
M11555	
M9837	
M10990	
M12455	
M5838	
M20144	
SIK903	
SIK904	
SIK901	
SIK909	
M27444	
M8764	

M10533
M27460
SIK417
M7999
M34738
M34379
M34743
M34744
M28453
M1543
M13367
M13332
M13340
M9502
M8476
M12475
M9801
M12319
M1544
M4275
M13931
M34010
M34011
M34009
M34008
M34013
M34014
M28713
M28715
M13209
M28717
M29389
M29400
M29392
M29394
M27884
M18197
M3576
M17595
M4723
M5960
M5856
M15644
M15645

M9844	
M14372	
M14482	
M14724	
M13574	
M14725	
M13801	
M1259	
M11829	
M1657	
M1652	
M1650	
M5915	
SIK143	
SIK146	
SIK403	
M1689	
M5762	
M4901	
M4973	
M4902	
M9173	
	97357
	65708
	69014
	69017
	69078
LGL7	
LG01	
LGL7a	
LGL7b	
LGL7c	
LGL7d	
LGL7e	
LGMa	
LGMb	
LGMc	
LGR196	
LGR196a	
LGR196b	
LGR8179	
LGR8178	
P610651	
P106086	

P1060836	
P1060837	
P610601	
P31166A1	
P31166A2	
P311653	
P61064	
P18754	
P106181	
P3116332	
P3912042	
P68	
BSP294	
BSP523	
BSP7191	
BSPi6	
BSP429	
BSP430	
BSP3173	
BSP6131	
BSP6139	
BSP1972ix	
BSP3156	
BSP3158	
BSP281	
BSP2060	
BSP2058	
BSP2059	
BSP676	
BSP6162	
	3467
	5972
	1887
Catb	
	6615
	26084
	11917
	1837
d	
	1953
	20831
	20830
RGM257491	
RGM257502	

RGM257500	
RGM257659	
RGM257652	
RGM257655	
RGM257654	
U01	
	7257
	21806
	10107
	7258
	92153
	37020
	86880
	91130
	93941
	93942
	93943
	67481
	28379
	67482
	4692
	92162
	6016
	8956
	7253
	7254
	7256
	39
	109
	159
	191
	43861
	22559
	22981
	43833
	60594
	2004
	4693
	92184
	92185
	4694
	3971
	3973
	3976

	3978
	92178
	18913
	18915
	70376
	4695
	92179
	27285
V70140	
	595
	74554
74554a	
	81137
81137a	
81137c	
KII2	
K01	
K02	
	1981
	2335
	62567
	2939
	19055
	19056
	19053
	19944
	19945
W1	
W2	
	96470
	6360
	3045
	96370

institution
IVPP
IVPP
IVPP
IVPP
IVPP
IVPP
IVPP
IVPP
IVPP
IVPP
IVPP
IVPP
IVPP
IVPP
IVPP
IVPP
IVPP
IVPP
IVPP
IVPP
IVPP
IVPP
IVPP
IVPP
IVPP
Senckenberg
Senckenberg
Senckenberg
Senckenberg
Senckenberg
Senckenberg
Senckenberg
Senckenberg
Senckenberg
Senckenberg
Senckenberg
Senckenberg
Senckenberg
SMNS
SMNS
SMNS
SMNS
SMNS

SMNS
NHM london
NHM london
NHM london
NHM london
NHM london
NHM london
NHM london
NHM london
NHM london
NHM london
NHM london
NHM london
NHM london
NHM london
NHM london
NHM london
NHM london
NHM london
NHM london
NHM london
NHM london
NHM london
NHM london
NHM london
NHM london
NHM london
NHM london
NHM london
NHM london
NHM london
NHM london
NHM london
NHM london
NHM london
NHM london
NHM london
NHM london
NHM london
NHM london
NHM london
NHM london
NHM london
NHM london

NHM london
NHM london
NHM london
NHM london
NHM london
NHM london
NHM london
NHM london
NHM london
NHM london
NHM london
NHM london
NHM london
NHM london
NHM london
NHM london
NHM london
NHM london
NHM london
NHM london
NHM london
NHM london
NHM london
NHM london
NHM london
NHM london
NHM london
NHM london
NHM london
NHM london
NHM london
NHM london
NHM london
NHM london
NHM london
NHM london
NHM london
NHM london
NHM london
NHM london
NHM london
NHM london
NHM london
NHM london

NHM london
NHM london
NHM london
NHM london
NHM london
NHM london
NHM london
NHM london
NHM london
NHM london
NHM london
NHM london
NHM london
NHM london
NHM london
NHM london
NHM london
NHM london
NHM london
NHM london
NHM london
NHM london
NHM london
NHM london
NHM london
NHM london
NHM london
NHM london
NHM london
NHM london
NHM london
NHM london
NHM london
NHM london
NHM london
NHM london
NHM london
NHM london
NHM london
NHM london
NHM london
NHM london
NHM london
NHM london

NHM london
NHM london
NHM london
NHM london
NHM london
NHM london
NHM london
NHM london
NHM london
NHM london
Tokyo NHM
Tokyo NHM
Tokyo NHM
Tokyo NHM
Tokyo NHM
Tokyo NHM
Tokyo NHM
Tokyo NHM
Tokyo NHM
Tokyo NHM
Tokyo NHM
Tokyo NHM
Tokyo NHM
Tokyo NHM
Tokyo NHM
Tokyo NHM
Tokyo NHM
Tokyo NHM
Tokyo NHM
Tokyo NHM
Tokyo NHM
Tokyo NHM
Tokyo NHM
Tokyo NHM
Tokyo NHM
Tokyo NHM
Tokyo NHM
Tokyo NHM
Tokyo NHM
Tokyo NHM
Tokyo NHM
Tokyo NHM
Tokyo NHM
Tokyo NHM

Tokyo NHM
Tokyo NHM
Tokyo NHM
Tokyo NHM
Tokyo NHM
Tokyo NHM
Tokyo NHM
Tokyo NHM
Tokyo NHM
Tokyo NHM
Tokyo NHM
Tokyo NHM
Tokyo NHM
Tokyo NHM
Tokyo NHM
Tokyo NHM
Tokyo NHM
Tokyo NHM
Tokyo NHM
Tokyo NHM
Tokyo NHM
Tokyo NHM
Tokyo NHM
Tokyo NHM
Tokyo NHM
Tokyo NHM
Tokyo NHM
Tokyo NHM
Tokyo NHM
Tokyo NHM
Tokyo NHM
Tokyo NHM
Tokyo NHM
Tokyo NHM
Tokyo NHM
Tokyo NHM
Tokyo NHM
Tokyo NHM
Tokyo NHM
Tokyo NHM
Tokyo NHM
Tokyo NHM
Tokyo NHM
Tokyo NHM

Tokyo NHM
Tokyo NHM
Tokyo NHM
Tokyo NHM
Tokyo NHM
Tokyo NHM
Tokyo NHM
Tokyo NHM
Tokyo NHM
Tokyo NHM
Tokyo NHM
Tokyo NHM
Tokyo NHM
Tokyo NHM
Tokyo NHM
Tokyo NHM
Tokyo NHM
Tokyo NHM
Tokyo NHM
Tokyo NHM
Tokyo NHM
Tokyo NHM
Lyon
Lyon
Lyon
Lyon
Lyon
Lyon
Lyon
Lyon
Lyon
Lyon
Lyon
Lyon
Lyon
Lyon
Lyon
Lyon
Lyon
Lyon
Lyon
Lyon
Augsburg
Augsburg

Augsburg
Augsburg
Augsburg
Augsburg
Augsburg
Augsburg
Augsburg
Augsburg
Augsburg
Augsburg
Augsburg
Augsburg
BSPG
BSPG
BSPG
BSPG
BSPG
BSPG
BSPG
BSPG
BSPG
BSPG
BSPG
BSPG
BSPG
BSPG
BSPG
BSPG
BSPG
BSPG
Leiden
Leiden
Leiden
Leiden
Leiden
Leiden
Leiden
Leiden
Leiden
Leiden
Leiden
Leiden
Leiden
Leiden

Leiden
Leiden
Leiden
Leiden
Leiden
Utrecht
LACM
LACM
LACM
LACM
LACM
LACM
LACM
LACM
LACM
LACM
LACM
LACM
LACM
LACM
LACM
LACM
LACM
LACM
LACM
LACM
LACM
LACM
LACM
LACM
LACM
LACM
LACM
LACM
LACM
LACM
LACM
LACM
LACM
LACM
LACM
LACM
LACM
LACM

LACM
LACM
LACM
LACM
LACM
LACM
LACM
LACM
UCMP
UCMP
NHM Wien
NHM Wien
NHM Wien
NHM Wien
NHM Wien
NHM Wien
NHM Wien
NHM Wien
NHM Wien
NHM Wien
NHM Wien
NHM Wien
NHM Wien
NHM Wien
NHM Wien
NHM Wien
NHM Wien
Isez Pan
Isez Pan
Isez Pan
Isez Pan
Isez Pan
Isez Pan

Locality
NA
Ertemte2
Ertemte2
Ertemte2
Ertemte2
Ertemte2
Ertemte2
Ertemte2
Ertemte2
NA
NA
Ertemte2
Ertemte2
Ertemte2
Ertemte2
Ertemte2
Ertemte2
Ertemte2
Ertemte2
Ertemte2
Ertemte2
Lu Feng
Lu Feng
Lu Feng
Lu Feng
NA
NA
NA
NA
NA
NA
NA
USA
NA
NA
NA
Japan
Japan
NA
NA
NA
NA
NA

NA
Russia
Spain
Spain
Spain
NA
Thailand
Japan
Taipei
Formosa
Japan
USA
Hainan
Hainan
Odung Valley
Odung Valley
Odung Valley
Odung Valley
Odung Valley
Yunnan
Yunnan
Yunnan
Yunnan
Sychuan
Sychuan
Sychuan
Russia
Russia
Russia
Russia
Russia
Asturie
ariege
ariege
Russia
Russia
Russia
NA
NA
NA
Japan
NA
NA
NA

Japan
Japan
Japan
NA
NA
NA
NA
NA
NA
NA
NA
NA
NA
NA
NA
NA
NA
NA
NA
NA
NA
NA
Japan
Japan
Japan
Japan
Japan
Japan
Japan
Japan
Japan
USA
USA
USA
USA
USA
USA
USA
USA
USA
USA
Malaya
USA
USA

USA
USA
Shantung
Shantung
Beijing
Beijing
Beijing
Beijing
Burma
Burma
USA
USA
USA
USA
USA
USA
USA
USA
USA
USA
Sado
Omi San
Sychuan
Sychuan
USA
USA
USA
USA
USA
Japan
Shizumura
Japan
Haynai
Korea
Japan
NA
NA
Japan
NA
NA
NA
NA
Ostia
LaGranya

Japan
Gansu
Yunnan
Sychuan
NA
Sansan
Saint Martin france
NA
Isle of Wight
Monte San Giovanni
Japan
Japan
Japan
Russia
Russia
Russia
Russia
Russia
Russia
Japan
Japan
Japan
Japan
Japan
Taiwan
Taiwan
Taiwan
Taiwan
Taiwan
Taiwan
Taiwan
Japan
Japan
Japan
Japan
Japan
Japan
Japan
India
India
India
India
Japan
Japan

Japan
Japan
Japan
Michigan
Malaysia
Malaysia
Malaysia
Malaysia
Thailand
Japan
Japan
Japan
Japan
Japan
Japan
Japan
Japan
Japan
Japan
Japan
Taiwan
Taiwan
Taiwan
Taiwan
Taiwan
Taiwan
Taiwan
Japan
Japan
Japan
Japan
Japan
Japan
Japan
Japan
Japan
Japan
Japan
Korea
Korea
Japan
Japan
Japan
Japan

Japan
Japan
Japan
Japan
Japan
Japan
Japan
Japan
Japan
Japan
Japan
Japan
Japan
Japan
Japan
Japan
Japan
Japan
Japan
Japan
Japan
Japan
NA
NA
NA
Sansan
La Grive
La Grive
La Grive
La Grive
La Grive
La Grive
La Grive
La Grive
La Grive
La Grive
La Grive
La Grive
La Grive
La Grive
La Grive
La Grive
NA
NA

NA
NA
NA
NA
NA
NA
NA
NA
NA
NA
NA
NA
Ehrenstein4
NA
Steinberg
Gaimershei
NA
NA
Petersbuch
NA
NA
Morhen
Petersbuch2
Petersbuch2
Vienhausen
Morhen19
Morhen19
Morhen19
HAAG2
Morhen13
Florida
Georgia
Russia
Russia
Russia
Russia
Montfort
La Motte
NA
ST Girons
Taiwan
Taiwan
Tegelen
Tegelen

Tegelen
Tegelen
Tegelen
Tegelen
Tegelen
Maramena
Ohio
Massachussets
Harbor island
Ohio
Pennsylvania
California
California
California
California
California
California
Florida
Florida
Florida
Georgia
Georgia
Lousiana
Michigan
Ohio
Ohio
Ohio
California
California
California
California
California
California
California
California
Washington
Oregon
Oregon
Oregon
Oregon
Oregon
Washington
Washington
Washington

Washington
Washington
Washington
Washington
Washington
Oregon
Washington
Washington
Nevada
Ricardo
Kohfidisch
Kohfidisch
Kohfidisch
Kohfidisch
Kohfidisch
Kohfidisch
Kohfidisch
Kohfidisch
Kohfidisch
Russia
Pennsylvania
Bangladesh
Russia
Russia
Russia
Russia
Russia
Weze1
Weze1
Weze1
Rebielice Kro1
Weze1
Rebielice Kro1

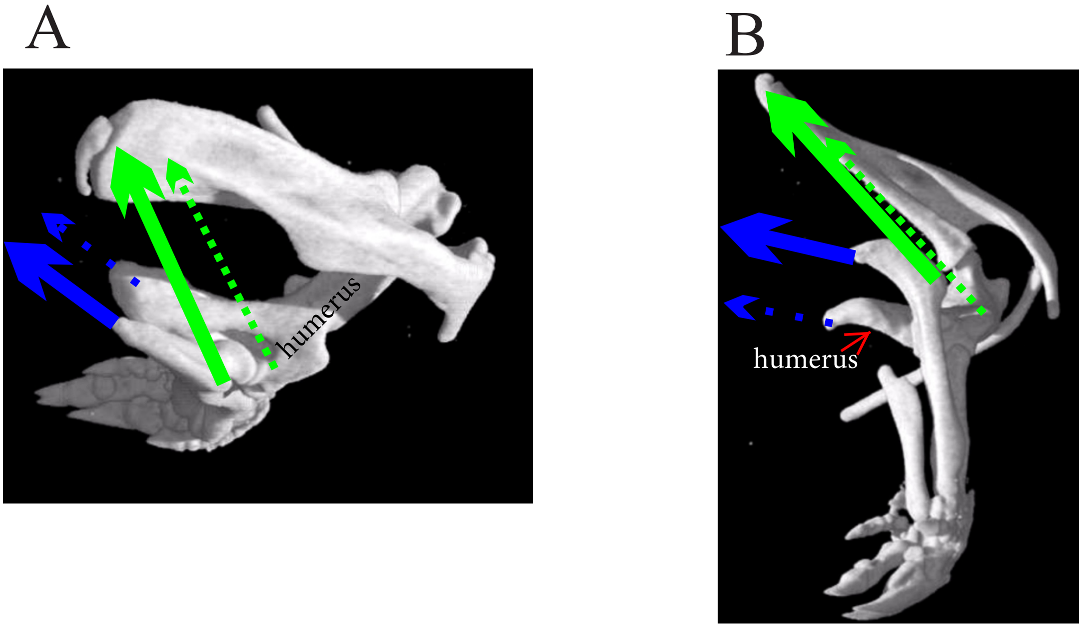
A
humerus
B
humerus

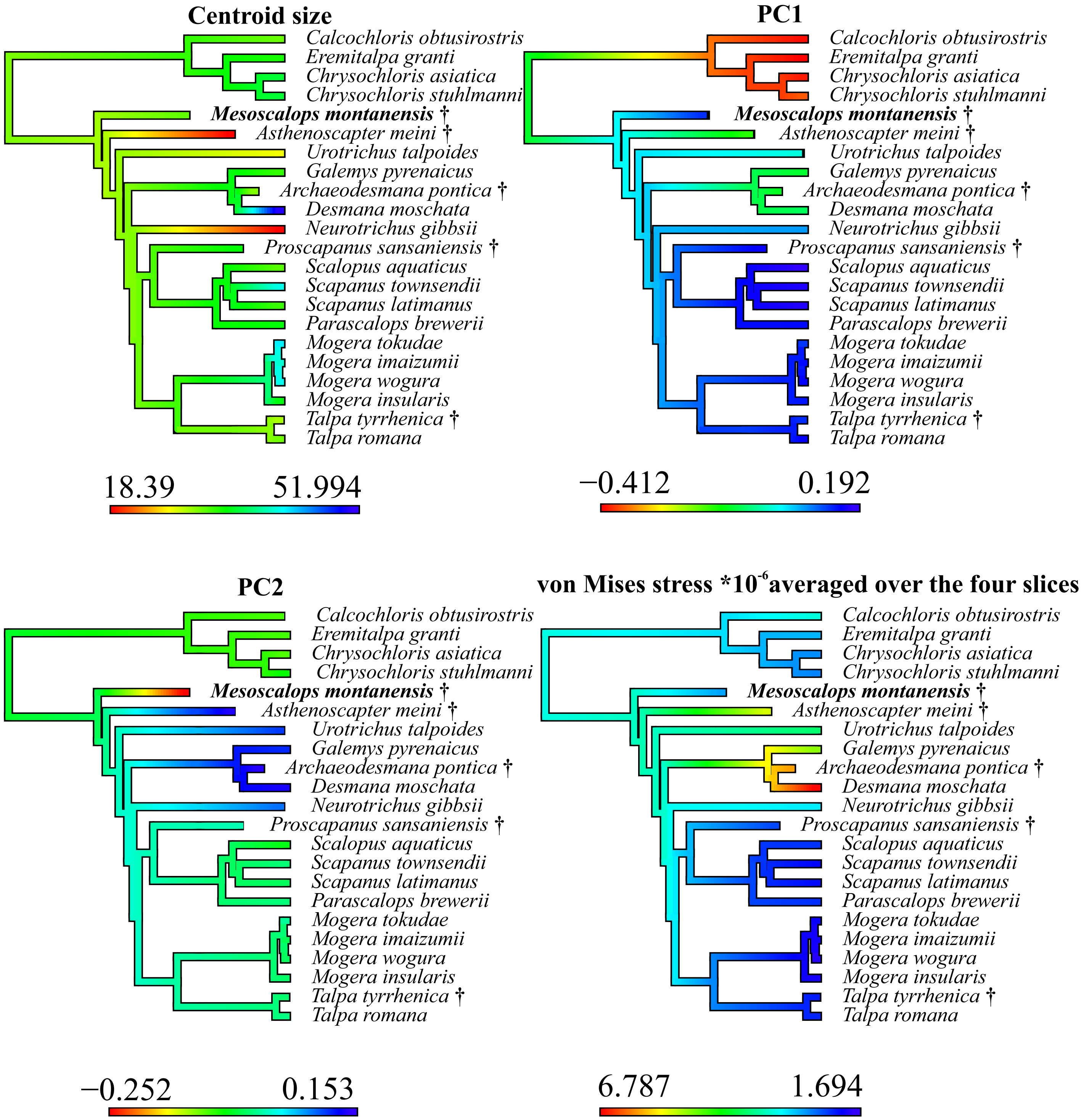
Centroid size
Calcochloris obtusirostris
Eremitalpa granti
Chrysochloris asiatica
Chrysochloris stuhlmanni
Mesoscalops montanensis †
Asthenoscapter meini †
Urotrichus talpoides
Galemys pyrenaicus
Archaeodesmana pontica †
Desmana moschata
Neurotrichus gibbsii
Proscapanus sansaniensis †
Scalopus aquaticus
Scapanus townsendii
Scapanus latimanus
Parascalops brewerii
Mogera tokudae
Mogera imaizumii
Mogera wogura
Mogera insularis
Talpa tyrrhenica †
Talpa romana
18.39
51.994
PC1
−0.412
0.192
PC2
−0.252
0.153
von Mises stress *10⁻⁶ averaged over the four slices
6.787
1.694